

การศึกษาการเผาไหม้ของละอองฝอยจากการฉีดเชื้อเพลิงปาล์มดีเซล



นายกาญจน์ ร่มพล

สถาบันวิทยบริการ

จุฬาลงกรณ์มหาวิทยาลัย

วิทยานิพนธ์นี้เป็นส่วนหนึ่งของการศึกษาตามหลักสูตรปริญญาวิศวกรรมศาสตรมหาบัณฑิต

สาขาวิชาวิศวกรรมเครื่องกล ภาควิชาวิศวกรรมเครื่องกล


คณะวิศวกรรมศาสตร์ จุฬาลงกรณ์มหาวิทยาลัย

ปีการศึกษา 2548

ISBN 974-53-2553-8

ลิขสิทธิ์ของจุฬาลงกรณ์มหาวิทยาลัย

THE FUNDAMENTAL STUDY ON CHARACTERISTIC OF PALM DIESEL SPRAY COMBUSTION



Mr. Karn Romphol

สถาบันวิทยบริการ
จุฬาลงกรณ์มหาวิทยาลัย

A Thesis Submitted in Partial Fulfillment of the Requirements
for the Degree of Master of Engineering Program in Mechanical Engineering

Department of Mechanical Engineering

Faculty of Engineering

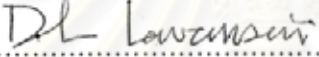
Chulalongkorn University

Academic Year 2005

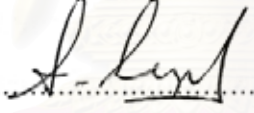
ISBN 974-53-2553-8

Thesis Title THE FUNDAMENTAL STUDY ON THE CHARACTERISTIC OF
PALM DIESEL SPRAY COMBUSTION
By KARN ROMPHOL
Field of study MECHANICAL ENGINEERING
Thesis Advisor ASSISTANT PROFESSOR KANIT WATTANAVICHIEEN, Ph.D.
Thesis Co-advisor PROFESSOR AKIHIKO AZETSU, Dr. Eng.


Accepted by the Faculty of Engineering, Chulalongkorn University in Partial
Fulfillment of the Requirements for the Master's Degree


..... Dean of Faculty of Engineering
(Professor Direk Lavansiri, Ph.D.)

THESIS COMMITTEE


..... Chairman
(Associate Professor Staporn Suprichakorn)


..... Thesis Advisor
(Assistant Professor Kanit Wattanavichien, Ph.D.)


..... Thesis Co-advisor
(Professor Akihiko Azetsu, Dr.Eng.)


..... Member
(Assistant Professor Chatchai Hongsa-Utain)

นายกาญจน์ ร่มพล : การศึกษาการเผาไหม้ของละอองฝอยจากการฉีดน้ำมันปาล์มดีเซล.

(THE FUNDAMENTAL STUDY ON THE CHARACTERISTIC OF PALM DIESEL SPRAY COMBUSTION) อ. ที่ปรึกษา: ผู้ช่วยศาสตราจารย์ ดร.คณิต วัฒนวิเชียร, อ. ที่ปรึกษาร่วม : Prof. Akihiko Azetsu, Dr. Eng. 239 หน้า. ISBN 974-53-2553-8

งานวิจัยนี้ได้ทำการศึกษาผลของการเผาไหม้ของละอองฝอยจากการฉีดน้ำมันปาล์มผสมดีเซลในห้องเผาไหม้จำลองที่มีปริมาตรคงที่ โดยควบคุมระยะเวลาการฉีดและความดันภายในห้องเผาไหม้ ผลของการเผาไหม้ของน้ำมันปาล์มที่ส่วนผสมและความดันการฉีดต่างๆ ได้ทำการวัดโดยใช้ Photo diode และการถ่ายภาพความเข้มแสงด้วย กล้องความไวแสงสูง (ICCD Camera) ผลที่ได้จากการวัดจะนำมาวิเคราะห์หาช่วงล่าช้าการจุดระเบิด (Ignition delay) และช่วงเวลาการเผาไหม้ (Combustion period) ส่วนอุณหภูมิการเผาไหม้และ ค่า KL factor ซึ่งจะเป็นค่าที่ใช้ในการประมาณค่า soot จะวิเคราะห์ด้วยวิธี Two-color

ผลการทดลองพบว่า ถ้าส่วนผสมปาล์มสกัด(refined palm)มากขึ้นก็จะมีผลทำให้ค่า Ignition delay และค่า Combustion period มีแนวโน้มที่จะลดลง อีกทั้งพื้นที่การเผาไหม้ที่มีอุณหภูมิสูง เกินกว่า 2400 K ของปาล์มดีเซล มีแนวโน้มที่จะน้อยกว่าดีเซล ขณะค่า KL factor ในช่วงเริ่มต้นการเผาไหม้ มีแนวโน้มที่จะมีค่าสูงขึ้นตามปริมาณปาล์มที่ผสม

ผลจากการถ่ายภาพละอองฝอย จากการฉีดน้ำมันปาล์มดีเซล 80% กับเชื้อเพลิงดีเซล ณ ความดันการฉีด 60 และ 100 MPa ยังพบว่าปาล์มดีเซล 80% มีค่าของมุมการฉีด(spray angle), ค่า spray penetration และค่าปริมาตรการฉีด (spray volume) น้อยกว่าเชื้อเพลิงดีเซล

ส่วนผลของการศึกษาการเผาไหม้ของน้ำมันปาล์มดิบไทย 10% ผสมดีเซล (CPO 10%) ณ ความดันการฉีด 100 MPa พบว่าการผลจากการเผาไหม้นั้น มีค่า Ignition delay และค่า Combustion period สั้นกว่าดีเซล อุณหภูมิการเผาไหม้จะต่ำกว่าดีเซลเล็กน้อยโดยเฉพาะในช่วงปลายของการเผาไหม้ ค่า KL factor และปริมาณความเข้มข้นของ Soot มีความแตกต่างกันน้อยมากเมื่อเทียบกับเชื้อเพลิงดีเซล ณ สภาวะการฉีดและการเผาไหม้ที่เท่ากัน

ภาควิชา.....วิศวกรรมเครื่องกล.....ลายมือชื่อนิสิต..... กกาญจน์ ร่มพล
สาขาวิชา.....วิศวกรรมเครื่องกล.....ลายมือชื่ออาจารย์ที่ปรึกษา..... ดร.คณิต วัฒนวิเชียร
ปีการศึกษา.....2548.....ลายมือชื่ออาจารย์ที่ปรึกษาร่วม..... Akihiko Azetsu

4470219121 : MAJOR MECHANICAL ENGINEERING

KEY WORD: PALM DIESEL / FLAME VISUALIZATION / COMBUSTION / TWO COLOR METHOD/ SPRAY

KARN ROMPHOL: THE FUNDAMENTAL STUDY ON THE CHARACTERISTIC OF PALM DIESEL SPRAY COMBUSTION. THESIS ADVISOR : ASST.PROF.KANIT WATTANAVICHIEEN, Ph.D., THESIS COADVISOR : PROF. AKIHIKO AZETSU, Dr. Eng., 239 pp. ISBN 974-53-2553-8

The study on the characteristics of palm diesel fuel spray combustion were conducted in a constant volume combustion chamber. With the fixed experimental conditions such as ambient pressure and injection events, the effects of refined palm blending percentage with diesel and injection pressure on spray combustion and flame structure were investigated using photo diode and ICCD camera. Two-color method was employed to measure combustion flame temperature and KL factors.

It was found that the higher the percentage of palm in the blend, the shorter the ignition delay and the shorter combustion period compared with diesel fuel. High temperature combustion area (over 2400 K) of palm diesel was also smaller than diesel. The amount of soot at the start of combustion was a little bit higher than diesel.

The results from fuel spray image, with 80%palm blended at injection pressure 60 and 100MPa, showed that spray penetration and spray angle were shorter and smaller than diesel fuel.

The effects of 10%CPO diesel at injection pressure of 100MPa on combustion and flame structure were also investigated. It was found that diesel blending with 10%CPO has shorter ignition delay and combustion period compared with conventional diesel fuel. High temperature combustion area (over 2400 K) of 10%CPO diesel was also smaller than diesel especially at the end of the combustion period. The amount of soot and soot concentration affected by this blending percentage were not significantly different from the diesel fuel.

Department..... Mechanical EngineeringStudent's signature.....*Karn Romphol*.....
 Field of study... Mechanical EngineeringAdvisor's signature...*Kanit Wattanaichien*.....
 Academic year2005.....Co-advisor's signature *Akihiko Azetsu*.....

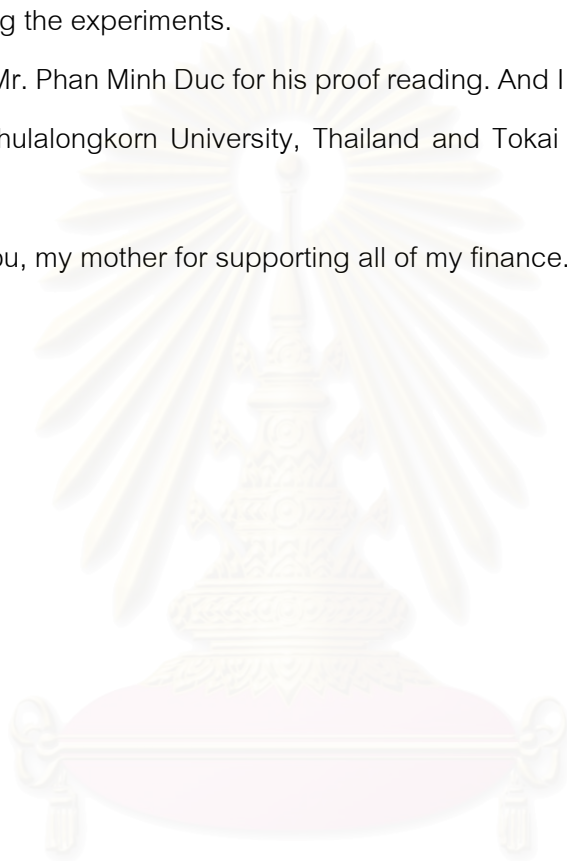
Acknowledgement

Author would like to thank Prof. Akihiko Azetsu and Dr.Kanit Wattanavichien for their supports and suggestions.

Thanks my research team, Mr Tadashi Matsuda, Mr. Tomo Fukui, Mr. Satoshi Kataoka, Mr. Yuuichi Shibasaki, Mr. Hiroaki Ito and Mr. Makoto Hiramoto for their assistance during the experiments.

Thanks Mr. Phan Minh Duc for his proof reading. And I would like to thank to all of my friends at Chulalongkorn University, Thailand and Tokai University, Japan for their helps.

Thank you, my mother for supporting all of my finance.



สถาบันวิทยบริการ
จุฬาลงกรณ์มหาวิทยาลัย

Contents

	page
Thai abstract	iv
English abstract	v
Acknowledgement.....	vi
Contents	vii
List of Tables.....	xiv
List of Figures	xv
Abbreviation and symbols	xxv
Chapter I Introduction.....	1
1.1 Introduction.....	1
1.2 Objective.....	1
1.3 Thesis scope	1
1.4 Thesis steps.....	1
1.5 Definition words	2
1.6 Expected results	2
Chapter II Theory and literature reviews	3
2.1 Characterization of liquid fuels.....	4
2.1.1 Heating Value	4
2.1.2 The specific gravity	4
2.1.3 Viscosity	4
2.1.4 Flash point	4
2.1.5 Auto-ignition temperature	5
2.1.6 Octane number.....	6
2.1.7 Cetane number	6
2.1.8 Smoke point.....	7
2.2 Thermodynamic properties of fuel-air before combustion	7
2.2.1 Mixing fuel and air	7
2.2.2 Ideal gas model for mixtures.....	7

	page
2.2.3 Actual gas model for mixtures.....	8
2.2.4 Fuel-Air Ratio	10
2.2.5 Water Vapor	10
2.2.6 Composition of the atmosphere	11
2.2.6.1 Composition of Standard Dry Air	12
2.2.6.2 Composition of Standard Moist Air	12
2.3 Thermodynamic of combustion	13
2.3.1 First law of thermodynamic	13
2.3.2 Heat of combustion	15
2.3.3 Energy of combustion	16
2.3.4 Chemical Equilibrium	17
2.3.5 Combustion stoichiometry	20
2.3.5.1 Composition Stoichiometry calculation sample.....	23
2.3.5.2 Mole fraction	25
2.3.5.3 Real Gas Model.....	26
2.4 Combustion Flames.....	26
2.4.1 Laminar premixed flames	27
2.4.2 Diffusion flames	28
2.5 Fuel spray theory.....	29
2.5.1 Practical steady-flow fuel spray flames.....	29
2.5.2 Fuel spray in diesel engine.....	31
2.5.2.1 Break-up length.....	31
2.5.2.2 Spray angle	32
2.5.2.3 Spray tip penetration	33
2.6 Momentum method to measure the injection rate	33
2.7 Palm Diesel.....	35
2.8 Two color method for flame visualization.....	36
2.9 Radical of combustion.....	37

	page
Chapter III Experimental apparatuses and methods	38
3.1 Fuel blending methods.....	38
3.2 Experiment apparatuses	38
3.2.1 Combustion chamber and components	39
3.2.1.1 Observation windows	41
3.2.1.2 Spark plug	42
3.2.1.3 Mixing propeller.....	43
3.2.1.4 Combustion chamber heater	44
3.2.1.5 Water cooling piping	45
3.2.1.6 Vacuum pump system.....	46
3.2.2 Injection systems	47
3.2.3 Injection rate sensor.....	51
3.2.4 Hydrogen combustion systems.....	52
3.2.5 Optical measurement system.....	54
3.2.5.1 Photo diode and photo sensor to detect luminous light emssion.....	54
3.2.5.2 The system for detecting the start of injection	55
3.2.5.3 Intensified CCD camera (ICCD).....	57
3.2.6 Control system for experiment	62
3.2.7 The experiment set up for studying on spray characteristics	64
Chapter IV Experimental procedure	65
4.1 Injection rate calculation	65
4.1.1 Peak Injection rate and injection pressure control.....	65
4.1.2 Injection rate and injection pressure control of experiment	67
4.1.3 Injection rate shaping for palm diesel blended at 20%, 40%, 60%, 80% and palm diesel 100%.....	70
4.2 The gas composition and ambient conditions inside combustion chamber after hydrogen combustion.....	71
4.3 The setting up of two color method system	74

4.3.1 Experimental apparatus set up for two color method camera calibration	74
4.3.2 Virtual image position equation	75
4.3.3 Calibration experiment method	75
4.3.4 Calibration experiment results.....	77
4.4 The combustion period and ignition delay calculation.....	78
4.5 The effects of combustion chamber heating temperature on fuel spray combustion characteristic	79
4.5.1 Effected on flame visualization.....	79
4.5.2 Effected on combustion ignition delay and combustion period	81
4.6 Images processing for two color method	83
4.6.1 ICCD camera image processing.....	83
4.6.2 Calculation of two color method.....	84
4.7 The effect of threshold value on fuel combustion flame images	85
4.8 Experiment process.....	90
4.9 Experiment flow chart.....	91
4.9.1 The study on refined palm oil	92
4.9.1.1 Ignition delay of the combustion and fuel combustion period.....	92
4.9.1.2 Combustion flame visualization.....	93
4.9.1.2.1 The study on combustion of palm diesel 60% at injection pressure 60 MPa and 100 MPa	93
4.9.1.2.2 The study on combustion of palm diesel 60% 80% and palm 100%	94
4.9.2 The study on Thai CPO 10%	94
4.9.3 The study on fuel spray characteristics of high percentage palm diesel	95

	page
Chapter V Experiment results	96
5.1 The study on refined palm oil	96
5.1.1 Ignition delay of the combustion	96
5.1.2 Fuel combustion period	98
5.1.3 Combustion flame visualization.....	101
5.1.3.1 The study on combustion of palm diesel 60% at injection pressure 60 MPa and 100 MPa	101
5.1.3.1.1 Intensity distribution of combustion flame	101
5.1.3.1.2 Combustion flame temperature distribution	104
5.1.3.1.3 Combustion flame temperature histogram	115
5.1.3.1.4 KL factor of combustion flame distribution	119
5.1.3.1.5 KL factor histogram	130
5.1.3.1.6 The analysis of flame temperature and KL factor	134
5.1.3.2 The study on combustion of palm diesel 60%, 80% and palm 100% at injection pressure 100 MPa	140
5.1.3.2.1 Intensity distribution of combustion flame	141
5.1.3.2.2 Combustion flame temperature and KL factor distribution.....	143
5.1.3.2.3 Combustion flame temperature histogram	147
5.1.3.2.4 KL factor histogram	151
5.1.3.2.5 The analysis of flame temperature and KL factor	155
5.2 The Study of Thai crude palm oil 10% (CPO 10%).....	161
5.2.1 Combustion period and ignition delay	161
5.2.2 Combustion flame visualization.....	163
5.2.2 1 Intensity distribution of combustion flame.....	163
5.2.2 2 Combustion flame temperature and KL factor distribution.....	164
5.2.2 3 Combustion flame temperature histogram.....	168

	page
5.2.2 4 KL factor of combustion flame histogram	173
5.2.2 5 The analytical of combustion flame images	178
5.3 Effect on fuel spray characteristics of high percentage palm diesel blended	183
5.3.1 The images of diesel and palm diesel 80% injection	183
5.3.2 Reflected light source intensity and spray characteristics	185
5.3.3 Effected on spray characteristics	186
5.3.3 1 Spray angle	186
5.3.3 2 Spray volume	187
5.3.3 3 Spray penetration	189
Chapter VI Conclusion and suggestion	191
6.1 The study on combustion of refined palm oil	191
6.1.1 Ignition delay of the combustion	191
6.1.2 Fuel combustion period	191
6.1.3 Combustion flame visualization	192
6.1.3.1 The study on combustion visualization of palm diesel 60% at injection pressure 60 MPa and 100MPa	192
6.1.3.2 The Study on combustion visualization of palm diesel 60%, 80% and palm 100% at injection pressure 100 MPa	192
6.2 The study of Thai COP 10% blend	193
6.2.1 Ignition delay of the combustion	193
6.2.2 Combustion flame visualization	193
6.3 The effect on spray characteristics of high percentage palm diesel blended	193
6.4 Suggestions	194
6.4.1 The experimental apparatuses	194
6.4.1.1 Injection systems	194
6.4.1.2 Optical sensors	194

	page
6.4.2 Camera calibration for two color method	194
6.4.2.1 Calibration for two color method	194
6.4.2.2 Calibration back ground image.....	194
6.4.3 Constant for limited wave-length range ($\alpha = 1.38$).....	195
6.4.4 Experiments	195
6.4.4.1 Combustion experiments.....	195
6.4.4.2 Spray experiments.....	195
6.4.5 Palm diesel	195
References.....	196
Bibliography.....	198
Appendices	
Appendix A.....	201
Appendix B.....	207
Appendix C.....	209
Appendix D.....	233
Appendix E.....	235
Author Biography	239

สถาบันวิทยบริการ
จุฬาลงกรณ์มหาวิทยาลัย

List of tables

Table	page
2-1 Flash point and auto-ignition temperature pure fuels in air at 1 atm	5
2-2 Stoichiometric complete combustion of several fuels in air	23
2-3 Property of crude palm oil.....	35
3-1 Combustion chamber pressure sensor and control.....	40
3-2 Propeller's driving motor specification	43
3-3 Piezo and components specification.....	49
3-4 Line pressure sensor specification	50
3-5 Injection sensor specification	51
3-6 Radical photo sensor specification	56
3-7 ICCD Light specification	61
3-8 ICCD camera lens and filter specification	61
3-9 Light source lamp specification.....	64
4-1 The relation of injection rate, injection pressure and injection period (by Piezo voltage control)	70
4-2 Hydrogen combustion mixing gas composition.....	72
4-3 Standard heat of formation	72
4-4 The relation temperature of tungsten lamp and input amplifier	76
4-5 Test matrix of the study on refined palm spray combustion	92
4-6 Test matrix of refined palm combustion visualization	93
4-7 Camera delay time for refined palm Combustion flame visualization of the study on combustion of palm diesel 60% at injection pressure 60 MPa and 100MPa.....	93
4-8 Camera delay time for refined palm Combustion flame visualization of the study on combustion of palm diesel 60%, 80% and 100% palm oil.....	94
4-9 Camera delay time for refined palm Combustion flame visualization of the study on combustion of That CPO 10%.....	94
4-10 Camera delay time for study visualization.....	95

List of figures

Figure	page
2-1 Block diagram of diesel combustion	3
2-2 Molecular weight of octane-air mixture and their products of combustion at 560 °R	10
2-3 Moisture content of air	11
2-4 Equilibrium composition of products of combustion of mixtures of octane C ₈ H ₁₈ and air	19
2-5 Excess air versus equivalence ratio	22
2-6 Bunsen burner flame	27
2-7 Candle flame in air showing reaction zone	28
2-8 Region of steady gas jet	30
2-9 Schematic of the development of a gas jet & vapor profiles	30
2-10 Parameter of spray	31
2-11 Break-up behavior of a liquid jet.....	32
2-12 The effect of injection pressure on spray angle	32
2-13 Spray tip penetration at various injection pressure	33
2-14 Pressure pick up and calculation profile	33
3-1 Experiment apparatuses	39
3-2 Pressure chamber and components	40
3-3 Combustion chamber pressure sensor	40
3-4 Observation window component	41
3-5 Glass Heater	41
3-6 Spark plug system	42
3-7 Spark plug position at combustion chamber	42
3-8 Spark plug control box.....	42
3-9 Mixing propeller	43
3-10 Mixing propeller driving motor	43
3-11 Propeller driving motor control box	43
3-12 Combustion chamber and heater	44

Figure	page
3-13 Transformer of heaters.....	44
3-14 Combustion chamber and cooling water line.....	45
3-15 Schematic of the vacuum pump system	46
3-16 Vacuum pump.....	46
3-17 Vapor trap.....	46
3-18 The Schematic of injector system.....	47
3-19 Pressure gauge and valve	47
3-20 Hydraulic Pump.....	48
3-21 Injector system components.....	48
3-22 Piezo stacks type	49
3-23 The relation between Piezo voltage and fuel injection rate.....	49
3-24 Injection rate sensor.....	51
3-25 Schematic of hydrogen combustion system	52
3-26 Oxygen, Air and hydrogen tanks.....	53
3-27 Gas Valves	53
3-28 Gas pressure inside the combustion vessel	53
3-29 Schematic diagram of optical sensor.....	54
3-30 Optical sensor: (a) Side, (b) Top	55
3-31 Schematic diagram of start injection measurement system	55
3-32 He-Ne laser Photo diode.....	56
3-33 He-Ne laser	56
3-34 Cross section through the optical part of an intensified CCD camera	57
3-35 The Camera system	59
3-36 ICCD Camera and parts	60
3-37 ICCD camera and Two color method set up.....	60
3-38 Control sequence of experiment	63
3-39 System controller and components	63
3-40 Experiment apparatus set up for studying of fuel spray	64
4-1 Piezo voltage shap for maximum injection rate setting up.....	66
4-2 The maximum injection rate of each injection pressure.....	66

Figure	page
4-3 Piezo Voltage shaping control	67
4-4 Injection rate shaping measured from pick up sensor.....	68
4-5 Piezo voltage shape for injection pressure 40, 60, 80 and 100 MPa.....	69
4-6 The injection rate of palm 20% and diesel at injection pressure 40, 60, 80 and 100 MPa	69
4-7 The injection rate of 20, 40, 60, 80%palm diesel, 100%palm and diesel at injection pressure 100 MPa.....	70
4-8 The injection rate of 20, 40, 60% palm diesel and diesel at injection pressure 60 MPa.....	71
4-9 Gas pressure inside combustion vessel.....	73
4-10 The schematic diagram of ICCD calibration for two color method.....	74
4-11 Calibration experiment for two color method	75
4-12 Tungsten ribbon intensity distribution at 1600 °C.....	77
4-13 Calibration graph for two color method.....	77
4-14 The data of optical sensor	78
4-15 Calculation of combustion period.....	78
4-16 Combustion flame intensity distribution (Red filter) at combustion chamber heating temperature 80 °C and 100°C	79
4-17 Section intensity data of red filter along Y-axis 150 and 250 at combustion chamber heating temperature 80 °C and 100 °C	80
4-18 Ignition delay at 80 °C and 100 °C chamber heating temperature at injection pressure 40 MPa and 100 MPa.....	81
4-19 Combustion period at 80 °C and 100 °C chamber heating temperature at injection pressure 40 MPa and 100 MPa.....	82
4-20 ICCD camera image processing for two color method.....	83
4-21 Calculation flow diagram of two color method	84
4-22 Intensity of Diesel combustion flame at injection pressure 40MPa Combustion at 3.0 MPa , 1.9 msec after started injection.....	85

Figure	page
4-23 Sectional data of red filter along Y-axis (50, 100, 150, 200 and 250) Diesel Injection pressure 40MPa Combustion at 3.0 MPa 1.9 msec after started injection.....	86
4-24 The relation of threshold value and temperature and KL factor distribution with different threshold value of 400, 900 and 1400 counts.....	87
4-25 Average temperature with different thresholds 400, 900 and 1400 (counts)	88
4-26 Total KL factor with different thresholds 400, 900 and 1400 (counts)	88
4-27 Average KL factor with different thresholds 400, 900 and 1400 (counts)	89
4-28 Numerical calculation of combustion area with different the threshold values and combustion flame images taken at 1.4, 2.4, 3.9 and 4.2 msec after start of injection.....	89
4-29 The experimental flow chart.....	91
5-1 Ignition delay at ambient pressure 2.0 and 3.0 MPa * Combustion chamber heating temperature 80 °C	96
5-2 Ignition delay of palm diesel 20%, 40%, 60% and diesel at injection pressure 60 and 100 MPa, ambient pressure 3.0 MPa	97
5-3 Ignition delay at ambient pressure 3.0 MPa, Injection pressure 100 MPa	98
5-4 Fuel combustion period at ambient pressure 2.0 and 3.0 MPa * Combustion chamber heating temperature 80 °C	99
5-5 Combustion period of palm diesel 20%,40%, 60% and diesel at injection pressure 60 and 100 MPa at ambient pressure 3.0 MPa	100
5-6 Fuel combustion period at ambient pressure 3.0 MPa injection pressure 100 MPa.....	101
5-7 Intensity distribution of combustion flame palm diesel 60% injection pressure 60 MPa.....	102
5-8 Intensity distribution of combustion flame palm diesel 60% injection pressure 100 MPa.....	103
5-9 Combustion flame temperature distribution of Diesel fuel and Palm diesel 60 % 0.7 msec after started injection, 100MPa and 60MPa.....	104

Figure	page
5-10 Combustion flame temperature distribution of Diesel fuel and Palm diesel 60 % 0.8 msec after started injection, 100MPa and 60MPa.....	105
5-11 Combustion flame temperature distribution of Diesel fuel and Palm diesel 60 % 0.9 msec after started injection, 100MPa and 60MPa.....	106
5-12 Combustion flame temperature distribution of Diesel fuel and Palm diesel 60 % 1.0 msec after started injection, 100MPa and 60MPa.....	107
5-13 Combustion flame temperature distribution of Diesel fuel and Palm diesel 60 % 1.1 msec after started injection, 100MPa and 60MPa.....	108
5-14 Combustion flame temperature distribution of Diesel fuel and Palm diesel 60 % 1.2 msec after started injection, 100MPa and 60MPa.....	109
5-15 Combustion flame temperature distribution of Diesel fuel and Palm diesel 60 % 1.4 msec after started injection, 100MPa and 60MPa.....	110
5-16 Combustion flame temperature distribution of Diesel fuel and Palm diesel 60 % 1.9 msec after started injection, 100MPa and 60MPa.....	111
5-17 Combustion flame temperature distribution of Diesel fuel and Palm diesel 60 % 2.4 msec after started injection, 100MPa and 60MPa.....	112
5-18 Combustion flame temperature distribution of Diesel fuel and Palm diesel 60 % 2.9 msec after started injection, 100MPa and 60MPa.....	113
5-19 Combustion flame temperature distribution of Diesel fuel and Palm diesel 60 % 3.4 msec after started injection, 100MPa and 60MPa.....	114
5-20 Flame Temperature histogram of Diesel and Diesel 60%, 60 MPa and 100 MPa, 0.9 msec after started injection.....	115
5-21 Flame Temperature histogram of Diesel and Diesel 60%, 60 MPa and 100 MPa, 1.4 msec after started injection.....	116
5-22 Flame Temperature histogram of Diesel and Diesel 60%, 60 MPa and 100 MPa, 1.9 msec after started injection.....	117
5-23 Flame Temperature histogram of Diesel and Diesel 60%, 60 MPa and 100 MPa, 2.4 msec after started injection.....	118
5-24 Combustion flame KL factor distribution of Diesel fuel and Palm diesel 60 % 0.7 msec after started injection, 100MPa and 60MPa.....	119

Figure	page
5-25 Combustion flame KL factor distribution of Diesel fuel and Palm diesel 60 % 0.8 msec after started injection, 100MPa and 60MPa.....	120
5-26 Combustion flame KL factor distribution of Diesel fuel and Palm diesel 60 % 0.9 msec after started injection, 100MPa and 60MPa.....	121
5-27 Combustion flame KL factor distribution of Diesel fuel and Palm diesel 60 % 1.0 msec after started injection, 100MPa and 60MPa.....	122
5-28 Combustion flame KL factor distribution of Diesel fuel and Palm diesel 60 % 1.1 msec after started injection, 100MPa and 60MPa.....	123
5-29 Combustion flame KL factor distribution of Diesel fuel and Palm diesel 60 % 1.2 msec after started injection, 100MPa and 60MPa.....	124
5-30 Combustion flame KL factor distribution of Diesel fuel and Palm diesel 60 % 1.4 msec after started injection, 100MPa and 60MPa.....	125
5-31 Combustion flame KL factor distribution of Diesel fuel and Palm diesel 60 % 1.9 msec after started injection, 100MPa and 60MPa.....	126
5-32 Combustion flame KL factor distribution of Diesel fuel and Palm diesel 60 % 2.4 msec after started injection, 100MPa and 60MPa.....	127
5-33 Combustion flame KL factor distribution of Diesel fuel and Palm diesel 60 % 2.9 msec after started injection, 100MPa and 60MPa.....	128
5-34 Combustion flame KL factor distribution of Diesel fuel and Palm diesel 60 % 3.4 msec after started injection, 100MPa and 60MPa.....	129
5-35 KL factor histogram of Diesel and Diesel 60%, 60 MPa and 100 MPa, 0.9 msec after started injection.....	130
5-36 KL factor histogram of Diesel and Diesel 60%, 60 MPa and 100 MPa, 1.4 msec after started injection.....	131
5-37 KL factor histogram of Diesel and Diesel 60%, 60 MPa and 100 MPa, 1.9 msec after started injection.....	132
5-38 KL factor histogram of Diesel and Diesel 60%, 60 MPa and 100 MPa, 2.4 msec after started injection.....	133
5-39 Flame area of Diesel and Palm Diesel 60%, 60 MPa and 100 MPa 0.7-1.2 msec after started injection	134

Figure	page
5-40 Flame area of Diesel and Palm Diesel 60%, 60 MPa and 100 MPa 0.9-3.4 msec after started injection	135
5-41 High temperature area of Diesel and Palm Diesel 60%, 60 MPa and 100 MPa 0.9-3.4 msec after started injection	136
5-42 Total KL factor of Diesel and Diesel 60%, 60 MPa and 100 MPa 0.7-1.2 msec after started injection	137
5-43 Total KL factor of Diesel and Diesel 60%, 60 MPa and 100 MPa 0.9-3.4 msec after started injection	138
5-44 Average KL factor of Diesel and Diesel 60%, 60 MPa and 100 MPa 0.9-3.4 msec after started injection	139
5-45 Force pressure data obtained from pick up sensor, 100 MPa	140
5-46 The combustion flame light intensity of diesel palm diesel 60%, 80% and palm 100%.....	141
5-47 Combustion flame temperature and KL factor distribution, Diesel fuel , Palm diesel 60 %,80 % and Palm 100 % (0.9 msec after started injection)	143
5-48 Combustion flame temperature and KL factor distribution, Diesel fuel , Palm diesel 60 %,80 % and Palm 100 % (1.4 msec after started injection)	144
5-49 Combustion flame temperature and KL factor distribution, Diesel fuel , Palm diesel 60 %,80 % and Palm 100 % (1.9 msec after started injection)	145
5-50 Combustion flame temperature and KL factor distribution, Diesel fuel , Palm diesel 60 %,80 % and Palm 100 % (2.4 msec after started injection)	146
5-51 Flame temperature histogram of Diesel and 60%, 80% Palm Diesel and palm 100 %, 0.9 msec after started injection	147
5-52 Flame temperature histogram of Diesel and 60%, 80% Palm Diesel and palm 100 %, 1.4 msec after started injection	148
5-53 Flame temperature histogram of Diesel and 60%, 80% Palm Diesel and palm 100 %, 1.9 msec after started injection	149
5-54 Flame temperature histogram of Diesel and 60%, 80% Palm Diesel and palm 100 %, 2.4 msec after started injection	150

Figure	page
5-55 KL factor histogram of Diesel and 60%, 80% Palm Diesel and palm 100 % 0.9 msec after started injection.....	151
5-56 KL factor histogram of Diesel and 60%, 80% Palm Diesel and palm 100 % 1.4 msec after started injection.....	152
5-57 KL factor histogram of Diesel and 60%, 80% Palm Diesel and palm 100 % 1.9 msec after started injection.....	153
5-58 KL factor histogram of Diesel and 60%, 80% Palm Diesel and palm 100 % 2.4 msec after started injection.....	154
5-59 Flame area of Diesel, 60%,80% Palm Diesel and palm 100 % 0.9-2.4 msec after start of injection.....	155
5-60 Average temperature of Diesel and 60%, 80% Palm Diesel and palm 100 % 0.9-2.4 msec after started injection	156
5-61 High temperature area of Diesel and 60%, 80% Palm Diesel and palm 100 % 0.9-2.4 msec after started injection	157
5-62 Total KL factor of Diesel and 60%, 80% Palm Diesel and palm 100 % 0.9-2.4 msec after started injection	158
5-63 Average KL factor of Diesel and 60%, 80% Palm Diesel and palm 100 % 0.9-2.4 msec after started injection	159
5-64 The voltage of luminous flame intensity obtained from side photo diode	160
5-65 The injection rate of Thai CPO 10% and diesel.....	161
5-66 Ignition delay of diesel and Thai CPO 10%.....	162
5-67 Fuel combustion period of diesel and Thai CPO 10%	162
5-68 Combustion flame intensity distribution of diesel and Thai CPO 10%.....	163
5-69 Combustion flame temperature and KL factor distribution of Diesel fuel and Thai CPO 10% 0.9 msec after start of injection	164
5-70 Combustion flame temperature and KL factor distribution of Diesel fuel and Thai CPO 10% 1.4 msec after start of injection	165
5-71 Combustion flame temperature and KL factor distribution of Diesel fuel and Thai CPO 10% 1.9 msec after start of injection	166

Figure	page
5-72 Combustion flame temperature and KL factor distribution of Diesel fuel and Thai CPO 10% 2.4 msec after start of injection	167
5-73 Flame temperature histogram of Diesel and Thai CPO 10% 0.9 msec after started injection.....	168
5-74 Flame temperature histogram of Diesel and Thai CPO 10% 1.15 msec after started injection.....	169
5-75 Flame temperature histogram of Diesel and Thai CPO 10% 1.4 msec after started injection.....	169
5-76 Flame temperature histogram of Diesel and Thai CPO 10% 1.65 msec after started injection.....	170
5-77 Flame temperature histogram of Diesel and Thai CPO 10% 1.9 msec after started injection.....	170
5-78 Flame temperature histogram of Diesel and Thai CPO 10% 2.15 msec after started injection.....	171
5-79 Flame temperature histogram of Diesel and Thai CPO 10% 2.4 msec after started injection.....	171
5-80 Flame temperature histogram of Diesel and Thai CPO 10% 2.65 msec after started injection.....	172
5-81 KL factor histogram of Diesel and Thai CPO 10% 0.9 msec after started injection.....	173
5-82 KL factor histogram of Diesel and Thai CPO 10% 1.15 msec after started injection.....	174
5-83 KL factor histogram of Diesel and Thai CPO 10% 1.4 msec after started injection.....	174
5-84 KL factor histogram of Diesel and Thai CPO 10% 1.65 msec after started injection.....	175
5-85 KL factor histogram of Diesel and Thai CPO 10% 1.9 msec after started injection.....	175
5-86 KL factor histogram of Diesel and Thai CPO 10% 2.15 msec after started injection.....	176

Figure	page
5-87 KL factor histogram of Diesel and Thai CPO 10% 2.4 msec after started injection.....	176
5-88 KL factor histogram of Diesel and Thai CPO 10% 2.65 msec after started injection.....	177
5-89 Flame area of Diesel and Thai CPO 10% 0.9-2.65 msec after start of injection.....	178
5-90 Average flame temperature Diesel and Thai CPO 10% 0.9-2.65 msec after start of injection.....	179
5-91 High temperature Area of Diesel and Thai CPO 10% 0.9-2.65 msec after start of injection.....	180
5-92 Total KL factor of Diesel and Thai CPO 10% 0.9-2.65 msec after start of injection.....	181
5-93 Average KL factor of Diesel and Thai CPO 10% 0.9-2.65 msec after start of injection.....	182
5-94 Spray image of Diesel and Palm diesel 80%, at injection pressure 100 MPa	183
5-95 Spray image of Diesel and Palm diesel 80%, at injection pressure 60 MPa	184
5-96 Intensity of fuel spray at the center place of the nozzle	185
5-97 The calculation of spray angle.....	186
5-98 Spray angle of Diesel and Palm diesel 80%	187
5-99 The calculation of spray volume	187
5-100 Spray Volume of Diesel and Palm diesel 80%	188
5-101 Spray penetration of Diesel and Palm diesel 80%	189
B-1 Non linear graph equation.....	208
D-1 The emissivity of well-defined tungsten ribbon as a function of wave length at dotted parts of the curves are obtained by extrapolation	234
E-1 Background raw data	236
E-2 Sectional along Y-axis	237
E-3 Sectional along X-axis	237
E-4 Calibration background image (by simulation)	238

Abbreviation and symbols

Abbreviation	Explanation	Units
a	Acceleration	m/s^2
A	Area	mm^2
ASCII	American Standard Code for Information Interchange	
ASTM	American Society for Testing and Materials Standards	
A/D	Analog to digital	
b	Burned (subscript)	
C_v	Specific heat at constant volume	$kJ/kg \cdot K$
C_p	Specific heat at constant pressure	$kJ/kg \cdot K$
C_i	The constant of fuel injection system	$kJ/kg \cdot K$
CI	Cetane index	
CN	Cetane number	
C_1	Constant of Plank equation ($2\pi \times 3.742 \times 10^{-16}$)	$W/m^2 \mu m$
C_2	Constant of Plank equation (1.439×10^{-2})	mK
C_i	Constant of injection system	
CO	Carbon monoxide	
CO ₂	Carbon dioxide	
CH _{1,8}	Kerosene	
CH ₄	Methane	
C ₃ H ₈	Propane	
CCD	Charge coupled device (camera)	
CPO	Crude palm oil	
D	Spray diameter	mm
D_s	Distance of subject to lens	cm
D_i	Distance of image to lens	cm
E_c	Energy of combustion	kJ/kg
E_{ig}	Internal energy of a unit mass of liquid fuel	kJ/kg
E_s	Sensible internal energy per unit mass of mixture	kJ/kg
E_{sa}	Sensible internal energy per unit mass of air	kJ/kg

Abbreviation	Explanation	Units
E_{sf}	Sensible internal energy per unit mass of fuel	kJ/kg
E_{sr}	Sensible internal energy per unit mass of residual gas	kJ/kg
E_v	Sensible internal energy per unit mass of water vapor	kJ/kg
E_u	Internal energy of a unit mass of liquid water	kJ/kg
F	Mass ratio of fuel to dry air	
F_i	Force of fuel injection	N
F_c	Stoichiometric chemically correct fuel-air ratio	
F_R	The fraction of the chemically correct ratio (the relative fuel-air ratio)	
f_s	The stoichiometric fuel/air ratio by weight	
f_a	The actual fuel/air mass ratio	
f	Residual gas fraction	
f_L	Lens focus	cm
f'	The residual fraction including water vapor	
G	Gravity	m/s^2
H ₂ O	Water	
H ₂	Hydrogen	
H_u	The enthalpy of a unit mass of liquid water	kJ/kg
H	Enthalpy	kJ/kg
h	Mass ratio water vapor to dry air	
\bar{h}_i	Enthalpy per unit mass	kJ/kg
ICCD	Intensified CCD (camera)	
J	Joule's law coefficient	
K	Absorption constant per unit flame thickness and is independent of wave length	
K_e	Equilibrium coefficient	
L	Flame thickness	μm

Abbreviation	Explanation	Units
M	Total mass of gaseous mixture	kg
M_a	Total mass of Air	kg
M_r	Total mass of residual gas	kg
M_f	The mass of fuel	kg
M_u	The mass of water vapor	kg
\bar{M}	Molecular weight	$kg/kmol$
MCP	Micro channel plate	
m	Mass	kg
m'	Rate of mass flow	mg/s
m_{air}	Mass of Air	kg
m_{fuel}	Mass of fuel	kg
m_{as}	Stoichiometric air mass	kg
\dot{m}_p	Injection rate	g/s
n	Mole fraction	
n_a	Mole of air	mol
n_{as}	Mole of stoichiometric air	mol
n_f	Mole of stoichiometric fuel	mol
n_{O_2}	Mole of oxygen	mol
n_{N_2}	Mole of nitrogen	mol
n_{tot}	Total dry air mole	mol
N_a	Total number of air	
N_f	Total number of fuel	
N_r	Total number of residual gas	
N_v	Total number of water vapor	
N_2	Nitrogen	
NO	Nitrogen oxide (incomplete equilibrium)	
NO_2	Nitrogen dioxide	
$N_o(\lambda, T)$	Intensity of radiation	$W/m^2 \mu m$
O_2	Oxygen	

Abbreviation	Explanation	Units
OH	Hydroxyl groups (incomplete equilibrium)	
P	Pressure	MPa
P_{air}	Partial pressure	kPa
P_{H_2O}	Partial pressure	kPa
P_{sat}	Partial pressure	kPa
PC	Personal computer	
q	Heat transfer to the system	kJ
Q_c	The heat released during experiment	kJ
Q_{ch}	The higher heat of combustion of the fuel	kJ
\hat{R}	Universal gas constant	$kJ/kgmol \cdot K$
R	Specific gas constant (\hat{R}/M)	$kJ/kg \cdot K$
S	The mass specific mixture entropy	$kJ/kg \cdot K$
\bar{S}	The molar specific mixture entropy	$kJ/kg \cdot K$
T	Temperature	K
t	Time	s
TM	Mid-boiling temperature	K
\bar{T}	Average temperature	K
T_a	The apparent temperature	K
\bar{u}	Internal energy per unit mass	kJ/kg
u	Velocity	m/s
U	Internal energy	kJ
V	Volume	m^3
W	The rate work	W
W_e	Electrical power	W
W_s	Shaft power	W
x_i	Mass fraction	
y_i	Mole fraction	
y_{N_2}	Mole fraction of nitrogen (by volume)	
y_{O_2}	Mole fraction of nitrogen (by volume)	

Abbreviation	Explanation	Units
ϕ	Relative humidity	%
dx/dt	Velocity	m/s
λ	Wave length	μm
α	Constant for limited wave length range ($\alpha=1.38$)	
ε	Emissivity	
α_c	Number of carbon	
β_h	Number of hydrogen	
γ_o	Number of oxygen	
ω	Specific humidity	
Δu	Different of velocity	m/s
Δt	Different of time	s
Δx	Different of distance	m
ρ	Density of fuel	g/m^3
ΔP	Different of pressure drop across nozzle	MPa

สถาบันวิทยบริการ
จุฬาลงกรณ์มหาวิทยาลัย

CHAPTER I

INTRODUCTION

1.1 Introduction

According to the increasing of green-house effect caused by the increase of carbon dioxide (CO₂) vegetable oil such as palm oil becomes an interesting alternative fuel because of its carbon cycle. In order to optimize the use of vegetable oil in a diesel engine, we still need to learn more on its combustion characteristics. Therefore, this thesis aimed to study the combustion phenomenon of palm diesel

1.2 Objective

- 1.2.1 To study palm diesel combustion characteristics.
- 1.2.2 To Study effect on palm diesel spray phenomenon.

1.3 Thesis scope

- 1.3.1 The fuel used in the experiment was palm diesel.
- 1.3.2 The experiment was done in a constant volume combustion chamber.

1.4 Thesis steps

- 1.4.1 Study the fundamental of fuel spray characteristics, flame temperature measurement and experiment equipment hand books.
- 1.4.2 Setup and calibrate the experimental apparatuses
- 1.4.3 Set the experimental parameters, combustion conditions, injection rate and piezo voltage movement shape and control timing.
- 1.4.4 Do experiment and analyze data.
- 1.4.5 Make conclusion and suggestion.

1.5 Definition words

1.5.1 Reference diesel is diesel fuel that was used during experiment.

1.5.2 Commercial Diesel is diesel fuel sold in usual market.

1.5.3 CPO diesel is crude palm oil blended with reference diesel.

1.5.4 Palm diesel is refined palm diesel blended with reference diesel.

1.6 Expected results

1.6.1 The palm diesel fuel spray and spray combustion characteristics will be more understood.

1.6.2 I wish the results of this work will be useful for developing a high performance with low emission engine.

1.6.3 More clear understanding on palm diesel spray combustion characteristics.



สถาบันวิทยบริการ
จุฬาลงกรณ์มหาวิทยาลัย

CHAPTER II

THEORY AND LITERATURE REVIEW

Diesel combustion processes are very complex and their detailed mechanisms are not well understood. The primary factor which controls the diesel combustion is the mixture formation as shown in Fig. 2-1.

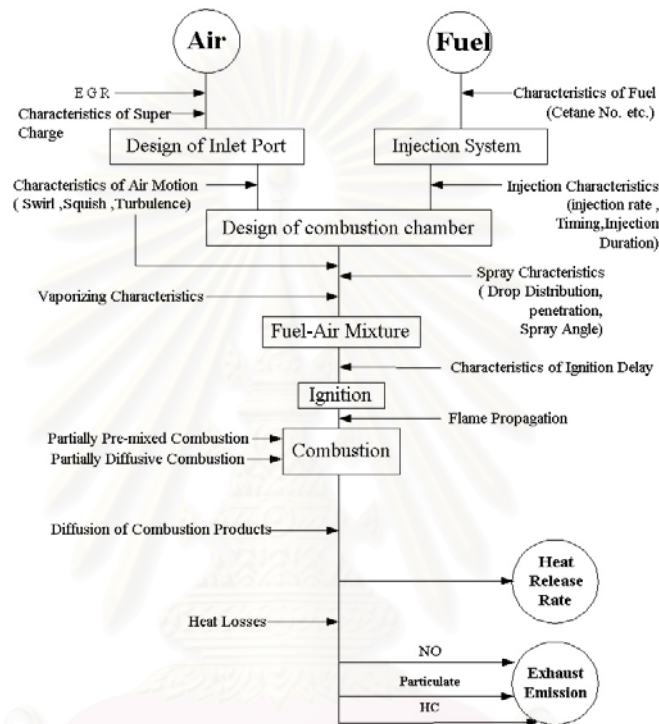


Fig.2-1 Block diagram of diesel combustion [4]

The mixture formation is controlled by the characteristics of the injection system, the nature of air swirl and turbulence in the cylinder, and spray characterization. The next factor of diesel combustion is ignition delay and the flame development after the ignition, that is, the combustion rate. The combustion in the diesel engine is heterogeneous combustion, that is a combination of partially pre-mixed combustion and partially diffusive combustion.

The air-fuel mixing processes, including atomization and vaporization, at the edges of the spray are followed by the ignition of these regions and progressive diffusive burning of the remainder of the spray. Therefore, accurate descriptions of the behavior of atomizing and vaporizing fuel in the spray are important for any kind of models to comprehend and describe the processes of air-fuel mixing and subsequent combustion.[4]

2.1 Characterization of Liquid Fuels

Important properties of liquid fuels include the heating value, specific gravity, viscosity, flash point, auto ignition temperature, distillation curve, sulfur content, vanadium and lead content, octane number (for gasolines), cetane number (for diesel fuels), and smoke point (for gas turbine fuels). [2]

2.1.1 **Heating value** for liquid fuels is determined by combustion with pressurized oxygen in a bomb calorimeter. This device is a stainless steel container which is surrounded by a large water bath. The large bath ensures that the final product temperature will be only very slightly above the initial reactant temperature of 25°C. The combustion is carried out for a lean mixture to ensure complete combustion.

2.1.2 **The specific gravity** is the density of the fuel divided by the density of water at the same temperature.

2.1.3 **Viscosity** of a liquid is a measure of its resistance to flow. For a liquid fuel, viscosity indicates the ease at which it can be pumped and the ease of atomization. Viscosity of liquids decreases with increasing temperature. There are several standard tests for viscosity. Sometimes pour point is used as a simple indicator of viscosity. The pour point is an indication of the lowest temperature at which a fuel oil can be stored and still be capable of flowing under very low forces in a standard apparatus.

2.1.4 **Flash point** is an indication of the maximum temperature at which a liquid fuel can be stored and handled without serious fire hazard. The flash point is the minimum temperature at which fuel will rapidly catch fire when exposed to an open flame located above the liquid. An example of flash point concern is the ignitability of the mixture above liquid fuel in a partially full fuel tank. Gasoline, which has a flash point of -43°C, is typically so volatile that the mixture is too rich to burn. Diesel fuel (flash point of 52°C) is so nonvolatile that the mixture is too lean to burn. However, gasoline-diesel fuel mixtures or alternative fuels such as methanol may pose a danger.

2.1.5 **Auto-ignition temperature** is the lowest temperature required to initiate self-sustained combustion in a standard combustion in a standard container in atmospheric air in the absence of a spark of flame. The auto-ignition temperature of the alkanes (paraffins) decreases with increasing molecular weight. Isooctane has a much higher auto-ignition temperature than octane. Ethane, ethylene, and ethanol have progressively decreasing auto-ignition temperatures. Carbon monoxide has a high auto-ignition temperature. In general, auto-ignition temperatures are an indication of the relative difficulty of combusting a fuel. Since the auto-ignition temperature varies with the geometry of the hot surface and other factors such as pressure, other tests such as octane number and cetane number are used for engine fuels. [2]

Table 2-1 Flash point and auto-ignition temperature of pure fuels in air at 1 atm [2]

Substance	Flash point(°C)	Autoignition(°C)
Methane	-188	537
Ethane	-135	472
Propane	-104	470
n-Butane	-60	365
n-Octane	10	206
Isooctane	-12	418
n-Cetane	135	205
Methanol	11	385
Ethanol	12	365
Acetylene	Gas	305
Carbon monoxide	Gas	600
Hydrogen	Gas	400

Source: Barton and Sarofin. *Fossil Fuel Combustion* : A source Book.

©1991, Wiley by permission of John Wiley and Sons, inc.

2.1.6 **Octane number** indicates the tendency of gasoline to knock (onset of auto-ignition) when the compression ratio in a spark-ignition engine is raised. The octane number of a fuel is measured by comparing the performance of the fuel with the performance of mixtures of isooctane and n-heptane in a standardized sparkignition engine. [2]

2.1.7 **Cetane number**, in compression-ignition engines the time between start of injection and onset of combustion is known as the ignition delay. Cetane number (CN) ranks fuels according to their ignition delay when undergoing a standard test. Because cetane (n-hexadecane) is one of the fastest-igniting hydrocarbons in fuel, it is assigned a cetane number of 100. Isocetane (heptamethylnonane) ignites slowly and is arbitrarily assigned a cetane number of 15. A fuel is compared with mixtures of the reference fuels in a standardized prechamber diesel engine and rated by the mixture which most nearly matches the ignition delay of the test fuel. The cetane number of the reference mixture is defined by.

$$\text{CN} = (\% \text{ n-cetane}) + 0.15 (\% \text{ heptamethylnonane}) \quad (2-1)$$

In the cetane number test the injection is fixed at 13° before top dead center and the compression ratio is changed until combustion of the test fuel starts at top dead center. The standard mixture is found which gives the same ignition delay at these fixed conditions of injection timing and compression ratio. The tests are run at 900 rev/min with 100°C water temperature and 65.55°C inlet air. Because the test engine is a pre-chamber design, the cetane number is a best only a relative scale when applied to open-chamber engines. The test is particularly questionable for low-cetane fuels (CN < 35).

In many cases CN is computed from correlations based on the chemical structure and physical properties of the fuel rather than engine tests. For example, the aniline point (temperature at which aniline and the fuel are miscible), API gravity (G),

and midboiling temperature (TM) are often used to correlate cetane number. The ASTM (D976) correlation is

$$CN = -420.34 + 0.016G^2 + 0.192G \log(TM) + 65.01(\log TM)^2 - 0.0001809(TM)^2 \quad (2-2)$$

where TM is °F and log is to base 10. Such calculated values of CN are more correctly designated as the cetane index (CI) to make clear that they are different from the measured value.

2.1.8 **Smoke point** measures the tendency of a liquid fuel to form soot. It is determined experimentally by burning the fuel in a special wick lamp and slowly increasing the height of the flame until smoke begins to appear. The maximum height of smokeless flame in millimeters is the smoke point. Hence, the higher the smoke point, the lower is the tendency of the fuel to form soot. Smoke point is used especially for gas turbine fuels.

2.2 Thermodynamic properties of fuel-air mixtures before combustion

2.2.1 Mixing fuel and air [7]

The thermodynamic properties of fuel-air mixtures depend on the following characteristics:

- (a). Composition of the fuel
- (b). Fuel-air ratio
- (c). Water-vapor content
- (d). Residual-gas content

2.2.2 Ideal Gas Model for Mixtures

The mass m of a mixture is equal to the sum of the mass of n components

$$m = \sum_{i=1}^n m_i \quad (2-3)$$

The mass fraction, x_i , of any given species is defined as:

$$x_i = \frac{m_i}{m} \quad \text{and} \quad \sum_{i=1}^n x_i = 1 \quad (2-4)$$

The mixture internal energy U and enthalpy H (units: kJ) is:

$$U = mu = \sum_{i=1}^n m_i u_i \quad H = mh = \sum_{i=1}^n m_i h_i \quad (2-5)$$

2.2.3 Actual Gas Model for Mixtures [3]

In dealing with such mixtures the following definitions are used :

F = mass ratio of fuel to dry air

F_c = stoichiometric or chemically correct fuel-air ratio

$F_R = F/F_c$, or the fraction of the chemically correct ratio, here called the relative fuel-air ratio

f = residual-gas fraction, defined as the ratio mass of residuals to the mass of dry air plus fuel residual gas

h = mass ratio water vapor to dry air.

From these relations

$$F = F_R F_c \quad (2-6)$$

and, since,

$$M = M_a + M_f + M_r + M_v \quad (2-7)$$

the following can be derived :

$$\frac{M_a}{M} = \frac{1-f}{1+F+h(1-f)} \quad (2-8)$$

$$\frac{M_f}{M} = \frac{F(1-f)}{1+F+h(1-f)} \quad (2-9)$$

$$\frac{M_r}{M} = \frac{f(1+F)}{1+F+h(1-f)} \quad (2-10)$$

$$\frac{M_v}{M} = \frac{h(1-f)}{1+F+h(1-f)} \quad (2-11)$$

where M is total mass of gaseous mixture, and subscripts a , f , r , and v refer to air, fuel, residual gas, and water vapor, respectively.

Since the total number of moles, N is equal to the sum of the moles of each constituent,

$$N = N_a + N_f + N_r + N_v \quad (2-12)$$

it follows that

$$N = \frac{M_a}{29} + \frac{M_f}{m_f} + \frac{M_r}{m_r} + \frac{M_v}{18} \quad (2-13)$$

The molecular weight of the mixture is the total mass divided by the number of moles. Dividing equation 2-7 by equation 2-13 and substituting the masses shown by equation 2-8 to 2-11 gives

$$m = \frac{M}{N} = \frac{1 + F + h(1 - f)}{(1/29 + F/m_f + h/18)(1 - f) + f(1 + F)/m_r} \quad (2-14)$$

where N is the number of moles and m is the molecular weight in each case. Since, $N = 1$, the molecular weight and the mass of the mixture in that figure are given by equation 2-14. The molecular weight of octane is 112, and the molecular weight of dry octane-air mixtures both burned and unburned is given in figure 2-2.

Since the internal energy of a mixture is equal to the sum of the internal energies of its constituents, we can write

$$E_s = \frac{(E_{sa} + FE_{sf} + hE_v)(1 - f) + fE_{sr}(1 + F)}{1 + F + h(1 - f)} \quad (2-15)$$

in which E_s refers to sensible internal energy per unit mass of mixture. The sensible enthalpy will have a corresponding relation to the enthalpy of a unit mass of each constituent. The energy and enthalpy of one mole of gas is obtained by multiplying equation 2-15 by the molecular weight, equation 2-14.

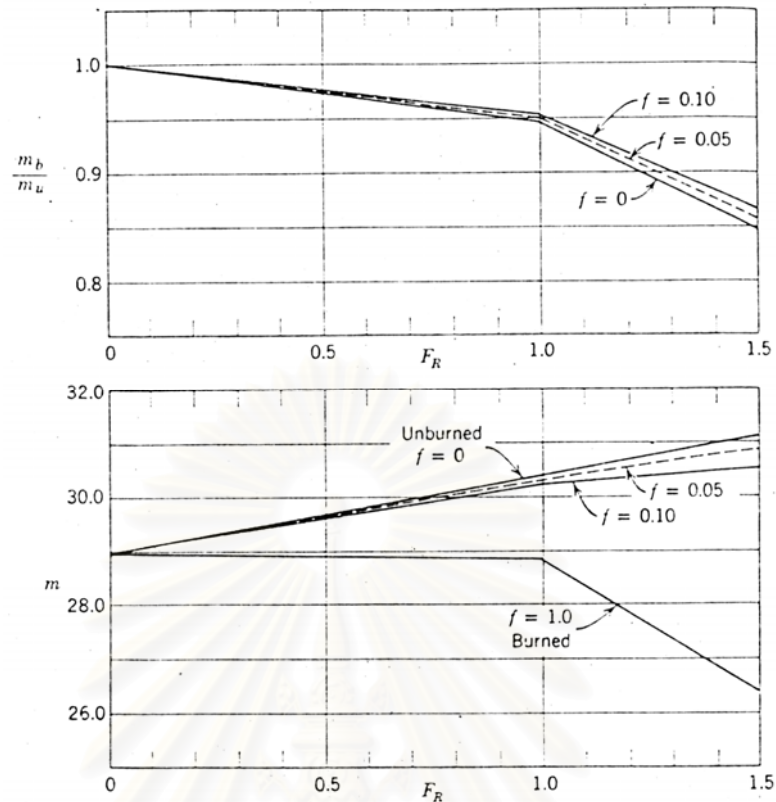


Fig. 2-2 Molecular weight of octane-air mixture and their products of combustion at 560°R : m = molecular weight ; subscript b is burned ; u is unburned [3]

2.2.4 Fuel-Air Ratio

F_R , the fuel-air ratio is defined as follows :

$$F_R = F/F_c \quad (2-16)$$

where F_c is the "chemically correct," or stoichiometric fuel-air ratio.

2.2.5 Water Vapor. Edson and Taylor have shown that variations in residual-gas or water-vapor content have little effect on the efficiency of fuel-air cycles, and therefore for thermodynamic purposes water vapor can be treated as an equal mass of residual gas. Calling f' the residual fraction including water vapor:

$$f' = \frac{M_r + M_v}{M_a + M_f + M_r + M_v} \quad (2-17)$$

and therefore :

$$f' = \frac{f(1+F) + h(1-f)}{1+F + h(1-f)} \quad (2-18)$$

However, the molecular weight should be computed from equation 2-14 and equations 2-8 to 2-15 should be used with the true values of f and h .

2.2.6 Composition of the atmosphere

Dry atmospheric air consists of 23% oxygen and 76% nitrogen by weight, plus small amounts of CO_2 and "rare" gases, principal among which is argon. By volume, these percentages are 21% O_2 , 78% N_2 and, 1% other gases. For thermodynamic purposes the other gases are taken to be the equivalent of an equal amount of nitrogen. The molecular weight of dry air is 28.85 or 29 within the limits of accuracy of most computations. Figure 2-3 shows limits of moisture and droplet content.

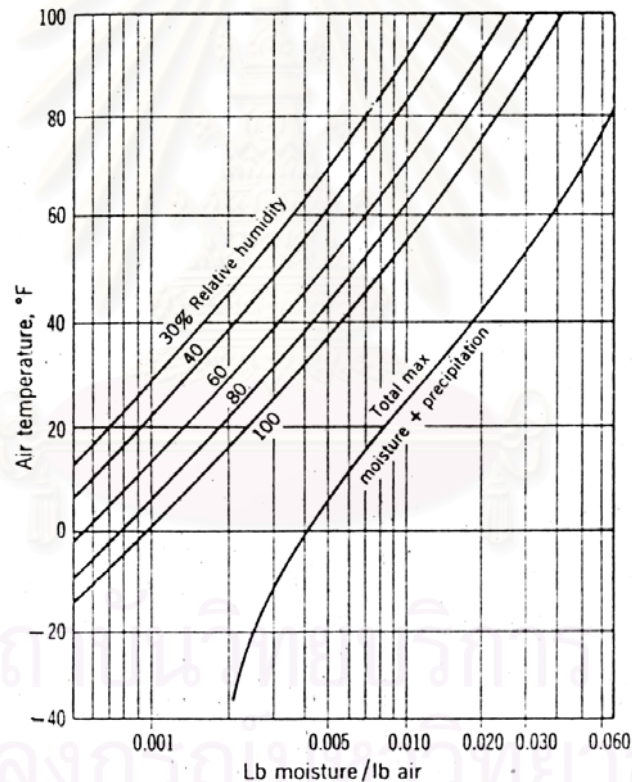


Fig. 2-3 Moisture content of air. [3]

In addition to the above ingredients, atmospheric air contains water vapor in percentages varying with temperature and the degree of saturation. The latter varies

with time and place from near zero to near 100%. In addition to evaporated water, air may contain a considerable amount of water suspended in the form droplets.

2.2.6.1 Composition of Standard Dry Air [7]

For combustion dry air is taken to be composed of 21% O₂ and 79% N₂ by volume (mole fraction).

$$\frac{n_{N_2}}{n_{O_2}} = \frac{n_{N_2}}{n_{tot}} \cdot \frac{n_{tot}}{n_{O_2}} = \frac{y_{N_2}}{y_{O_2}} = \frac{0.79}{0.21} = 3.76 \quad (2-19)$$

For every mole of O₂ there are 3.76 moles of N₂.

The molecular weight of air is

$$\begin{aligned} \bar{M}_{air} &= \sum_{i=1}^n y_i \bar{M}_i = y_{O_2} \cdot \bar{M}_{O_2} + y_{N_2} \cdot \bar{M}_{N_2} \\ &= 0.21(32) + 0.79(28) = 28.84 \text{ kg/kmol} \end{aligned} \quad (2-20)$$

2.2.6.2 Composition of Standard Moist Air [7]

Atmospheric air always contains some amount of water vapour. The amount of water in moist air at T is specified by the **specific humidity**, ω , or the **relative humidity**, ϕ , defined as follows:

$$\omega = \frac{m_{H_2O}}{m_{air}} \quad \phi = \frac{P_{H_2O}}{P_{sat}(T)} \quad 0 < \phi < 1 \quad (2-21)$$

The two are related by:

$$\omega = \frac{m_{H_2O}}{m_{air}} = \frac{\bar{M}_{H_2O} \cdot n_{H_2O}}{\bar{M}_{air} \cdot n_{air}} = \left(\frac{18}{29}\right) \left(\frac{P_{H_2O}}{P_{air}}\right) = 0.62 \left(\frac{P_{H_2O}}{P - P_{H_2O}}\right) = 0.62 \left(\frac{\phi \cdot P_{sat}(T)}{P - \phi \cdot P_{sat}(T)}\right) \quad (2-22)$$

The number of moles of water can be calculated knowing ω or ϕ

$$n_{H_2O} = \frac{m_{H_2O}}{\bar{M}_{H_2O}} = \frac{\omega \cdot m_{air}}{\bar{M}_{H_2O}} = \frac{\omega \cdot (n_{air} \cdot \bar{M}_{air})}{\bar{M}_{H_2O}} = \frac{\omega \cdot n_{air}}{0.62} \rightarrow \frac{n_{H_2O}}{n_{air}} = 1.61 \cdot \omega \quad (2-23)$$

2.3 Thermodynamic of combustion [2]

2.3.1 First law of thermodynamic

For a thermodynamic system, the first law of thermodynamics in rate form states that the time rate of change of energy of the system is equal to the rate at which work is done on the system plus the rate at which heat is transferred to the system, the first law of thermodynamics may be written as,

$$\frac{d(mu)}{dt} = \dot{W} + q \quad (2-24)$$

When $m = \text{mass}$

$q = \text{heat transfer to the system}$

$W = \text{The rate work is done to the system consisted of shaft power, electrical power, and power due to moving boundaries.}$

$u = \text{internal energy per unit mass is. If the work transfer for a system of volume } V \text{ is restricted to mechanical work due to uniform system pressure against a moving boundary of area } A \text{ moving outward with a velocity } dx/dt, \text{ then the power is}$

$$\dot{W} = -pA \frac{dx}{dt} = -p \frac{dV}{dt} \quad (2-25)$$

Then the first law for a system becomes

$$\frac{d(mu)}{dt} = -p \frac{dV}{dt} + q \quad (2-26)$$

The thermodynamic properties of the system can be evaluated if the whole system is assumed uniform. If the system is not uniform, it may be divided into subsystems of cells, each of which is assumed uniform. The properties of the whole system are then obtained by summing the cell values. For example, dividing the system into J cells each of volume V_j and assigning properties p_j, T_j, p_j to each cell, the system energy is,

$$mu = \sum_{j=1}^J p_j V_j u_j \quad (2-27)$$

The average temperature \bar{T} of a non-uniform mixture of ideal gases in J cells is obtained by applying the ideal gas law and assuming that the pressure is the same in each cell, so that

$$\sum_j p_j v_j = pV = \sum_i N_j \hat{R} T_j = N \hat{R} \bar{T} \quad (2-28)$$

Solving for \bar{T} ,

$$\bar{T} = \frac{pV}{N \hat{R}} = \sum_j \frac{N_j T_j}{N} = \sum_j x_j T_j \quad (2-29)$$

where x_j is the mole fraction of species j . The average temperature defined in this way is the mole average temperature. If each cell has the same composition, then $\bar{T} = pV/mR$ is the mass average temperature. However, even for a system of uniform composition,

$$m\bar{u}(\bar{T}) \neq \sum_j m_j \bar{u}_j(\bar{T}) \quad (2-30)$$

if the specific heat C_c is a function of temperature so that u is a nonlinear function of T .

By integration equation 2-24 with respect to time the closed-system energy balance becomes.

$$m(u_2 - u_1) = -W_{12} + Q_{12} \quad (2-31)$$

where $W_{12} = \int_{t_1}^{t_2} p \frac{dV}{dt} dt$ and $Q_{12} = \int_{t_1}^{t_2} q dt$ (2-32)

For a uniform system with constant pressure the energy equation, equation 2-24 simplifies to

$$\frac{d(mu + pV)}{dt} = q \quad (2-33)$$

or $\frac{d(mh)}{dt} = q$ (2-34)

Integration of equation 2-34 gives

$$m(h_2 - h_1) = Q_{12} \quad (2-35)$$

If the chemical composition is constant, the chemical energy does not change, and for ideal gases,

$$u_2 - u_1 = \int_{T_1}^{T_2} C_v dT \quad (2-36)$$

$$h_2 - h_1 = \int_{T_1}^{T_2} C_p dT \quad (2-37)$$

Where $C_p = C_v + R$

For the open-system version of equation 2-24 is

$$\frac{d(mu)}{dt} + \sum_i \dot{m}_i \left(h_i + \frac{V_i^2}{2} \right) = q + \dot{W} \quad (2-38)$$

The first term in this equation represents the time rate of change of energy in the system. In this equation \dot{m}_i is the flow rate through flow area i at the system boundary, and h_i is the enthalpy of the fluid as it crosses boundary surface area i . The flow rates are given positive values for flow out of the system and negative values for flow into the system. The enthalpy includes sensible enthalpy and chemical energy of the mixture of gases at position i . The $V_i^2/2$ term is the kinetic energy of the flow crossing boundary surface area i , q is the rate of heat transfer to the system, and \dot{W} is the power added to the system. In general, $\dot{W} = -p(dV/dt) + \dot{W}_s + \dot{W}_e$ where \dot{W}_s = shaft power and \dot{W}_e = electrical power. For steady flow with one stream flowing in and one stream flowing out of the control volume, the open-system energy equation may be simplified to, [2]

$$\dot{m} \left(h_2 - h_1 + \frac{V_2^2}{2} - \frac{V_1^2}{2} \right) = q + \dot{W} \quad (2-39)$$

2.3.2 Heat of Combustion [3]

Starting with the calorimeter and its contents at a known temperature, the mixture is ignited. After which the bomb and its contents are cooled to the initial temperature, which is usually low enough so that most of the water in the products condenses to the liquid state. The heat released by this process, Q_c is carefully

measured. Since the process occurs at constant volume, Q_c is equal to the internal energy of the fuel-oxygen mixture above a base of zero energy of CO_2 , H_2O , and O_2 at the temperature of the experiment.

To determine heat of combustion, the following quantity is computed:

$$Q_{ch} = \frac{1}{M_f} \left[Q_c + \frac{V}{J} (p_2 - p_1) \right] \quad (2-40)$$

where Q_c is the heat released during the experiment, M_f is the mass of fuel used, V is the container volume, and p_2 and p_1 are pressures in the bomb after and before combustion.

Q_{ch} is known as the higher heat of combustion of the fuel.

Another quantity, known as the lower heat of combustion of the fuel, is computed as follows:

$$Q_c = Q_{ch} + M_u H_u / M_1 \quad (2-41)$$

where M_u is the mass of water vapor in the combustion products and H_u is the enthalpy of a unit mass of liquid water at the experimental temperature, referred to a base of water vapor. Since H_u is a negative number, Q_c is smaller than Q_{ch} .

Customarily, Q_c is used as the basis for computing the thermal efficiency of engines. All thermal efficiency values in this volume are computed on this basis.

2.3.3 Energy of Combustion

This quantity could be measured by measuring the heat released at constant volume, starting with unburned gaseous fuel and O_2 at the base temperature and ending with gaseous CO_2 , H_2O , and O_2 at the same temperature. However, E_c can be computed from the bomb-calorimeter experiment previously described by using the following relation:

$$E_c = \frac{1}{M_f} (Q_c + M_v E_v) - E_{ig} \quad (2-42)$$

In the above expression

M_f = mass of fuel used

M_v = mass of water in products

E_v = internal energy of a unit mass of liquid water above a base of water vapor at the experimental temperature

E_{ig} = the internal energy of a unit mass of liquid fuel above a base of gaseous fuel at the experimental temperature. If the fuel was gaseous when put in the bomb, this quantity is taken as zero

Both E_v and E_{ig} are negative numbers, since the internal energy of the gas is greater than that of the liquid.

Equation 2-42 assumes that the bomb experiment was carried out at the base temperature for E_c . Small differences between the base and the experimental temperature can be ignored without appreciable error. [3]

2.3.4 Chemical Equilibrium

For thermodynamic purposes it may be assumed that the products of combustion of the common fuels are made up of various combinations of oxygen, hydrogen, carbon, and nitrogen. The way in which these elements are combined after combustion and the proportion of the various compounds in the mixture depends not only on the proportions present in the original mixture but also on the temperature, the pressure, and the extent to which chemical equilibrium has been approached.

When two substances react chemically with each other the reaction does not necessarily proceed to the point at which one of the substances is completely consumed. Before this happens, an equilibrium condition may be reached in which not only products of the reaction are present but also appreciable amounts of the original reacting substances and, in many cases, intermediate compounds. The proportions at

equilibrium of the products of a given reaction and the original or intermediate substances depend on the original proportions and on the temperature and pressure after the reaction has taken place. In general, exothermal reactions, that is, reactions which increase the temperature, such as the combustion process, are less complete at high temperatures than at low temperatures.[3]

In fuel-air mixtures at equilibrium after combustion appreciable amounts of the following substances may be present ;



The quantitative treatment of chemical equilibrium rests upon a relationship of the partial pressures.

$$\omega A + \chi B = y C + z D \quad (2-43)$$

$$\frac{p^u_C \cdot p^z_D}{p^u_A \cdot p^z_B} = K_e \quad (2-44)$$

where ω , χ , y , and z are the respective numbers of moles of the substances involved, p is the partial pressure of the substance denoted by the subscript, and K_e is the equilibrium coefficient, which is a function of the temperature.

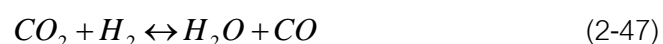
The general equation can be applied to the products of combustion of a fuel-air mixture containing compounds which tend to react with each other with a change in temperature.



For which the equilibrium coefficient at a given temperature is

$$K_{e1} = \frac{(p_{\text{CO}_2})^2}{(p_{\text{CO}})^2 (p_{\text{O}_2})} \quad (2-46)$$

And



for which

$$K_{e2} = \frac{(p_{\text{H}_2\text{O}})(p_{\text{CO}})}{(p_{\text{CO}_2})(p_{\text{H}_2})} \quad (2-48)$$

These equilibrium coefficients, together with those for other possible reactions between the products of combustion, have been determined for various temperatures and may be used to determine the partial pressure ratios, hence the relative amounts of the various constituents at any given temperature. Figure 2-4 shows the equilibrium composition of the products of combustion of octane (C_8H_{18}) and air for three different fuel-air ratios over the range from 1393.51- 2782.40 °C.

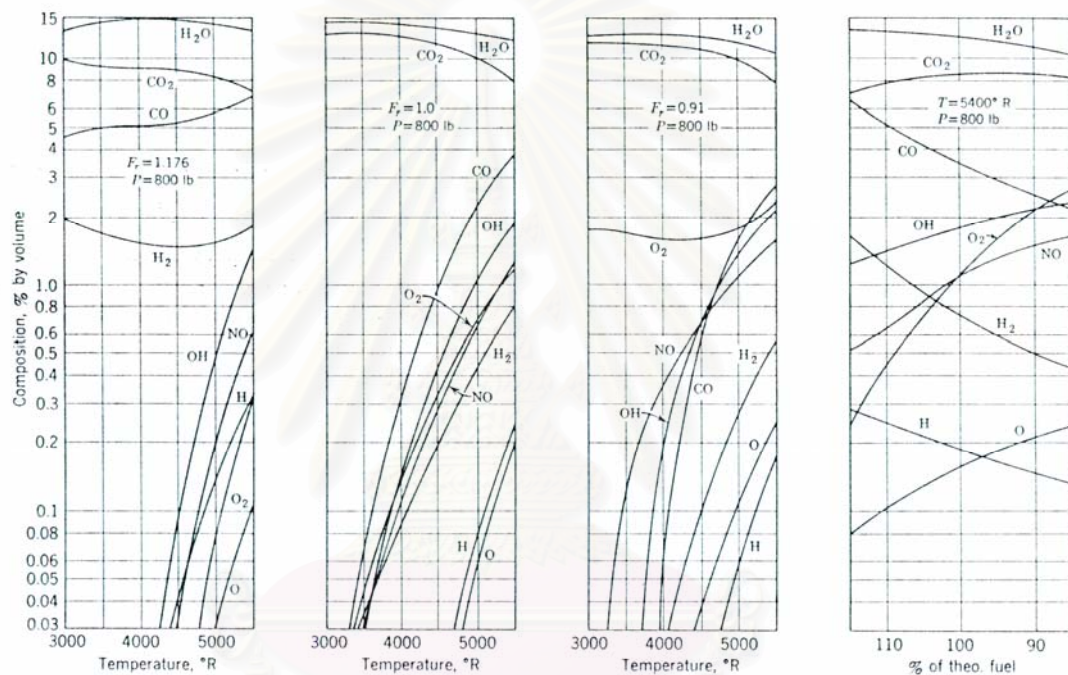


Fig. 2-4 Equilibrium composition of products of combustion of mixtures of octane C_8H_{18} and air [3]

สถาบันวิทยบริการ
จุฬาลงกรณ์มหาวิทยาลัย

2.3.5 Combustion stoichiometry [2]

When molecules undergo chemical reaction, the reactant atoms are rearranged to form new combinations. For example, hydrogen and oxygen react to form water:



Two atoms of hydrogen and one atom of oxygen form one molecule of water, since the number of atoms of H and O must be the same on each side of the equation.

The relative masses of the molecules are obtained by multiplying the number of moles of each species by the respective molecular weights (which have units of kg/kgmol in the SI system of units). For the hydrogen-oxygen reaction above,

$$(1 \text{ kmol } H_2) \left(\frac{2 \text{ kg}}{\text{kgmol } H_2} \right) + \left(\frac{1}{2} \text{ mol } O_2 \right) \left(\frac{32 \text{ kg}}{\text{kgmol } O_2} \right) = (1 \text{ kmol } H_2O) \left(\frac{18 \text{ kg}}{\text{kgmol } H_2O} \right) \quad (2-50)$$

and the mass of the reactants equals the mass of the products, although the moles of reactants do not equal the moles of products. For a fixed p and T and ideal gases,

$$1 \text{ volume } H_2 + \frac{1}{2} \text{ volume } O_2 = 1 \text{ volume } H_2O \quad (2-51)$$

Thus, when ideal gases react at constant T and p , the volume may change.

For a fuel containing carbon, hydrogen and oxygen which is burned to completion with a stoichiometric amount of air, atom balances on C, H, O, and N atoms yield the following general expression:

$$C_{\alpha_c} H_{\beta_h} O_{\gamma_o} + \left(\frac{\alpha_c + \beta_h}{4} - \frac{\gamma_o}{2} \right) (O_2 + 3.76 N_2) \rightarrow \alpha_c CO_2 + \left(\frac{\beta_h}{2} \right) H_2O + 3.76 \left(\alpha_c + \frac{\beta_h}{4} - \frac{\gamma_o}{2} \right) N_2 \quad (2-52)$$

when α , β and γ_o are the number of carbon, hydrogen, and oxygen atoms in a molecule of fuel. Alternatively, α , β and γ_o are the mole fractions of the carbon,

hydrogen, and oxygen from the ultimate analysis of the fuel. The moles of stoichiometric air per mole of fuel are:

$$\frac{n_{as}}{n_f} = 4.76 \left(\frac{\alpha_c + \beta_h}{4} + \frac{\gamma_o}{2} \right) \quad (2-53)$$

The stoichiometric fuel/air ratio by weight is

$$f_s = \frac{m_f}{m_{as}} = \frac{M_f n_f}{M_a n_{as}} \quad (2-54)$$

$$= \frac{M_f}{29.0(\alpha + \beta/4 - \gamma/2)(4.76)} \quad (2-55)$$

The percent excess air is the actual air used minus the stoichiometric air all divided by the stoichiometric air times 100:

$$\begin{aligned} \% \text{ excess air} &= \frac{100(m_a - m_{as})}{m_{as}} \\ &= \frac{100(n_a - n_{as})}{n_{as}} \\ &= \frac{100(n_{O_2} - n_{O_{2(s)}})}{n_{O_{2(s)}}} \end{aligned} \quad (2-56)$$

Percent theoretical air is the amount of air actually used divided by the stoichiometric air:

$$\% \text{ theoretical air} = \left(\frac{m_a}{m_{as}} \right) 100 = \left(\frac{n_a}{n_{as}} \right) 100 \quad (2-57)$$

Hence,

$$\% \text{ excess air} = \% \text{ theoretical air} - 100 \quad (2-58)$$

For example, 110% theoretical air is a lean mixture with 10% excess air ; 85% theoretical air is a rich mixture which is 15% deficient in air.

Sometimes equivalence ratio is used instead of excess air to describe a combustible mixture. The equivalence ratio F is defined as the actual fuel/air mass ratio f divided by the stoichiometric fuel/air mass ratio f_s :

$$F = \frac{f}{f_s} \quad (2-59)$$

Excess air is directly related to equivalence ratio. Using equation 2-56, it follows that

$$\% \text{ excess air} = \frac{100(1 - F)}{F} \quad (2-60)$$

Equation 2-60 is plotted in Figure 2-5. For lean mixtures, excess air tends to infinity, and this is why the use of equivalence ratio is preferred for internal-combustion engines, which often run lean. Note that $1/(1 + f)$ is the mass of air to mass of mixture ratio, and $f/(1 + f)$ is the mass of fuel to mass of mixture ratio.

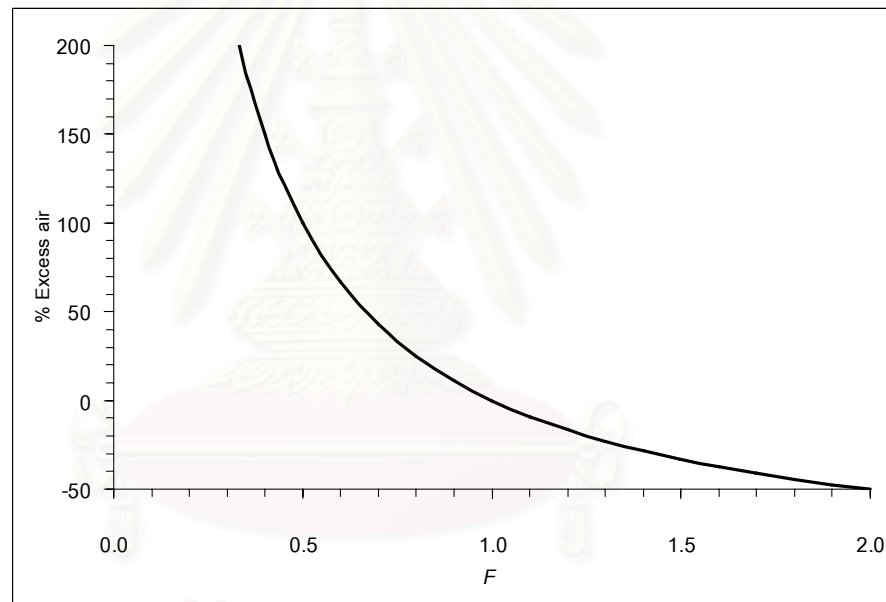


Fig 2-5 Excess air versus equivalence ratio [2]

Excess air can be deduced by measuring the composition of the products. If the products are complete, then the numerator in equation 2-56 can be replaced by the moles of oxygen in the products, $(n_{O_2})_{prod}$. The stoichiometric moles of oxygen in the denominator of equation 2-56 can be obtained from the nitrogen in the products, $(n_{N_2})_{prod}$. Since gaseous measurements are usually done in terms of mole fraction, n 's are replaced by x 's by dividing the numerator and denominator by the total moles in the

products. Referring to the products and noting that $(n_{N_2})_{prod} = (n_{N_2})_{reactants}$, the excess air becomes,

$$\begin{aligned} \% \text{ excess air} &= \left[\frac{(n_{O_2})_{prod}}{(n_{N_2})_{prod} / 3.76 - (n_{O_2})_{prod}} \right] 100 \\ &= \left[\frac{(x_{O_2})_{prod}}{(x_{N_2})_{prod} / 3.76 - (x_{O_2})_{prod}} \right] 100 \end{aligned} \quad (2-61)$$

Typical values of the stoichiometric air-to-fuel ratio, the inverse ratio f_s , and the volume percent of CO_2 in the dry products are shown in Table 2-2 for various fuels. Concentrations in the dry products are used when water is condensed out of the products before gas analysis in order to protect the gas monitoring instruments. [2]

Table 2-2 Stoichiometric complete combustion of several fuels in air

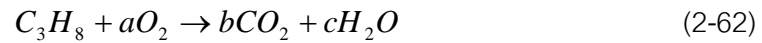
Fuel	m_{as}/m_f	f_s	CO_2
			(% by volume in dry products)
Methane	17.2	0.0581	11.7
Gasoline	14.7	0.0580	14.9
Methanol	6.5	0.154	15.1
Ethanol	9.0	0.111	15.1
No. 1 fuel oil	14.8	0.0676	15.1
No. 6 fuel oil	13.8	0.0725	15.9
Bituminous coal*	10.0	0.100	18.2
Wood*	5.9	0.169	20.5

*Dry basis.

2.3.5.1 Combustion Stoichiometry calculation sample [7]

If sufficient oxygen is available, a hydrocarbon fuel can be completely oxidized, the carbon is converted to carbon dioxide (CO_2) and the hydrogen is

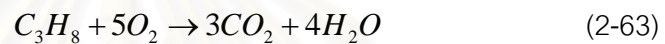
converted to water (H_2O). The overall chemical equation for the complete combustion of one mole of propane (C_3H_8) with oxygen is:



Elements cannot be created or destroyed, so

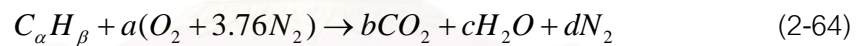
$$\begin{aligned} \text{C balance:} & \quad b = 3 \\ \text{H balance:} & \quad 2c = 8 \rightarrow c = 4 \\ \text{O balance:} & \quad 2b + c = 2a \rightarrow a = 5 \end{aligned}$$

Thus the above reaction is:

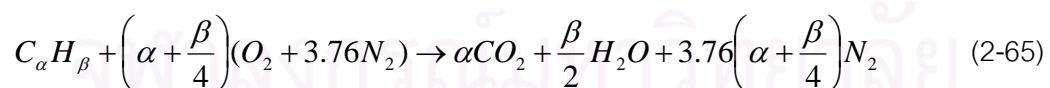


Air contains molecular nitrogen N_2 , when the products are low temperature, the nitrogen is not significantly affected by the reaction, it is considered inert.

The complete reaction of a general hydrocarbon $C_\alpha H_\beta$ with air is:

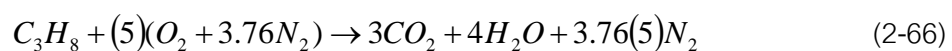


$$\begin{aligned} \text{C balance:} & \quad a = b \\ \text{H balance:} & \quad \beta = 2c \rightarrow c = \beta/2 \\ \text{O balance:} & \quad 2a = 2b + c \rightarrow a = b + c/2 \rightarrow a = \alpha + \beta/4 \\ \text{N balance:} & \quad 2(3.76)a = 2d \rightarrow d = 3.76a/2 \rightarrow d = 3.76(\alpha + \beta/4) \end{aligned}$$



The above equation defines the **stoichiometric** proportions of fuel and air

Example: For propane (C_3H_8) $\alpha = 3$ and $\beta = 8$



The stoichiometric *mass* based air/fuel ratio for C_aH_b fuel is:

$$(A/F)_s = \frac{m_{air}}{m_{fuel}} = \frac{(\sum n_i \bar{M}_i)_{air}}{(\sum n_i \bar{M}_i)_{fuel}} = \frac{\left(\alpha + \frac{\beta}{4}\right) \bar{M}_{O_2} + 3.76 \left(\alpha + \frac{\beta}{4}\right) \bar{M}_{N_2}}{\alpha \bar{M}_C + \beta \bar{M}_H} \quad (2-67)$$

Substituting the respective molecular weights and dividing top and bottom by α one gets the following expression that only depends on the ratio of the number of hydrogen atoms to carbon atoms (β/α) in the fuel.

$$(A/F)_s = \frac{1}{(F/A)_s} = \frac{\left(1 + \frac{(\beta/\alpha)}{4}\right)(32 + 3.76 \cdot 28)}{12 + (\beta/\alpha) \cdot 1} \quad (2-68)$$

Note above equation only applies to stoichiometric mixture

For methane (CH_4), $\beta/\alpha = 4 \rightarrow (A/F)_s = 17.2$

For octane (C_8H_{18}), $\beta/\alpha = 2.25 \rightarrow (A/F)_s = 15.1$

2.3.5.2 Mole fraction

The total number of moles in the mixture is

$$n = \sum_{i=1}^n n_i \quad (2-69)$$

The **mole fraction**, y_i , of any given species is defined as:

$$y_i = \frac{n_i}{n} \quad \text{and} \quad \sum_{i=1}^n y_i = 1 \quad (2-70)$$

The mixture internal energy U and enthalpy H (units: kJ) is:

$$U = \sum_{i=1}^n n_i \bar{u}_i \quad H = \sum_{i=1}^n n_i \bar{h}_i \quad (2-71)$$

where n_i are molar specific values (units: kJ/kmol)

The mixture molar specific internal energy and enthalpy (units kJ/ kmol) is:

$$\bar{u} = \sum_{i=1}^n y_i \bar{u}_i \quad \bar{h} = \sum_{i=1}^n y_i \bar{h}_i \quad (2-72)$$

The mixture molecular weight, M , is given by:

$$\bar{M} = \frac{m}{n} = \frac{\sum_{i=1}^n m_i}{n} = \sum_{i=1}^n \frac{n_i \bar{M}_i}{n} = \sum_{i=1}^n y_i \bar{M}_i \quad (2-73)$$

The **partial pressure** of a component, P_i , in the mixture (units: kPa) is:

$$y_i = \frac{n_i}{n} = \frac{P_i V / RT}{PV / RT} = \frac{P_i}{P} \quad \text{or} \quad P_i = y_i P \quad (2-74)$$

2.3.5.3 Real Gas Model

The mass specific mixture entropy (units: kJ/kg K) at P , T is

$$s = \sum_{i=1}^n x_i (s_i^o - R_i \ln(P_i / P)) - R \ln(P / P_o) \quad (2-75)$$

The molar specific mixture entropy (units: kJ/mol K) is:

$$\bar{s} = \sum_{i=1}^n y_i (\bar{s}_i^o - R_i \ln y_i) - \bar{R} \ln(P / P_o) \quad (2-76)$$

Note, if the mixture pressure is at 1 bar the second terms drops out.

2.4 Combustion Flame [2]

There are two basic idealized types of flames: *premixed flames*, and *diffusion flames*. Premixed flames arise from the combustion of gaseous reactants which are perfectly mixed prior to combustion. A premixed flame is a rapid, essentially constant-pressure, exothermic reaction of gaseous fuel and oxidizer which radiates light and heat and propagates as a thin zone with speeds of less than a few meters per second. Laminar premixed flames have a unique burning velocity for a given fuel-oxidizer mixture. Turbulence increases the burning velocity. Diffusion flames arise from the combustion of separate gaseous fuel and oxidizer streams which combust as they mix. Diffusion flames are dominated by the mixing of the reactants, which can be either laminar or turbulent, and reaction takes place at the interface between the fuel and oxidizer.

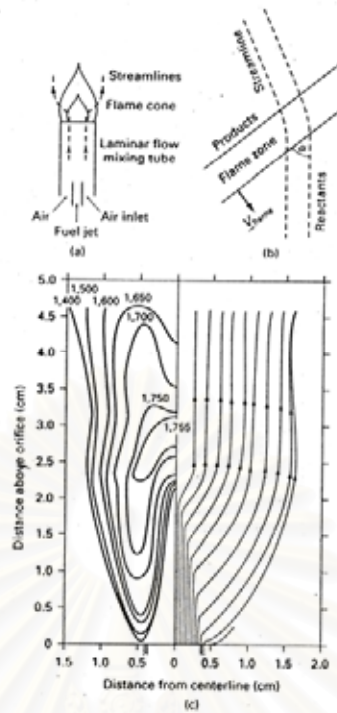


Fig 2-6 Bunsen burner flame: (a) schematic of burner , (b) flow diagram , and (c) streamline and temperature ($^{\circ}\text{C}$) for a laminar slot burner [2]

2.4.1 Laminar premixed flames

A combustion reaction started at a local heat source in a quiescent fuel-air mixture at ambient conditions will propagate initially as a laminar flame. Chemical reaction takes place in a relatively thin zone, and the flame moves at a fairly low velocity. For stoichiometric hydrocarbon mixtures in ambient air the flame is approximately 1 mm thick and moves at about 0.5 m/s, the pressure drop through the flame is very small (about 1 Pa), and the temperature in the reaction zone is high (2200-2600 K). Within the flame reaction zone a multitude of active radicals are formed in the high temperature part of the flame and diffuse upstream to attack the fuel.

The familiar Bunsen burner, shown schematically in Figure 2-6 (a) provides an example of a stationary laminar premixed flame, provided that the reactants flow through the tube under laminar conditions. Fuel enters under a slight positive pressure at the

base of the burner and entrains air, which mixes in the burner tube. The flame zone is cone-shaped.

Figure 2-6 (b) shows the streamlines relative to the flame zone, and Figure 2-6 (c) shows isotherms and streamlines for a slot burner. A slot burner with a rectangular cross section will produce a tent-shaped flame similar to the cone of a Bunsen burner. The observed peak temperature in the flame is slightly reduced from the adiabatic temperature due to radiation losses. A fuel-air mixture with a slower burning velocity will have a more pointed tip.

2.4.2 Diffusion flames

Diffusion flames take place when the sources of fuel and oxidizer are physically separated so that the energy release rate is limited primarily by the mixing process. There is no fundamental flame speed as in the case of premixed flames, and the flames are not one-dimensional. Chemical kinetics plays a secondary role in the behavior of diffusion flames. Diffusion flames occur with flowing gases, with vaporization of liquid fuels, and with devolatilization of solid fuels. Flames from liquid and solid fuels will be considered in later chapters.

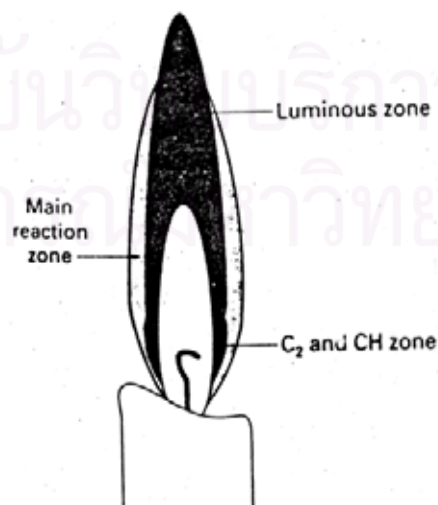


Fig. 2-7 Candle flame in air showing reaction zone [2]

A candle flame, shown in Figure 2-7, is an example of a diffusion flame. Wax is melted, flows up the wick and is vaporized. Air flows upward due to natural convection. The reaction zone is between the air and fuel zones. Air diffuses inward and fuel diffuses outward. In hydrocarbon flames soot particles are produced, giving rise to intense luminosity.

2.5 Fuel spray theory

2.5.1 Practical steady-flow fuel spray flames are of two basic types. [2]

a) Atomized by high-pressure air (or steam), which have such high momentum that the entrained air is sufficient for combustion.

b) Atomized by high liquid pressure which have relatively low momentum such that the dimensions of the flame are primarily determined by the surrounding air flow.

The fuel sprays used in direct-injection reciprocating engines are unsteady, so that their length varies with time. Although some of these sprays, such as those used in direct-injected spark-ignited engines, are of much lower pressure and momentum than the typical high-momentum diesel spray, all of the in-cylinder engine sprays tend to influence the air motion significantly.

Given a spray droplet size and velocity distribution near the spray nozzle, relationships for droplet motion, vaporization, and agglomeration may be modeled. For some sprays such as the air atomization sprays and the very-high-pressure (1400 atm) diesel sprays, the spray momentum is large and the droplet size is very small. For such sprays the droplets may vaporize quickly and the spray may be approximated as a gas jet. The gas jet problem for a steady jet is well worked out if the jet and air are traveling in the same direction. For a jet in cross flow, only approximate models and empirical formulations are available. Calculations using 3-D numerical codes exist for transient liquid sprays and gas jets, but have not yet been validated.

As a simple example, consider a gas jet in a stagnant surrounding gas. As gas leaves the nozzle, a boundary layer grows along the outer portion of the jet stream. The inner region that is unaffected by the boundary layer gradually diminishes until the boundary layer has filled the entire jet region. After a transition region, the profiles become fully developed. The behavior is very similar to the opposite problem of the entry region in pipe flow. The unaffected core region is about 4 to 5 nozzle diameters long, and the transition region is about 10 diameters long. Figure 2-8 show the various regions.



Fig.2-8 Region of steady gas jet [2]

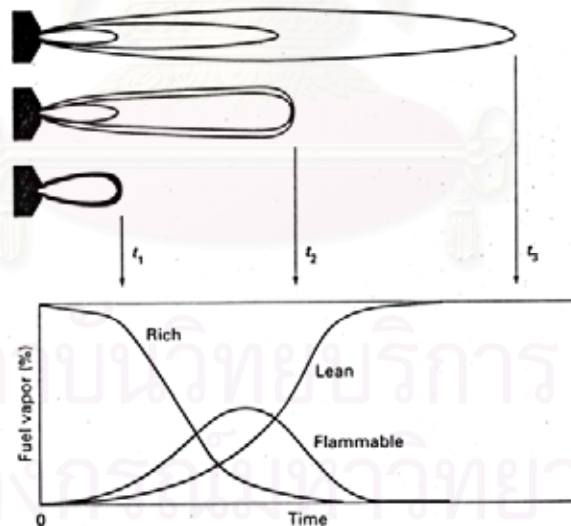


Fig.2-9 At top, schematic of the development of a gas jet. At Bottom, fuel vapor profiles are shown versus time for each of the three envelope regions, shown in the schematic [2].

2.5.2 Fuel spray in diesel engine [4]

The fuel injected from the nozzle into the combustion chamber of the diesel engine disintegrates into numerous drops of different sizes and concentrations in the spray. Figure 2-10 shows the main parameters that express the aspect of a diesel spray.

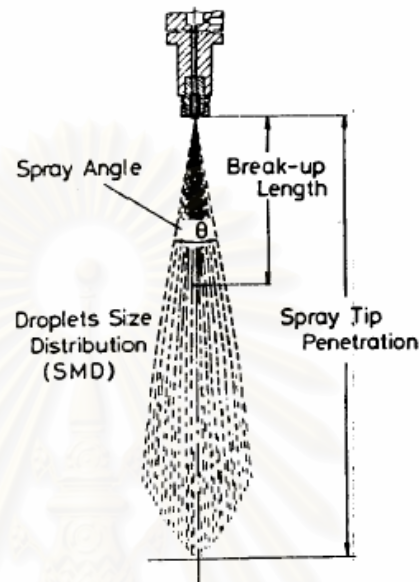


Fig. 2-10 Parameter of spray [4]

The motion of the spray tip and break-up length give clues as to the understanding of the disintegrating process of a fuel jet. Spray angle and drop size distribution are the results of this disintegrating process. These four parameters of the spray are related to each other in the disintegrating process and affect, the mixture formation through aerodynamic and thermodynamic processes in the combustion chamber of the diesel engine.

2.5.2.1 Break-up length

The injected liquid does not break up instantly after injection. There is some unbroken portion which is referred to as the liquid break-up length. Break-up lengths average between 10 to 30 mm and appear to be present for injection velocities above 200 m/s. Extensive experimental studies on the break-up phenomena of low velocity jets have been shown in figure 2-11. Increasing ambient pressure, the break-up length decreases. And break-up length increases with an increase in injection velocity.

When injection velocity is further increased, the wavy flow is not observed and break-up length decreases. This region is called a spray.

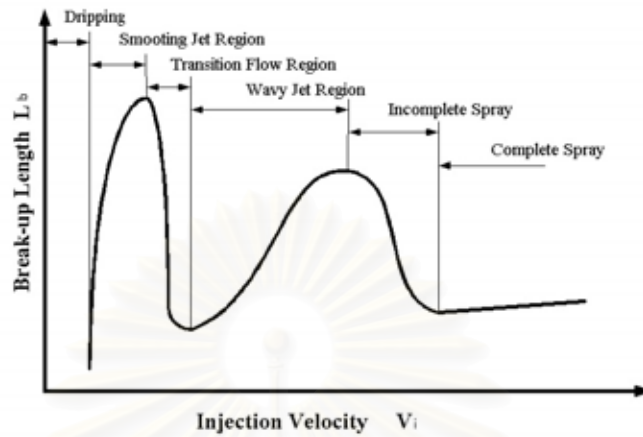


Fig.2-11 Break-up behavior of a liquid jet [4]

2.5.2.2 Spray angle

Figure 2-12 shows the effect of injection pressure on the spray angle. The spray angle increases with an increase in injection velocity, takes the maximum value and reaches an almost constant value in a complete spray region.

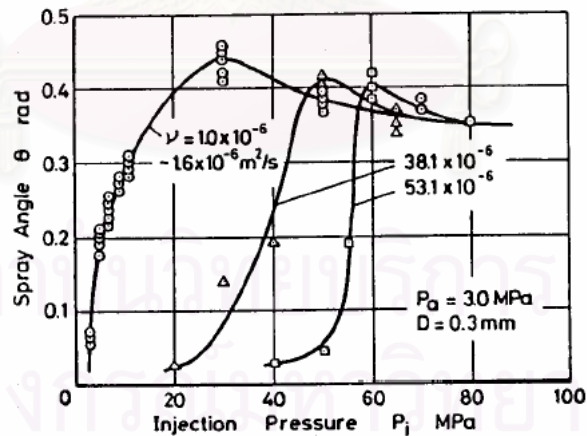


Fig. 2-12 The effect of injection pressure on spray angle [4]

The maximum spray angle appeared at the injection velocity where the feature of a spray shifted from an incomplete spray type to a complete one. The injection pressure where the maximum spray angle occurs increases with an increase in the liquid kinematic viscosity; this indicates that the transition velocity also increases with the viscosity. But the transition velocity is almost independent of the nozzle hole diameter.

2.5.2.3 Spray tip penetration

The speed and extent to which the fuel spray penetrates in the combustion chamber has an important influence on air utilization and fuel-air mixing rate. So spray tip penetration of the intermittent diesel spray was measured with the aid of photographic techniques at various ambient temperatures, ambient pressures injection pressures and injection durations. Figure 2-13 shows the effect of injection pressure on spray tip penetration under constant ambient pressure and injection duration. [4]

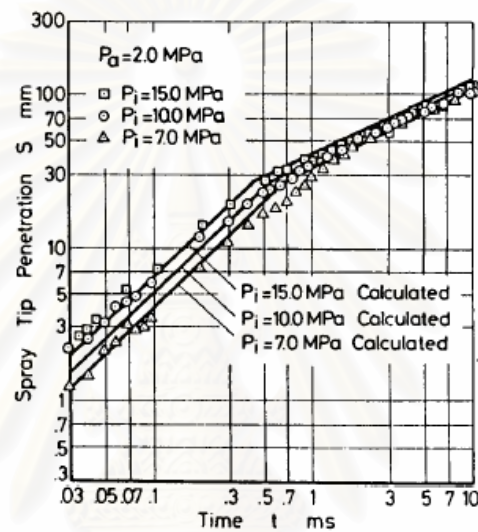


Fig. 2-13 Spray tip penetration at various injection pressures [4]

2.6 Momentum method to measure the injection rate

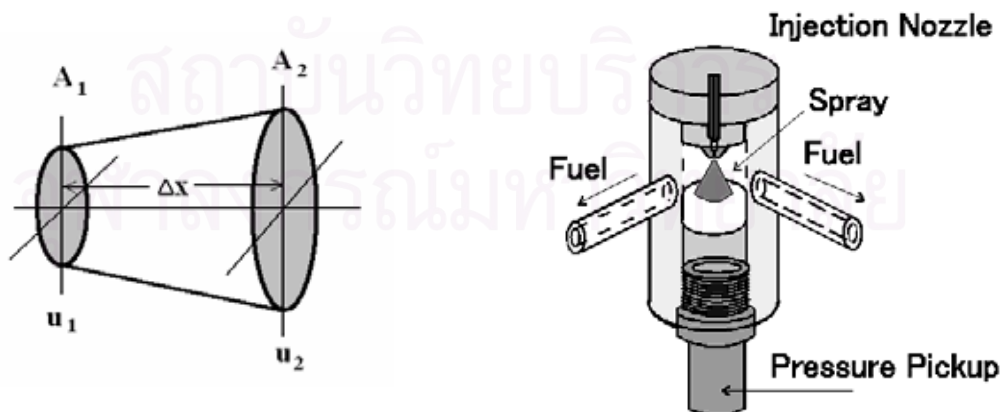


Fig.2-14 Pressure pick up and calculation profile

From Newton's second law;

$$F_i = ma \quad (2-77)$$

Where F_i = Force of fuel injection

m = mass

a = acceleration

$$F_i = m \frac{\Delta u}{\Delta t} \quad (2-78)$$

$$F_i = m' \Delta u \quad (2-79)$$

Where u = velocity

t = time

m' = rate of mass flow

And from $m = \rho V$ (2-80)

Where V = volume

ρ = density

$$m = C_i \rho \Delta x A$$

$$\frac{m}{\Delta t} = C_i \rho \frac{\Delta x}{\Delta t} A$$

$$m' = C_i \rho u A \quad (2-81)$$

Where Δx = distance

A = section Area

C_i = constant

Combined equation 2-79 and equation 2-81

$$m' = C_{i1} \rho \left(\frac{F_i}{m'} \right) A$$

$$(m')^2 = C_{i1} \rho F_i A$$

$$m' = \sqrt{C_{i1} \rho F_i A}$$

$$m' = C_{i2} \sqrt{F_i} \quad , \quad C_{i2} = \sqrt{C_{i1} \rho A} \quad (2-82)$$

$$m' = f(F_i) \quad (2-83)$$

Mass flow rate is the function of square root force.

2.7 Palm Diesel

Palm oil is the oil extracted from mesocarp of palm seed by heating and compressing. Palm oil could be classified into 2 types;

- a) Palm oil for industry
- b) Palm oil for consumer (such as Crude palm oil and Refined palm oil)

Some property of crude palm diesel 10% is showing in table 2-3

Table 2-3 Property of crude palm oil [5], [13]

Property	Test method	Specification
Relative Density at 50/20 °C	CAC/RM9	0.891-0.899
Refractive Index at n_D 50 °C	IUPAC(1979)	1.455-1.456
Water vapor at temperature 105 °C (%wt)	IUPAC(1979)	≤ 0.2
Insoluble impurities (%wt)	IUPAC(1979)	≤ 0.05
Iodine value (Wijis)	IUPAC(1979)	50-55
Saponification value milligram potassium hydroxide per sample 1 g	IUPAC(1979)	190-209
Unsaponifiable matter (g) per sample 1 kg	IUPAC(1979)	≤ 12
Acid value milligram potassium hydroxide per sample 1 g	IUPAC(1979)	≤ 4
Peroxide value milligram equivalent peroxide oxygen per sample 1 kg	IUPAC(1979)	≤ 10
Beta carotene (mg / kg)	AOAC(1984)	500-2000

2.8 Two color method for flame visualization [9], [11]

The principle of 2 color method

The relation between the intensity of monochromatic radiation from the black body, the wave and temperature of the black body can be expressed by Plank's equation.

$$N_0(\lambda, T) = C_1 \lambda^{-5} \left[\exp\left(\frac{C_2}{\lambda T}\right) \right]^{-1} \quad (2-84)$$

$N_0(\lambda, T)$ is an intensity of radiation from black body ($\text{W/m}^2 \mu\text{m}$) at wave length (λ), C_1 and C_2 are constants ($C_1=3.742 \times 10^{-16} \text{Wm}^2, C_2=1.439 \times 10^{-2} \text{mK}$). If the temperature is under 3000 K, Plank's equation can be approximated by Wien's equation.

$$N_0(\lambda, T) = C_1 \lambda^{-5} \exp\left(\frac{-C_2}{\lambda T}\right) \quad (2-85)$$

For a non-black body, it is necessary to introduce a new factor (ϵ_λ) called the monochromatic emissivity. Thus for non-black body:

$$N(\lambda, T) = \epsilon_\lambda N_0(\lambda, T) = \epsilon_\lambda C_1 \lambda^{-5} \exp\left(\frac{-C_2}{\lambda T}\right) \quad (2-86)$$

where $N(\lambda, T)$ is the intensity of radiation from non-black body and may also be represented mathematically by

$$N(\lambda, T) = N_0(\lambda, T_a) = C_1 \lambda^{-5} \exp\left(\frac{-C_2}{\lambda T_a}\right) \quad (2-87)$$

where T_a is the apparent temperature and defined as the temperature at which a black body would have the same monochromatic intensity of radiation as the non-black body.

In general, monochromatic emission is not equal at different wave lengths. It has been shown by Hottel and Broughton that the mono chromatic emission of a luminous flame is expressed by an equation of the form

$$\epsilon_\lambda = 1 - \exp\left(\frac{-KL}{\lambda^\alpha}\right) \quad (2-88)$$

where K = absorption constant per unit flame thickness and is independent of wave length

L = flame thickness

α = constant for limited wave-length range ($\alpha=1.38$)

Equating equation 2-86, equation 2-87 and solved KL factor by equation 2-88.

$$KL = -\lambda^\alpha \ln \left[1 - \exp \left\{ \frac{C_2}{\lambda} \left(\frac{1}{T} - \frac{1}{T_a} \right) \right\} \right] \quad (2-89)$$

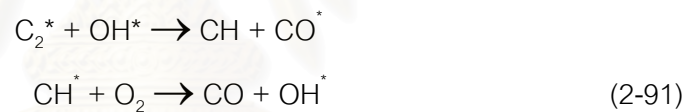
Two equations can be written for two different wave lengths by subscript 1 and 2. Equating the two KL terms, which are equal over a limited wave length range, and rearranging, give the following,

$$\lambda_1^\alpha \ln \left[1 - \exp \left\{ \frac{C_2}{\lambda_1} \left(\frac{1}{T} - \frac{1}{T_{a1}} \right) \right\} \right] = \lambda_2^\alpha \ln \left[1 - \exp \left\{ \frac{C_2}{\lambda_2} \left(\frac{1}{T} - \frac{1}{T_{a2}} \right) \right\} \right] \quad (2-90)$$

if $\lambda_1, \lambda_2, \alpha_1$ and α_2 are known and the two apparent temperatures are measured, true temperature (T) can calculate from the equation 2-90. [9]

2.9 Radical of combustion [9]

The radical of the hydrocarbon combustion is produced the OH radical at which the combustion is occurred following chemical reaction 2-91.



The wave length of OH radical is around 306.5 nm to 308.9 nm.

CHAPTER III

EXPERIMENTAL APPARATUSES AND METHODS

3.1 Fuel blending methods

This experiment was done with crude palm oil and refined palm oil. The blending methods for both oils were closely the same:

- a) Heat palm oil up to 60 °C.
- b) Blended them together at mixing percentage of 10, 20, 40, 60 and 80 %.
- c) Maintain the fuel temperature at 40 °C before loaded into heating fuel tank.

3.2 Experimental apparatuses

The constant volume combustion chamber system was assembled in year 2003.

The system includes:

- a) Test base and combustion chamber:
 - Observation window glass
 - Mixing propeller
 - Heater and cooling water
- b) Injection system:
 - Fuel line
 - Fuel tank
 - Pump and valve
 - Injector
- c) Hydrogen combustion system:
 - Gas tank (Air, O₂, H₂)
 - Piping and valve
- d) Optical sensor and ICCD camera:
 - Photo diode and photo sensor
 - ICCD camera (LA vision Flame Star II)

With his helps, Dr.Yoshifumi Wakisaka, the electric control system was completely installed. Fuel injection system, combustion chamber systems and optical measurement system was installed properly with relative position, as shown in figure 3-1.

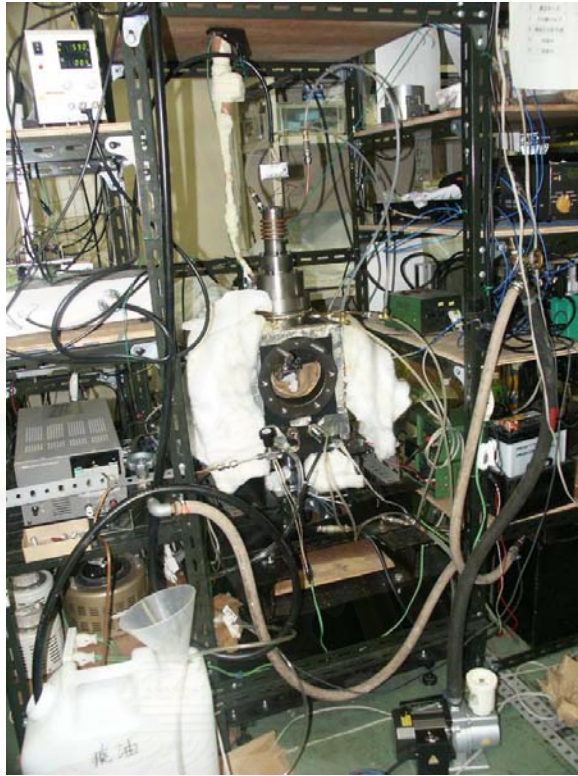


Fig.3-1 Experimental apparatuses

3.2.1 Combustion chamber and components

The visualization of fuel spray and combustion flame structure inside the actual engine is very difficult. Although this combustion chamber had relatively large volume (2200 cc) compared to diesel engine combustion chamber, more details of flame structure could be observed.

This combustion chamber was made form cubic steel and drilled holds at all sides; top side for nozzle and injection systems, bottom side for mixing propeller and the other sides for window observation glass and spark plugs, as shown in figure 3-2. Specification and picture of the pressure sensor used to measure the pressure inside the chamber is shown in table 3-1 and figure 3-3.

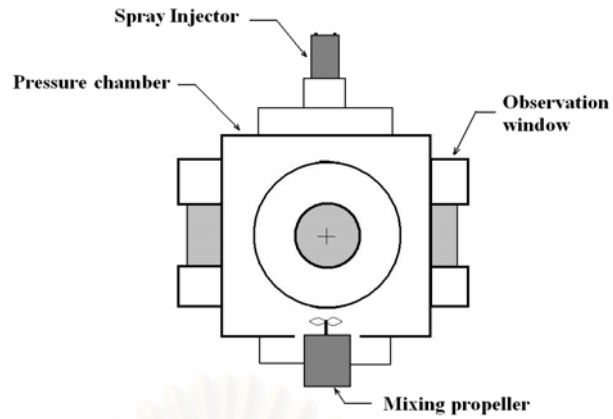


Fig.3-2 Pressure chamber and components



Fig.3-3 Combustion chamber pressure sensor

Table 3-1 Combustion chamber pressure sensor and control

Inside combustion chamber pressure sensor	Kyowadengyo
Max pressure	50 kgf / cm ²
Capacity	1527 (×10 ⁻⁶) μ Strain
AD board Interface AZI-3141	12 bit 4 channel FIFO memory : 4k word/ch
Input	±5, ±10, 0~+10 V
Conversion time	10 μ s

3.2.1.1. Observation window

The observation window is installed at the one side of combustion chamber. The special crystal type of glass was selected and installed as shown in figure 3-4.



Fig.3-4 Observation window component

The glass window was also heated by heater, shown in figure 3-5. Glass heater was always put at the observation windows and removed only when the measurement was being done to protect the window from crack.



Fig.3-5 Glass Heater

3.2.1.2. Spark plug

Two spark plugs at two sides of the chamber were used for starting the hydrogen combustion. The schematic of spark plug system is shown in figure 3-5. The start timing of spark plug is fully controlled by 9 channel delay and this timing affected the rising shape of H_2 combustion pressure inside the vessel.

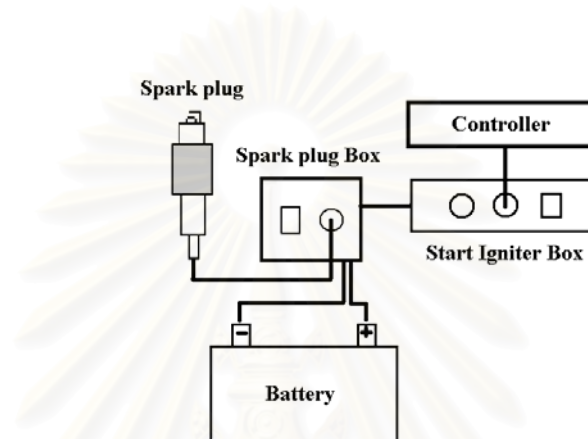


Fig.3-6 Spark plug system



Fig.3-7 Spark plug position
at combustion chamber



Fig 3-8 Spark plug control box

3.2.1.3. Mixing propeller

Mixing propeller was installed at the bottom of the combustion vessel for:

- Mixing gases; Air, O₂ and H₂ before start of the hydrogen combustion.
- Maintaining the high temperature gas around the nozzle after hydrogen combustion.
- Helping to drain the combusted away of the combustion chamber.

In this experiment, the mixing propeller stopped 0.5 msec before start of combustion for 1 second width. Specification of propeller's driving motor is shown in table 3-2.



Fig 3-9 Mixing propeller



Fig 3-10 Mixing propeller driving motor



Fig 3-11 Propeller driving motor control box

Table 3-2 Propeller's driving motor specification

Mixing motor	Oriental	
Frequency	50 / 60	Hz
Torque	3000 / 2600	gcm
Speed	1300 / 1550	rpm

3.2.1.4. Combustion chamber heater

The combustion chamber was heated up to 100 °C by an electrical heater for preventing the individual ghost light which might occur at low temperature, as shown in figure 3-12. The temperature was controlled by changing the transformer in put voltage, as shown in figure 3-13.

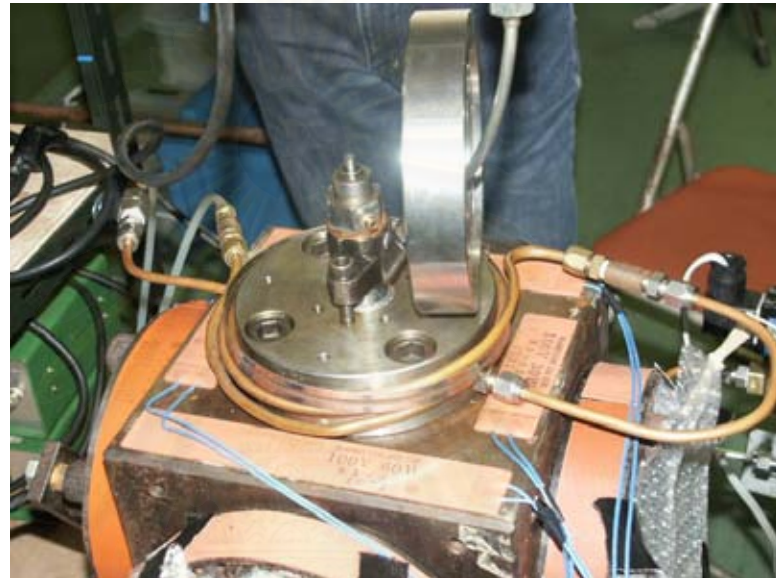


Fig.3-12 Combustion chamber and heater

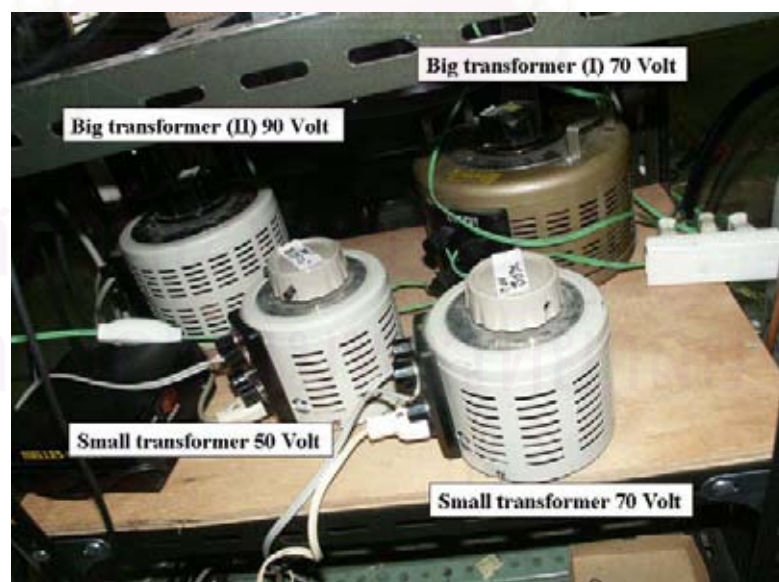


Fig.3-13 Transformer of heaters

3.2.1.5. Water cooling pipe

The top of combustion chamber and inside pressure sensor were cooled when conducting the experiment, as shown in figure 3-14 and 3-3. The cooling water was maintained the constant temperature around injector ($\sim 40^{\circ}\text{C}$) to decrease the thermal effect on the nozzle system.



Fig.3-14 Combustion chamber and cooling water line

สถาบันวิทยบริการ
จุฬาลงกรณ์มหาวิทยาลัย

3.2.1.6. Vacuum pump system

The vacuum pump system was used to remove the combusted gas in the combustion chamber. The schematic of the vacuum pump system is shown in figure 3-15. The combusted gas was sucked passing the vapor trap to prevent the water vapor of the combustion getting into the vacuum pump. Vacuum pump and vapor trap are shown in figure 3-16 and 3-17.

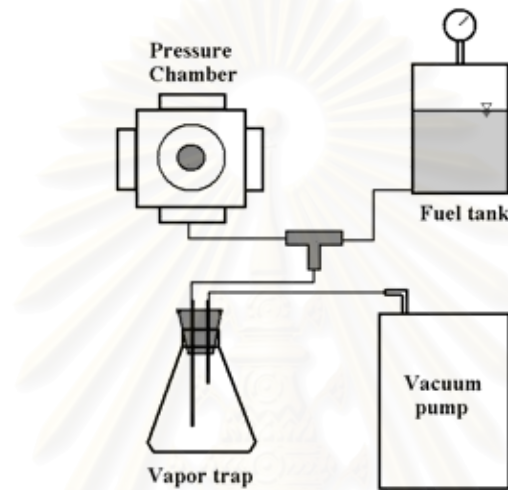


Fig.3-15 Schematic of the vacuum pump system



Fig.3-16 Vacuum pump



Fig.3-17 Vapor trap

3.2.2 Injection systems

The injection system components were 2.2 liter fuel tank, high pressure hydraulic pump, inlet and outlet valve, main pressure gauge and Piezo & injector, as shown in figure 3-18. The picture of main pressure gauge and inlet & outlet valve and hydraulic pump are shown in figure 3-19 and 3-20.

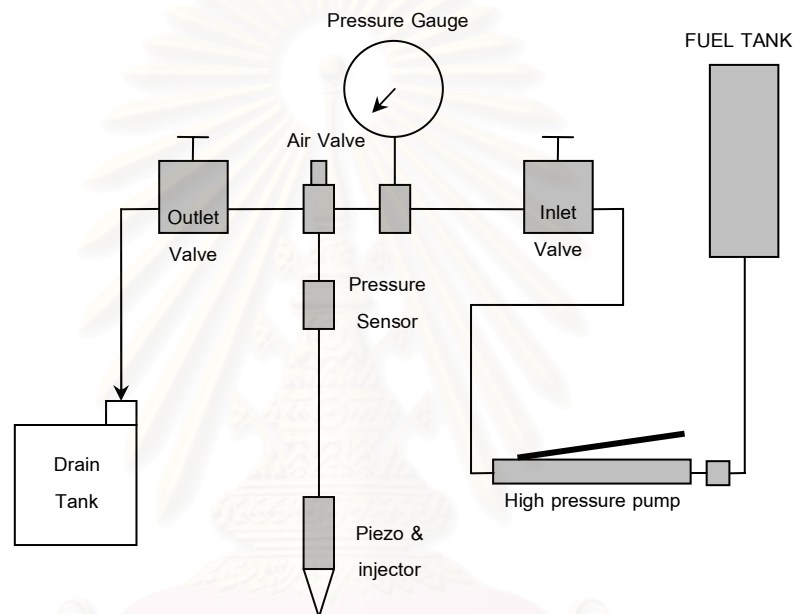


Fig 3-18 The Schematic of injector system



Fig 3-19 Pressure gauge and valve



Fig 3-20 Hydraulic Pump

A special single hold nozzle (diameter 0.20 mm) was used and connected to piezo actuator with extended pressure pin. The assembly of the injector system is shown in figure 3-21.

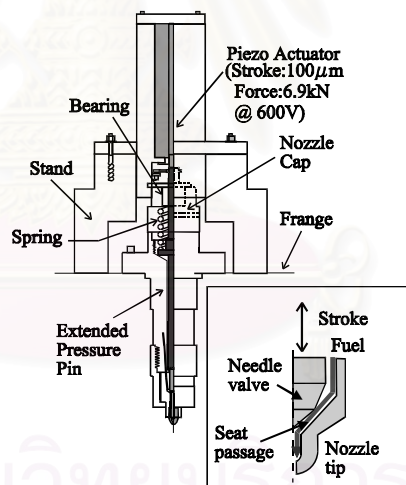


fig 3-21 Injector system components [1]

Piezo used in this experiment was piezo stack type that consisted of a large number of contacted ceramic discs and connected the electrodes arranged at both sides of the ceramic disc, as shown in figure 3-22.

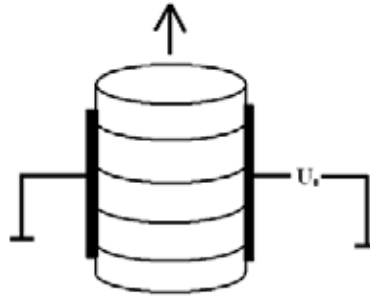


Fig 3-22 Piezo stacks type

The injection was controlled by changing Piezo voltage. The relation between Piezo voltage and injection rate is shown in figure 3-23.

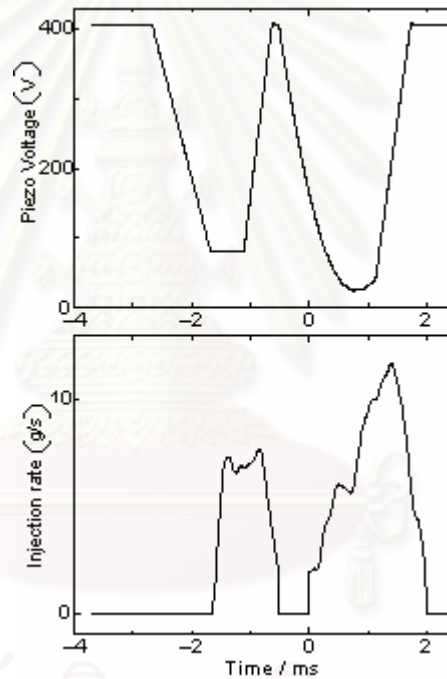


Fig 3-23 The relation between Piezo voltage and fuel injection rate [6]

Table 3-3 Piezo and components specification

Piezo Acurator	Denso stacks type
Size	118.5 ± 1.6 mm, ϕ 30.2 ± 0.2 mm
Wight	570 g
Capacity	5.4 μ F
Maximum moving length	600 V, 105 ± 16 μ m
Power	6900 N

Table 3-3 Piezo and components specification (continue)

DC Power Supply	Matsusada precision	
Output Voltage	0 – 650	V
Output Ampere	0 – 0.1	A
Output ripple	10 m	Vrms

DA Board Micro science MDA – 2898 BPC	12 bit 2 channel 4KB(2048 data) FIFO memory
Analog (DA) input	$\pm 5, \pm 10, 0 \sim +10$ V
DA data out put	port I/O, DMA
Clock frequency	1 MHz

AD Board Micro science ADM – 4898BPC-4-16 KW	12 bit 4 channel FIFO memory
input	$\pm 10, \pm 5, \pm 2.5, \pm 2$ V
AD data out put	port I/O, DMA
Clock frequency	8 MHz

Table 3-4 Line pressure sensor specification

Injection Pressure Sensor	Kyowadengyo	
Max pressure	1000	kgf / cm ²
Capacity	2010 ($\times 10^{-6}$)	μ Strain
Clock Frequency	3	kHz

3.2.3 Injection rate sensor

One parameter of this experiment was injection rate set close to maximum (peak) injection rate of this nozzle (diameter 0.20 mm). The measurement apparatus was injection rate sensor, called "Pickup sensor"

Pickup sensor was a pressure sensor capacity which mounted to the nozzle by aluminum case, shown in figure 3-13.

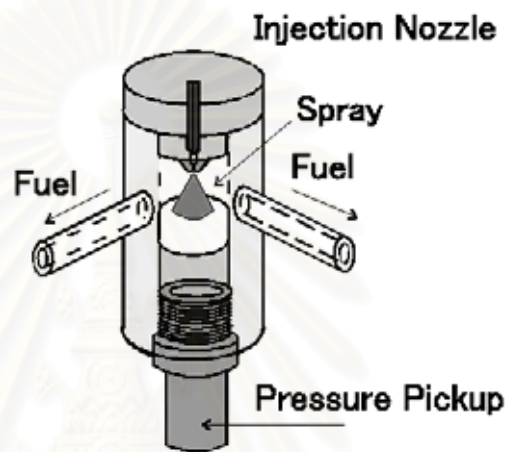


Fig3-24 Injection rate sensor

Table 3-5 Injection sensor specification

Injection rate Sensor	Kyowadengyo	
Max pressure	2	kgf / cm ²
Capacity	1646 ($\times 10^{-6}$)	μ Strain
Clock Frequency	3	kHz

3.2.4 Hydrogen combustion system

Experimental conditions were simulated close to the real diesel condition. The considered parameters are air-fuel ratio, air density, oxygen concentration, high ambient pressure and temperature. Schematic of hydrogen combustion system which was used to increase ambient temperature and pressure inside the combustion chamber is shown in figure 3-25 and the gas tank and gas valve are shown in figure 3-26 and 3-27.

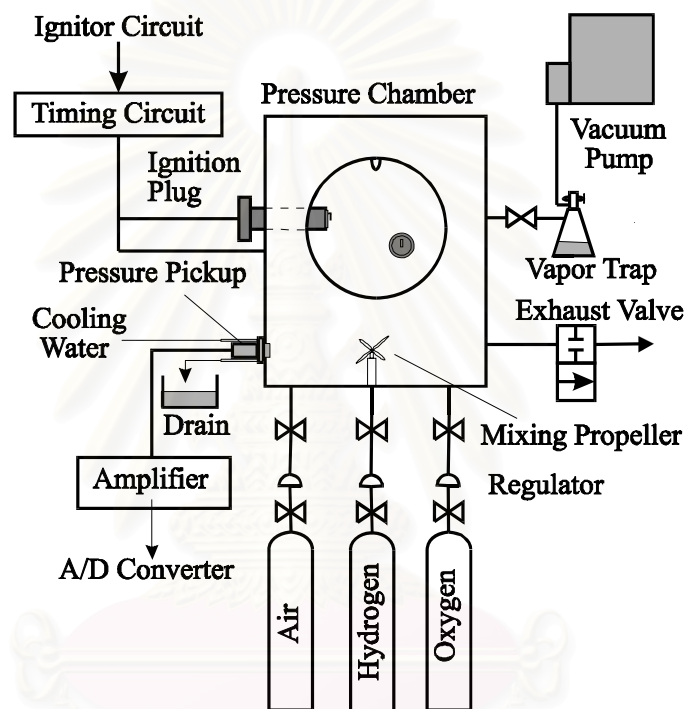


Fig.3-25 Schematic of hydrogen combustion system

Air, oxygen and hydrogen at proper mixture were charged to the chamber and ignited by spark plug ignition. After the pressure and temperature rose up to the required condition, the nozzle started to spray the fuel and fuel flame could be visualized. Figure 3-28 shows Gas pressure inside the combustion vessel after the hydrogen combustion and the position which fuel was injected.



Fig 3-26 Oxygen, Air and hydrogen tanks



Fig 3-27 Gas Valves

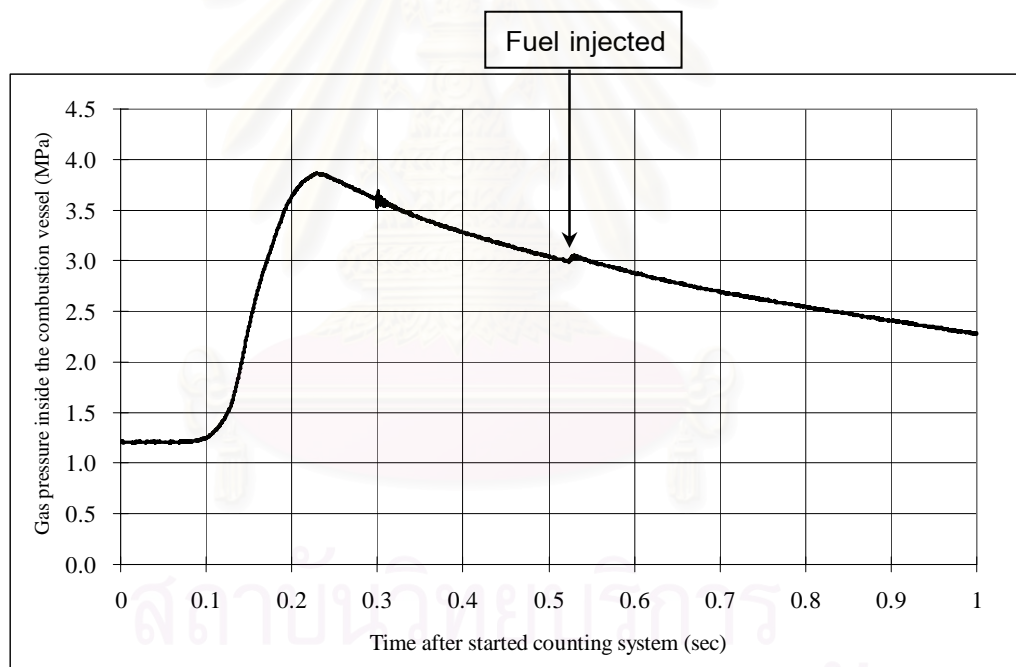


Fig 3-28 Gas pressure inside the combustion vessel

3.2.5 Optical measurement system

Optical measurement system was used to measure the combustion luminous light emission. The system consisted of Photo diode, photo sensor and ICCD camera.

3.2.5.1 Photo diode and photo sensor to detect luminous light emission

This system was used to measure the ignition delay and combustion period of fuel combustion, as shown figure 3-30. In figure 3-30(a) is the head of fiber glass which connected to 2 sensors, one for detecting OH-radical and another for detecting luminous emission called "Side". In figure 3-30(b), "Top" is the photodiode located at the top of the combustion chamber that was used to detect and measure luminous flame at the bottom of the chamber.

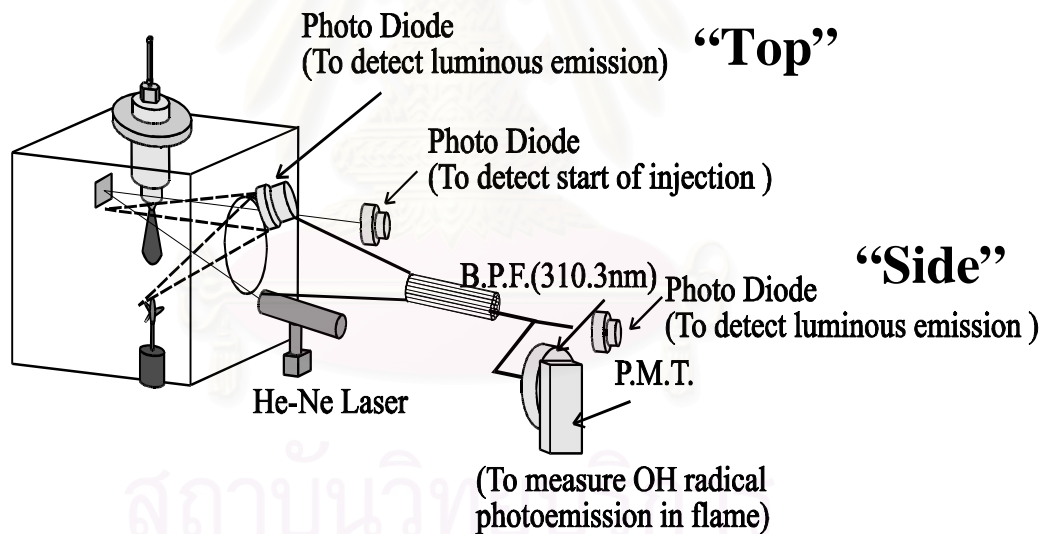


Fig 3-29 Schematic diagram of optical sensor [9]

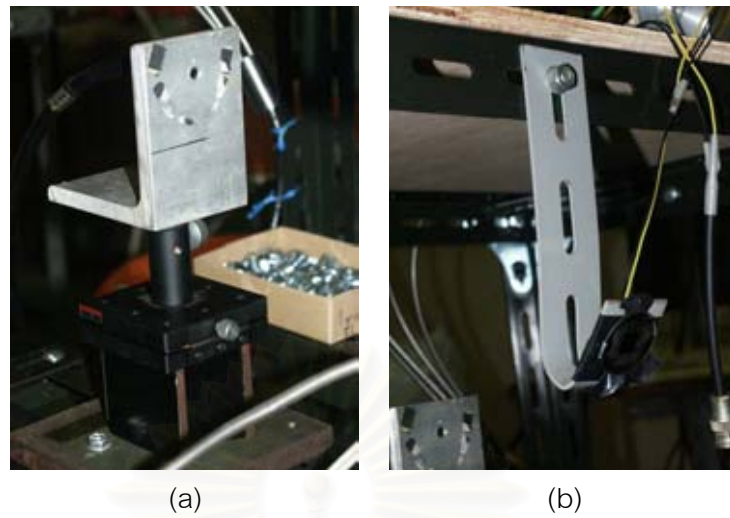


Fig 3-30 Optical sensor: (a) Side, (b) Top

3.2.5.2 The system for detecting the start of injection

From figure 3-31, the start of fuel injection was measured by pointing the He-Ne laser to the tip of the nozzle. Laser reflected by mirror to the photo diode was cut as fuel sprays started. This signal will be the start of the spray. The ignition delay is calculated by using this laser signal data and OH-radical data.

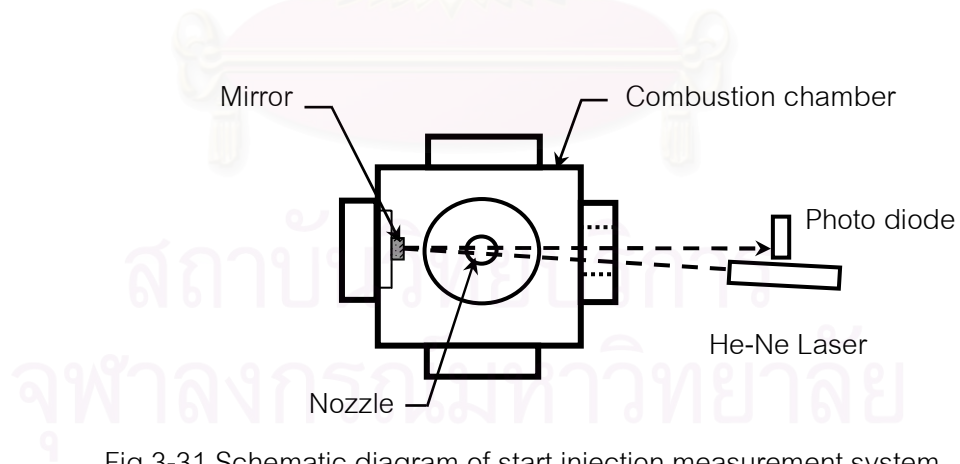


Fig 3-31 Schematic diagram of start injection measurement system

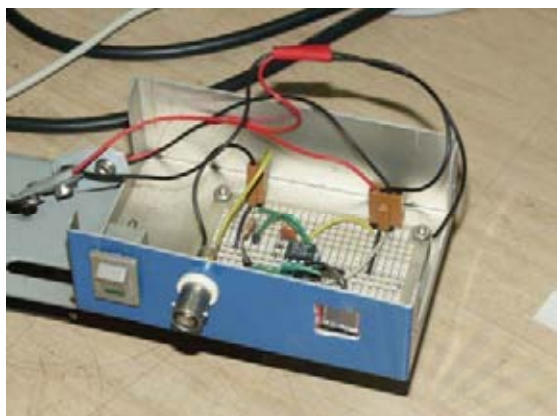


Fig 3-32 He-Ne laser Photo diode



Fig 3-33 He-Ne laser

Table 3-6 Radical photo sensor specification

Radical Measurement Metal Interference	Nihonsinkukugaku MIF-W
Center Wave Length	310.3 nm
Transmittance	18.3 %
Half Band Width	16.6 nm

Photo Multiplier S1226-44BK	Hamamatsu photonics silicon photo diode
Wave Length	320 ~ 1000 nm
Sensitivity	0.35 A / W
Effective Size	13 mm ²

Photo Multiplier S1227-1010BR	Hamamatsu photonics silicon photo diode
Wave Length	320 ~ 1000 nm
Sensitivity	0.42 A / W
Effective Size	100 mm ²

Table 3-6 Radical photo sensor specification (continue)

Photo Diode S1226-44BK	Hamamatsa photonics silicon photo diode
Wave Length	320 ~ 1000 nm
Sensitivity	0.35 A / W
Effective Size	13 mm ²

Photo Diode S1227-1010BR	Hamamatsa photonics silicon photo diode
Wave Length	320 ~ 1000 nm
Sensitivity	0.42 A / W
Effective Size	100 mm ²

3.2.5.3 Intensified CCD Camera (ICCD) [8]

An intensified CCD camera is a CCD detector coupled with an image intensifier in front of lens. The combination of CCD and image intensifier has several advantages compared to the use of CCD alone, such as;

- Ultimate sensitivity; it is possible to measure single photon.
- UV extended spectral sensitivity down to 180 nm(with quartz entrance window)
- An extremely short shutter speed of several nsec (optical gating)

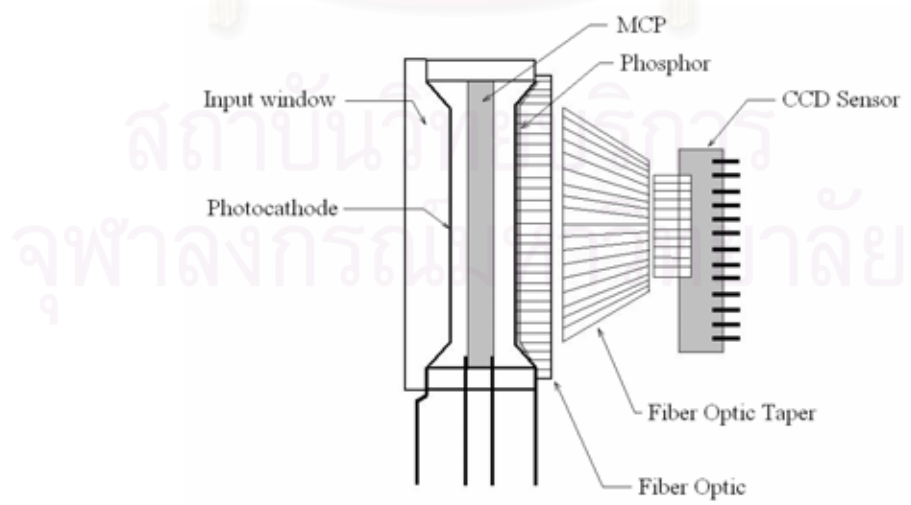


Fig 3-34 Cross section through the optical part of an intensified CCD camera

The composition inside ICCD camera shown in figure 3-34 are;

1) **Photo Cathode:** The image is focused onto the photo cathode plane. Impinging photons generate electrons inside the photo cathode material. Only during the image intensifier gate time, a negative voltage is applied to the photo cathode. Hence, only during this gating time electrons are accelerated towards the MCP.

2) **Microchannel plate(MCP):** The MCP is 1 mm thin plate with an array of $10\mu\text{m}$ holes that are grouped in a hexagonal structure. Between entrance and exit planes of the MCP is a high voltage, so that the electrons hitting the walls of the MCP channels. Generated secondary electrons depends strongly on the MCP voltage (at maximum it is ca.1000).This voltage is set via the image intensifier gain.

3) **Phosphor:** after leaving the MCP the electron cloud is pulled by a voltage of 6000V onto the phosphor. For each electron hitting the phosphor ca 200 "green" photons are generated. This phosphor image is mapped onto the CCD via fiber coupling.

4) **CCD:** The CCD collects the light emitted by the phosphor. The CCD acts as an integrating device. It hold the image information in a matrix of separated image elements (pixels). The photo electron charge of each pixel is read out via the CCD electronics. This analogue signal is digitized by the A/D converter and transferred to computer memory.

Through the image intensifier process the color information of the original image is lost. The photons of all wave length are intensified and the resulting phosphor image is proportional to the total incident light intensity. Still, the overall gain factor depends on a single photons wavelength (because the quantum efficiency of the photo cathode depends on the wavelength). For green incident light the image intensifier gives a light amplification of ca. 10^4 at maximum MCP voltage.[7]

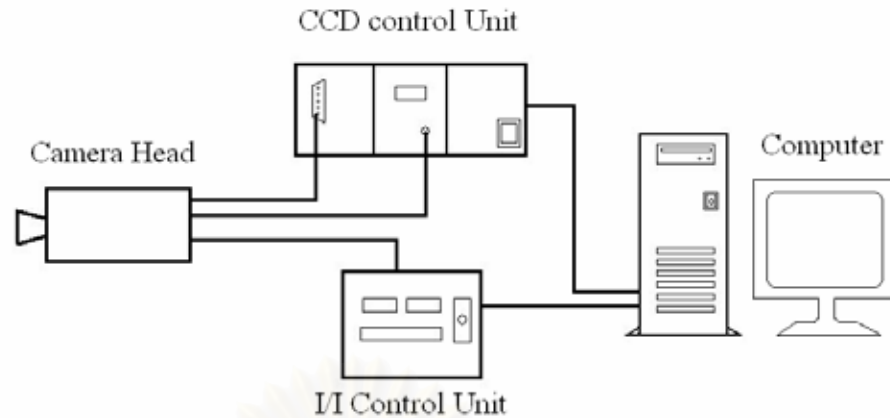


Fig. 3-35 The Camera system

Figure 3-35, the head of the camera system consists of an image intensifier that is coupled to the CCD sensor via fiber optics.

The image intensifier (I/I) is operated by the I/I control unit. It contains electronics to set the intensifier gain and the opening time (gate width) of the image intensifier.

The CCD is operated by the CCD control unit (CCU). It contains the CCD electronics and the thermoelectric (TE) stabilizer.

When acquiring an image, the information is stored on the CCD inside the camera head. The CCD image is read out to the CCD control unit. With the CCD electronics, the camera signal is processed and converted to an analogue slow scan video signal. This signal is transferred to an A/D Converter inside the PC. Here the analogue signal is digitized and stored in a buffer.

All these working steps have to be synchronized. The synchronization can be done either by an external clock or by the computer.

ICCD camera was installed on the X-Y adjustable plate and set the focus length at the nozzle tip position, 76 cm from front camera lens, as shown in figure 3-36.

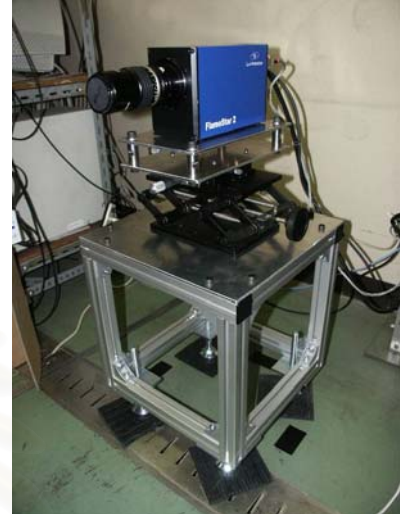
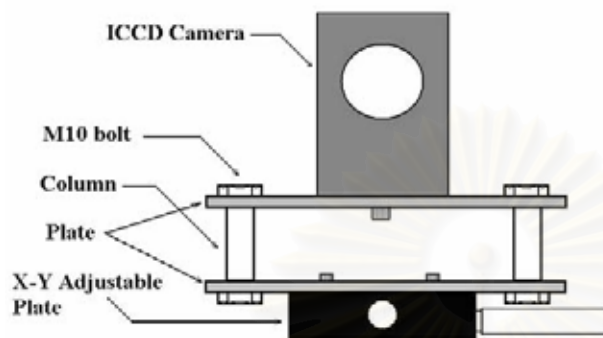


Fig 3-36 ICCD Camera and parts

Figure 3-37 shows the setting up of two color method. Two difference wave length filter 488 and 634 nm were mounted at the front of camera lens and the image was separated to be two by Vari len.

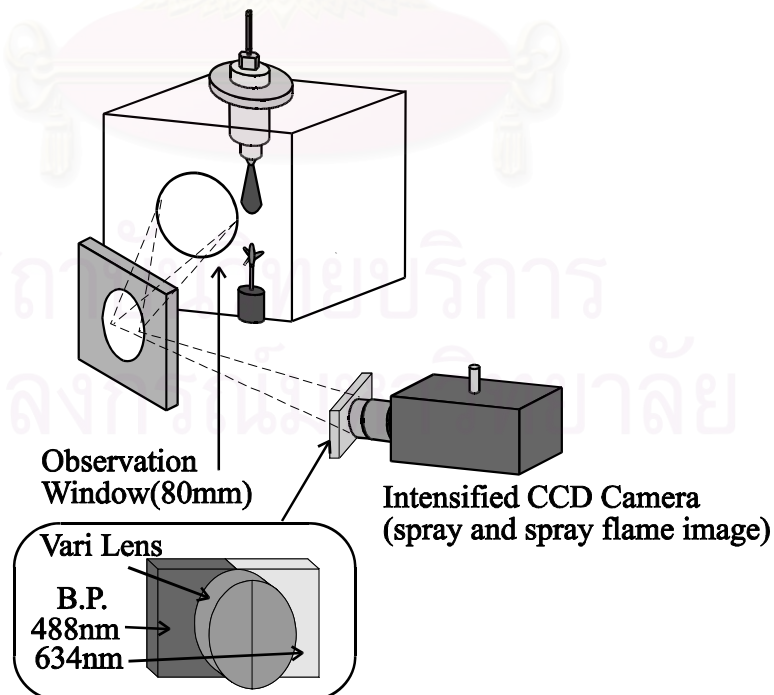


Fig 3-37 ICCD Camera and Two color method set up [9]

Table 3-7 ICCD camera specification

ICCD Camera	LA vision Flame star
Camera sensitivity (max)	60 counts / photo electron
Reference Pos	6.3 scales setting (Corresponds 1 to count / phot el.)
Min. gate	5 nsec
Dark image intensity (top)	200 counts Temp 25 °C
Read out frequency	1.8 MHz
Read out time / Frame	75 msec
RMS (single image)	2.0 counts Temp 10 °C
Computer System	Pentium III 500 MHz
Hard disk	10 GB
RAM	128 MB

Table 3-8 ICCD camera lens and filter specification

Lens:	Nikon 105 mm Diameter 52 mm, F1.8
Vari lens:	Kenko Vari Mirage 52
Filter1 Center wave length	488 nm
Transmittance	46 %
Full width at half max (FWHM)	11.3 nm

Table 3-8 ICCD camera lens and filter specification (continue)

Filter2 Center wave length	634	nm
Transmittance	40	%
Full width at half max (FWHM)	8.5	nm

3.2.6 Control system of experiment

Some experiment apparatus of control system are shown in figure 3-39 and to control the experimental combustion conditions and injection timing, the 9 channel and 4 channel delay pulse generators were used. The system flow chart is shown in figure 3-38. The system started after pushing the start button. The pulse (5 Volt) was generated to 9 channel delay generator, used only channel 1, 4, 6 and 7. The working steps of system are:

- a) Push start button: to generated pulse 5 voltage to 9 channel delay.
- b) Set 1st channel of 9 channel delay generated pulse, delayed 0.1 msec width 1 sec, to A/D converter, to start measuring ambient pressure inside combustion chamber.
- c) After delay 0.145 msec, set 7th channel generated pulse (width 0.005 msec) to start spark plug for hydrogen combustion.
- d) At experiment condition (3 MPa), fuel was injected after the mixing propeller stopped 0.05 msec, that was controlled by channel 4th and 6th (only ch.6th is minus voltage).

สถาบันวิทยบริการ
จุฬาลงกรณ์มหาวิทยาลัย

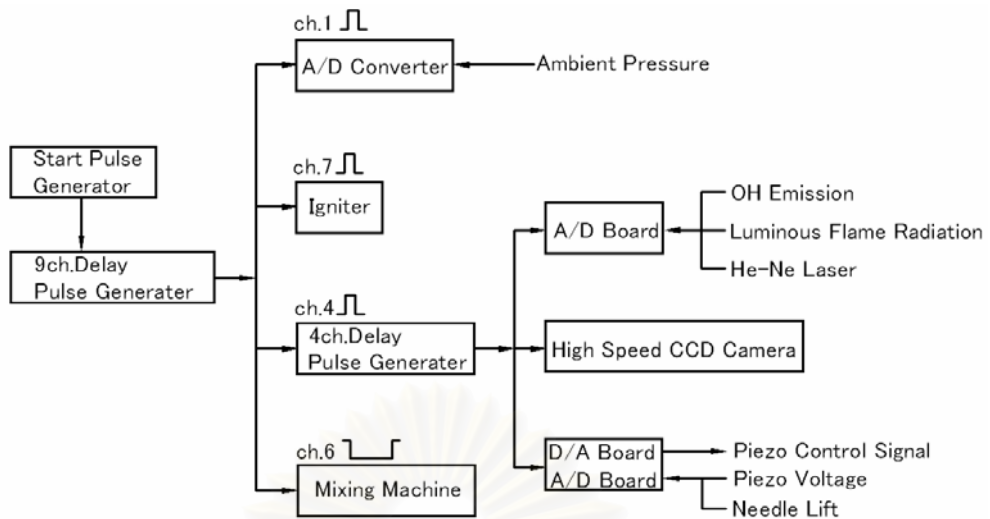
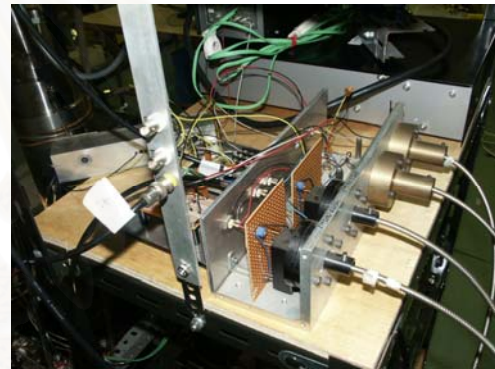


Fig.3-38 Control sequence of experiment



(a) 9 Channel delay pulse generator

(b) Photo sensor and diode circuit board



(c) Start pulse generator



(d) A/D board

Fig.3-39 System controller and components

3.2.7 The experimental set up for studying on spray characteristics

The study on spray characteristics was done with opening one side of the vessel and still heating up over 100 °C. The spray was illuminated by a tungsten lamp and the images were captured by ICCD camera with exposure time of 10 μ sec. The test was performed with diesel fuel and palm diesel 80 % at injection pressure of 100 and 60 MPa. Experiment apparatus set up for studying of fuel spray is shown in figure 5-40.

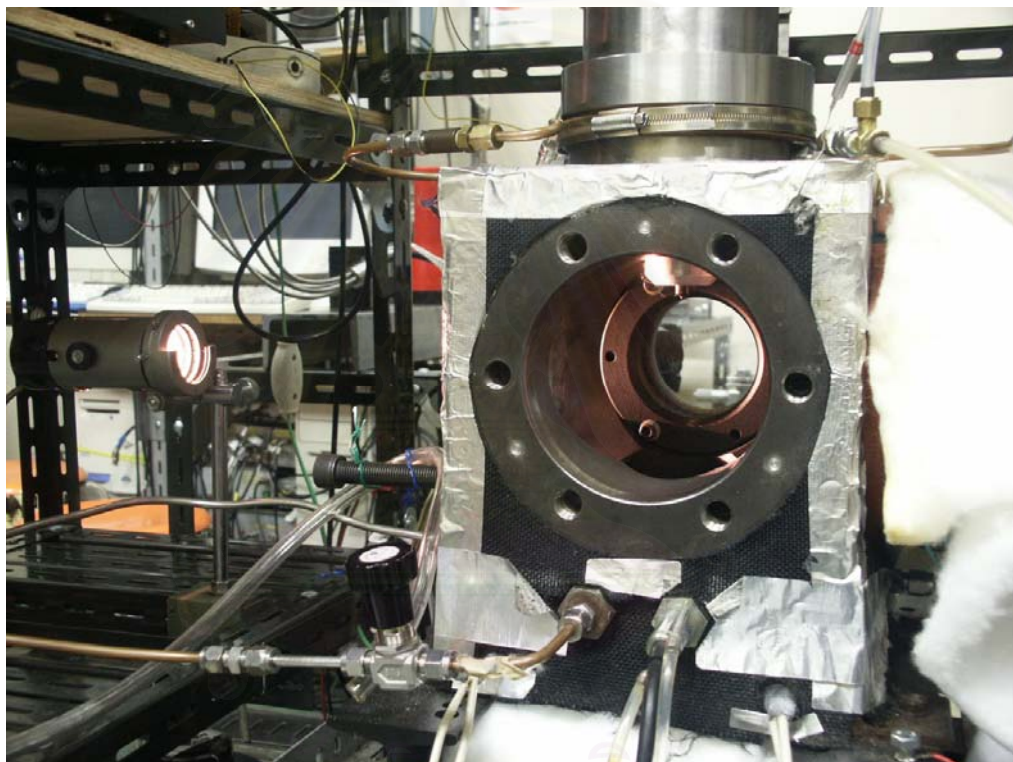


Fig. 3-40 Experiment apparatus set up for studying of fuel spray

Table 3-9 Light source lamp specification

Light source	Olympus
Lamp type	Tungsten lamp
Voltage	5 V

CHAPTER IV

EXPERIMENTAL PROCEDURE

This chapter describes the experimental procedure followed the experiment of investigation and examine the palm diesel spray and spray combustion characteristics. The main experimental conditions were studied and selected.

4.1 Injection rate calculation

4.1.1 Peak Injection rate and injection pressure control

The experiment was desired to study the effect injection pressure on combustion phenomenon. The relation between injection rate and pressure drop across the nozzle is described as below:

$$\dot{m}_p = C_i \sqrt{\Delta P_1}$$
$$\frac{\dot{m}_{P_1}}{\dot{m}_{P_2}} = \frac{\sqrt{\Delta P_1}}{\sqrt{\Delta P_2}} \quad (4-1)$$

\dot{m} is the injection rate (g/s)

C_i is the constant of fuel injection system as the function of nozzle minimum area, discharge coefficient, fuel density and pressure drop across the nozzle. [6]

ΔP_1 is pressure drop across the nozzle (MPa)

ΔP_2 is pressure drop across the nozzle (MPa)

The injection system was set, in order to achieve injection rate close to the peak of peak injection rate of nozzle, by adjusting the shim plate between the Piezo case and stand.

Figure 4-1 is the Piezo voltage shape for measuring the peak of the injection rate. The data obtained from "Pick up sensor", the pressure sensor which mounted to nozzle tip and measured the force of fuel spray, was used of calculated the average injection rate by dividing pick up injected fuel weight with injection period.

The results have to relate as equation 4-1. The injection rate of this experiment at injection pressure 40 MPa, 60MPa, 80MPa and 100MPa is shown in figure 4-2 and the constant factor (C_i) of each injection pressure could also calculated by this graph data.

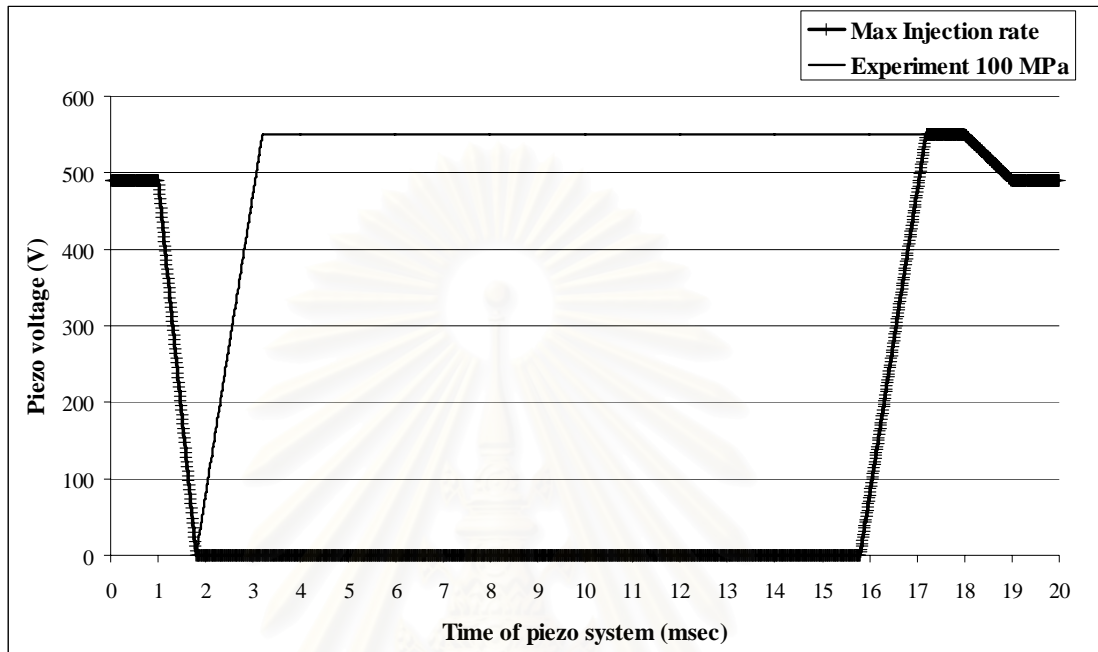


Fig. 4-1 Piezo voltage shape for maximum injection rate setting up

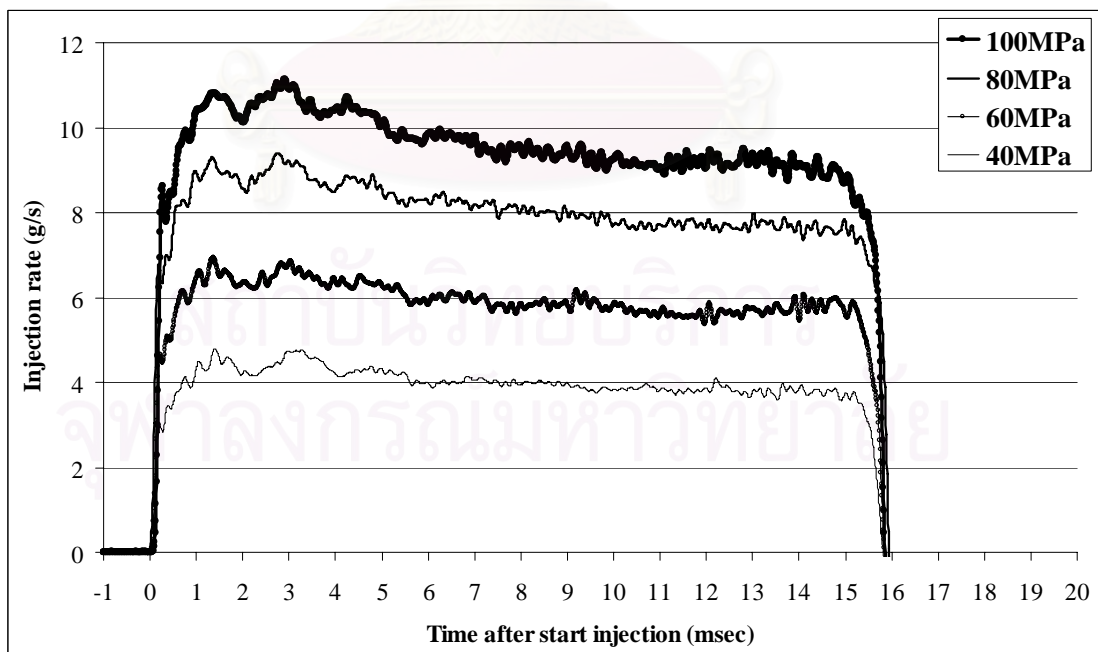


Fig. 4-2 The maximum injection rate of each injection pressure

4.1.2 Injection rate and injection pressure control of experiment

In the experiment, chosen Piezo voltage shape, as shown in figure 4-3, was chosen due to some reasons:

a) The higher slope of the shape could eliminate the effect of fuel viscosity which is high in case of our investigated palm fuel.

b) This injection period of this experiment is close to the phenomenon in a real engine.

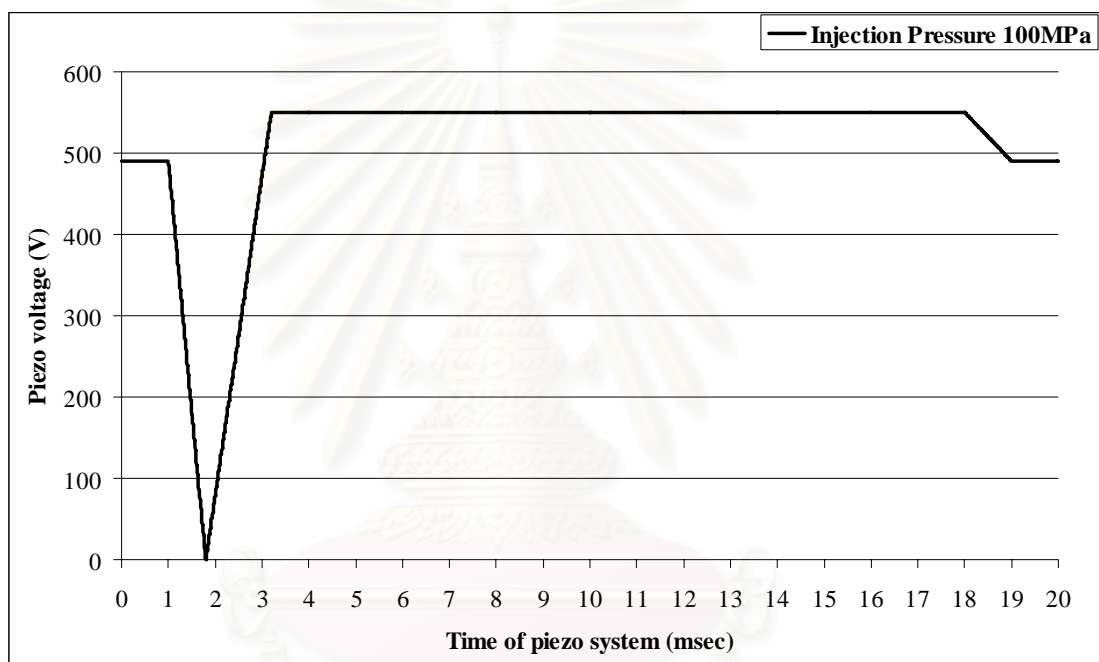


Fig 4-3 Piezo voltage shaping control

The results obtained from “Pick Up sensor” of diesel, palm diesel 60, 80% and 100% palm oil, are shown in figure 4-4. This data and constant factor (C_i) were used to calculate the fuel injection rate.

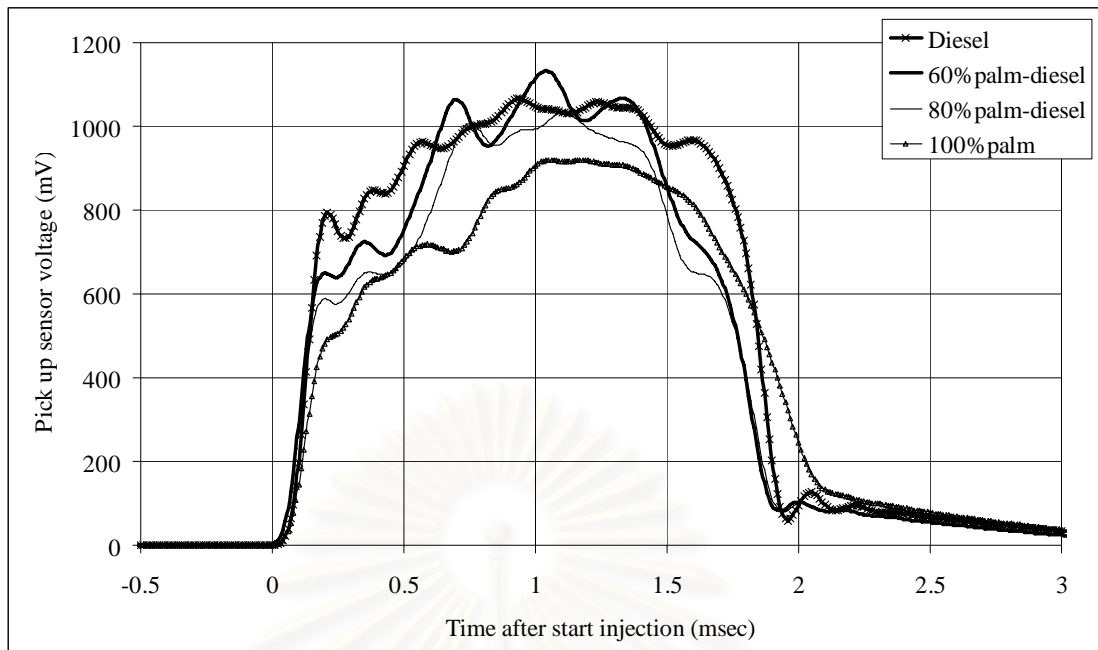


Fig 4-4 Injection rate shaping measured from pick up sensor (pressure sensor)

From the raw data of figure 4-4, the sensor voltage of palm diesel was lower than diesel fuel which meant that blended palm oil affected the fuel spray phenomena.

The repeat ability of the injection system set up was also checked by comparing the current figure 4-4 with that obtained in the previous experiments.

To adjust the injection system for injection pressure 40, 60, 80 and 100 MPa and maintain the injection mass 15 mg, extending the injection timing and changing shim plate were applied. Therefore, Piezo voltage shaping was adjusted as figure 4-5. The decreasing and rising slope were fixed for all injection pressures to obtain the similar injection rate shaping. By this method, the injection rate was obtained as shown in figure 4-6. The relation between injection rate, injection pressure and injection period are shown in table 4-1.

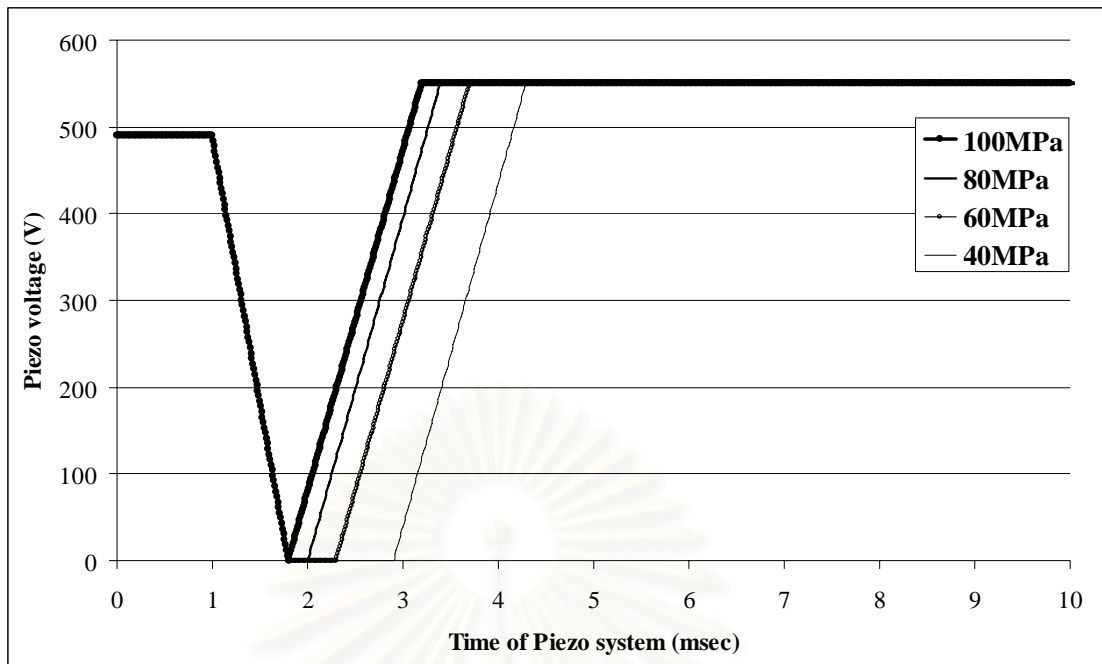


Fig. 4-5 Piezo voltage shape for injection pressure 40, 60, 80 and 100 MPa

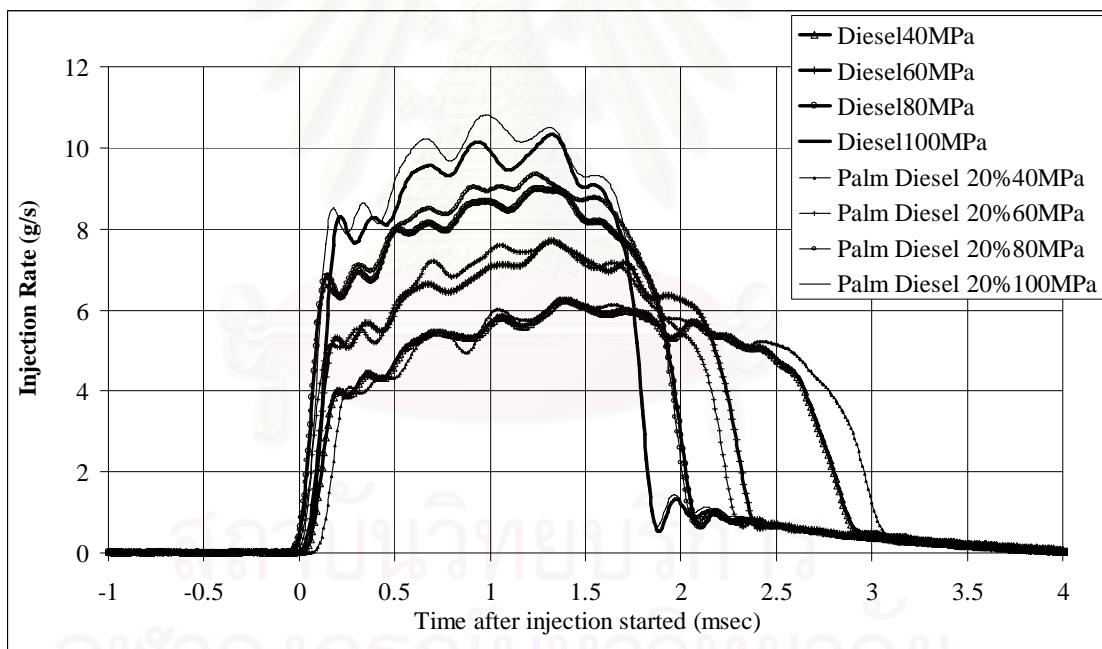


Fig. 4-6 The injection rate of palm 20% and diesel
at injection pressure 40, 60, 80 and 100 MPa

From figure 4-6, the increase of the injection period of each injection pressure was not constant because injection mass is the function of square root injection pressure as described in equation 4-1.

Table 4-1 The relation of injection rate, injection pressure and injection period
(by Piezo voltage control)

Injection Pressure	Injection rate (g/sec)	Injection period (by Piezo voltage control) (msec)
100 MPa	10.15	2.2
80 MPa	9.01	2.4
60 MPa	7.92	2.7
40 MPa	6.29	3.3

4.1.3 Injection rate shaping for palm diesel blended at 20%, 40%, 60%, 80% and palm diesel 100%

The same Piezo voltage shape was also applied for another percentage palm blend with injection pressure 60MPa and 100 MPa, as shown in figure 4-7 and 4-8. Only in the case of palm 100% experiments the injection period was extended by 0.4 msec to minimize the difference of the amount of injected fuel.

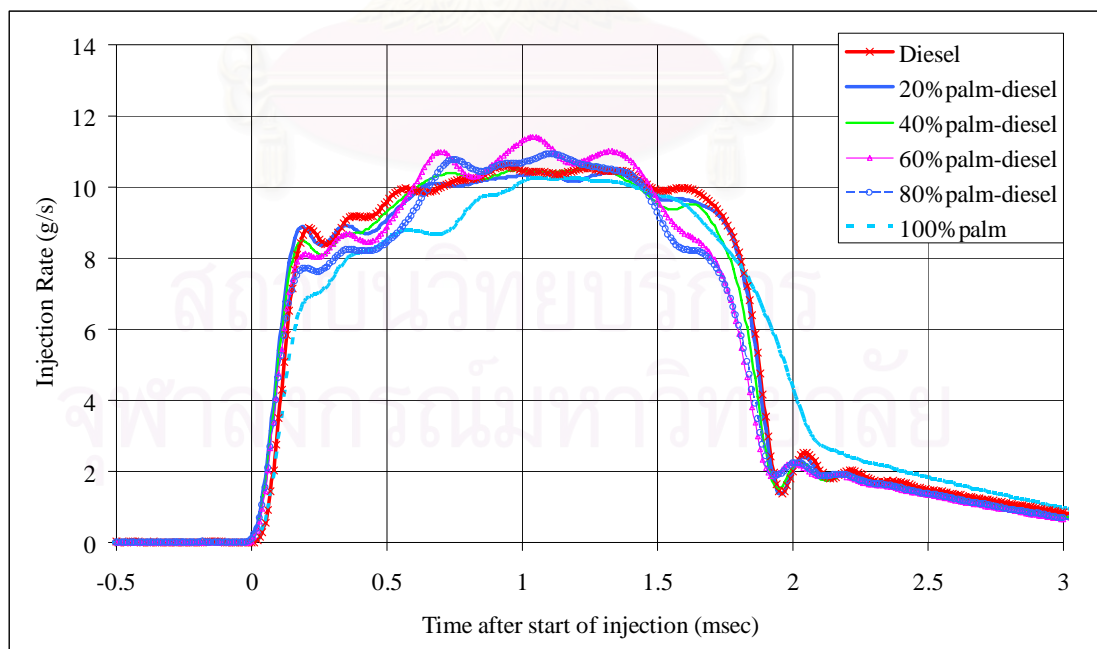


Fig. 4-7 The injection rate of 20, 40, 60, 80%palm diesel, 100%palm and diesel at injection pressure 100 MPa

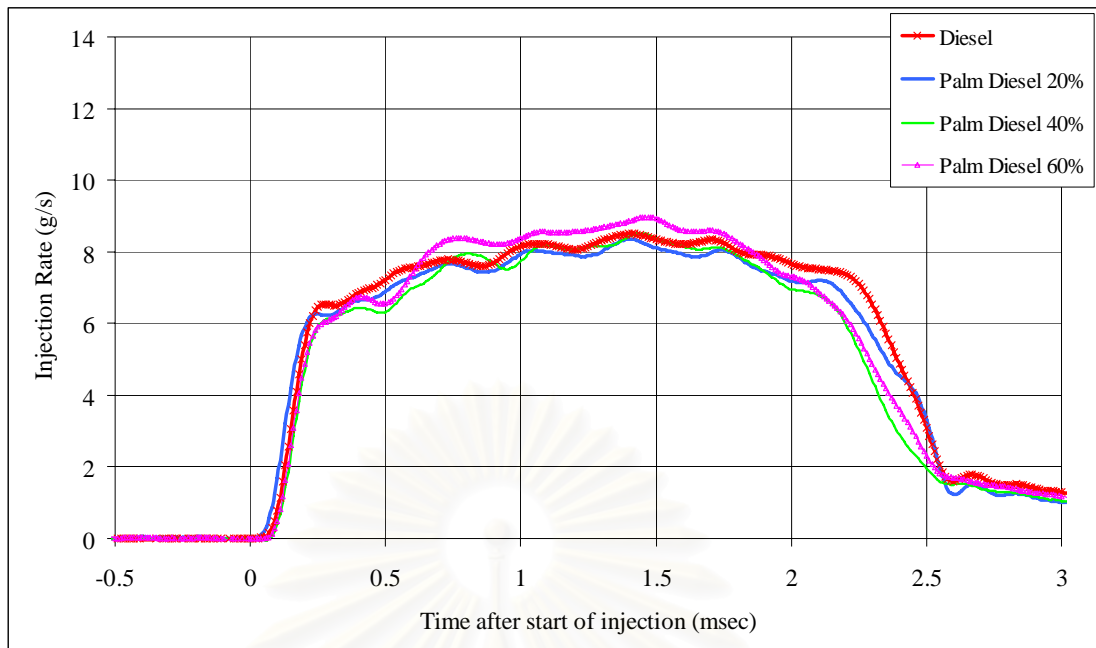


Fig. 4-8 The injection rate of 20, 40, 60% palm diesel and diesel at injection pressure 60 MPa

Since injection mass tends to decrease and start of injection tends to retard as palm percentage increase, the attempt to maintain injection mass at 15 mg and controlled the start of injection at same point was done by a little bit increasing the injection line pressure. This increase was less than 2% for injection pressure 100 MPa and less than 1% for injection pressure 60 MPa.

4.2 The gas composition and ambient conditions inside combustion chamber after hydrogen combustion

Environment inside the combustion chamber was made to be suitable for combusting the fuel spray at that similar to real engine. To obtain the proper conditions inside the chamber at the high temperature and pressure with Stoichiometric conditions, a mixture of O_2 , H_2 and air, shown in table 4-2, was applied and expected to create combustion environment with 21% O_2 by volume, calculated by Gordon program [9].

Table 4-2 Hydrogen combustion mixing gas composition

Before combustion		
Air	Hydrogen	Oxygen
84.5%	12.3%	10.3%

After combustion		
Nitrogen	H ₂ O	Oxygen
71 %	8 %	21 %

Table 4-3 Standard heat of formation

	$\Delta H_{f, 298}^0$ (MJ/kmol)		$\Delta H_{f, 298}^0$ (MJ/kmol)
H	218.11	C ₂ H ₄	52.50
H ₂	0	C ₂ H ₆	-84.72
H ₂ O	-241.99	C ₃ H ₆	20.43
H ₂ O(l)	-286.03	C ₃ H ₈	-103.92
N	472.96	<i>n</i> -C ₄ H ₁₀	-126.23
N ₂	0	<i>n</i> -C ₅ H ₁₂	-146.54
NO	90.35	<i>n</i> -C ₆ H ₁₄	-167.30
NO ₂	33.12	<i>n</i> -C ₇ H ₁₆	-187.95
O	249.36	<i>n</i> -C ₈ H ₁₈	-208.59
O ₂	0	C ₆ H ₆	82.98
OH	39.49	C ₇ H ₈	50.03
C(s)	0	CH ₃ OH	-201.30
CO	-110.60	C ₂ H ₅ OH	-235.46
CO ₂	-393.79	S	0
CH ₄	-74.92	SO ₂	-297.04
C ₂ H ₂	226.88	SO ₃	-396.02
		NH ₃	-45.92



$$\begin{aligned} \Delta H_{298}^0 &= 1x(\Delta H_{f,298}^0)_{\text{H}_2\text{O}} - 1x(\Delta H_{f,298}^0)_{\text{H}_2} - 1/2x(\Delta H_{f,298}^0)_{\text{O}_2} \quad (4-3) \\ &= 1x(-241.99) - 0 - 0 \\ &= -241.99 \text{ MJ/kmol} \end{aligned}$$

$$\begin{aligned} \text{H}_2\text{O}; \quad 1 \text{ kmol} &= 18 \text{ kg} \\ -(-241.99)/18 &= 13.443 \text{ MJ/kg} \end{aligned}$$

By using the standard heat formation, the heat of hydrogen combustion could be estimated as 13.4 MJ/kg. But the actual chemical combustion was more complicated, therefore, the combustion temperature was calculated by computational program for chemical combustion "CHEMKIN". The equilibrium closed homogeneous combustion model was selected and the result of the maximum combustion temperature was approximately 1200 °C.

Figure 4-9 represents the gas pressure inside combustion vessel after combusting the hydrogen at the selected proper gas mixing composition and starting time. The pressure inside the vessel rose up to 3.9 MPa and decreased caused by the effect of the heat transfer to the ambient.

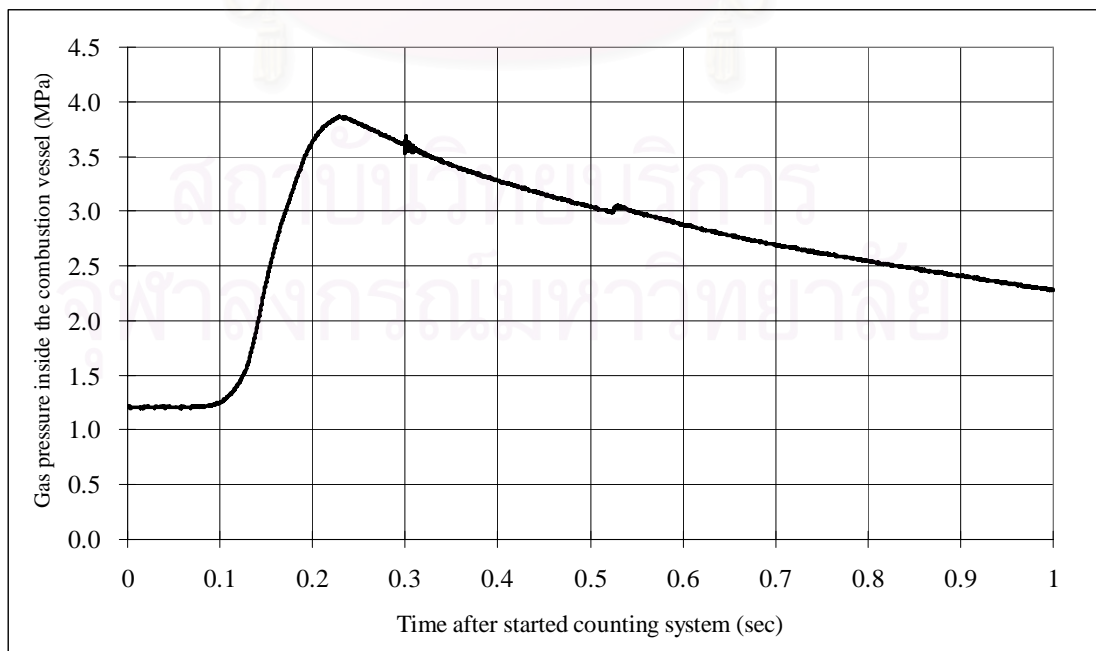


Fig. 4-9 Gas pressure inside combustion vessel

4.3 The setting up of two color method system

ICCD camera used in the experiments was Lavision Flame star II, the camera was focused away from the nozzle tip 76 cm from front lens, adjusted to obtain the clear and large flame images of both filters, red and blue.

The utilization of 2 color method, calibration graph was required for calculating apparent temperature (T_a) of the two monochromatic wave lengths. Apparent temperature (T_a) is the temperature at which a black body would have the same monochromatic intensity of radiation as the non-black body.

There are many methods for making the calibration graph:

- a) Calibrating with black body condition.

This method is difficult to obtain black body condition and consumes much time.

- b) Calibrating with tungsten ribbon.

This experiment was done with this method because using tungsten ribbon has several advantages:

- a) Easy to get proper condition
- b) Could repeat experiment many times.

4.3.1 Experimental apparatus set up for two color method camera calibration

Virtual images of a tungsten ribbon at varied temperatures from 1300 to 1600 °C (with step of 100 °C, done by varying the input electrical current) were taken with calibration systems as shown as in figure 4-10 and 4-11.

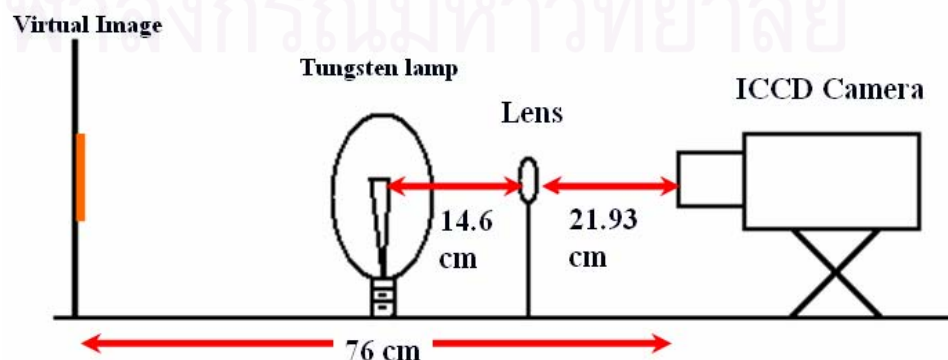


Fig 4-10 The schematic diagram of ICCD calibration for two color method

The position of lens and tungsten lamp is in relation with the camera lens focus length which was 76 cm (from front lens) in this study, virtual image would occur at this distance far from the front lens.



Fig 4-11 Calibration experiment for two color method

4.3.2 Virtual image position equation

The equation 4-2 was applied for calculating the virtual images position. The focus length of tungsten lamp lens was 20 cm and the result of the calculation, shown in figure 4-10

$$\frac{1}{f_L} = \frac{1}{D_s} + \frac{1}{D_i} \quad (4-2)$$

f_L = lens focus (lens for tungsten lamp)

D_s = Distance from subject to lens

D_i = Distance form image to lens

4.3.3 Calibration experiment method

The camera exposure 10 μ sec was selected and took the images of a tungsten ribbon on each filter by varying input electric current of the tungsten lamp at 1300, 1400,

1500 and 1600 °C. The relation between input electrical current and temperature of tungsten ribbon is shown in table 4-4.

Table 4-4 The relation temperature of tungsten lamp and input amplifier

Temperature (C)	Amplifier (A)
1000	6.94
1100	7.43
1200	8.03
1300	8.71
1400	9.48
1500	10.36
1600	11.26
1700	12.27
1800	13.37

The images of tungsten ribbon corresponding to red and blue filter were taken separately first at 1600 °C (11.26 A of the amplifier current) and then 1500, 1400, and 1300 °C. The calibration was repeated 5 times.

สถาบันวิทยบริการ
จุฬาลงกรณ์มหาวิทยาลัย

4.3.4 Calibration experimental results

The image results shown in figure 4-12 are the images from red and blue filter at temperature of tungsten ribbon 1600 °C. Calibration graph for two color method is presented in figure 4-13.



Fig 4-12 Tungsten ribbon intensity distribution at 1600 °C

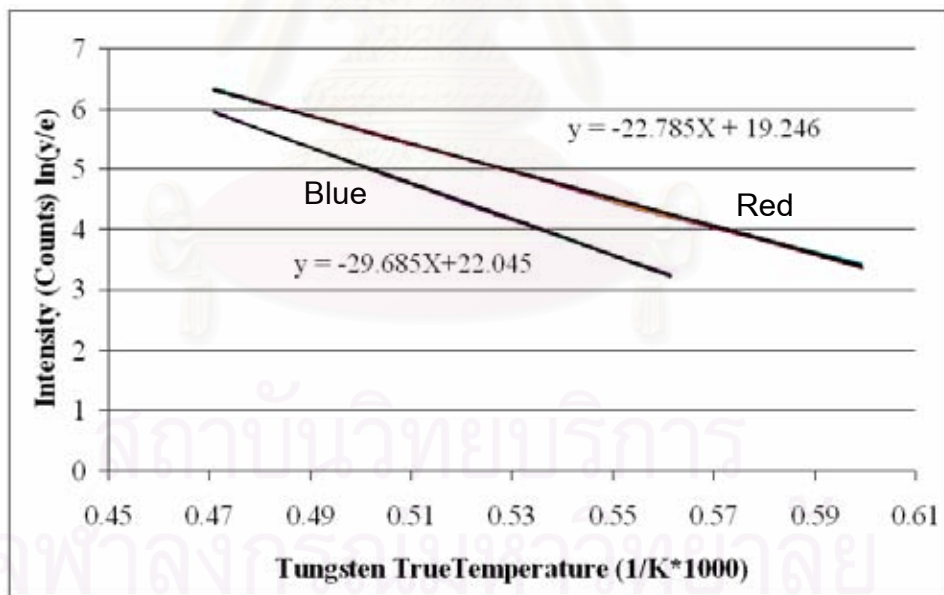


Fig. 4-13 Calibration graph for two color method

Y-axis is natural logarithm of tungsten ribbon's intensity divided by emissivity of well-defined tungsten ribbon in each temperature at wave length between 634 and 488 μm . X-axis is true temperature of tungsten lamp. The emissivity of well-defined tungsten ribbon as a function of wavelength is shown in appendix D. The equation

obtained from calibration graph was used to calculate the apparent temperature (T_a) of combustion flame intensity.

4.4 The combustion period and ignition delay calculation

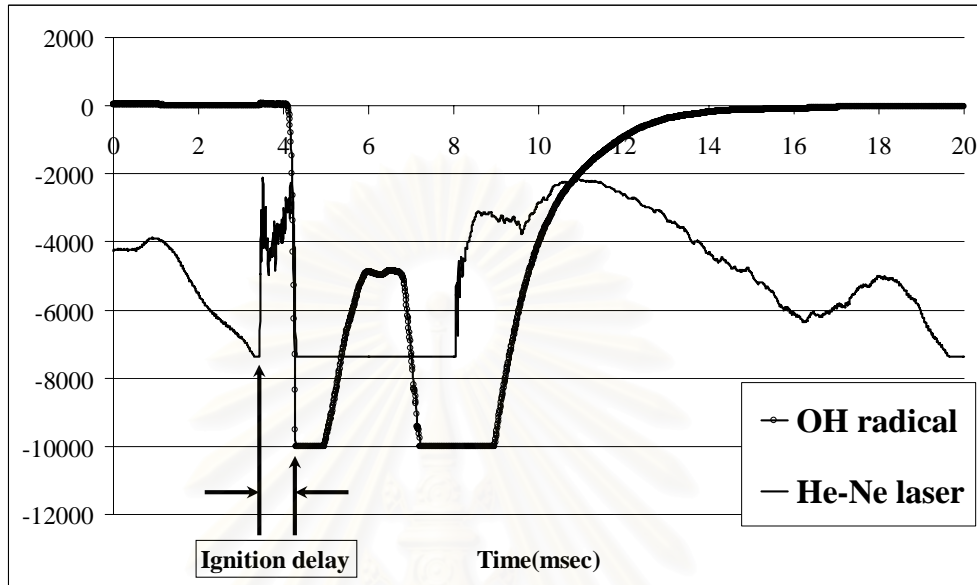


Fig. 4-14 The data of optical sensor

Ignition delay is calculated from time difference of start He-Ne laser pulse and the start of OH-radical as shown in figure 4-14.

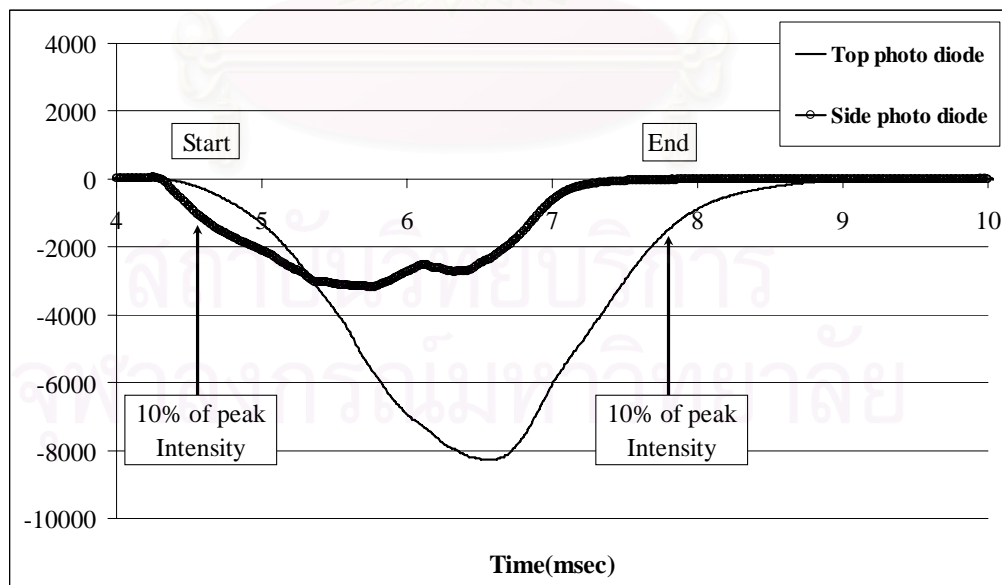


Fig. 4-15 Calculation of combustion period

Combustion period, shown in figure 4-15, is calculated from time difference of 10% of peak data obtained from side and top photo diodes.

4.5 The effects of combustion chamber heating temperature on fuel spray combustion characteristic

4.5.1 Effect on flame visualization

The clear images are required to analyze combustion flame temperature. 'Ghost light', the individual light, caused by not enough heating temperature of the vessel wall must be eliminated. Hence, the combustion chamber heating temperature is concerned.

The figure 4-16 shows the intensity distribution of flame at chamber temperature of 80°C and 100°C. The ghost light could be detected at 80°C but it has decreased after increasing the temperature up to 100°C. This light might be caused by from vaporization of water after hydrogen combustion started.

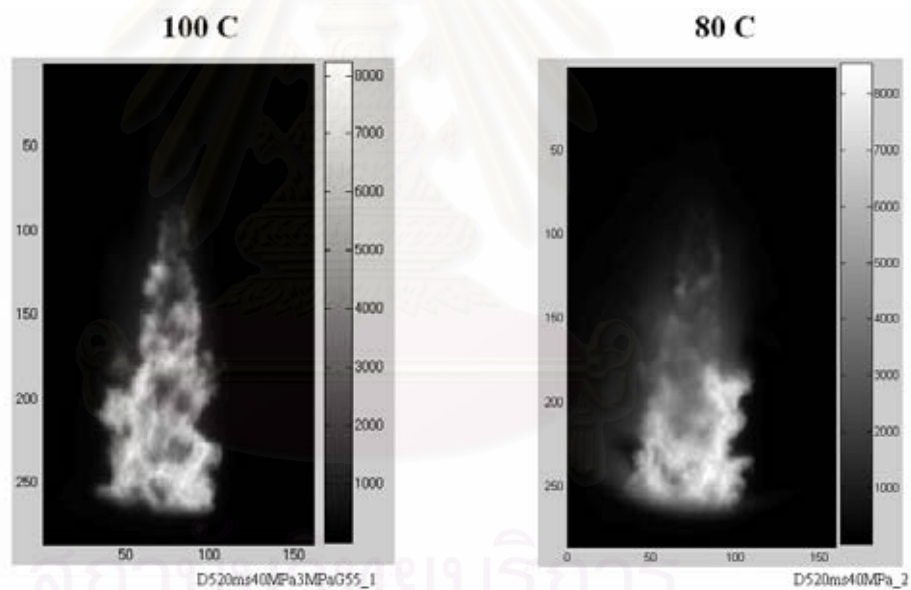


Fig 4-16 Combustion flame intensity distribution (Red filter) at combustion chamber heating temperature 80 °C and 100°C

In figure 4-14, the sectional data obtained at the pixel Y axis at position of pixel 150 and 250 shows more details of the difference between heating chamber 80°C and 100°C .

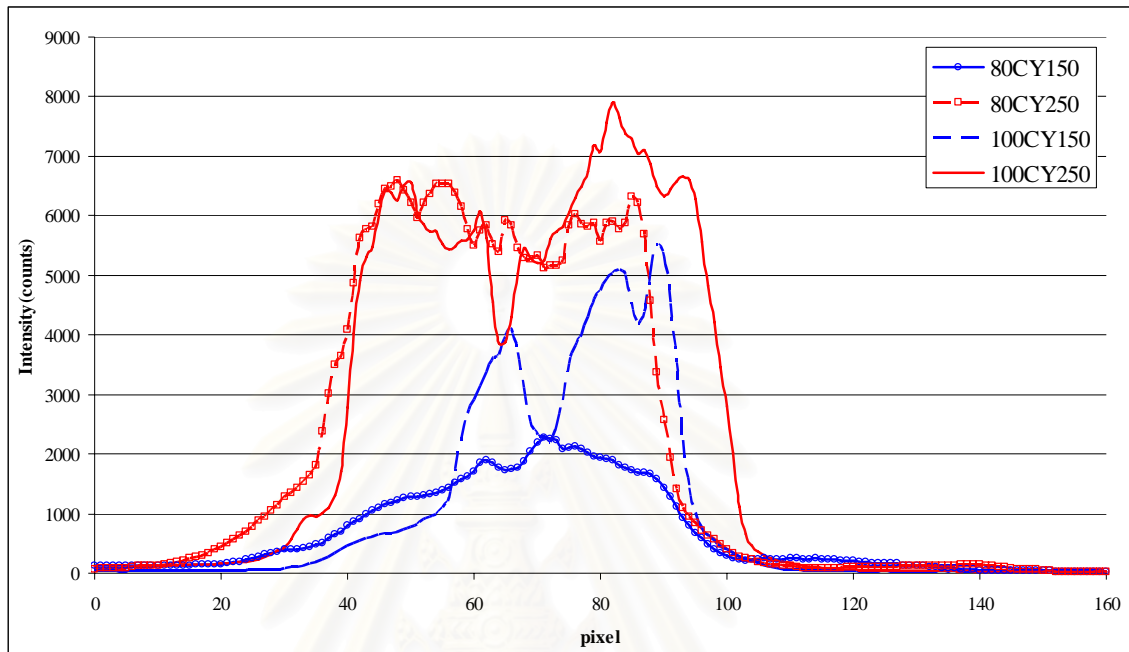


Fig 4-17 Section intensity data of red filter along Y-axis 150 and 250 at combustion chamber heating temperature 80°C and 100°C

The separation between back ground and combustion flame of 100°C could be clearly defined, at around 1000 counts, compared with at 80°C .

สถาบันวิทยบริการ
จุฬาลงกรณ์มหาวิทยาลัย

4.5.2 Effect on combustion ignition delay and combustion period

The effect of combustion chamber heating temperature was studied at 80 °C and 100 °C, injection pressure 40 MPa and 100 MPa. It was found that the effect on ignition delay was very small at both injection pressure.

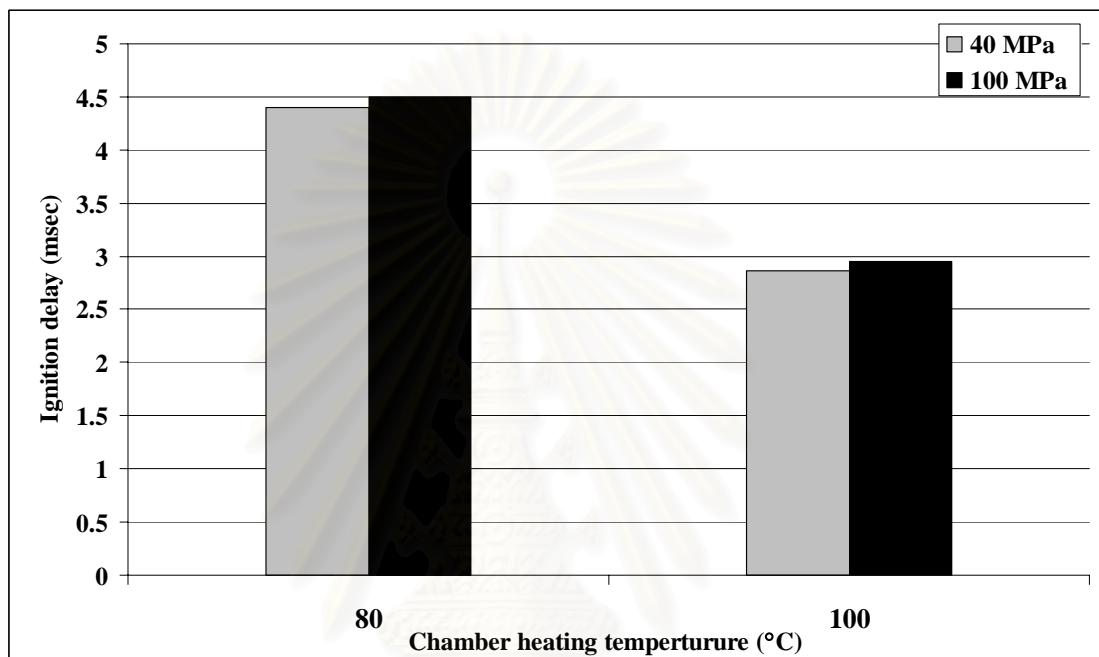


Fig 4-18 Ignition delay at 80 °C and 100 °C chamber heating temperature at injection pressure 40 MPa and 100 MPa

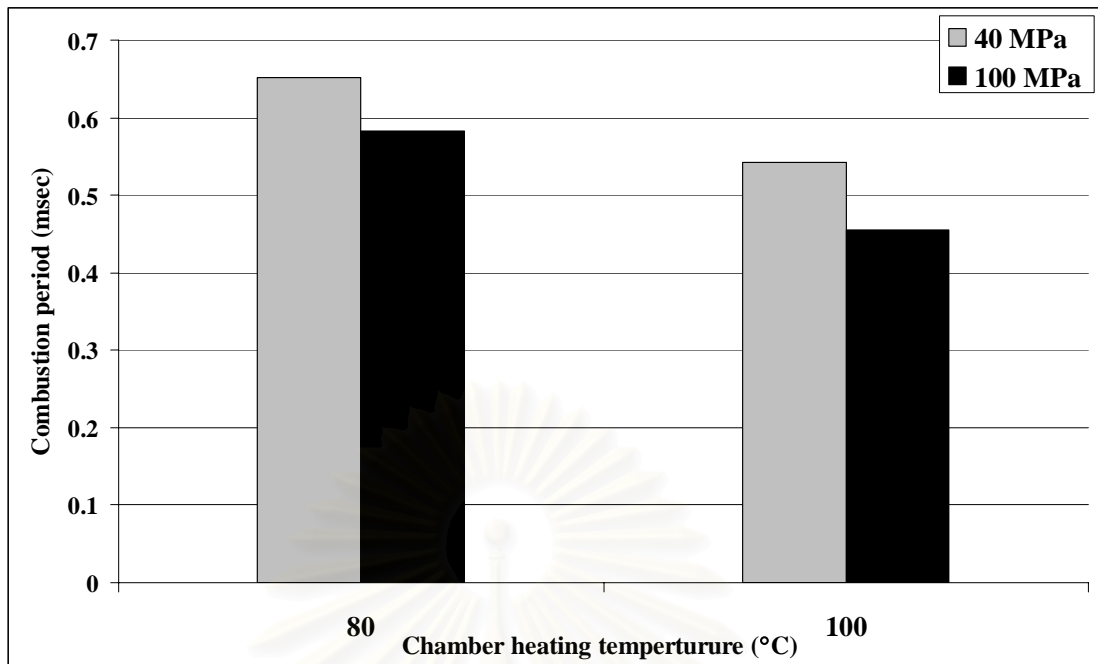


Fig 4-19 Combustion period at 80 °C and 100 °C chamber heating temperature at injection pressure 40 MPa and 100 MPa

Form the figure 4-19, it can be seen that the combustion period was decreased around 0.1 msec at injection pressure 40MPa and 100 MPa.

สถาบันวิทยบริการ
จุฬาลงกรณ์มหาวิทยาลัย

4.6 Images processing for two color method

This section explains the details of images processing of two color method which could be distinguished as 1) ICCD camera image processing and 2) the computational programming for two color method.

4.6.1 ICCD camera image processing

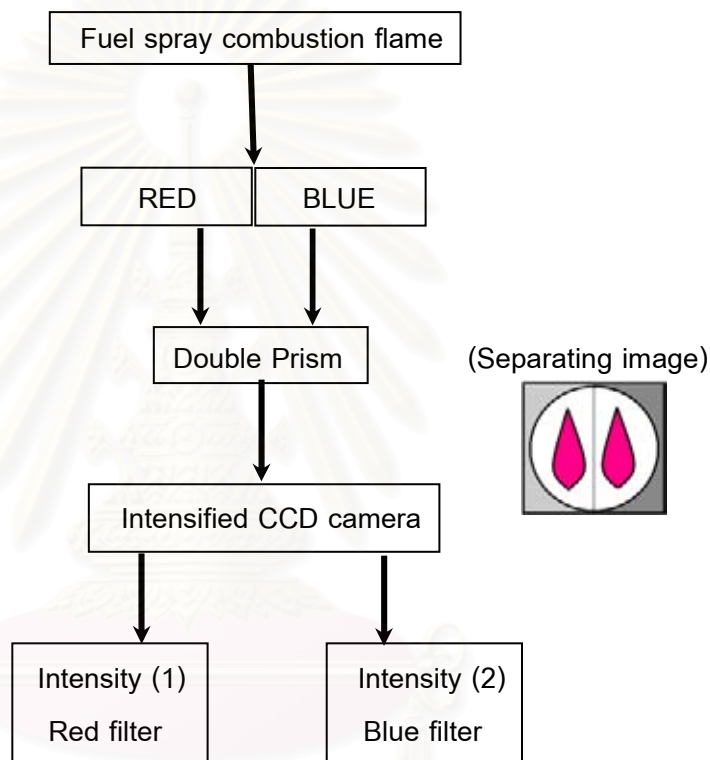


Fig.4-20 ICCD camera image processing for two color method

The fuel combustion light occurred after fuel was spray into the hot gas inside the combustion chamber. By photo technique, double prism (Vari lens) separated the picture to be two at left and right side of camera lens. At the same positions, the filters were mounted on and ICCD camera could take the combustion flame intensity of both wave lengths at the same time.

The experiment of visualization took combustion images flame by flame at list 3 times and changed camera delay times were done to take the images at other time periods.

4.6.2 The computational programming for two color method

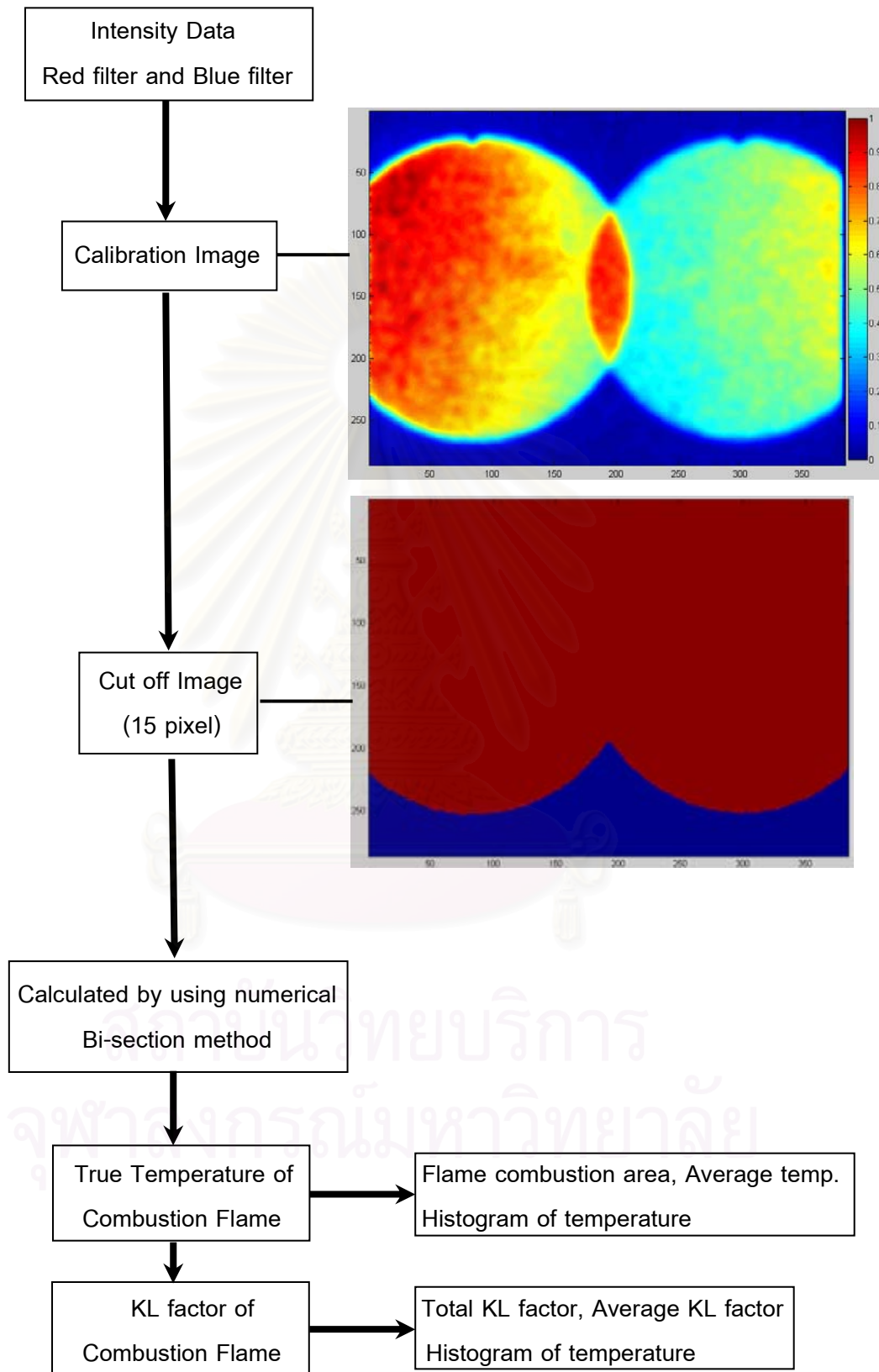


Fig.4-21 Calculation flow diagram of two color method

Consequent steps of programming process can be seen in figure 4-21. The data of light intensity was decoded to ASCII code and divided this data by “Calibration image” to adjust the image back ground.

“Cut off image” removed a part of all images to eliminate the combustion light reflected from the bottom of observation window glass, which caused strange light.

“Bi-section method” takes data from each filter, Red and Blue, at the same matrix dimension and calculates the true temperature of 2-dimensional combustion flame images.

The true temperature is then used to predict KL factor, flame combustion area, histogram, average value and total KL factor.

4.7 The effect of threshold value on fuel combustion flame images

Threshold value is the value of intensity which picks out the combustion area outline from the background. The threshold level was subjectively chosen by studying the combustion light intensity.

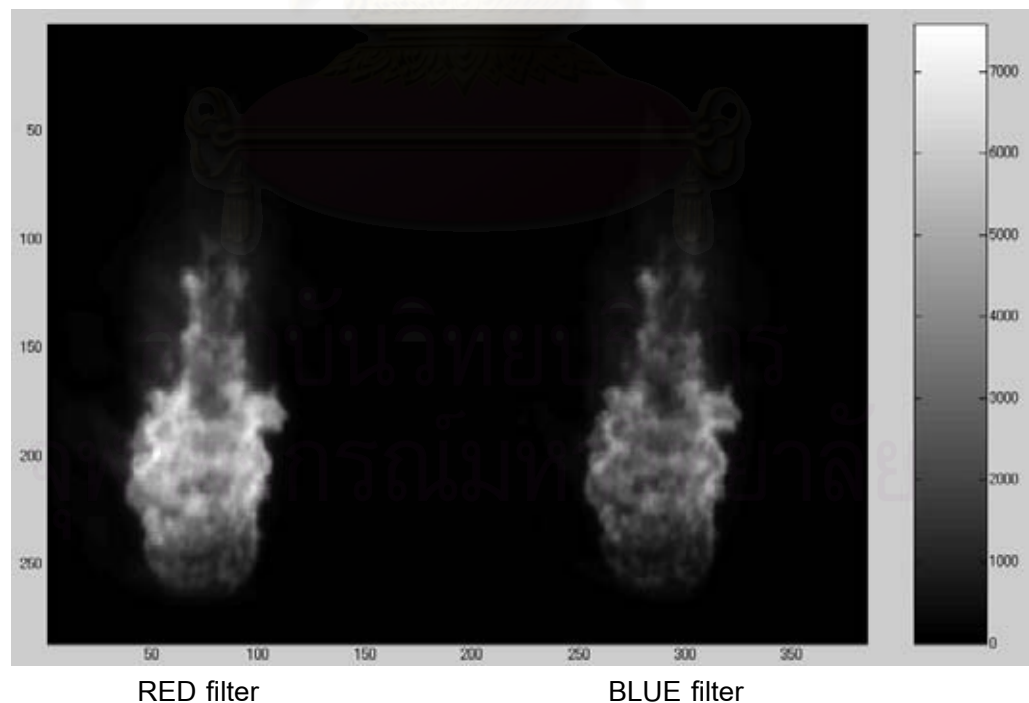


Fig.4-22 Intensity of Diesel combustion flame at injection pressure 40MPa

Combustion at 3.0 MPa , 1.9 msec after started injection

From figure 4-22, the diesel combustion flame intensity of red filter was selected and the data at Y-axis position 50, 100, 150, 200 and 250 were pick up and the result is shown in figure 4-23. The separation between background and combustion flame was determined corresponding to the changing of the data line gradient occurred at the range of intensity between 500 and 1500 counts.

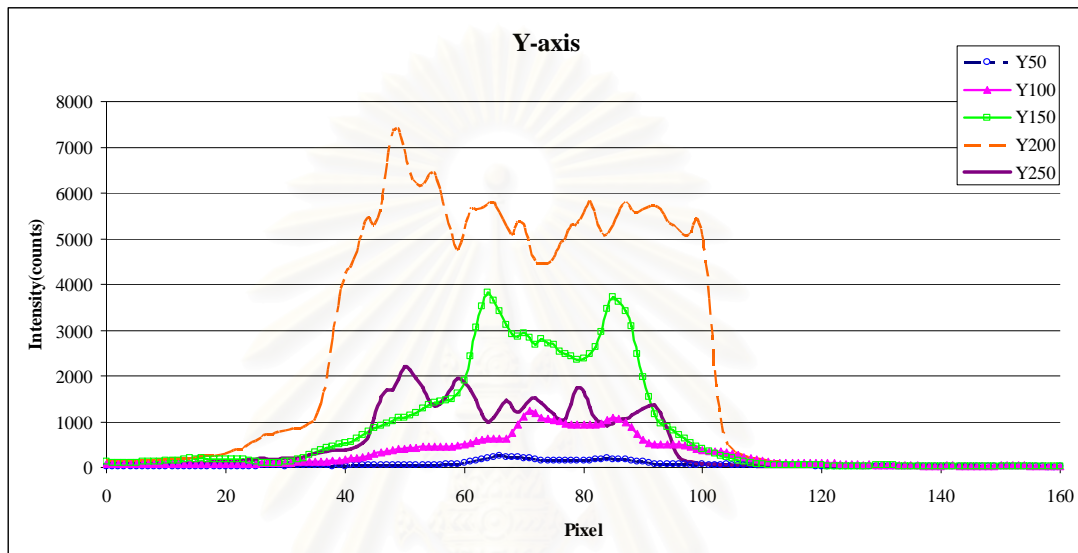


Fig.4-23 Sectional data of red filter along Y-axis (50, 100,150,200 and 250)

Diesel Injection pressure 40MPa Combustion at 3.0 MPa

1.9 msec after started injection

สถาบันวิทยบริการ
จุฬาลงกรณ์มหาวิทยาลัย

The threshold value 400, 900 and 1400 counts were chosen to calculate the flame temperature and KL factor distribution, as shown in figure 4-24. The effect of the threshold and combustion area was more clearly understood.

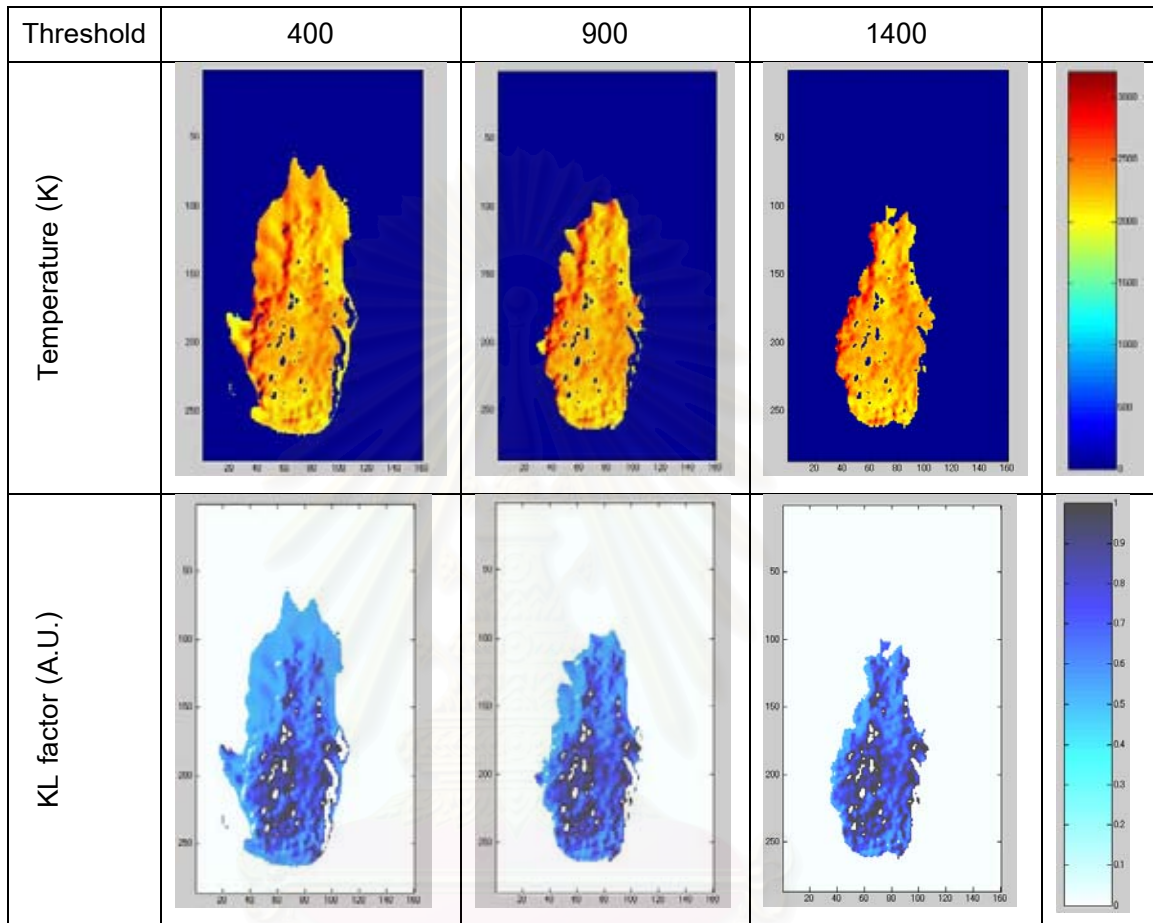


Fig.4-24 The relation of threshold value and temperature and KL factor distribution with different threshold value of 400, 900 and 1400 counts.

สถาบันวิทยบริการ
จุฬาลงกรณ์มหาวิทยาลัย

Average temperature, integration of KL factor and average KL factor predicted with difference thresholds are represented in figure 4-25, 4-26 and 4-27. With higher threshold the combustion area decreases, as seen clearly in figure 4-28, resulting high average temperature and average KL factor but lower integration of KL factor.

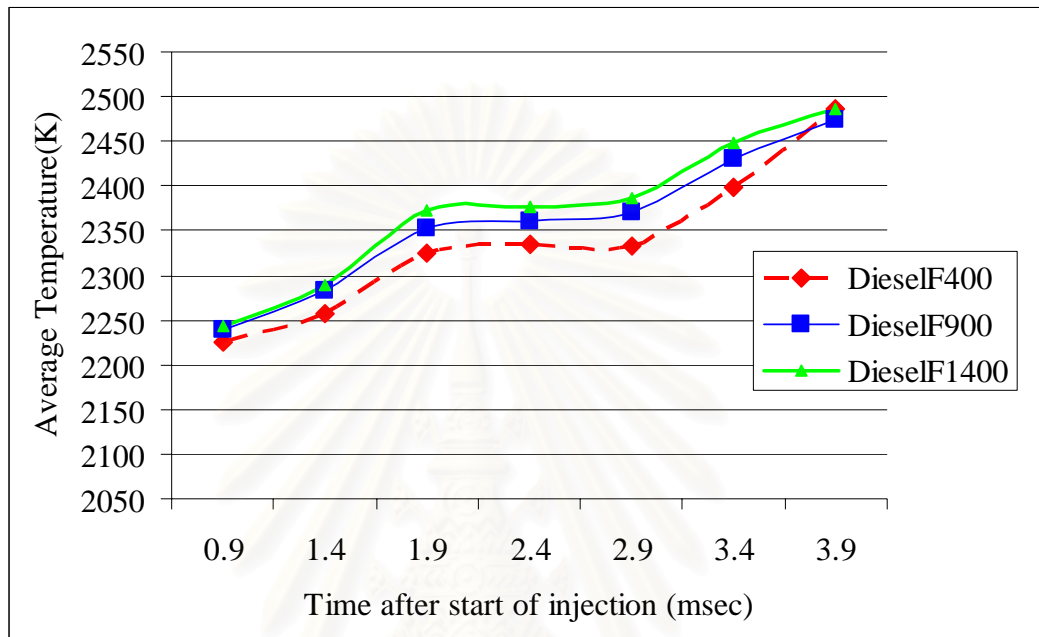


Fig.4-25 Average temperature with different thresholds 400, 900 and 1400 (counts)

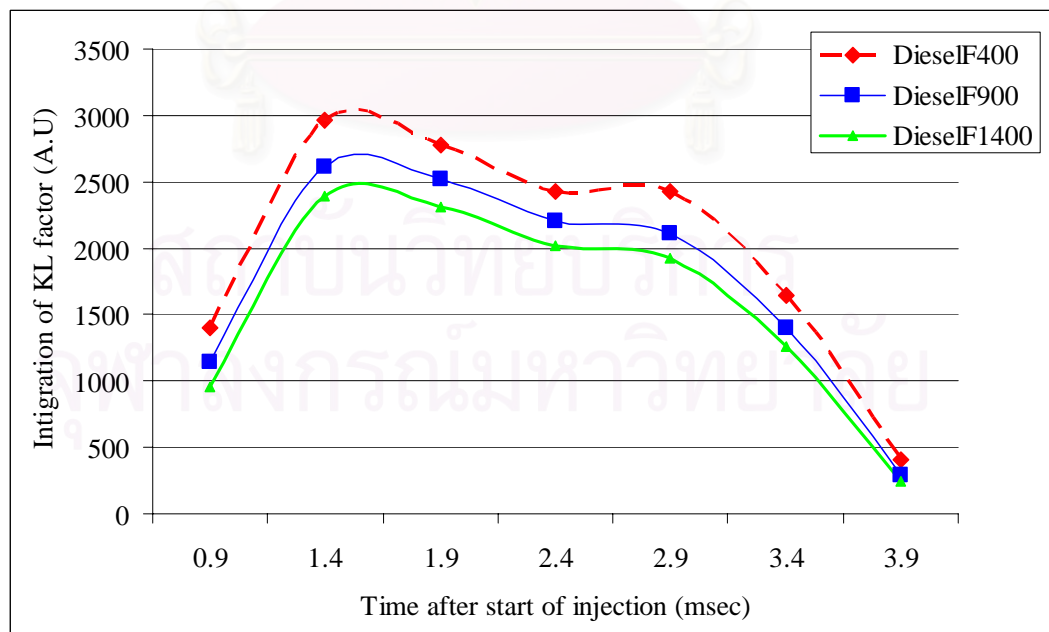


Fig.4-26 Total KL factor with different thresholds 400, 900 and 1400 (counts)

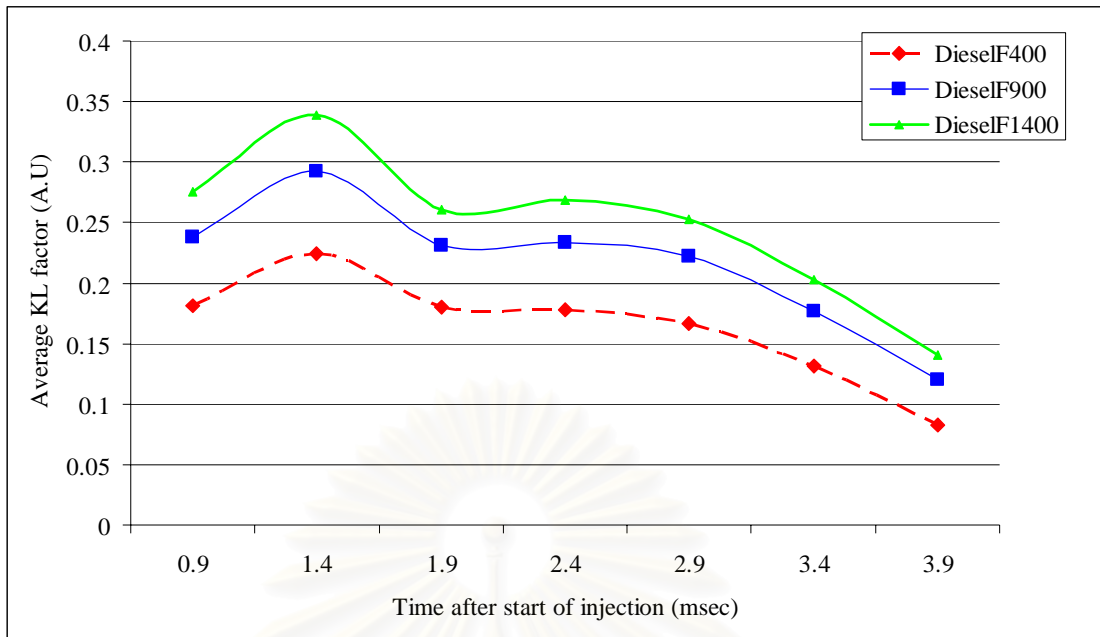


Fig.4-27 Average KL factor with different thresholds 400, 900 and 1400 (counts)

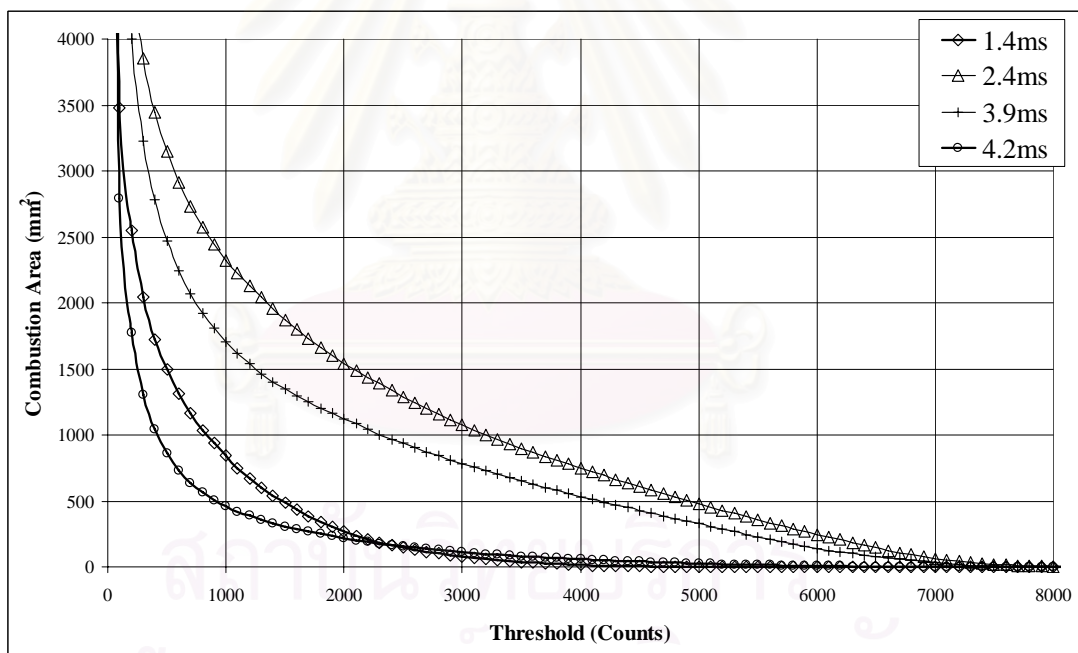


Fig.4-28 Numerical calculation of combustion area with different the threshold values and combustion flame images taken at 1.4, 2.4, 3.9 and 4.2 msec after start of injection

From figure 4-28, the suitable threshold value of images was changed with combustion timing. Therefore, in this experiment the threshold value at 20% from peak intensity of each image was selected.

4.8 Experimental Procedure

1. Cleanup the combustion chamber by acetone and alcohol.
2. Check the electrical cable.
3. Open the cooling water.
4. Close the chamber and heat up until 60°C , starting heat up observation window.
5. Heat the fuel line up to 40°C .
6. Turn on the control system.
7. Heat the palm diesel and diesel fuel and blending together.
8. After the temperature up to 100°C , load fuel into the heating tank.
9. Open the combustion chamber, maintain the temperature at 100°C ,
 - Check injection mass
 - Check injection rate shape
 - Start of the injection
 - He-Ne laser position
 - Check mixing propeller
10. Close the chamber.
11. Open the gas tank and adjust regulator to supply:
Air 40 Kg/cm^2 , H_2 4 Kg/cm^2 and O_2 4 Kg/cm^2
12. Check leak of chamber.
13. Conduct the experiment.
14. After finish the experiment;
 - Close the gas tank. Drain the H_2 and O_2 in line out.
 - Turn windows glass heater off.
 - Decrease the chamber heater to half, after the temperature is under 60°C , turn the chamber heater off.
 - As the temperature is under 40°C turn the cooling water off.

4.9 Experimental flow chart

The experiment started from heating the combustion chamber up to 100°C and fuel line up to 40°C. The proper fuel was loaded into the injection system line. The injection mass and injection rate shape were checked. Close the chamber, adjust and reset the control system. After that, turn on the electrical apparatuses: mixing propeller, starting control and measurement system (waiting for starting signal). Charge gas (Hydrogen, Air and Oxygen) into chamber, at the proper composition and then, pressure up the fuel in line pressure. Push start button to start all electrical apparatuses and measurement system. Finally, drain the combusted gas off by high pressure gas and vacuum pump, after pressure inside drops to atmospheric pressure, check crack on windows glass. Save and check the obtained data. The experimental flow chart is shown in figure 4-29.

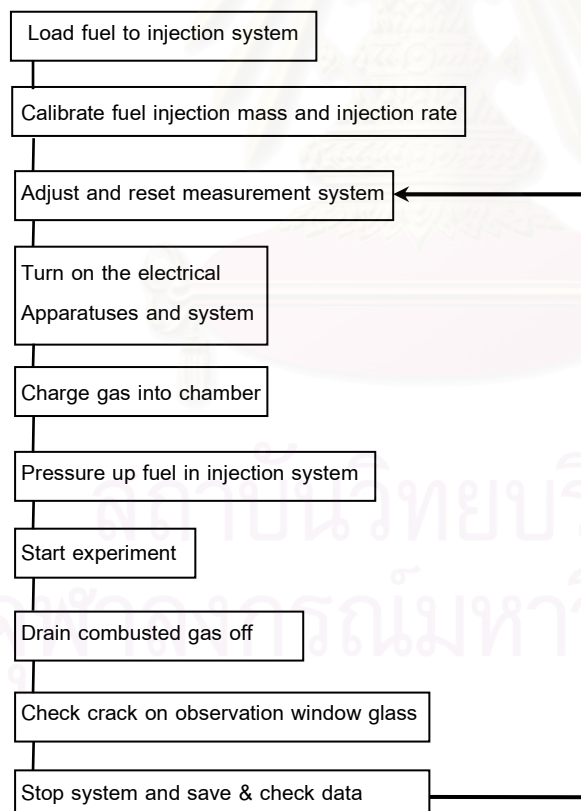


Fig. 4-29 the experimental flow chart

4.9.1 The study on refined palm oil

The experiment of refined palm was conducted as the experiment flow chart, shown in figure 4-29. The experiments of ignition delay, combustion period and combustion visualization were examined separately; first the experiments were conducted to measure the ignition delay and combustion period by photo diode and sensor. Then, the optical sensor was removed and the flame images were taken flame by flame by ICCD camera with different camera's delay times.

4.9.1.1 Ignition delay of the combustion and fuel combustion period

This study was done with varied ambient combustion condition (2.0 and 3.0 MPa), palm blended percentage and injection pressure and shown in table 4-5.

Table 4-5 Test matrix of the study on refined palm spray combustion

Combustion Condition 2.0 MPa						
Injection Pressure	Diesel	Palm diesel 20%	Palm diesel 40%	Palm diesel 60%	Palm diesel 80%	Palm 100%
40 MPa	⊗	⊗				
60 MPa	⊗	⊗				
80 MPa	⊗	⊗				
100 MPa	⊗	⊗				

Combustion Condition 3.0 MPa						
Injection Pressure	Diesel	Palm diesel 20%	Palm diesel 40%	Palm diesel 60%	Palm diesel 80%	Palm 100%
40 MPa	⊗	⊗				
60 MPa	⊗	⊗	⊗	⊗		
80 MPa	⊗	⊗				
100 MPa	⊗	⊗	⊗	⊗	⊗	⊗

4.9.3 The study on fuel spray characteristics of high percentage palm diesel Blended

This study was done by spraying the fuel into the chamber at the atmospheric pressure. The chamber heating temperature was still maintained at 100 °C. The control of the injection mass and injection rate was the same as combustion experiment. The test matrix is shown in table 4-10. By changing the camera delay time, the spray images were taken, flame by flame, from 0.1 to 0.7 msec, 0.1 msec step, after start of injection (until some part of fuel spray could not be observed) and at close to peak of injection rate, 1.0 and 1.2 msec after start of injection, for calculating spray angle.

Table 4-10 Camera delay time for spray visualization

Fuel	Injection pressure	Time after start of injection (msec)									
		0.1	0.2	0.3	0.4	0.5	0.6	0.7	1.0	1.2	
Diesel	60 MPa	⊗	⊗	⊗	⊗	⊗	⊗	⊗	⊗	⊗	⊗
	100 MPa	⊗	⊗	⊗	⊗	⊗	⊗	⊗	⊗	⊗	
Palm diesel 80%	60 MPa	⊗	⊗	⊗	⊗	⊗	⊗	⊗	⊗	⊗	⊗
	100 MPa	⊗	⊗	⊗	⊗	⊗	⊗	⊗	⊗	⊗	

CHAPTER V

EXPERIMENT RESULTS

5.1 The study on refined palm oil

The proper percentage blend of refined palm and diesel fuel was heated up by hot water (60°C) and kept 3 hours before loaded into the fuel injection system (heat up to 40 °C). The injection pressure was used to control the injection mass, in the micro-scale. This pressure was maintained with the range of less than 2% of injection pressure 100 MPa and less than 1% for other injection pressure, in attempt to keep the mass approximate 15 mg for all experiments.

5.1.1 Ignition delay of the combustion

The data obtained from He-Ne laser and OH-radical was used to calculate the ignition delay. It was found that palm diesel gave shorter ignition delay compared with diesel.

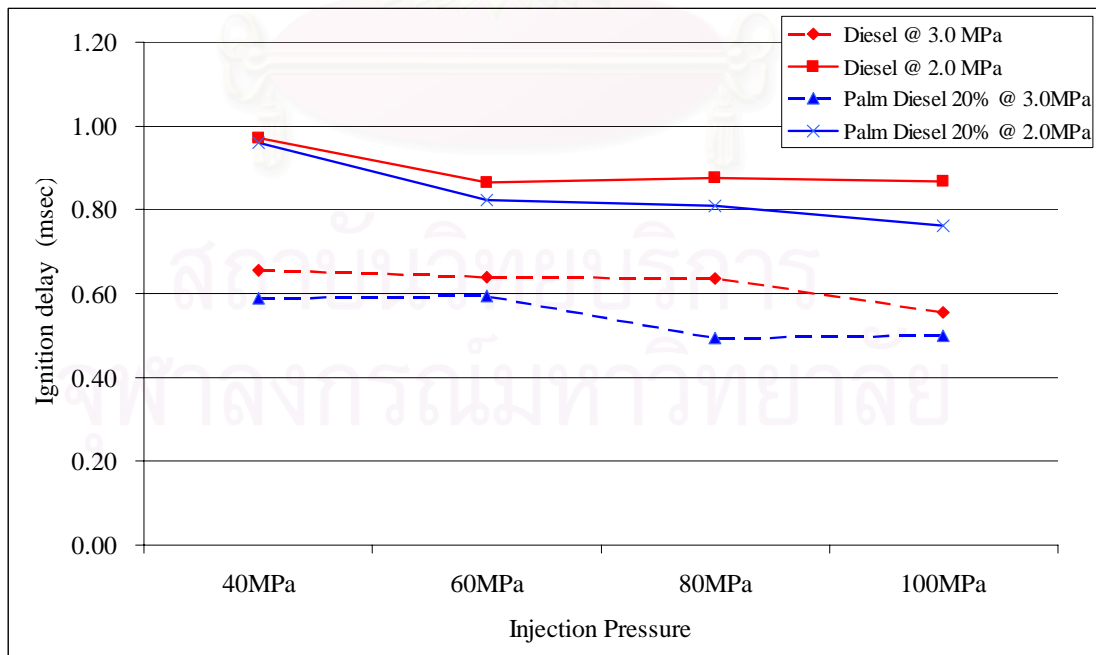


Fig.5-1 Ignition delay at ambient pressure 2.0 and 3.0 MPa.

* Combustion chamber heating temperature 80 °C

The ignition delay of palm diesel 20% were shorter than diesel at all injection pressure, though the combustion ambient were increase from 2.0 to 3.0 MPa, the ignition delay were still shorter, shown in figure 5-1

The study was done with the higher blending percentage. It was found that ignition delay was decreased with high percentage refined palm oil blended at both injection pressure 60 MPa and 100 MPa, shown in figure 5-2.

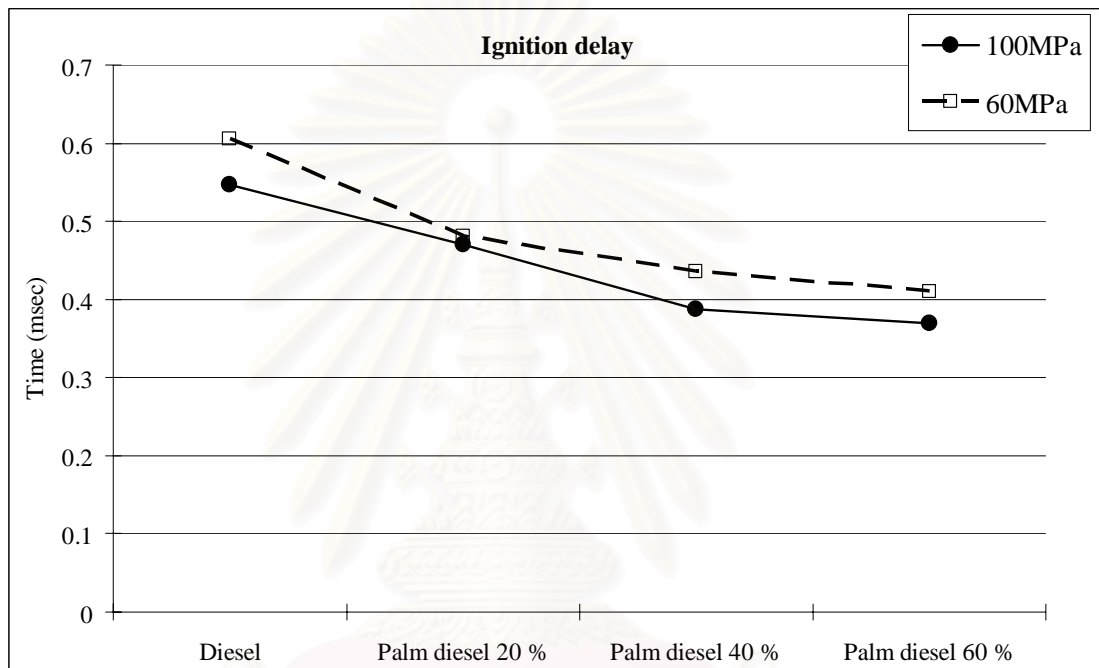


Fig.5-2 Ignition delay of palm diesel 20%, 40%, 60% and diesel

At injection pressure 60 and 100 MPa

Ambient pressure 3.0 MPa

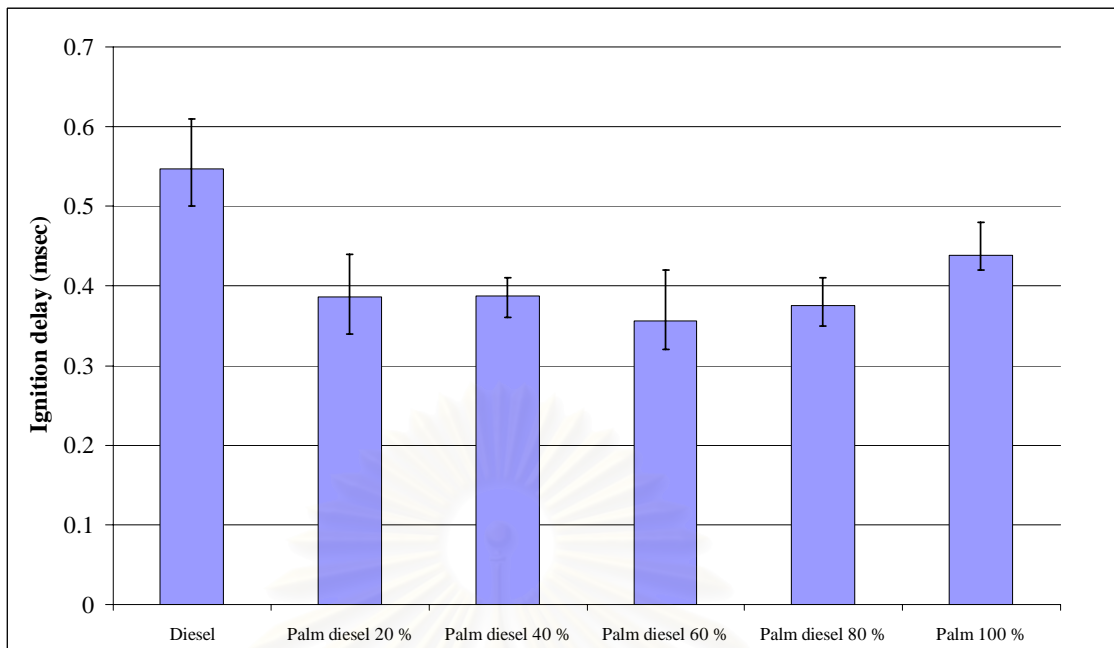


Fig.5-3 Ignition delay at ambient pressure 3.0 MPa

Injection pressure 100 MPa

The experiment was continued blended more the palm oil, up to palm diesel 80% and palm 100% at injection pressure 100 MPa. The ignition delays of fuels were also shorter than diesel fuel. Only in the case of palm 100%, the injection period was prolonged 0.4 msec to maintain the injection mass 15 mg.

5.1.2 Fuel combustion period

The data 10% of peak intensities obtained from two photo diodes (top and side) were selected to be the start and end of the combustion. The combustion results were shown that the combustion period of palm diesel 20% and diesel were a little bit difference at the low injection pressure and this value became close to diesel after increased the injection pressure.

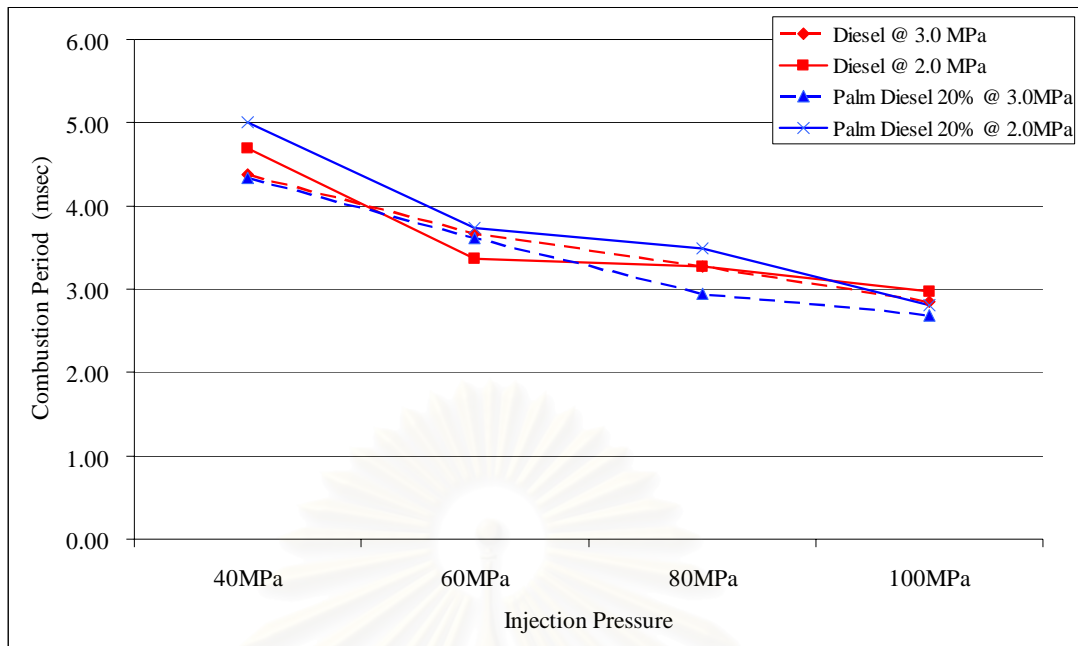


Fig.5-4 Fuel combustion period at ambient pressure 2.0 and 3.0 MPa

* Combustion chamber heating temperature 80 °C

From figure 5-4, the combustion period was decreased with the higher injection pressure. This might be the results of 1) short injection period and 2) better atomization as injection pressure increased.

สถาบันวิทยบริการ
จุฬาลงกรณ์มหาวิทยาลัย

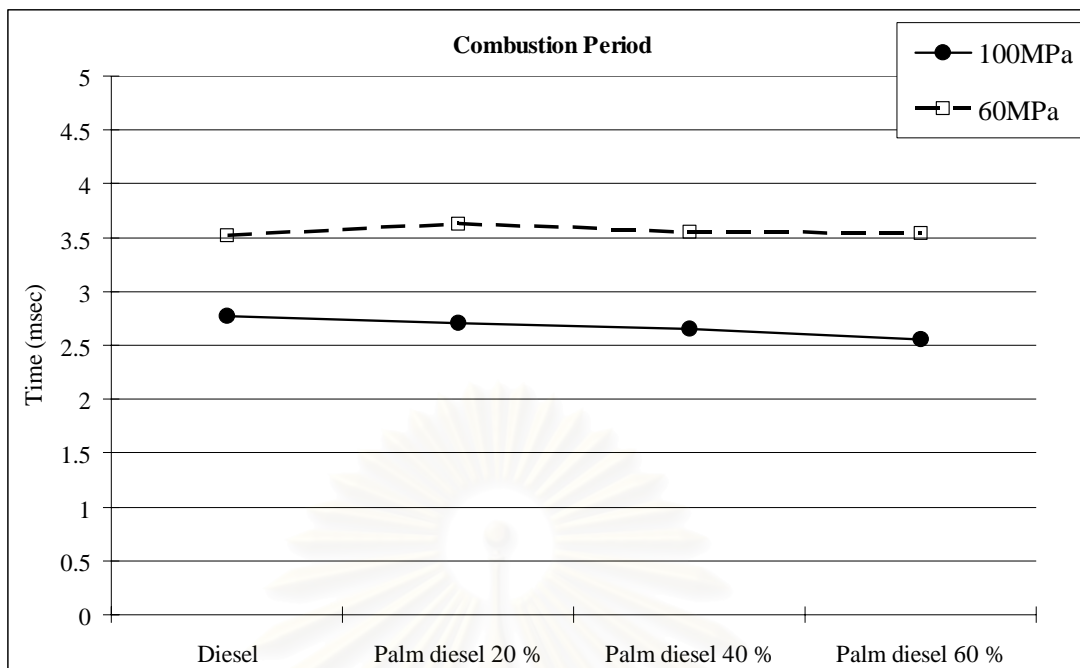


Fig.5-5 Combustion period of palm diesel 20%,40%, 60% and diesel at injection pressure 60 and 100 MPa at ambient pressure 3.0 MPa

The study on effect of palm blended percentage 20%, 40%, 60% on combustion period was done, revealing that at the injection pressure 60 MPa, the combustion period was rarely changed. However, in the case of injection pressure 100 MPa, the combustion period was seemed to decrease.

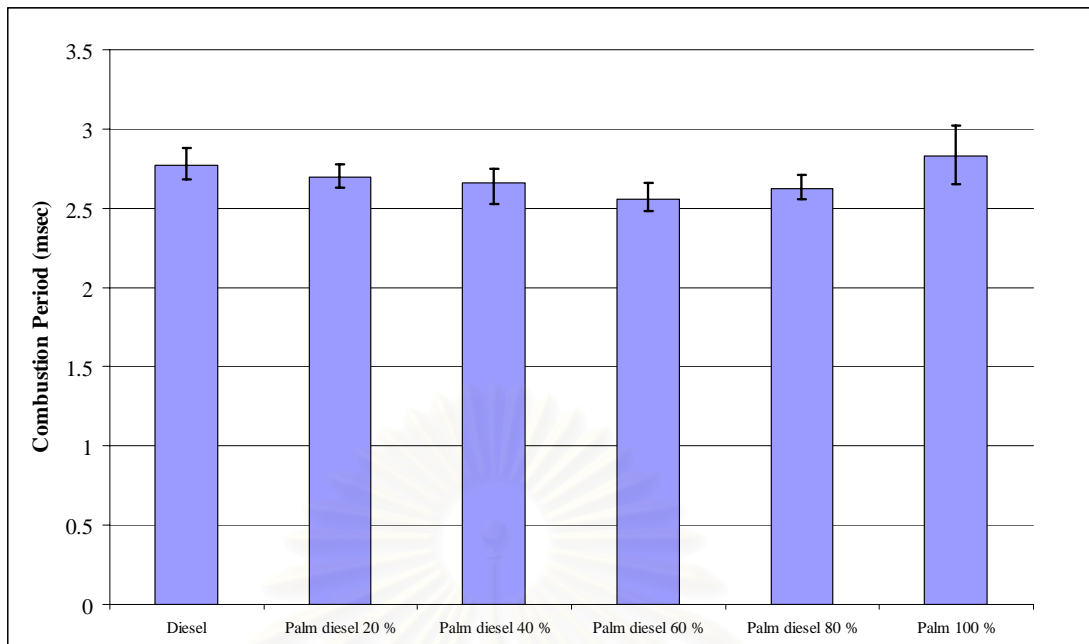


Fig.5-6 Fuel combustion period at ambient pressure 3.0 MPa
Injection pressure 100 MPa

The results shown in figure 5-6 show that the observed combustion period of palm blended at injection pressure of 100 MPa were shorter than diesel. The amount of injection fuel became slightly smaller and the injection period became slightly shorter with the increase of palm blended percentage. This may due to the higher viscosity of palm blended fuel. The shorter combustion period of palm blended fuel might be the results of these tendencies.

5.1.3 Combustion flame visualization

The 10 μ sec exposure time of ICCD camera was set and focus at the position of nozzle tip. The images were taken by vary delay time.

5.1.3.1. The study on combustion of palm diesel 60% at injection pressure 60 MPa and 100MPa

The study was conducted with the palm diesel 60% to investigate the effect of injection pressure at 100 MPa and 60 MPa and compared the results with diesel fuel.

5.1.3.1.1. Intensity distribution of combustion flame

Some images of diesel 60% at injection pressure 60 MPa and

100MPa were shown in figure 5-7, 5-8.

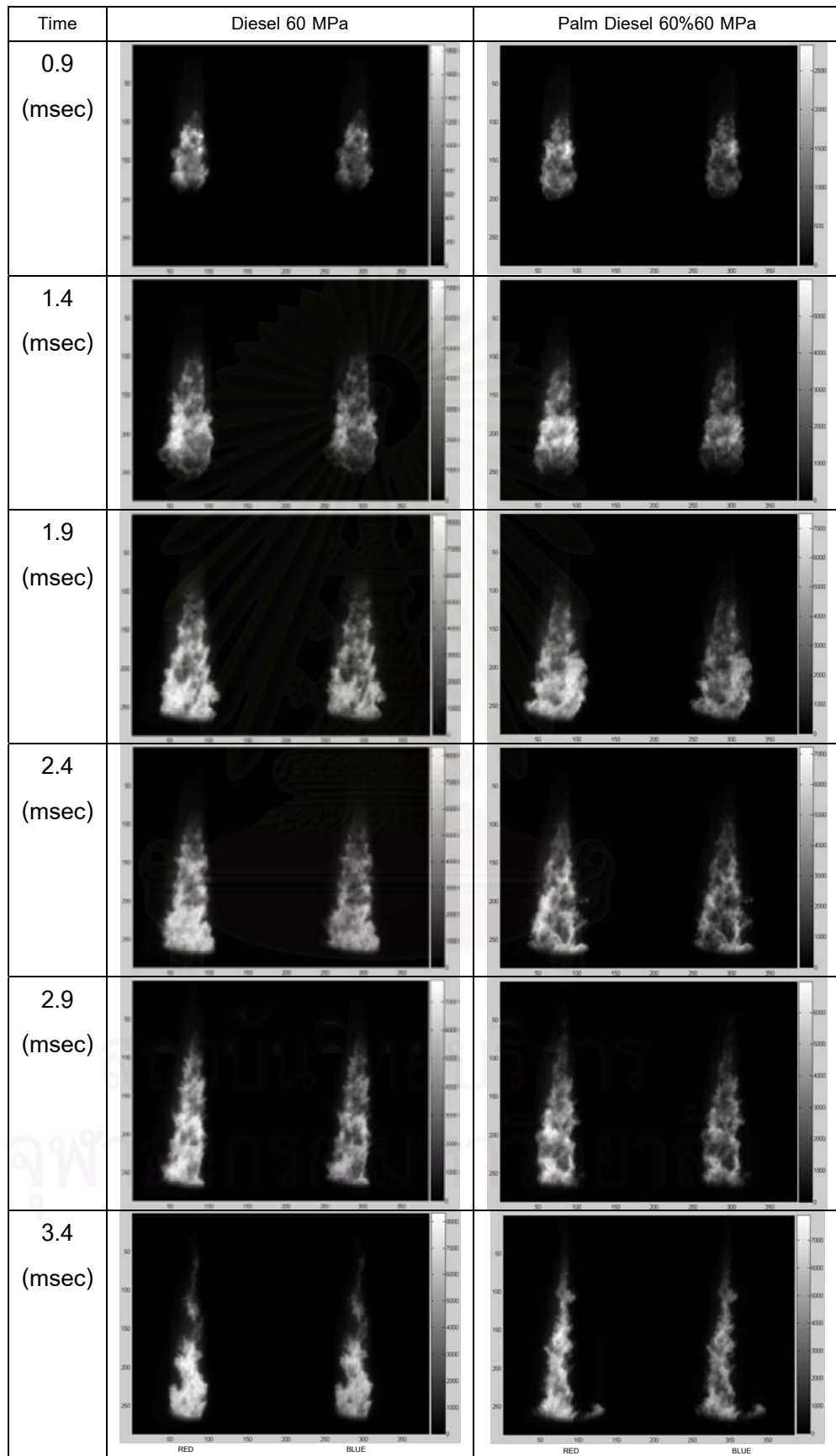


Fig.5-7 Intensity of combustion flame palm diesel 60%, Injection pressure 60 MPa

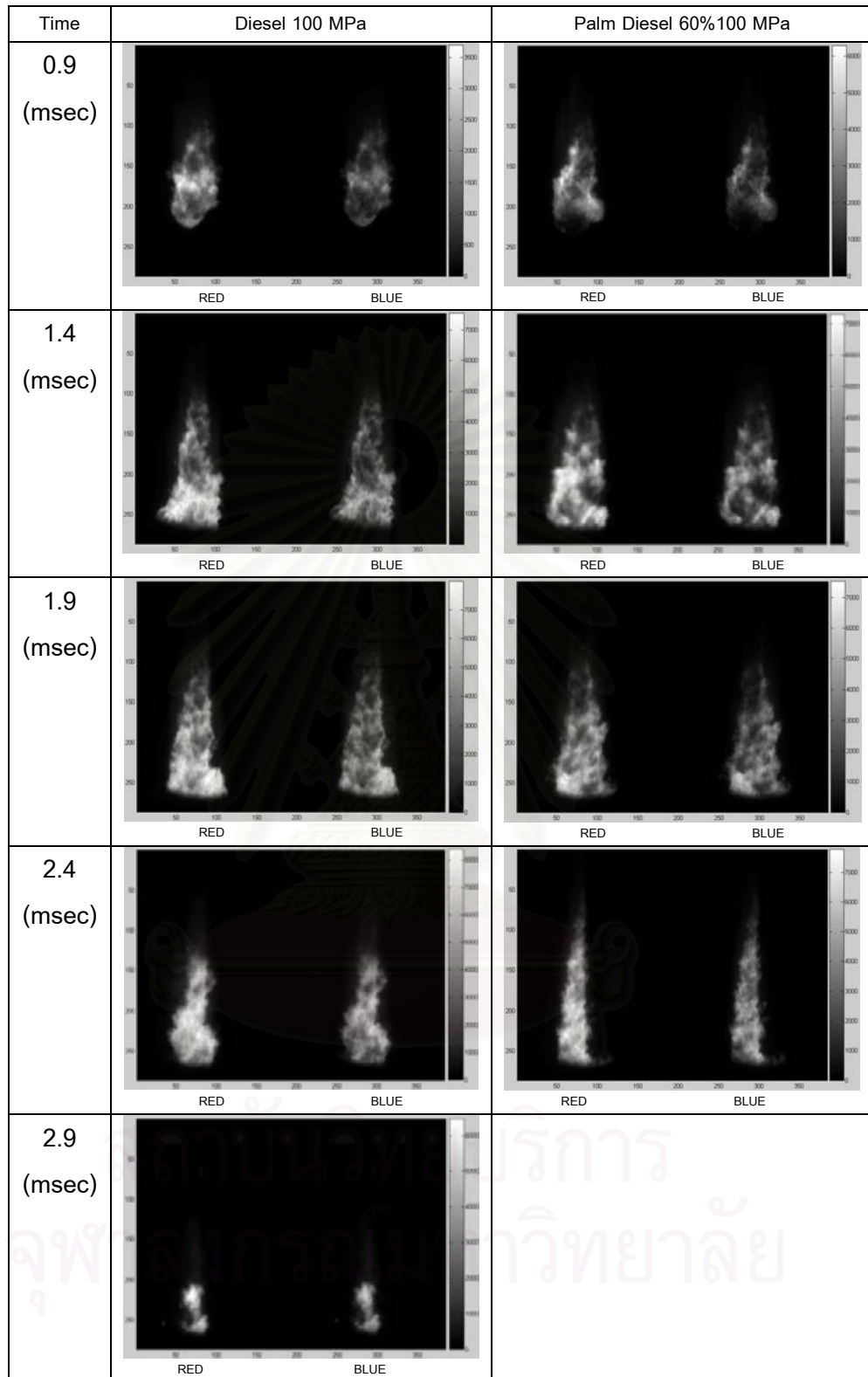


Fig.5-8 Intensity distribution of combustion flame, palm diesel 60%

Injection pressure 100 MPa

5.1.3.1.2. Combustion flame temperature distribution

The flame intensity data were complied with two color method. Some of calculated results of true temperature are shown in figure 5-9 to 5-19. The threshold value at 20% from the peak intensity of each image was selected.

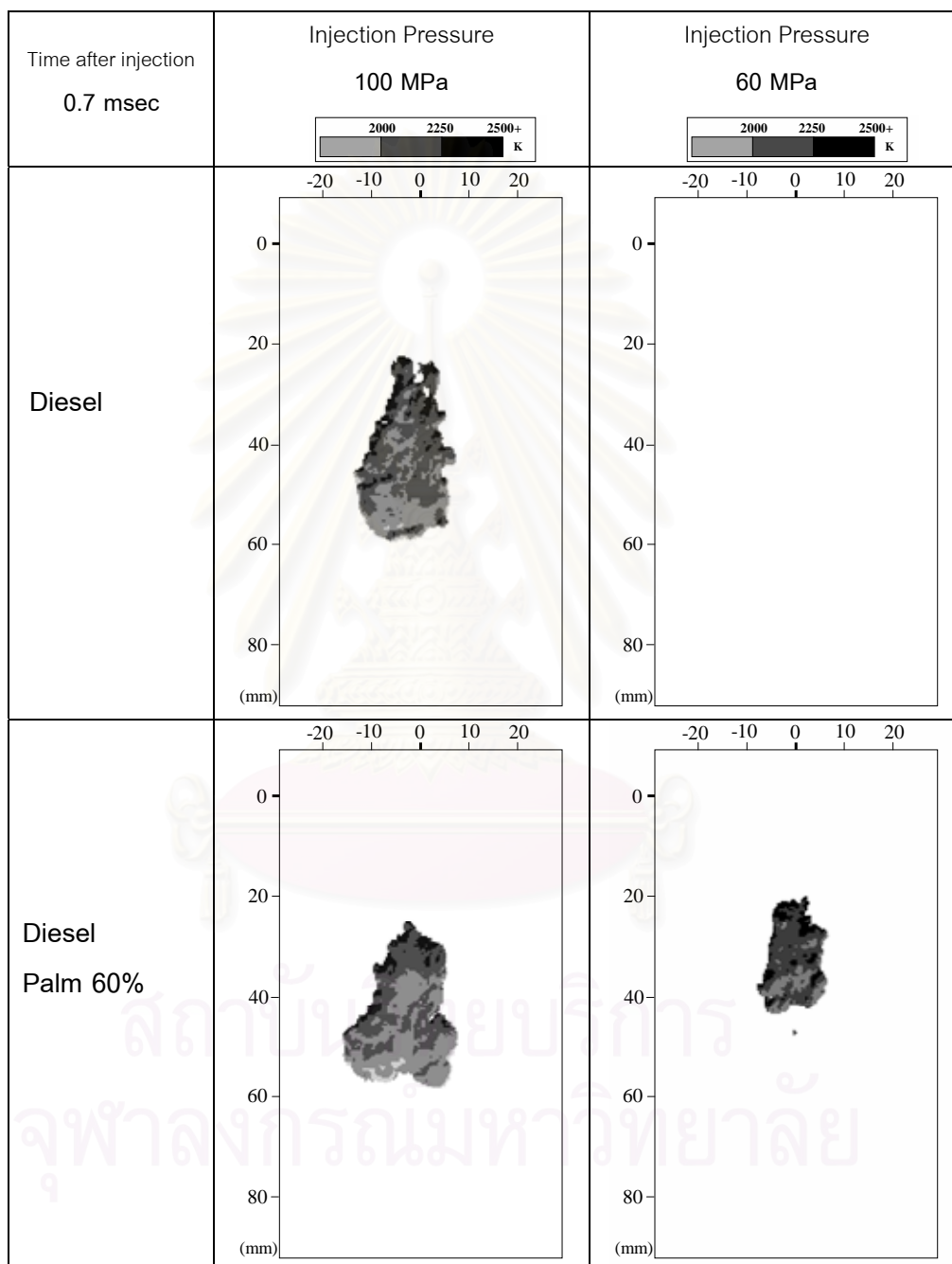


Fig.5-9 Combustion flame temperature distribution of Diesel fuel and Palm diesel 60 %

Injection pressure 100MPa and 60MPa , Combustion at 3.0 MPa

0.7 msec after start of injection ICCD camera Gain 5.5 width 10 μ sec

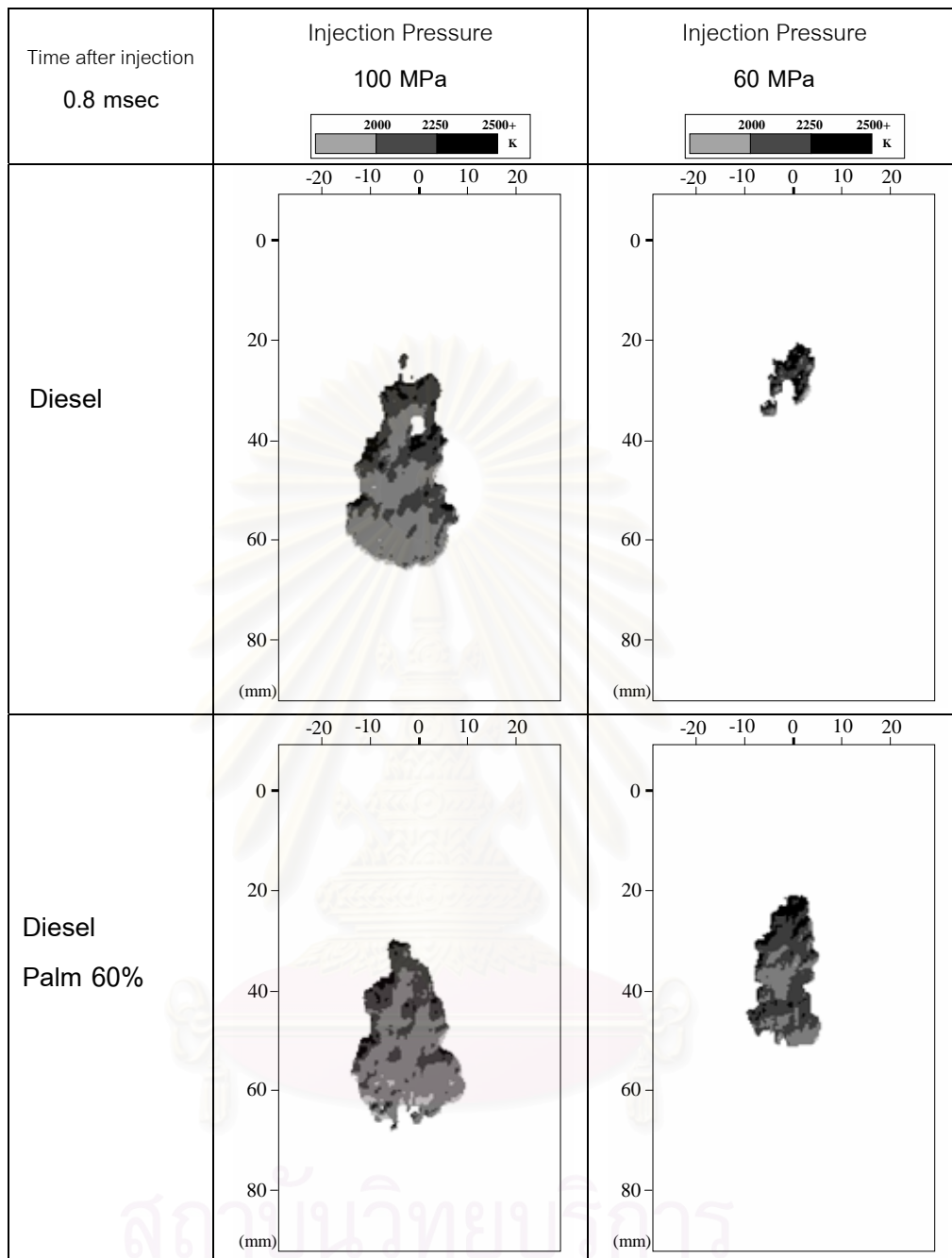


Fig.5-10 Combustion flame temperature distribution of Diesel fuel and Palm diesel 60 %

Injection pressure 100MPa and 60MPa, Combustion at 3.0 MPa

0.8 msec after start of injection, ICCD camera Gain 5.5, width 10 μ sec

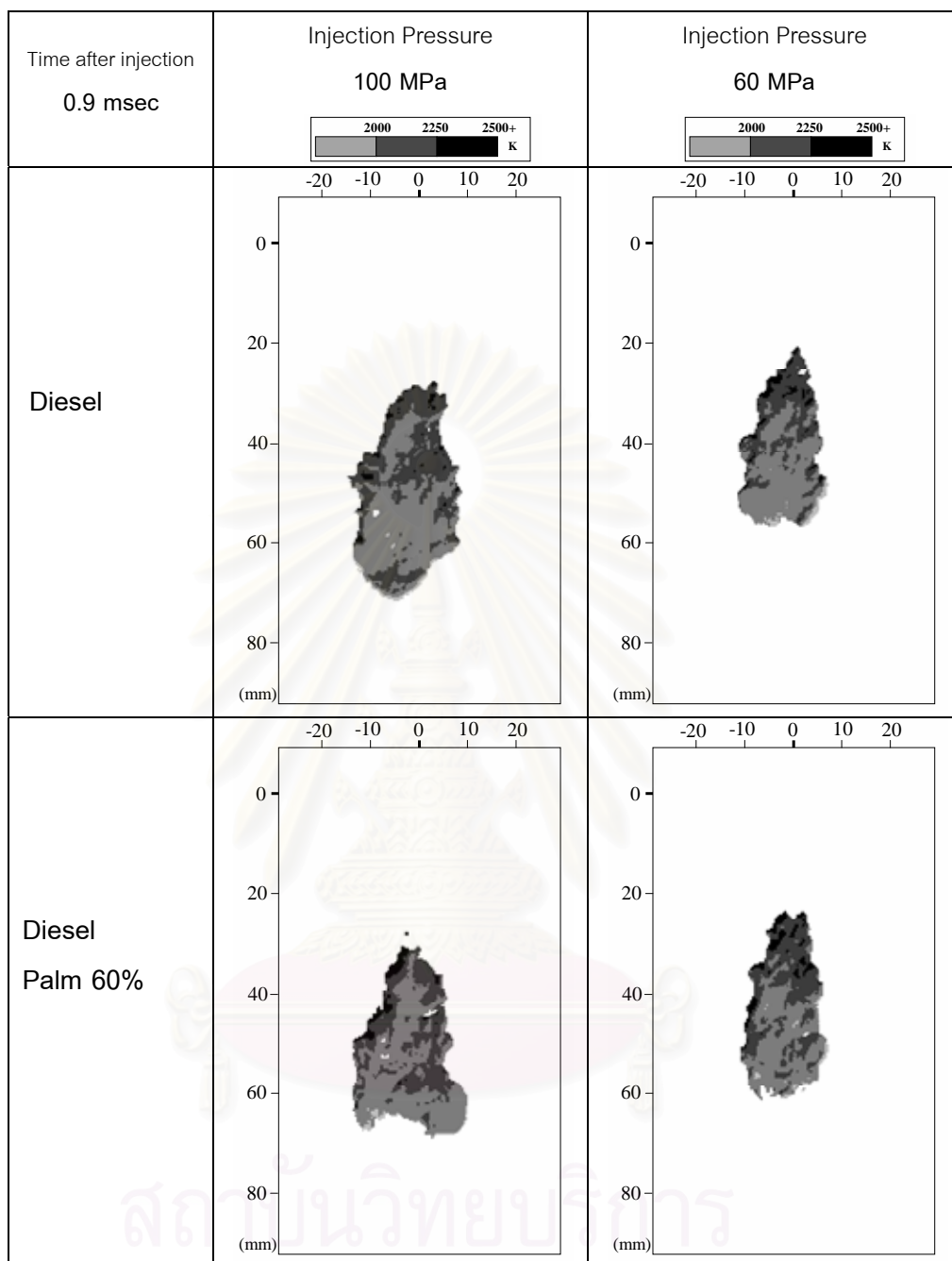


Fig.5-11 Combustion flame temperature distribution of Diesel fuel and Palm diesel 60 %

Injection pressure 100MPa and 60MPa, Combustion at 3.0 MPa

0.9 msec after start of injection, ICCD camera Gain 5.5, width 10 μ sec

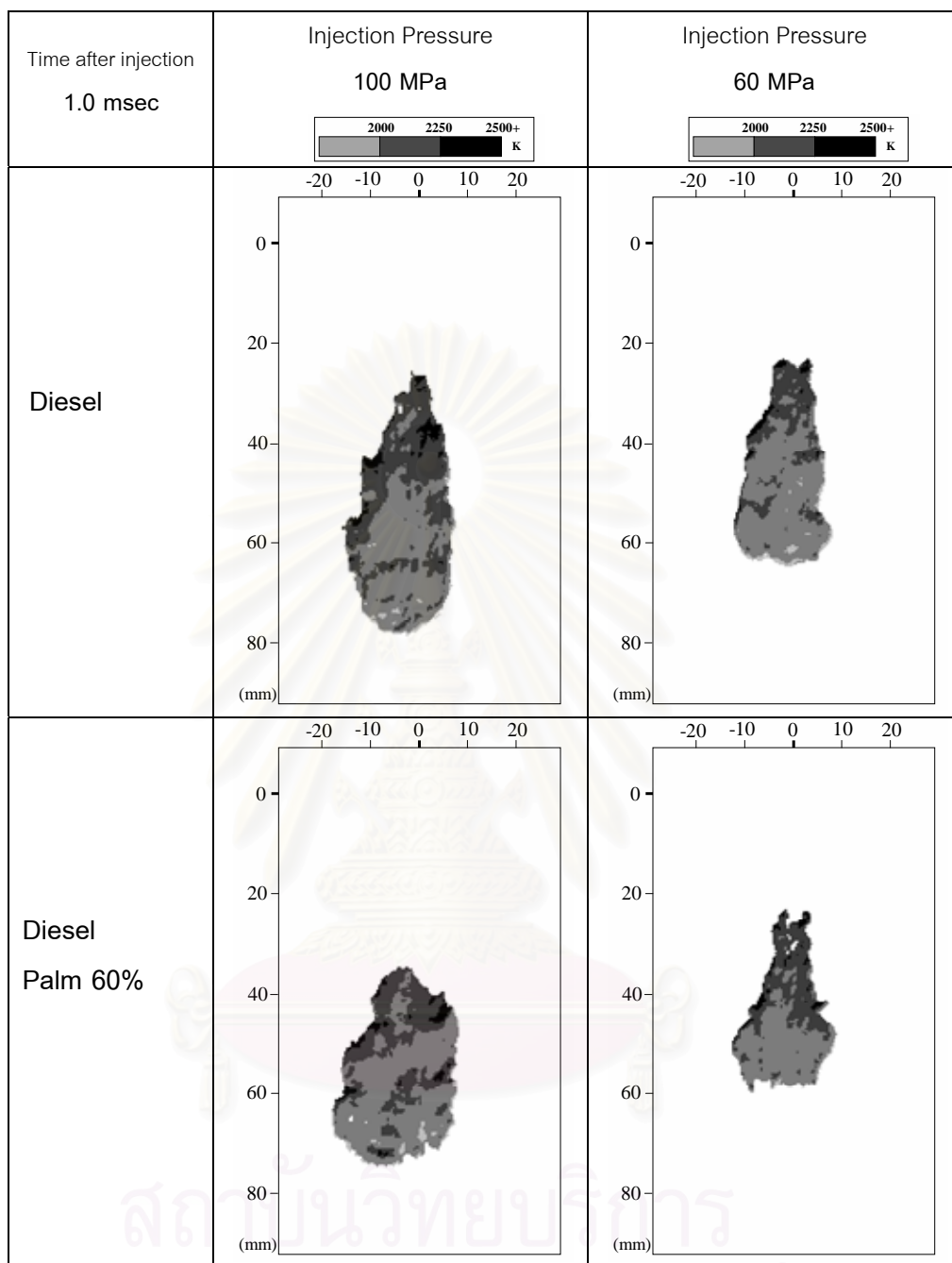


Fig.5-12 Combustion flame temperature distribution of Diesel fuel and Palm diesel 60 %

Injection pressure 100MPa and 60MPa, Combustion at 3.0 MPa

1.0 msec after start of injection, ICCD camera Gain 5.5, width 10 μ sec

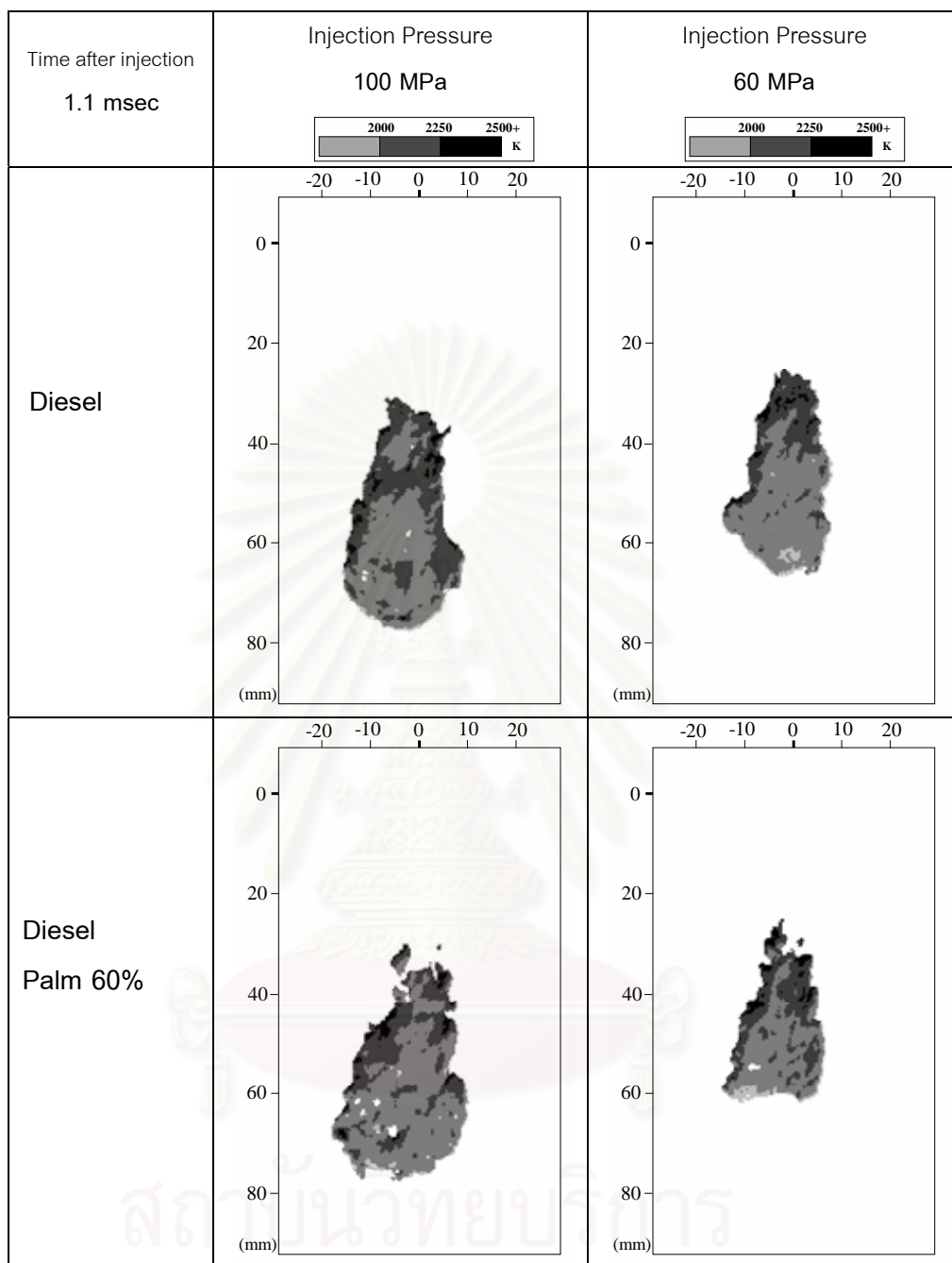


Fig.5-13 Combustion flame temperature distribution of Diesel fuel and Palm diesel 60 %

Injection pressure 100MPa and 60MPa, Combustion at 3.0 MPa

1.1 msec after start of injection, ICCD camera Gain 5.5, width 10 μ sec

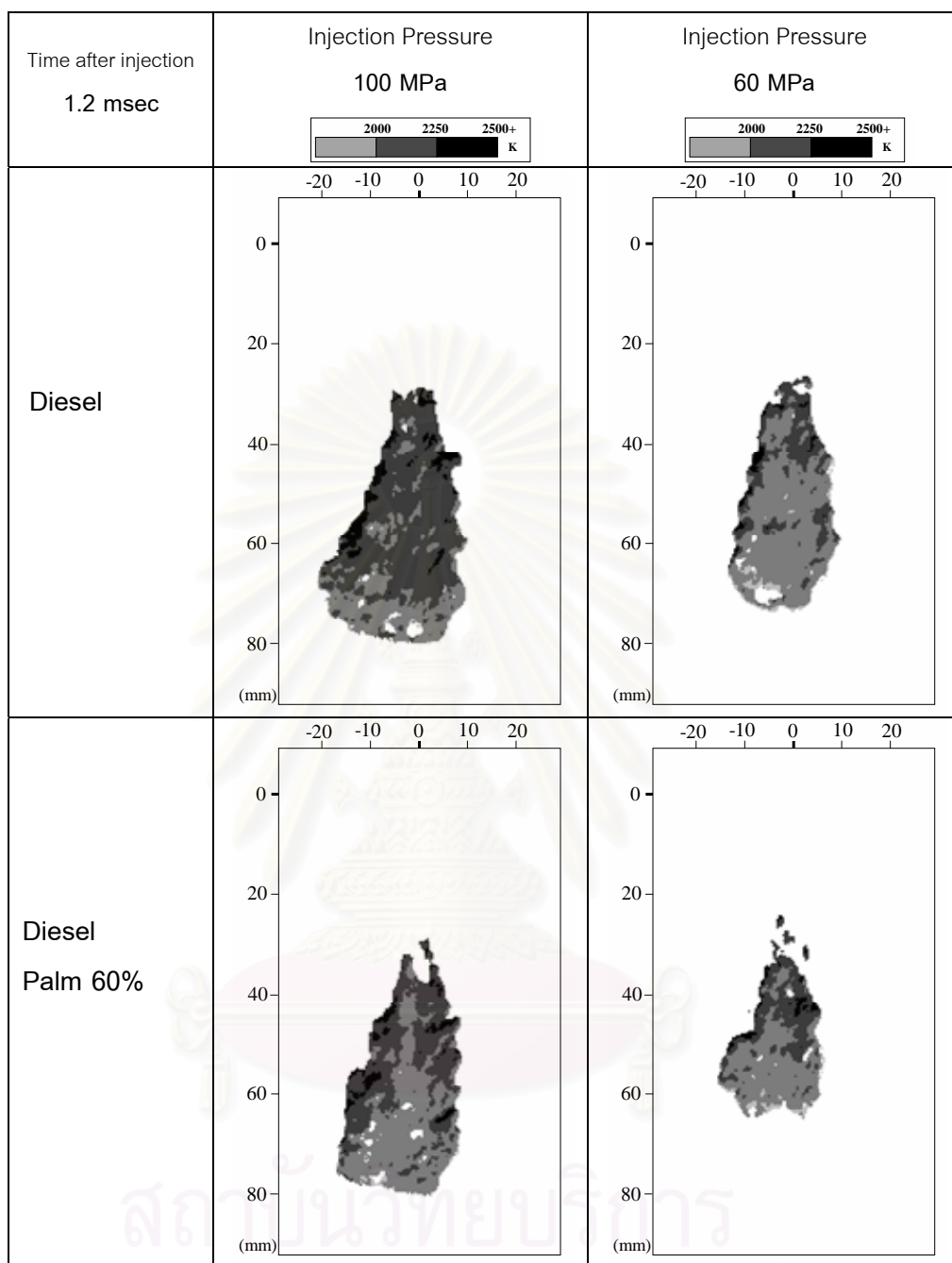


Fig.5-14 Combustion flame temperature distribution of Diesel fuel and Palm diesel 60 %

Injection pressure 100MPa and 60MPa, Combustion at 3.0 MPa

1.2 msec after start of injection, ICCD camera Gain 5.5, width 10 μ sec

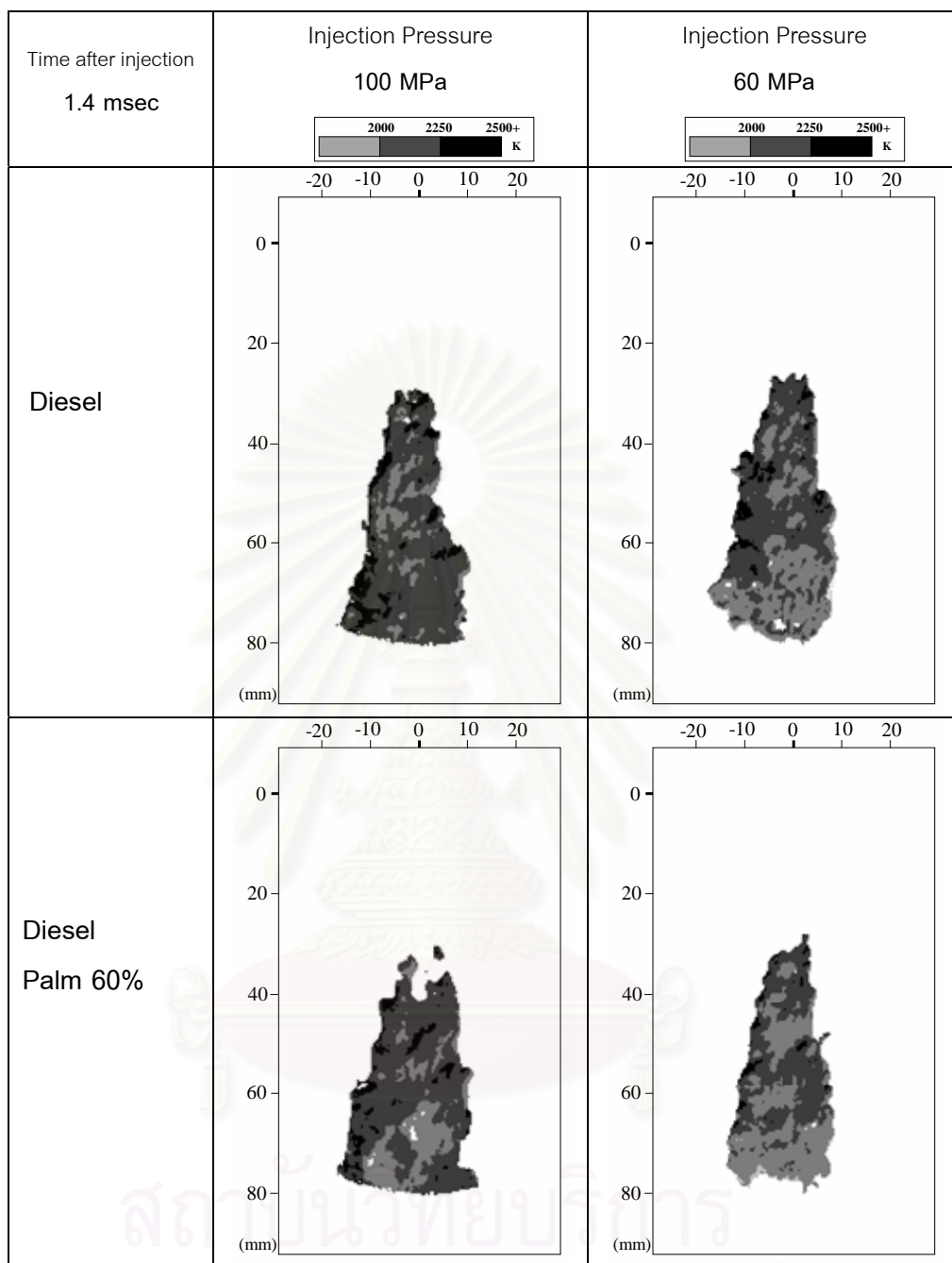


Fig.5-15 Combustion flame temperature distribution of Diesel fuel and Palm diesel 60 %

Injection pressure 100MPa and 60MPa, Combustion at 3.0 MPa

1.4 msec after start of injection, ICCD camera Gain 5.5, width 10 μ sec

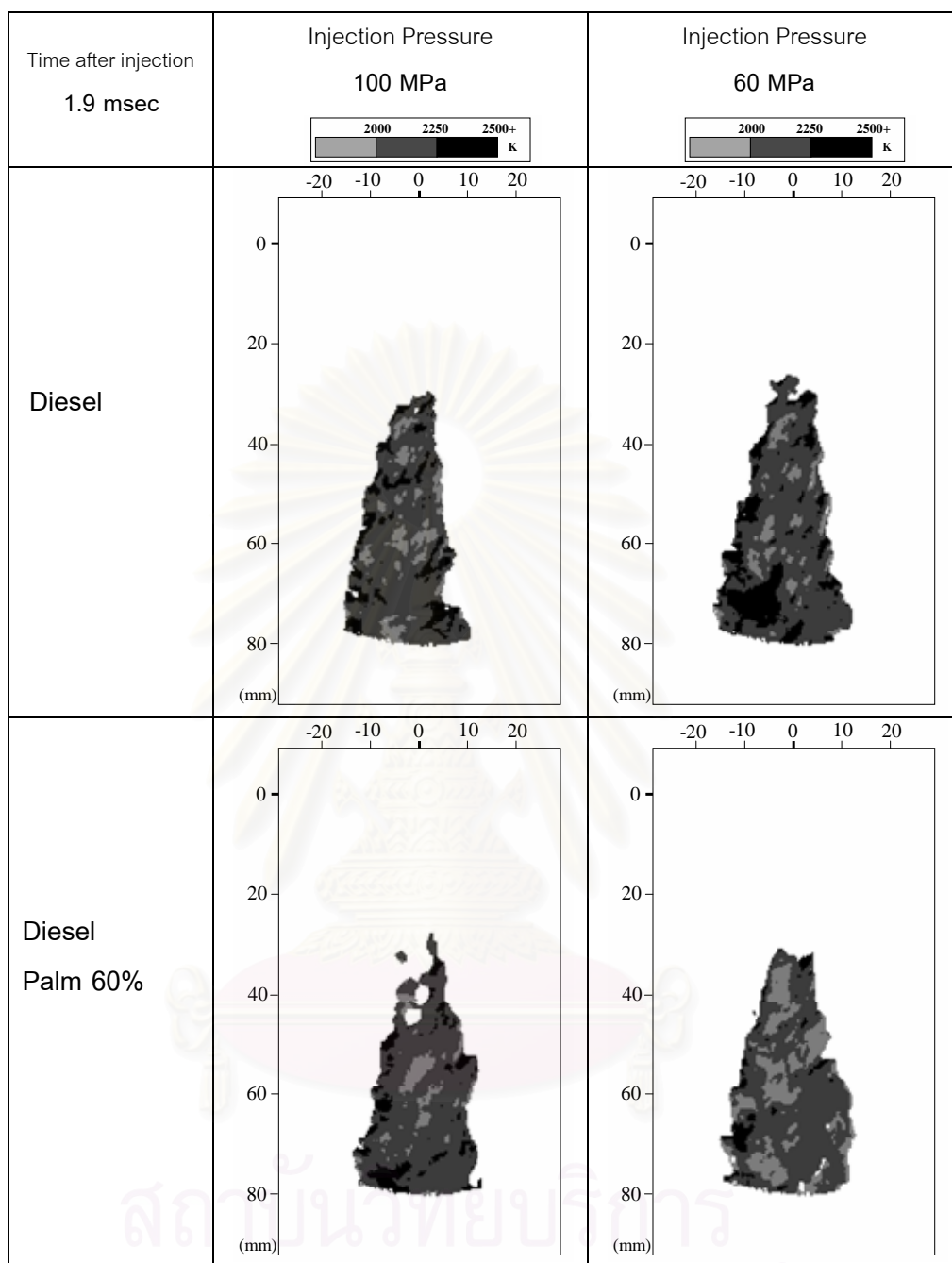


Fig.5-16 Combustion flame temperature distribution of Diesel fuel and Palm diesel 60 %

Injection pressure 100MPa and 60MPa, Combustion at 3.0 MPa

1.9 msec after start of injection, ICCD camera Gain 5.5, width 10 μ sec

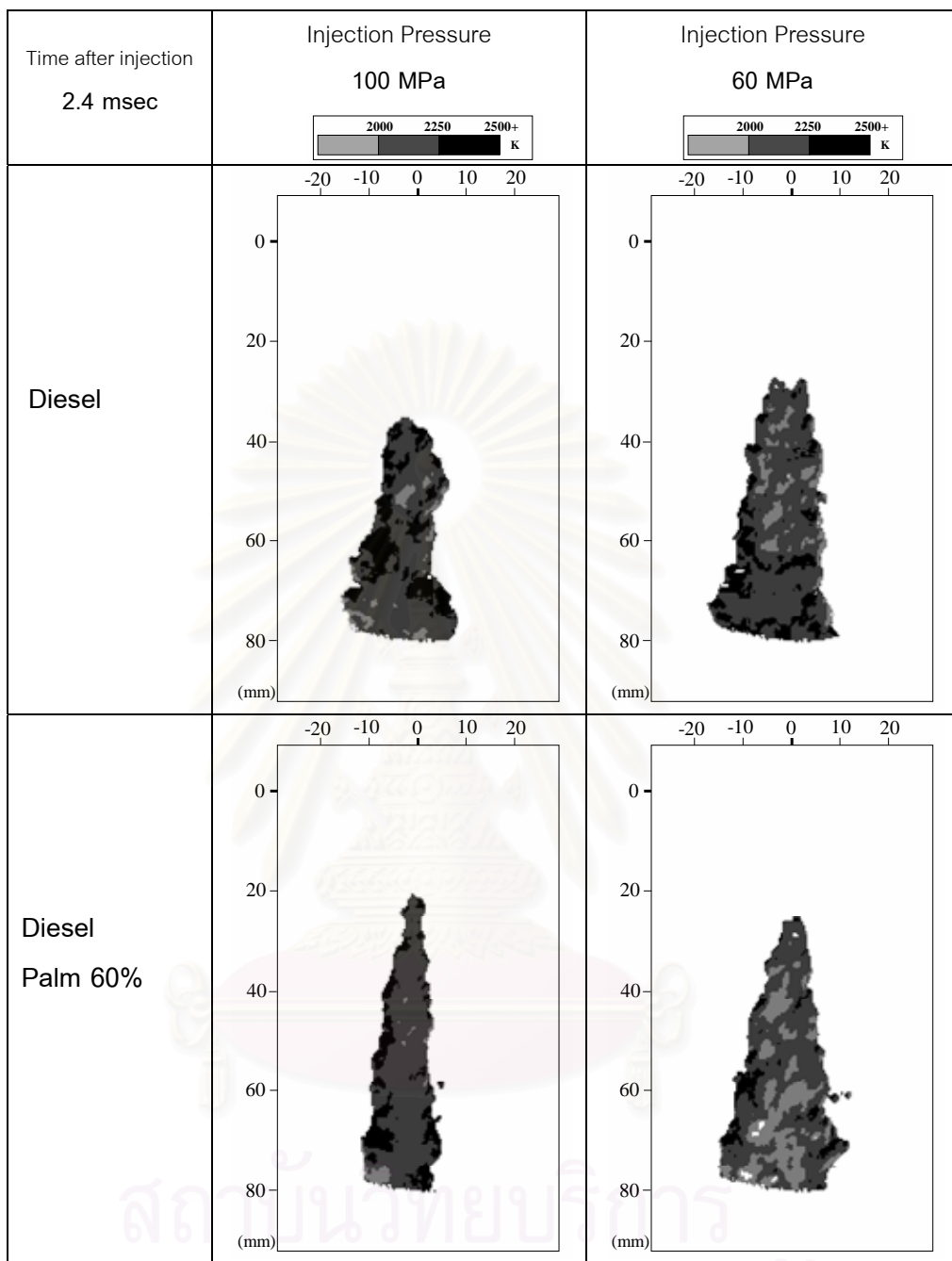


Fig.5-17 Combustion flame temperature distribution of Diesel fuel and Palm diesel 60 %

Injection pressure 100MPa and 60MPa, Combustion at 3.0 MPa

2.4 msec after start of injection, ICCD camera Gain 5.5, width 10 μ sec

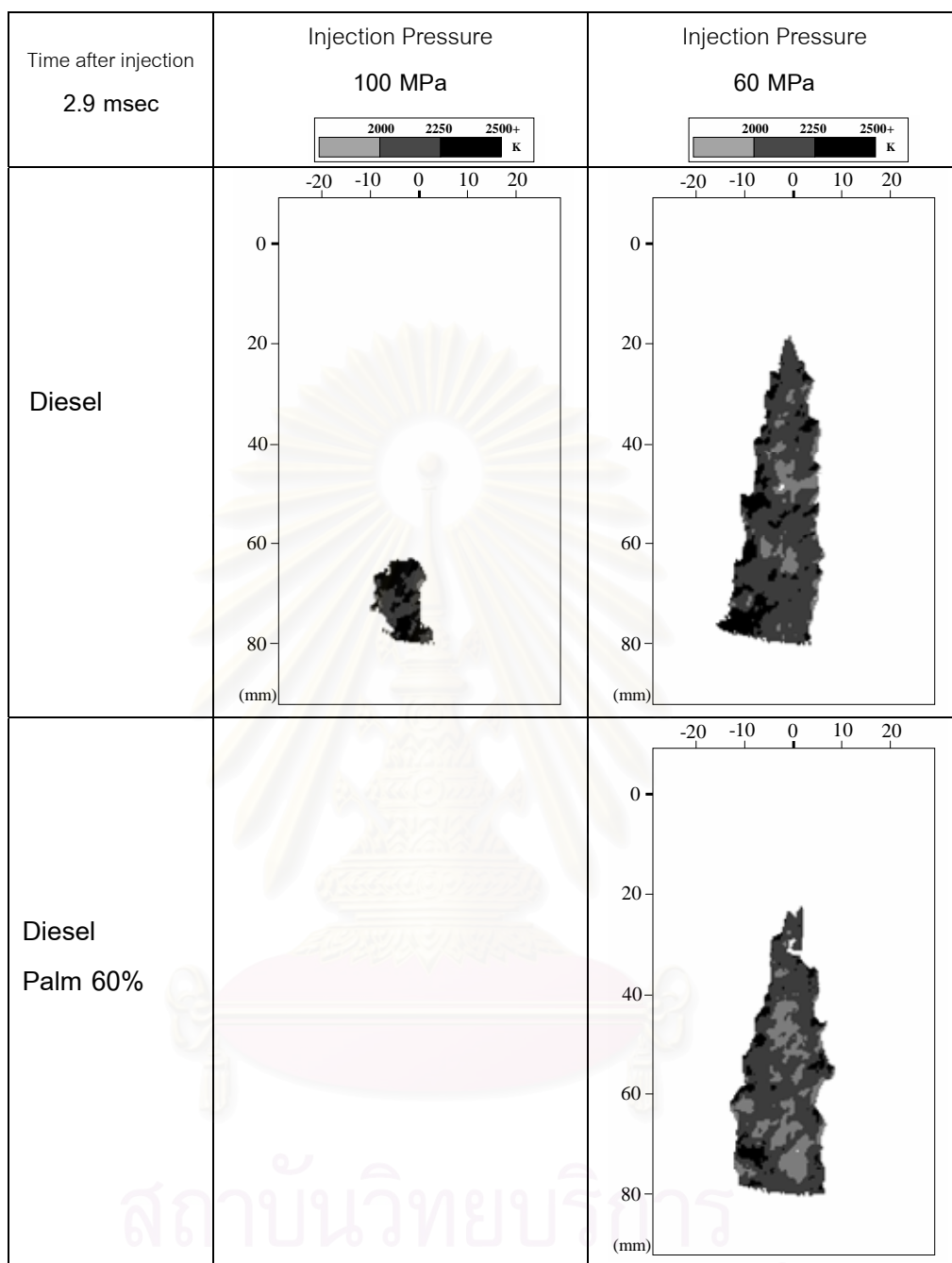


Fig.5-18 Combustion flame temperature distribution of Diesel fuel and Palm diesel 60 %

Injection pressure 100MPa and 60MPa, Combustion at 3.0 MPa

2.9 msec after start of injection, ICCD camera Gain 5.5, width 10 μ sec

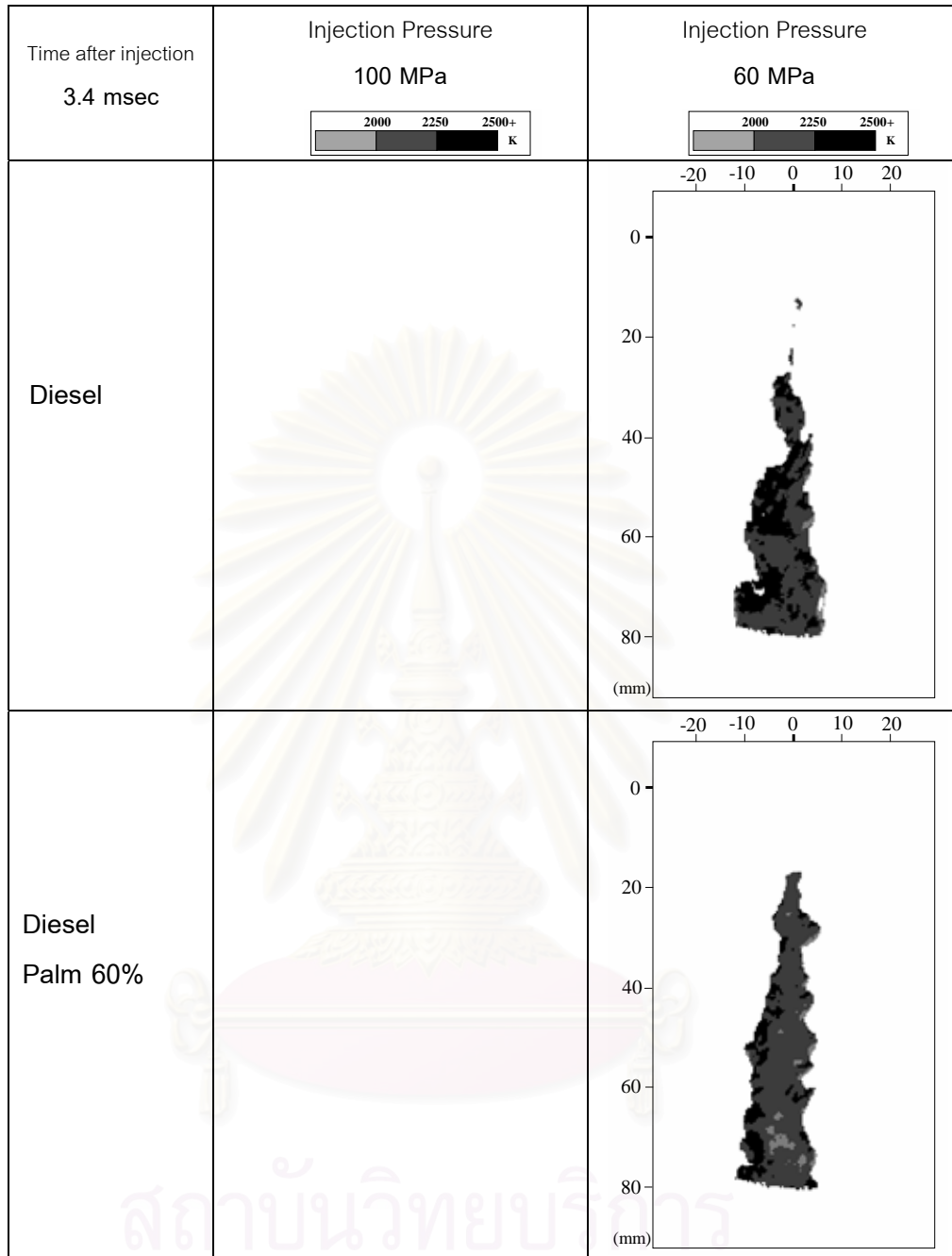


Fig.5-19 Combustion flame temperature distribution of Diesel fuel and Palm diesel 60 %

Injection pressure 100MPa and 60MPa, Combustion at 3.0 MPa

3.4 msec after start of injection, ICCD camera Gain 5.5, width 10 μ sec

5.1.3.1.3. Combustion flame temperature histogram

The temperature histogram was calculated by counting the number of combustion flame pixel and converting them to flame area (mm^2). The temperature interval of 50 K was selected and the data is shown from figure 5-20 to 5-23; taking images from time instant of 0.9, 1.4, 1.9 and 2.4 msec after start of combustion.

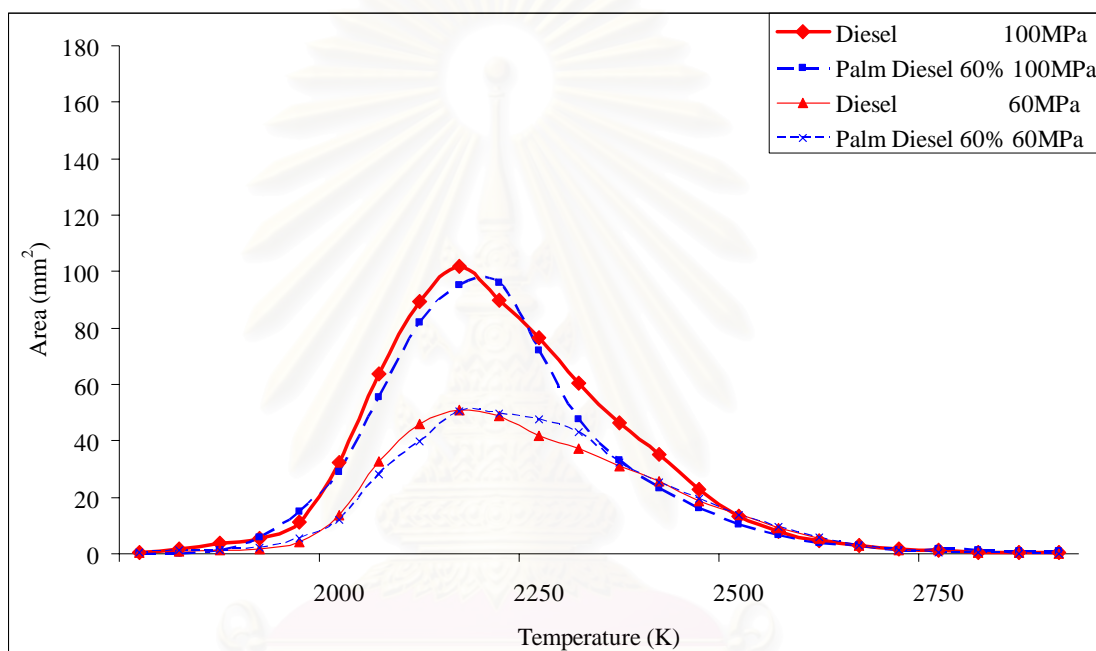


Fig. 5-20 Flame temperature histogram of Diesel and 60% Palm Diesel at injection pressure 60 MPa and 100 MPa Combustion at 3.0 MPa 930K 0.9 msec after start of injection

From figure 5-20, the combustion temperature of 100 MPa injection pressure was higher than 60 MPa and the difference between diesel palm 60% and diesel was very small.

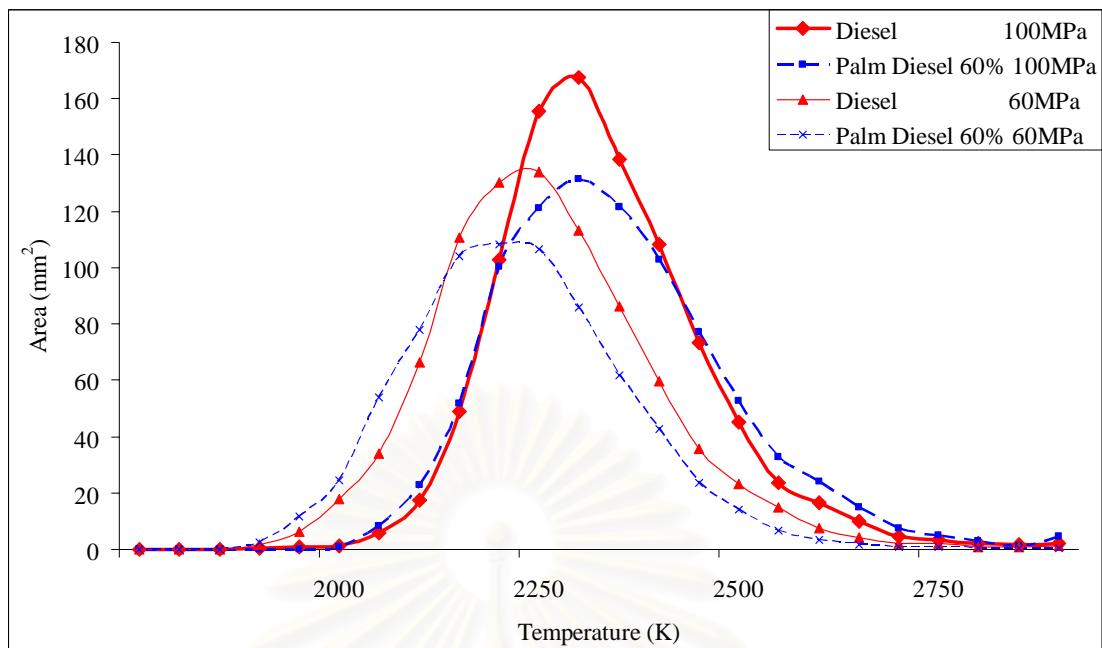


Fig. 5-21 Flame temperature histogram of Diesel and 60% Palm Diesel at injection pressure 60 MPa and 100 MPa Combustion at 3.0 MPa 930K 1.4 msec after start of injection

From figure 5-21, the combustion temperature of 100 MPa was higher than 60 MPa. The combustion temperature of diesel palm 60% was lower than diesel. Combustion area of diesel was larger than diesel palm 60% at both injection pressures.

สถาบันวิทยบริการ
จุฬาลงกรณ์มหาวิทยาลัย

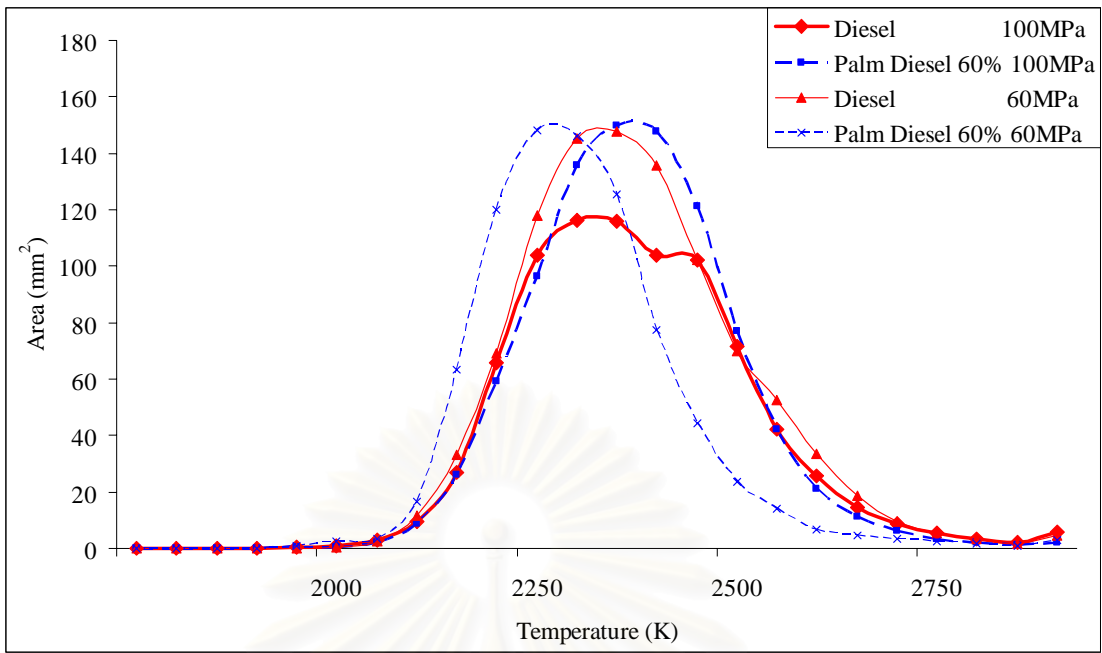


Fig. 5-22 Flame temperature histogram of Diesel and 60% Palm Diesel at injection pressure 60 MPa and 100 MPa Combustion at 3.0 MPa 930K 1.9 msec after start of injection

At injection pressure 60MPa, combustion temperature of palm diesel 60% was lower than diesel, combustion area was closely same size.

At injection pressure 100 MPa, combustion temperature for both fuel were the same but the combustion area of diesel was smaller, it might be caused by the faster burning rate of diesel.

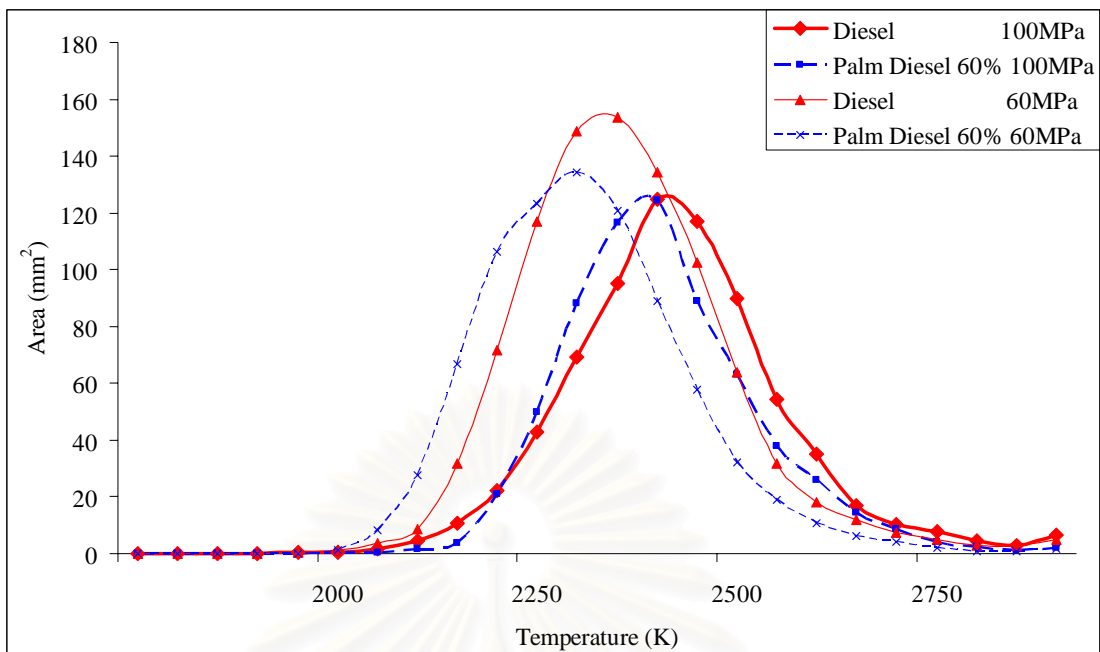


Fig. 5-23 Flame temperature histogram of Diesel and 60% Palm Diesel at injection pressure 60 MPa and 100 MPa Combustion at 3.0 MPa 930K 2.4 msec after start of injection

Finally, flame temperature of fuel injection pressure 60 MPa was higher than at 100 MPa because the longer injection period was set. Palm diesel combustion temperature was still lower than diesel with both injection pressures.

5.1.3.1.4. KL factor of Combustion flame distribution

The flame intensity data were complied with two color method. Some of calculated results of KL factor are shown in figure 5-24 to 5-34. The threshold value at 20% from the peak intensity of each image was selected.

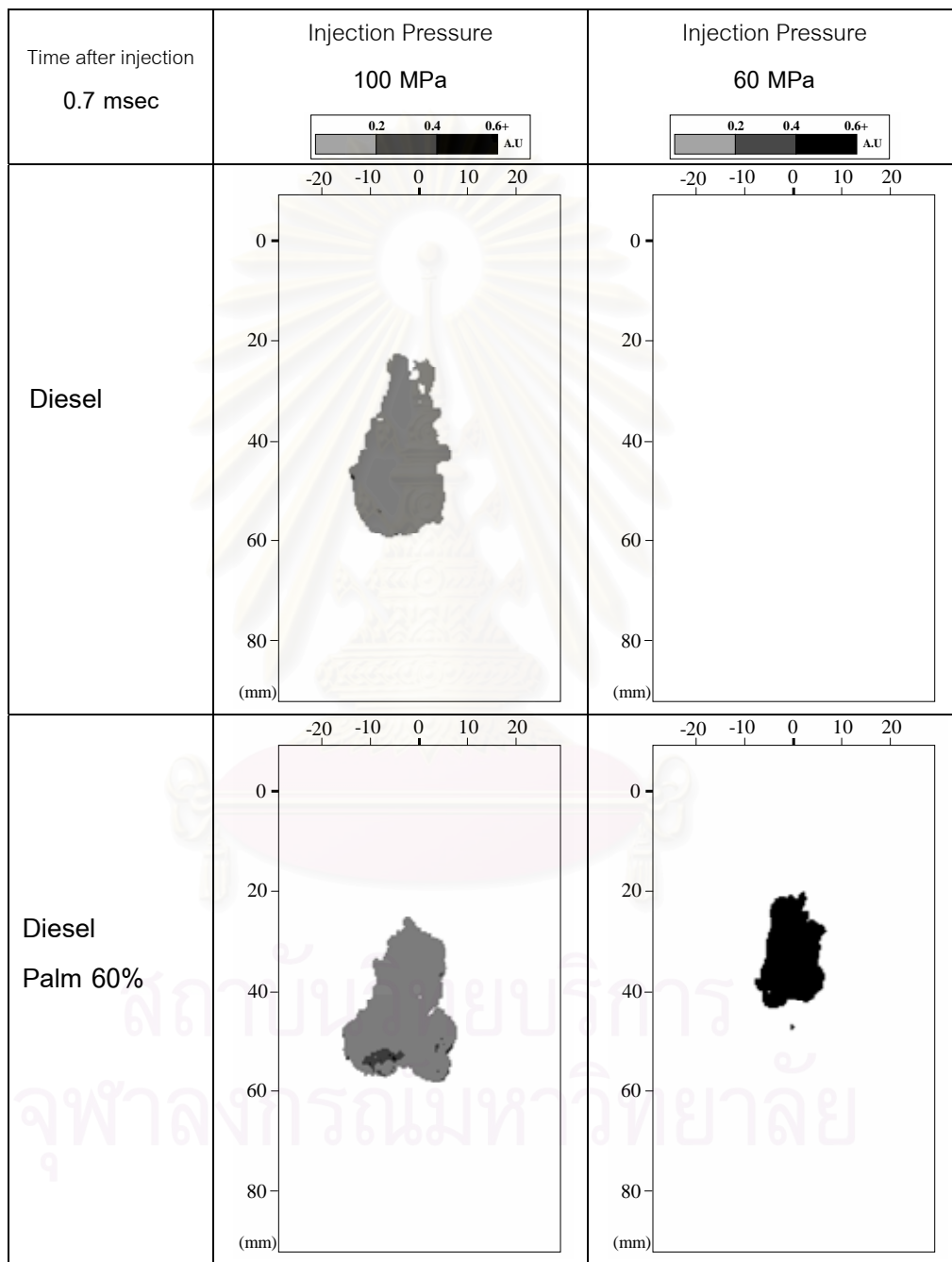


Fig.5-24 Combustion flame KL factor distribution of Diesel fuel and Palm diesel 60 %

Injection pressure 100MPa and 60MPa, Combustion at 3.0 MPa

0.7 msec after start of injection, ICCD camera Gain 5.5, width 10 μ sec

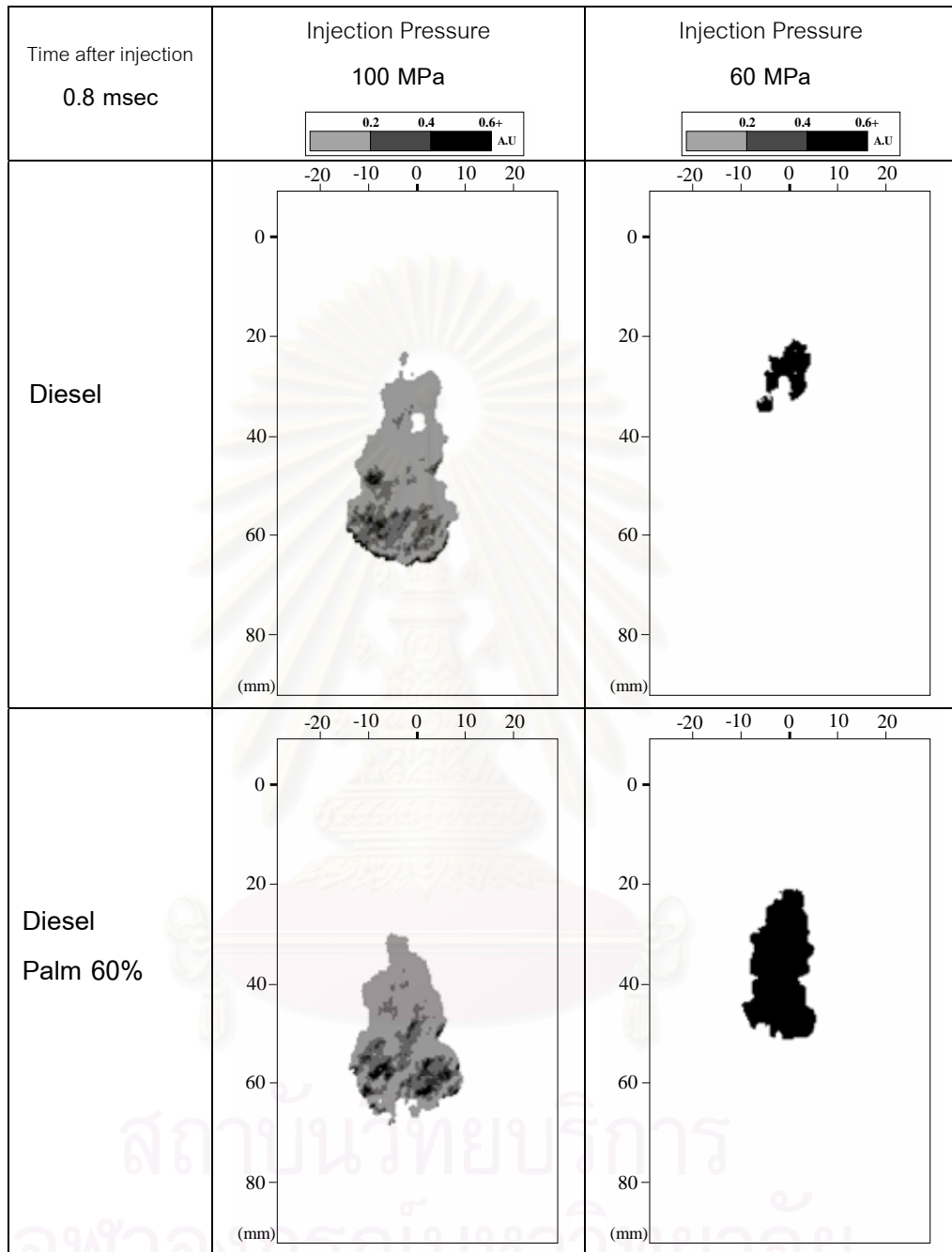


Fig.5-25 Combustion flame KL factor distribution of Diesel fuel and Palm diesel 60 %

Injection pressure 100MPa and 60MPa, Combustion at 3.0 MPa

0.8 msec after start of injection, ICCD camera Gain 5.5, width 10 μ sec

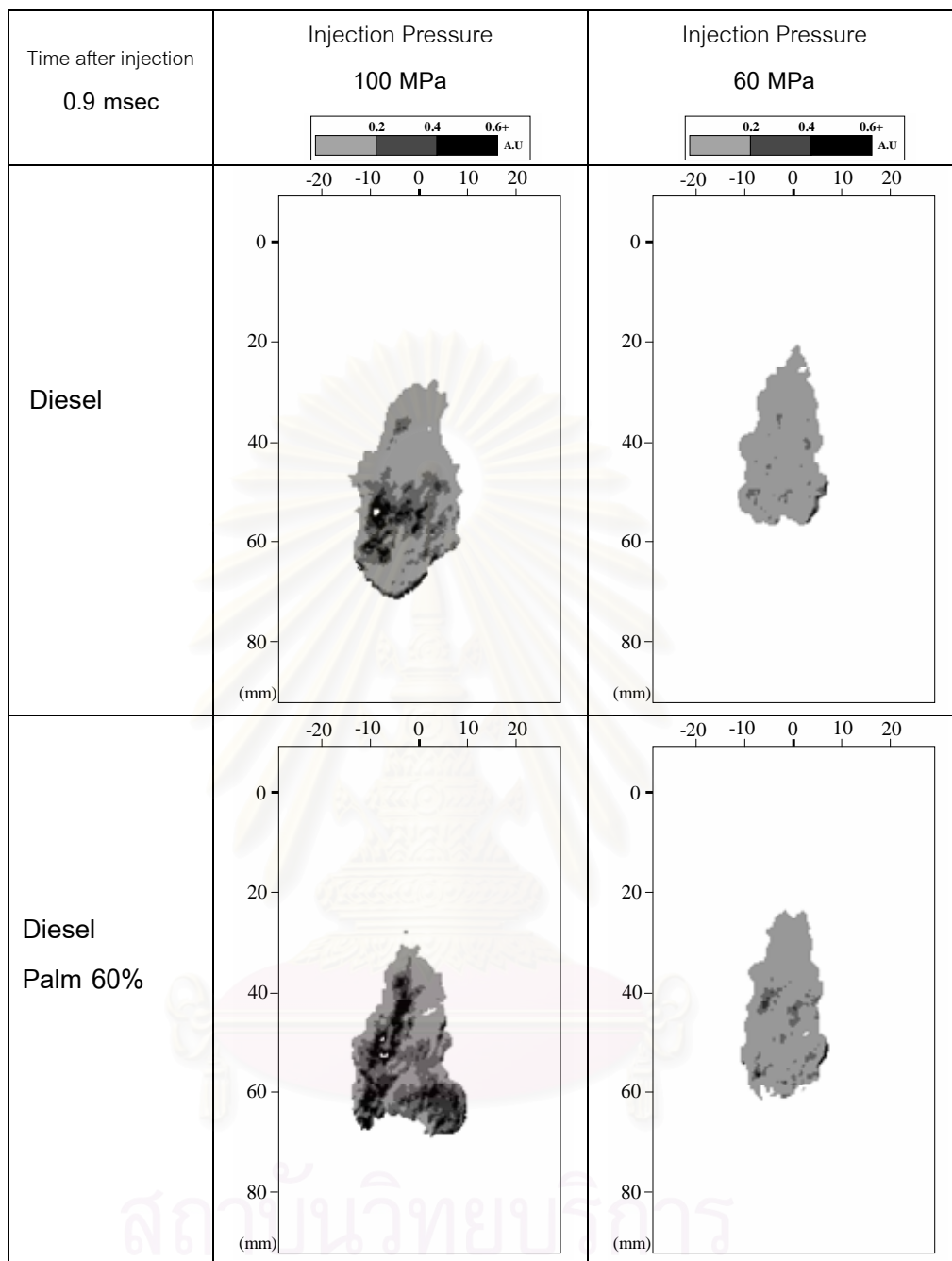


Fig.5-26 Combustion flame KL factor distribution of Diesel fuel and Palm diesel 60 %

Injection pressure 100MPa and 60MPa, Combustion at 3.0 MPa

0.9 msec after start of injection, ICCD camera Gain 5.5, width 10 μ sec

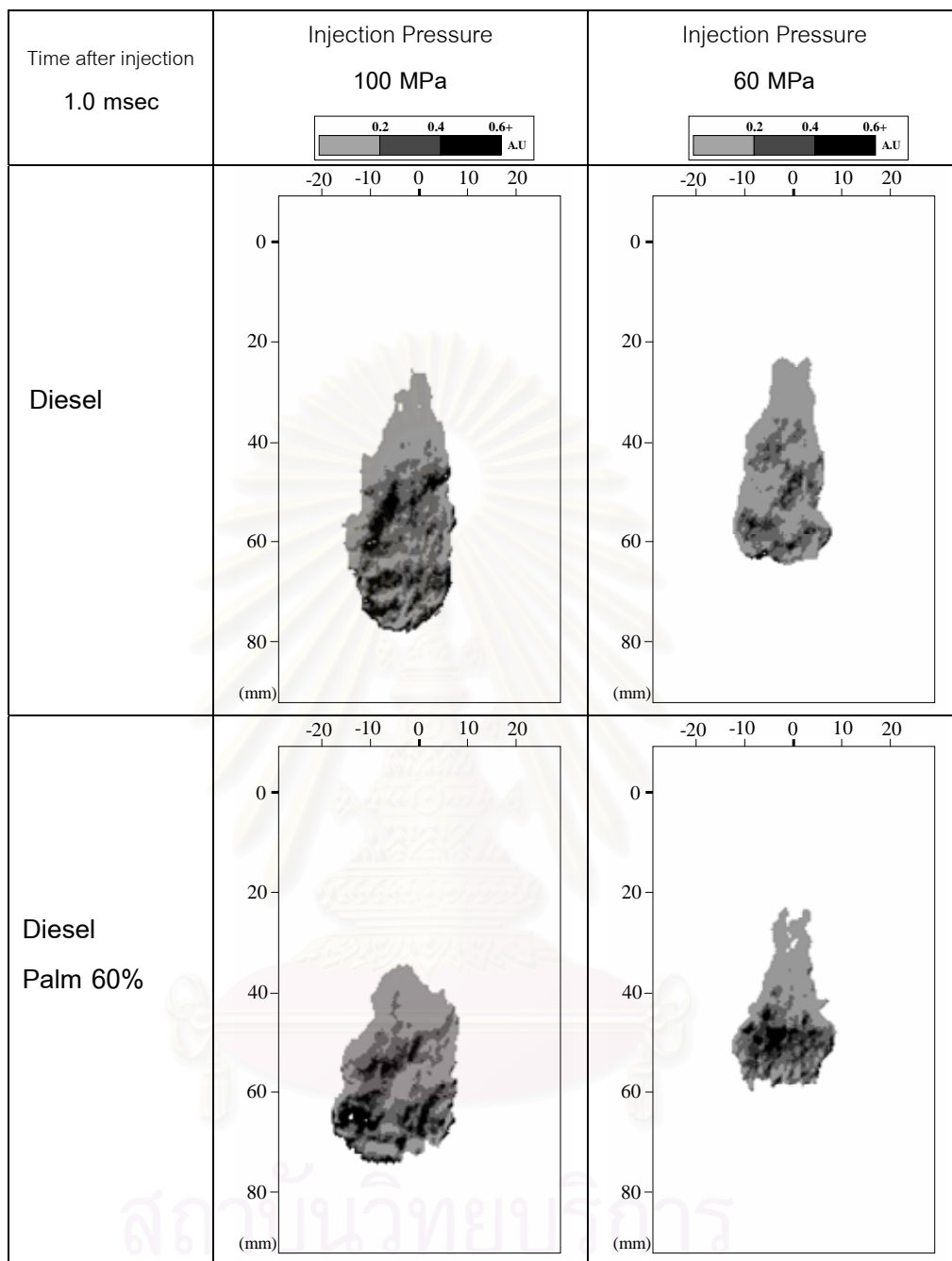


Fig.5-27 Combustion flame KL factor distribution of Diesel fuel and Palm diesel 60 %

Injection pressure 100MPa and 60MPa, Combustion at 3.0 MPa

1.0 msec after start of injection, ICCD camera Gain 5.5, width 10 μ sec

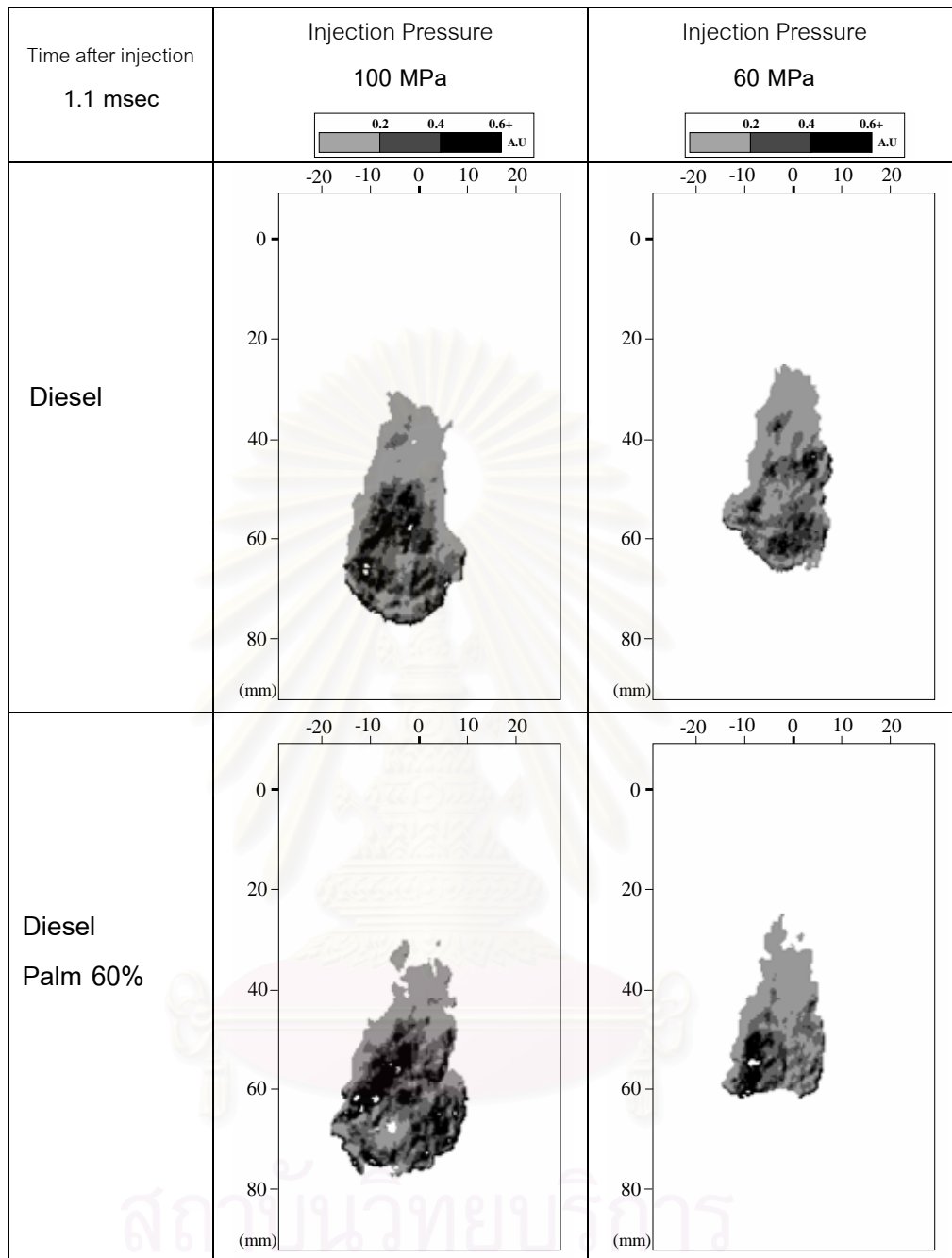


Fig.5-28 Combustion flame KL factor distribution of Diesel fuel and Palm diesel 60 %

Injection pressure 100MPa and 60MPa, Combustion at 3.0 MPa

1.1 msec after start of injection, ICCD camera Gain 5.5, width 10 μ sec

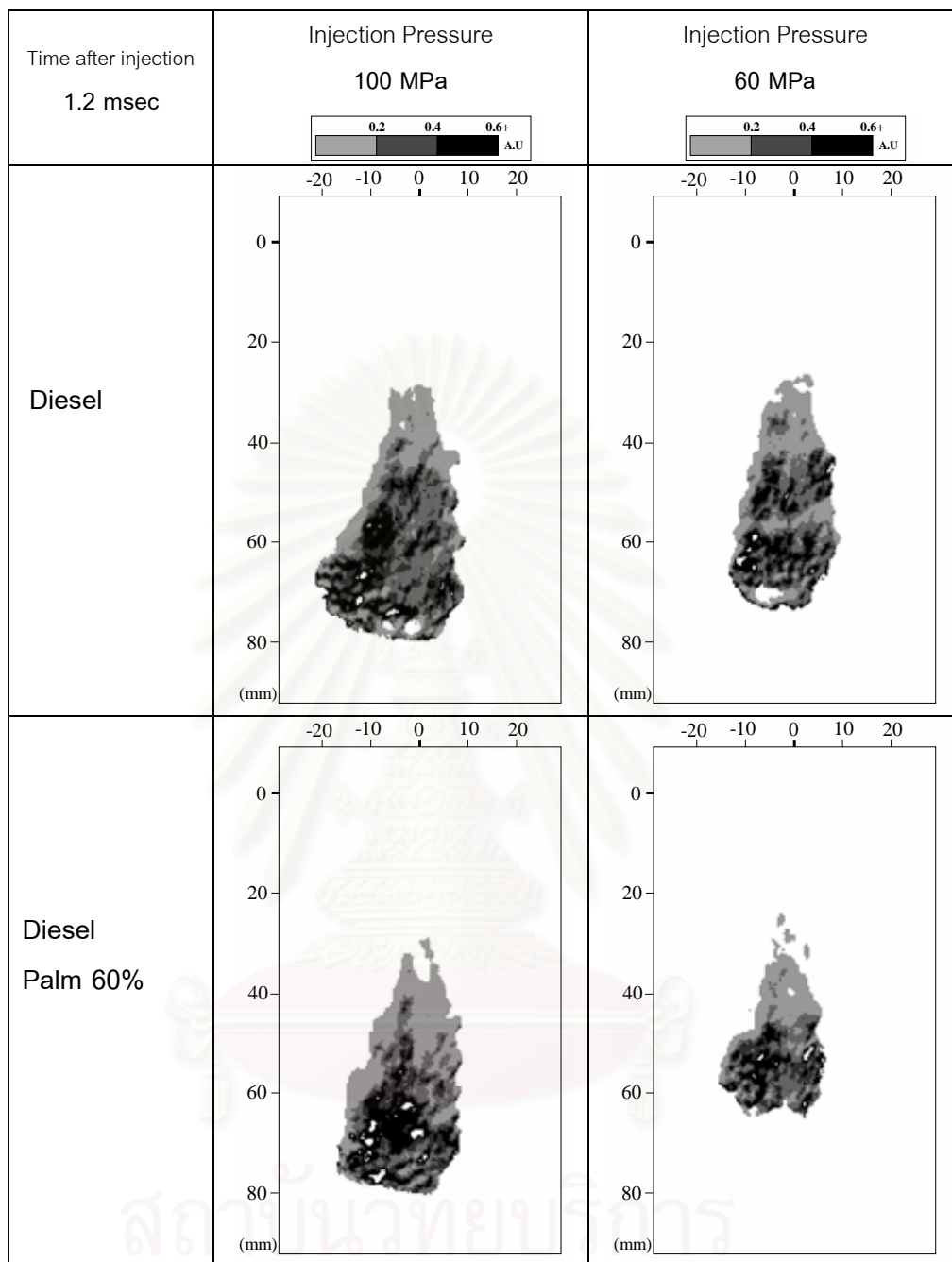


Fig.5-29 Combustion flame KL factor distribution of Diesel fuel and Palm diesel 60 %

Injection pressure 100MPa and 60MPa, Combustion at 3.0 MPa

1.2 msec after start of injection, ICCD camera Gain 5.5, width 10 μ sec

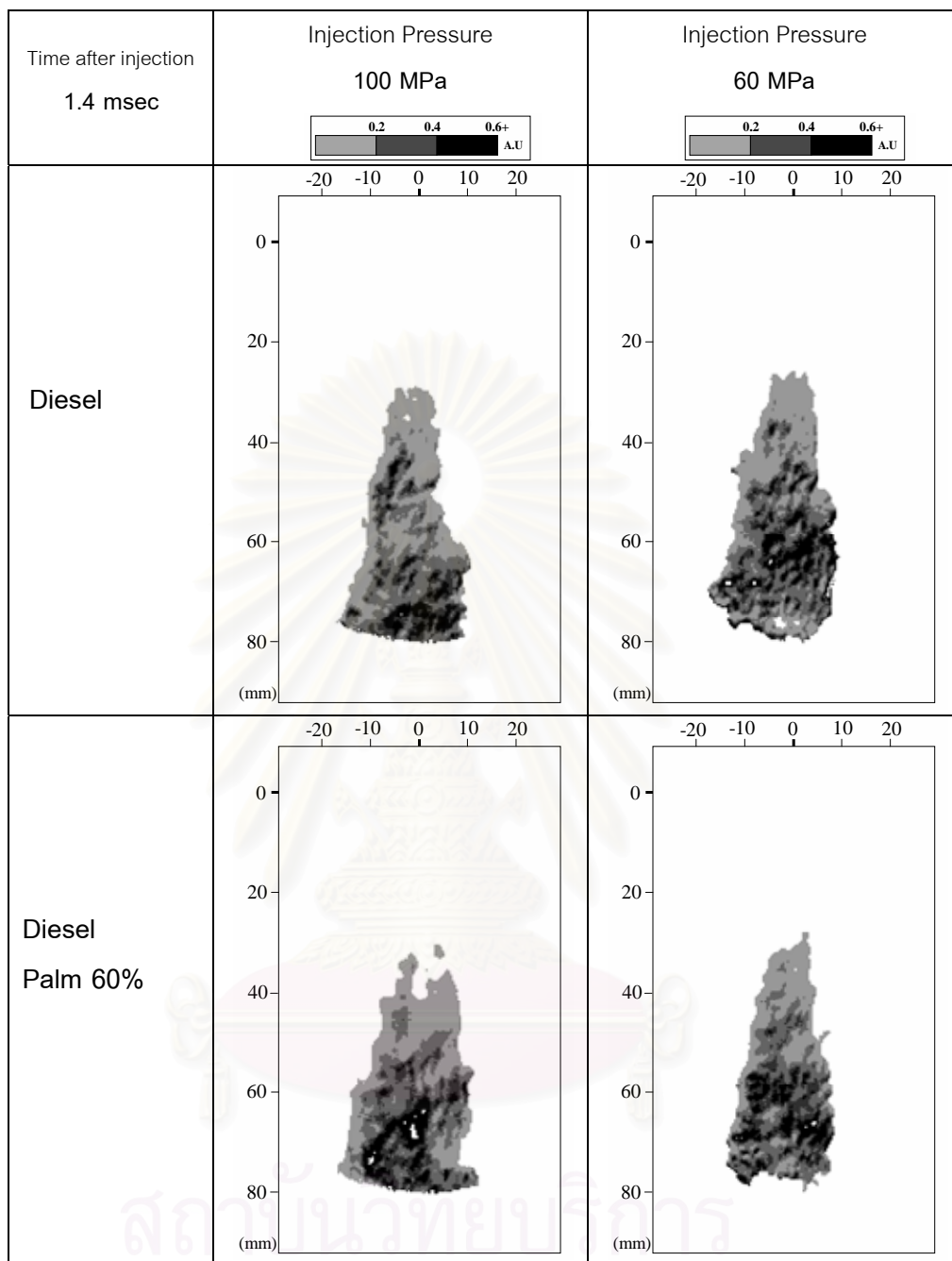


Fig.5-30 Combustion flame KL factor distribution of Diesel fuel and Palm diesel 60 %

Injection pressure 100MPa and 60MPa, Combustion at 3.0 MPa

1.4 msec after start of injection, ICCD camera Gain 5.5, width 10 μ sec

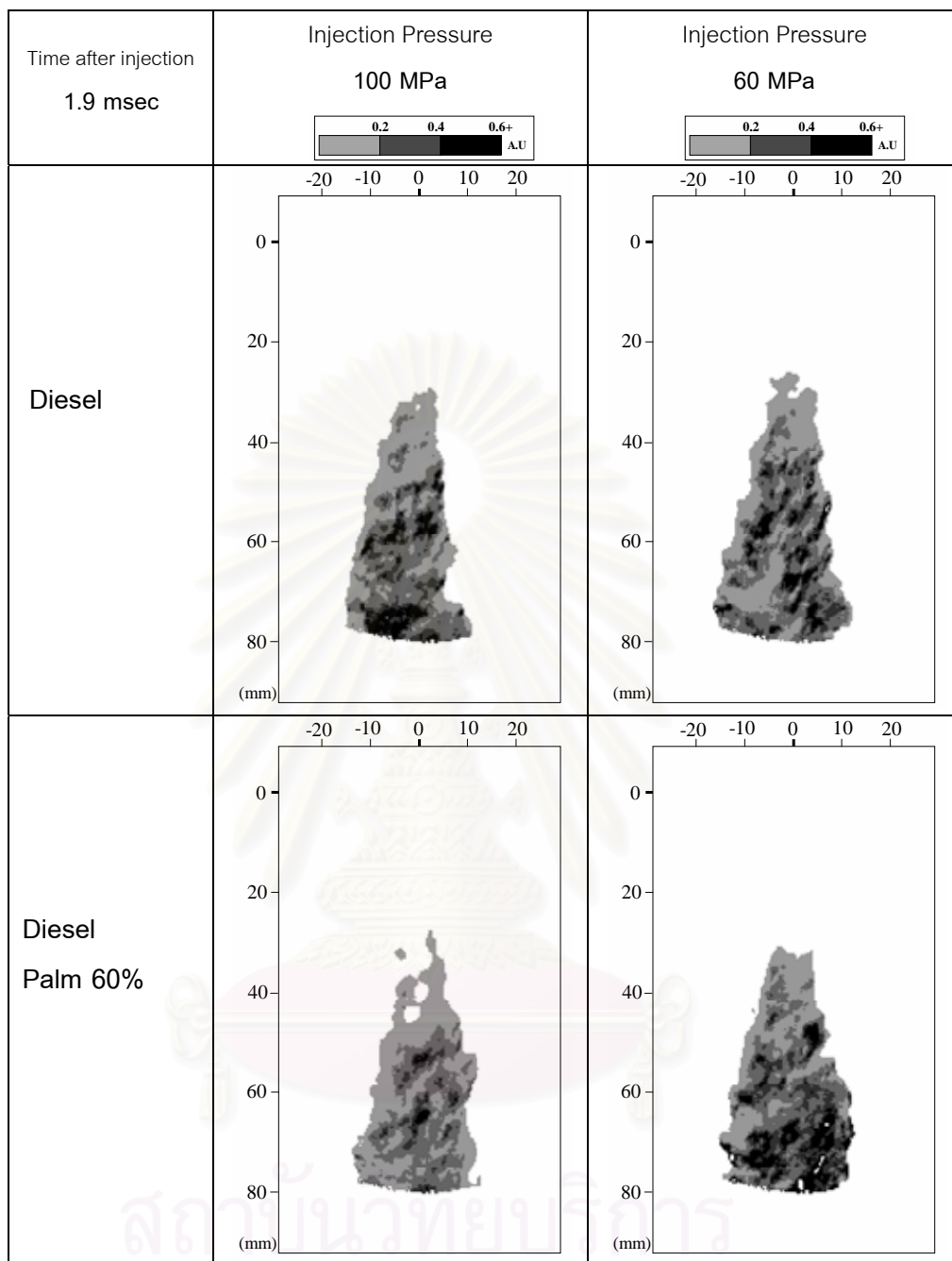


Fig.5-31 Combustion flame KL factor distribution of Diesel fuel and Palm diesel 60 %

Injection pressure 100MPa and 60MPa, Combustion at 3.0 MPa

1.9 msec after start of injection, ICCD camera Gain 5.5, width 10 μ sec

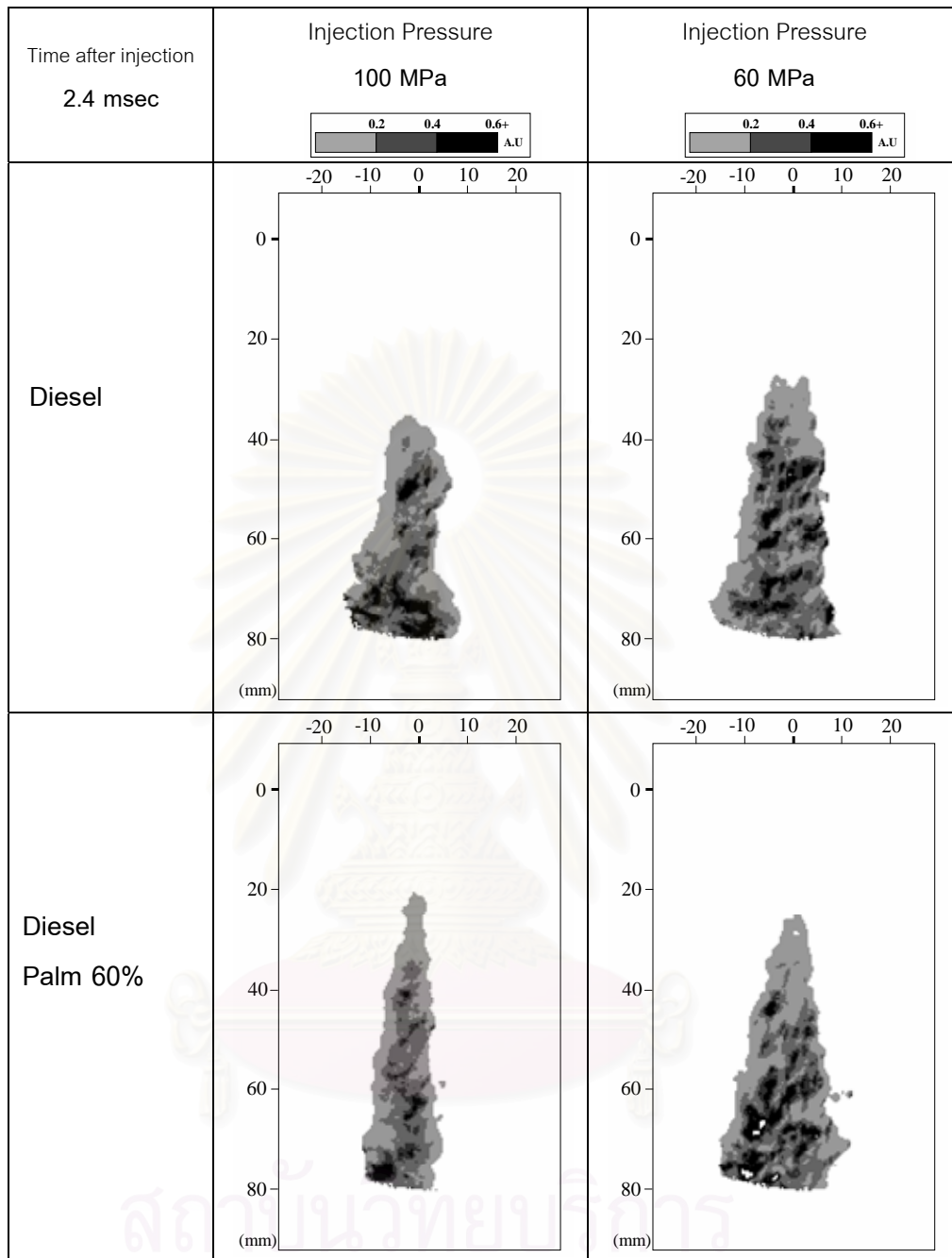


Fig.5-32 Combustion flame KL factor distribution of Diesel fuel and Palm diesel 60 %

Injection pressure 100MPa and 60MPa, Combustion at 3.0 MPa

2.4 msec after start of injection, ICCD camera Gain 5.5, width 10 μ sec

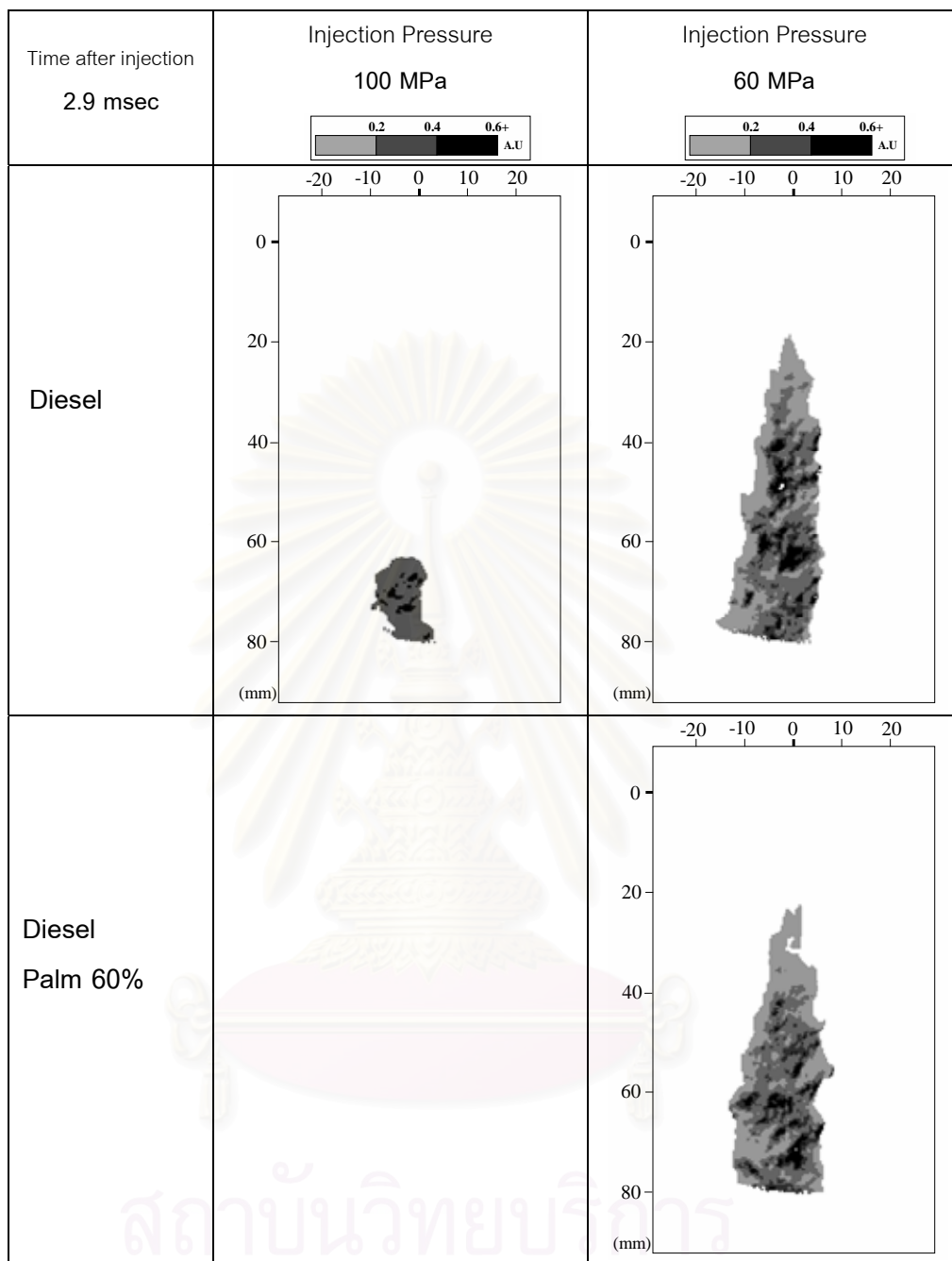


Fig.5-33 Combustion flame KL factor distribution of Diesel fuel and Palm diesel 60 %

Injection pressure 100MPa and 60MPa, Combustion at 3.0 MPa

2.9 msec after start of injection, ICCD camera Gain 5.5, width 10 μ sec

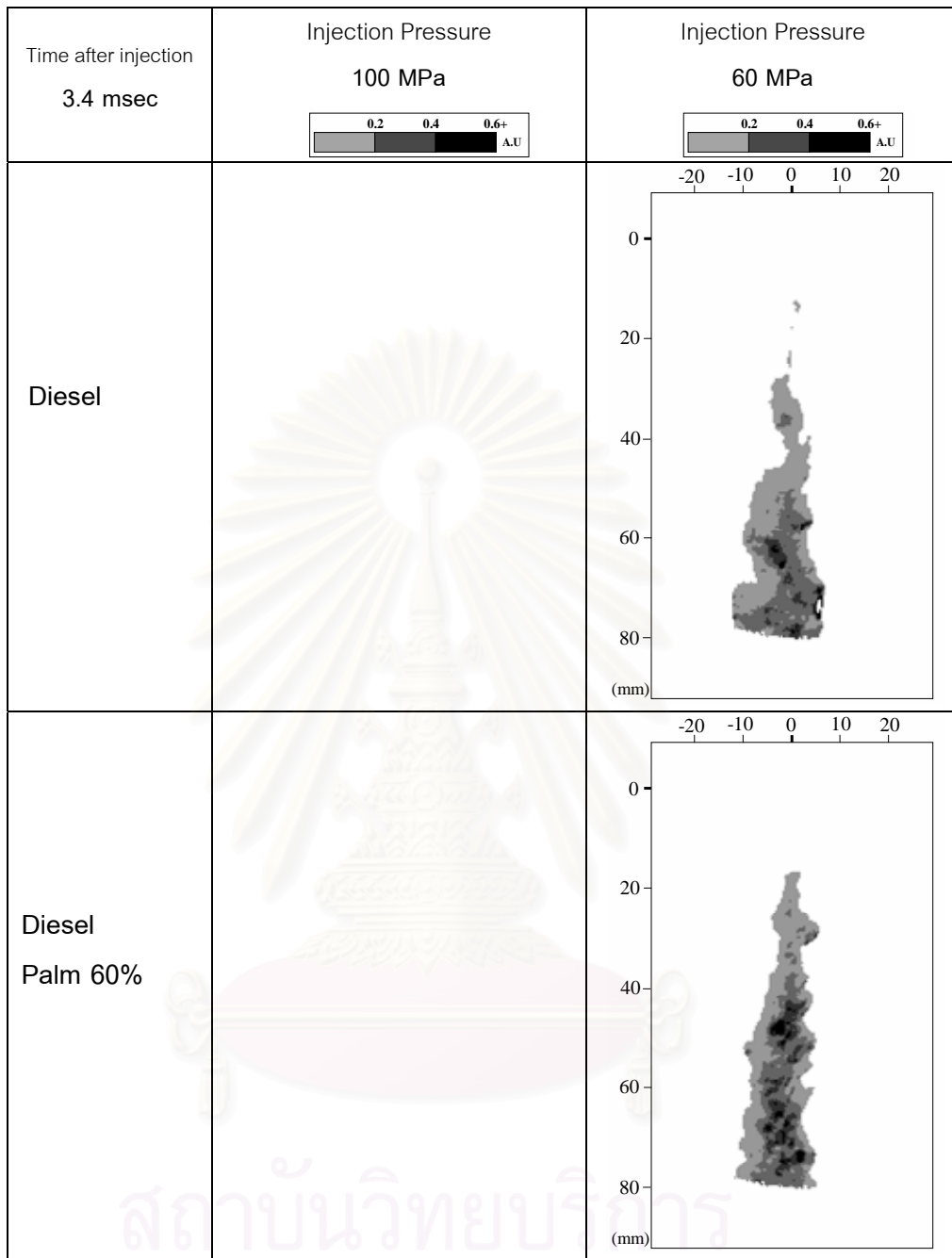


Fig.5-34 Combustion flame KL factor distribution of Diesel fuel and Palm diesel 60 %

Injection pressure 100MPa and 60MPa, Combustion at 3.0 MPa

3.4 msec after start of injection, ICCD camera Gain 5.5, width 10 μ sec

5.1.3.1.5. KL factor histogram

The KL factor histogram was calculated by evaluating the KL factor from the counted number of combustion flame pixel and converting them to flame area (mm^2). The KL factor interval was selected at 0.005 A.U. and the data are shown from figure 5-35 to 5-38, took the images from instant of 0.9, 1.4, 1.9 and 2.4 msec after start of combustion, respectively.

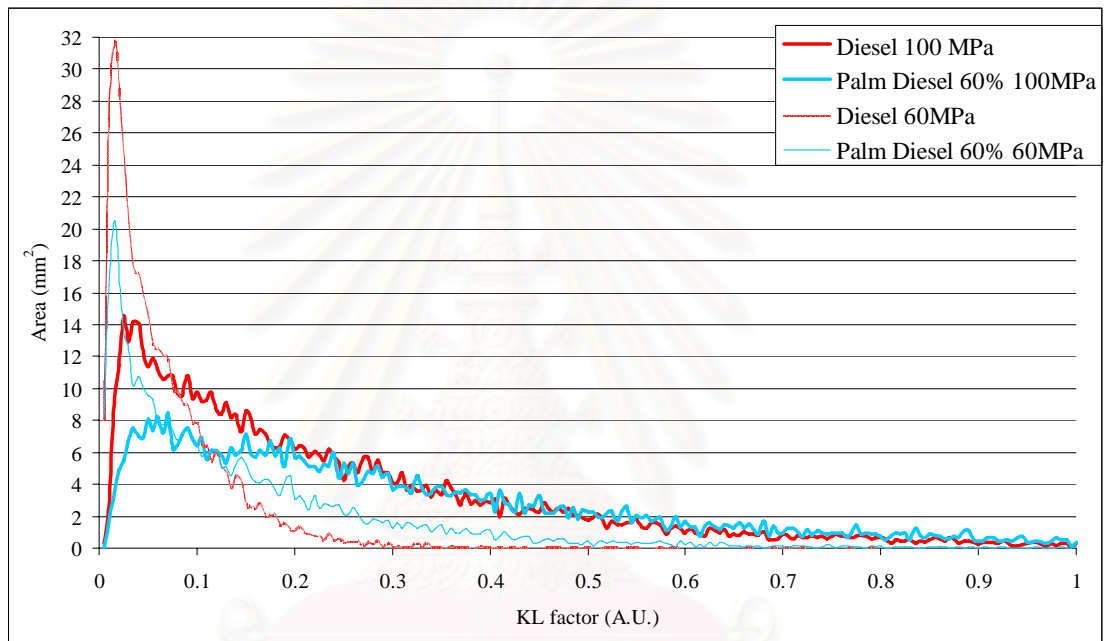


Fig. 5-35 KL factor histogram of Diesel and 60% Palm Diesel at injection pressure 60 MPa and 100 MPa, Combustion at 3.0 MPa 930K 0.9 msec after start of injection

From figure 5-35, low KL factor had a larger area at injection pressure 60 MPa compared with 100 MPa. The KL factor of palm diesel 60% seem to be lower than diesel.

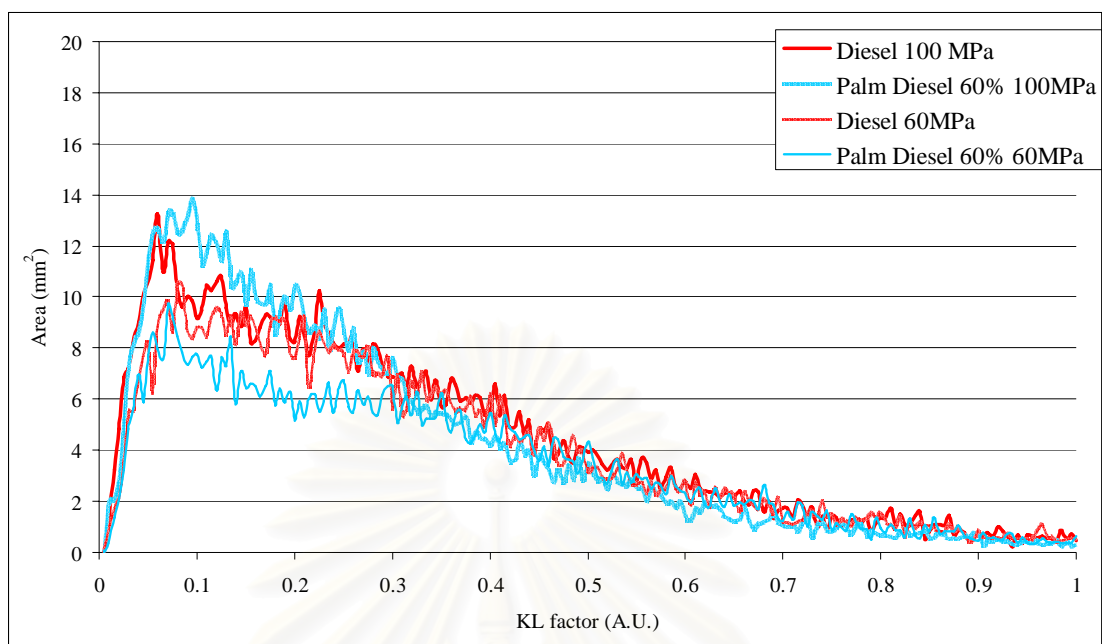


Fig. 5-36 KL factor histogram of Diesel and 60% Palm Diesel at injection pressure 60 MPa and 100 MPa, Combustion at 3.0 MPa 930K 1.4 msec after start of injection

The KL factor value of 100 MPa injection pressure was higher than 60 MPa. At 60 MPa injection pressure, the KL factor of palm diesel 60% was lower than diesel but at the 100 MPa, KL factor was higher.

สถาบันวิทยบริการ
จุฬาลงกรณ์มหาวิทยาลัย

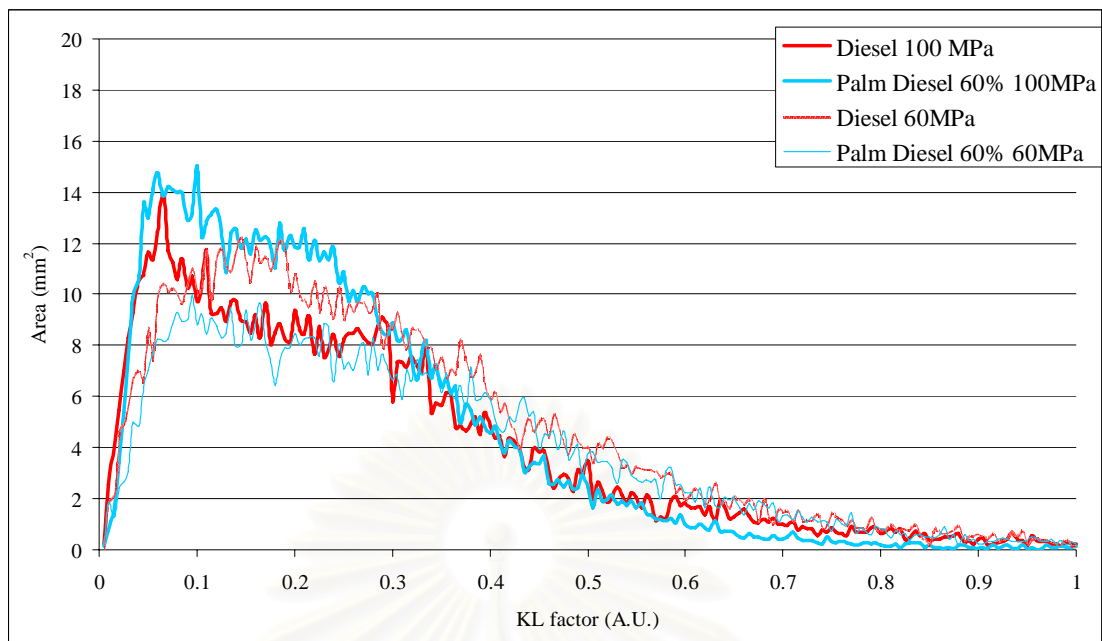


Fig. 5-37 KL factor histogram of Diesel and 60% Palm Diesel at injection pressure 60 MPa and 100 MPa, Combustion at 3.0 MPa 930K 1.9 msec after start of injection

The KL factor value of 100 MPa injection pressure was higher than 60 MPa. At 60 MPa injection pressure, the KL factor of palm diesel 60% was lower than diesel but at the 100 MPa, KL factor was higher.

สถาบันวิทยบริการ
จุฬาลงกรณ์มหาวิทยาลัย

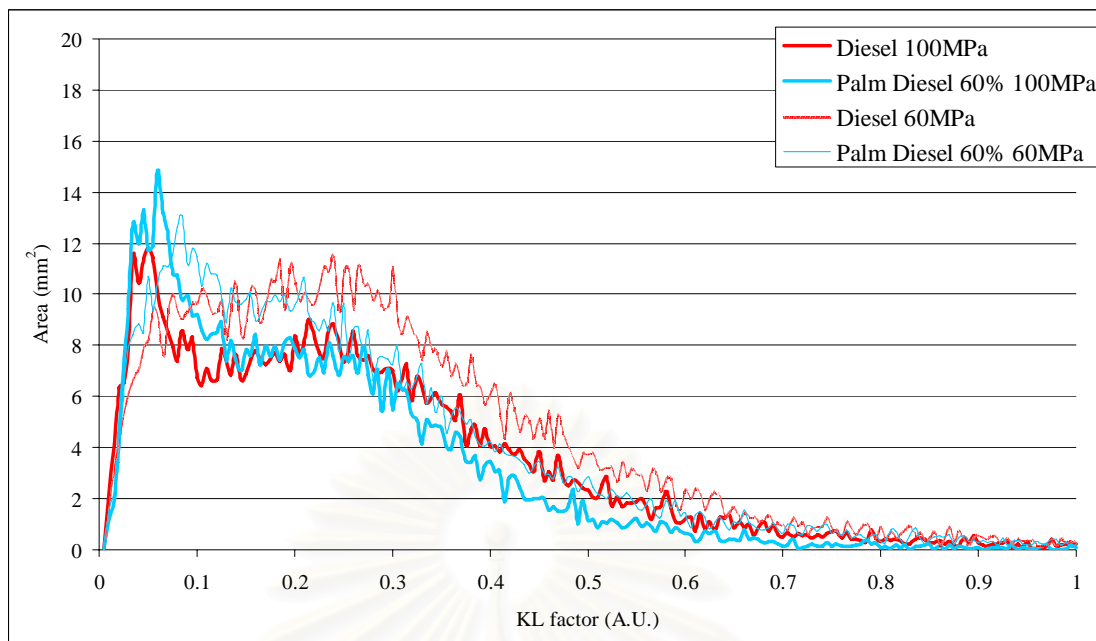


Fig. 5-38 KL factor histogram of Diesel and 60% Palm Diesel at injection pressure 60 MPa and 100 MPa, Combustion at 3.0 MPa 930K 2.4 msec after start of injection

At the end of the combustion, the KL factor of 60 MPa injection pressure, was higher than 100 MPa because the longer injection timing. KL factor of palm diesel seemed to be higher but the difference was very small.

From KL factor histogram, KL factor value was very low at the start of the combustion. At this time diesel fuel KL factor value were higher than palm diesel 60% at injection pressure 60 and 100 MPa.

At the injection pressure 100MPa, KL factor value could be higher than that at 60 MPa because of the larger combustion area.

The palm 60% produced lower KL factor at low injection pressure (60 MPa) but at the high injection pressure 100 MPa, the KL factor became higher compared with diesel fuel.

5.1.3.1.6. The analysis of flame temperature and KL factor

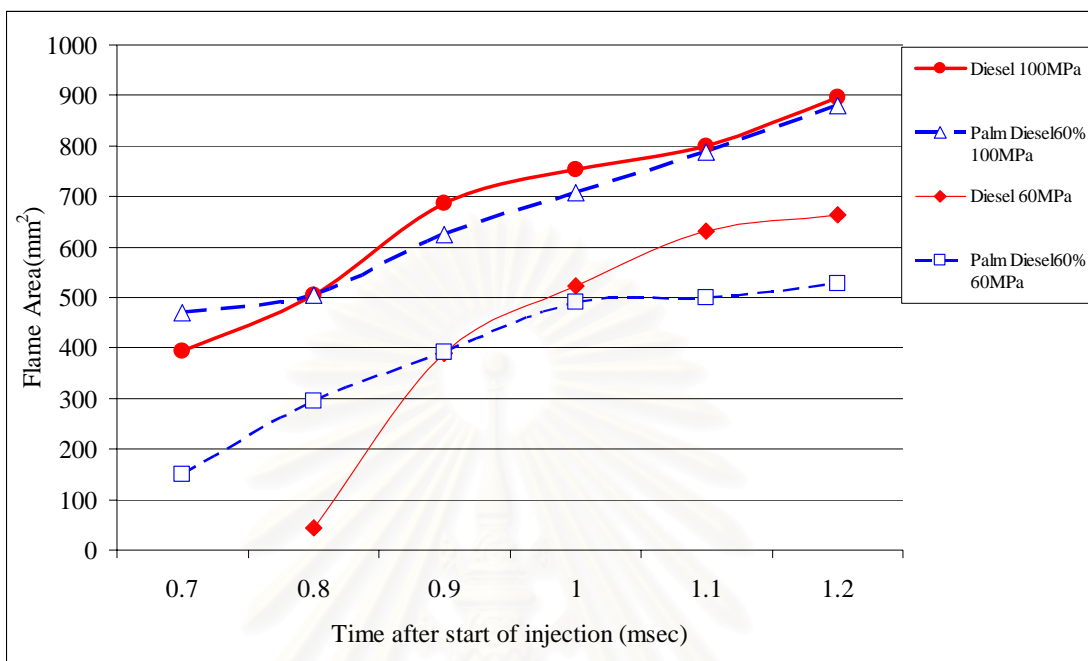


Fig. 5-39 Flame area of Diesel and 60% Palm Diesel at injection pressure 60 MPa and 100 MPa, Combustion at 3.0 MPa 930K 0.7-1.2 msec after start of injection

At start of combustion, the flame area of fuel injected at 100 MPa was larger than 60 MPa.

It could be observed that the difference between palm diesel 60% and diesel at 100 MPa was very small.

At 60 MPa injection pressure, the flame area increasing rate of diesel was higher than palm 60%.

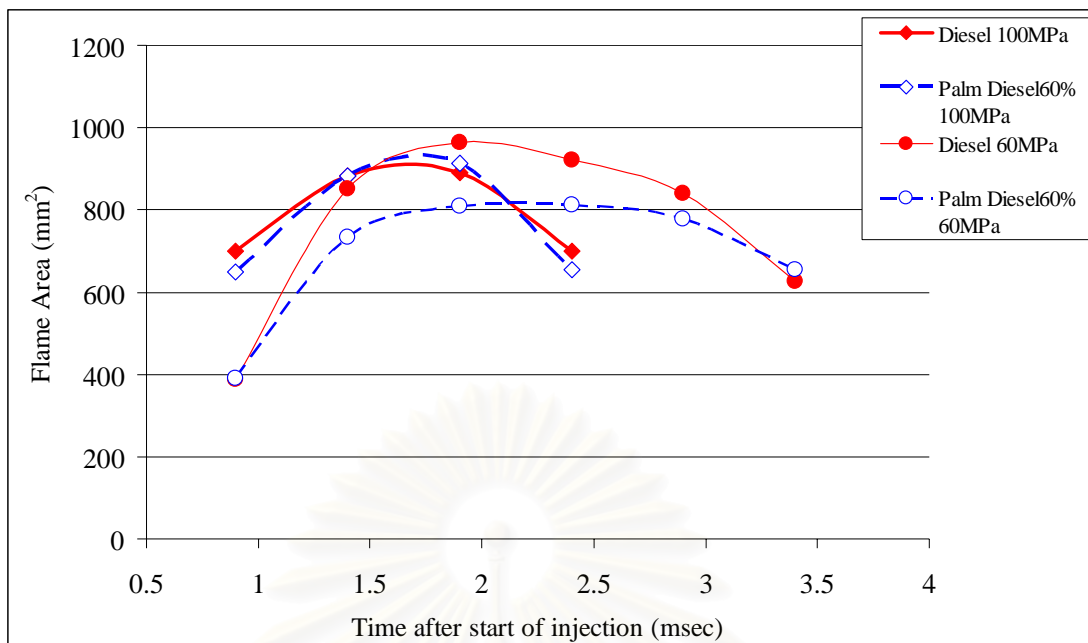


Fig. 5-40 Flame area of Diesel and 60% Palm Diesel at injection pressure 60 MPa and 100 MPa, Combustion at 3.0 MPa 930K 0.9-3.4 msec after start of injection

At the main combustion, injection pressure 100 MPa, the difference in flame area of diesel and palm 60% were very small.

In the case of injection pressure 60 MPa, flame area of diesel was larger than palm 60%.

It could be concluded that higher injection pressure caused larger flame area. This might be resulted from the better fuel atomization and combustion.

สถาบันวิทยบริการ
จุฬาลงกรณ์มหาวิทยาลัย

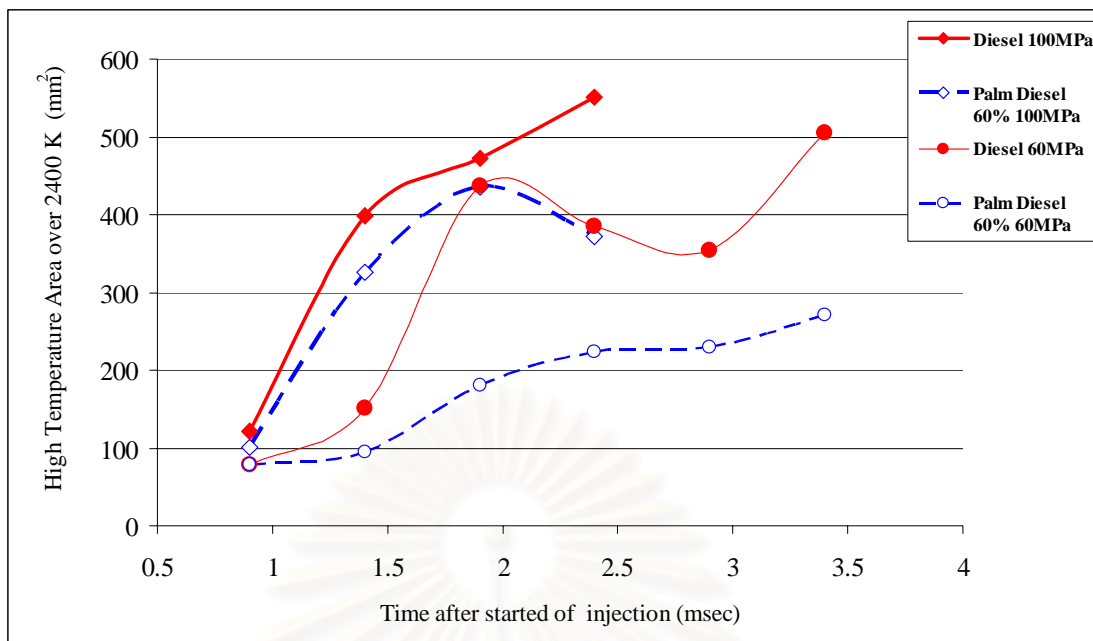


Fig. 5-41 High temperature area of Diesel and 60% Palm Diesel at injection pressure 60 MPa and 100 MPa, Combustion at 3.0 MPa 930K 0.9-3.4 msec after start of injection

The high temperature area (over 2400 K) produced by palm diesel 60% was smaller than that by diesel at both injection pressures.

The difference between both fuels was small at the high injection pressure (100 MPa), perhaps due to better fuel combustion.

สถาบันวิทยบริการ
จุฬาลงกรณ์มหาวิทยาลัย

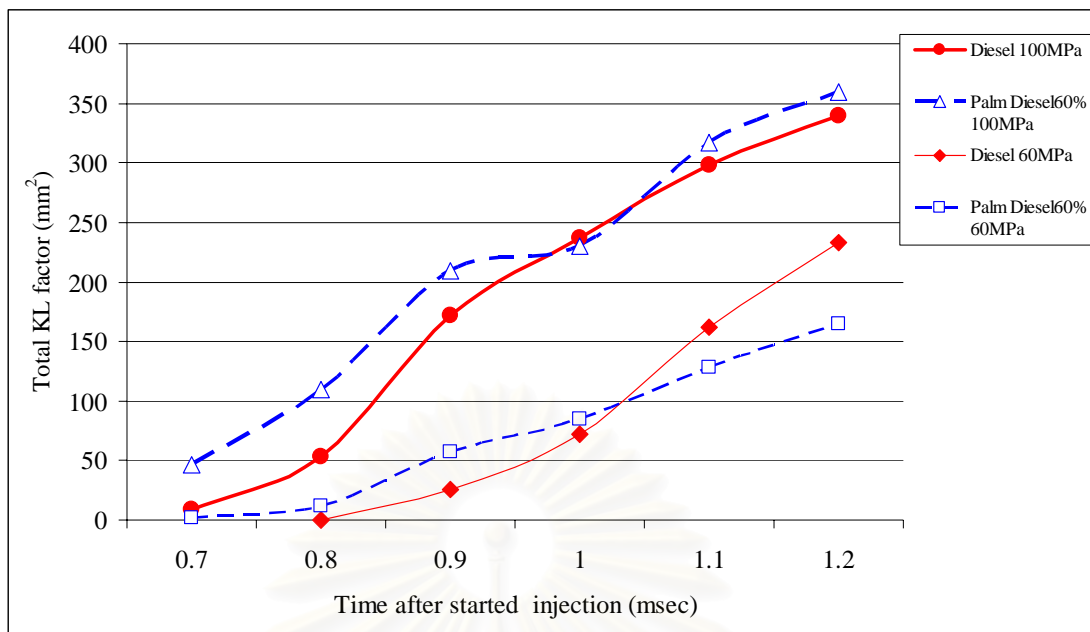


Fig. 5-42 Total KL factor of Diesel and 60% Palm Diesel at injection pressure 60 MPa and 100 MPa Combustion at 3.0 MPa 930K 0.7-1.2 msec after start of injection

Total KL factor is the summation of KL factor value at all flame area. This factor could be used to estimate the total soot of the combustion.

At the start of combustion total KL factor of palm 60%, 100 MPa was higher than in diesel.

The difference of KL factor was very small at low injection pressure (60MPa).

สถาบันวิทยบริการ
จุฬาลงกรณ์มหาวิทยาลัย

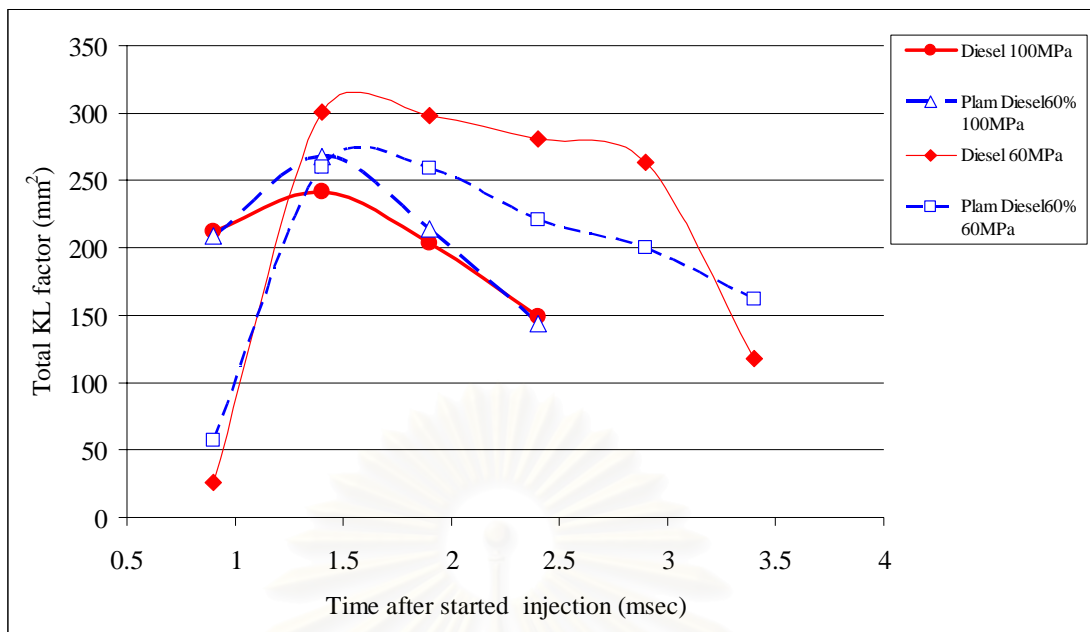


Fig. 5-43 Total KL factor of Diesel and 60% Palm Diesel at injection pressure 60 MPa and 100 MPa Combustion at 3.0 MPa 930K 0.9-3.4 msec after start of injection

At the main of combustion, total KL factor of palm 60%, 100 MPa was higher than in diesel.

In the case of 60 MPa injection pressure, total KL factor of palm 60% was lower than in diesel.

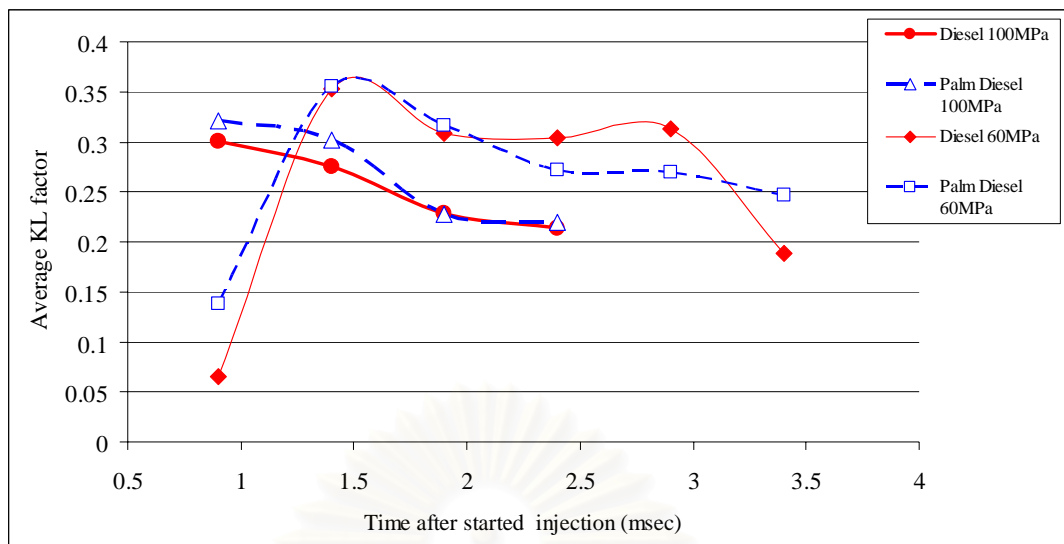


Fig. 5-44 Average KL factor of Diesel and 60% Palm Diesel at injection pressure 60 MPa and 100 MPa Combustion at 3.0 MPa 930K 0.9-3.4 msec after start of injection

The average KL factor was calculated from the total of KL factor divided by flame area at all flame area. This factor could be used to estimate the soot concentration of the combustion.

At the start of combustion average KL factor of palm 60%, 100 MPa was higher than in diesel but at the end of the combustion this value was at same level as palm diesel.

In the case of low injection pressure (60 MPa), the difference was very small with both fuels.

Combustion flame areas of palm diesel 60% were smaller than that of diesel at injection pressure of 60 MPa but after increasing the injection pressure up to 100 MPa, the area size was close to the diesel as shown in figure 5-39 and 5-40.

High temperature area of combustion flame (>2400 K) was calculated. It is shown in figure 5-41 that the high temperature area of palm diesel 60 % was smaller than diesel. The higher injection pressure caused the larger high temperature area.

Average KL factor shown in figures 5-44 is the total of KL factor over the flame area, shown in figure 5-43, divided by flame area. Soot concentration can be estimated based on KL factor. The soot concentration of palm diesel 60% seemed to be higher than diesel at the injection pressure of 100 MPa and 60 MPa.

5.1.3.2. The study on combustion of palm diesel 60%, 80% and palm 100% at injection pressure 100 MPa

Blend between commercial diesel and refined palm at the percentages of 60%, 80% and palm 100% were used in this study. The process for preparing the blend are; 1. Heat refined palm oil up to 60 °C, 2. Blend to diesel fuel, 3. Warm blend fuel up to 40 °C before loading into fuel tank. During the experiments, the fuel injection system had been also heated up to 40 °C to prevent the blended fuel becomes wax.

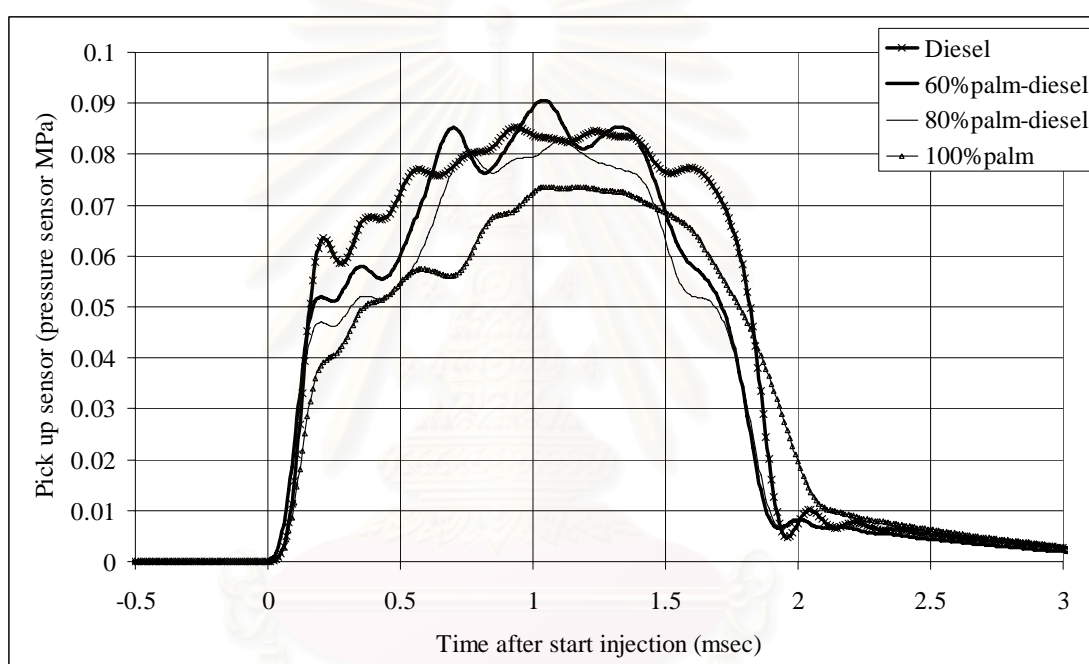


Fig. 5-45 Force pressure data obtained from pick up sensor at injection pressure 100 MPa

The rectangular injection rate shape was selected in this experiment. Fuel injection mass was set approximately 15 mg and injection pressure of 100 MPa was selected for this experiments.

The data obtained from pick up sensor (the pressure sensor for measuring force at the nozzle tip) is shown in figure 5-45. The force of injection was decreased with the higher percentage blended of palm oil. It can be concluded that the higher percentage palm diesel strongly affects the spray phenomena.

5.1.3.2.1. Intensity distribution of combustion flame.

In each following images, the left part is corresponding with red filter and the right part is with blue filter.

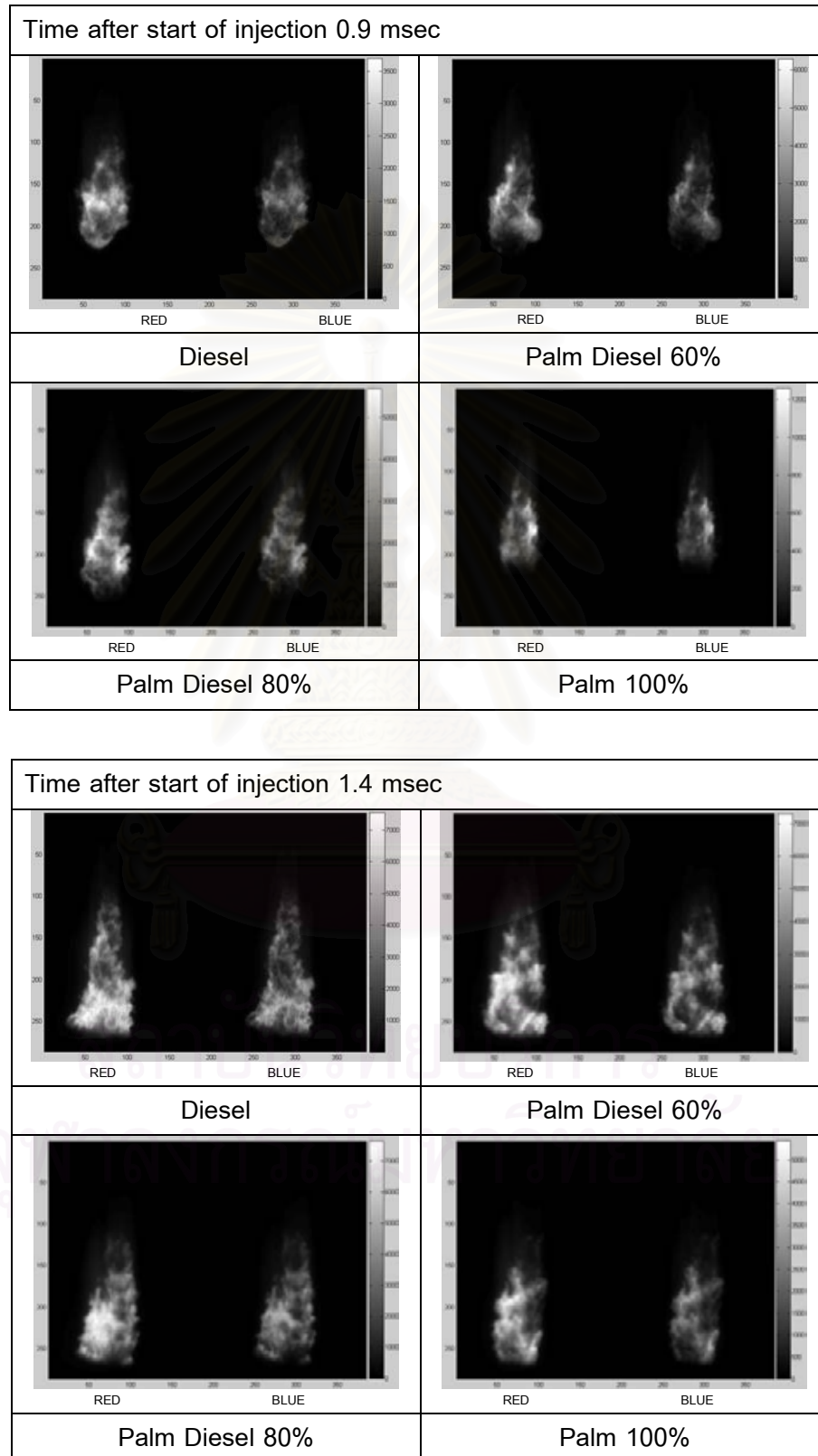


Fig. 5-46 The combustion light intensity of diesel, palm diesel 60%, 80% and palm 100%

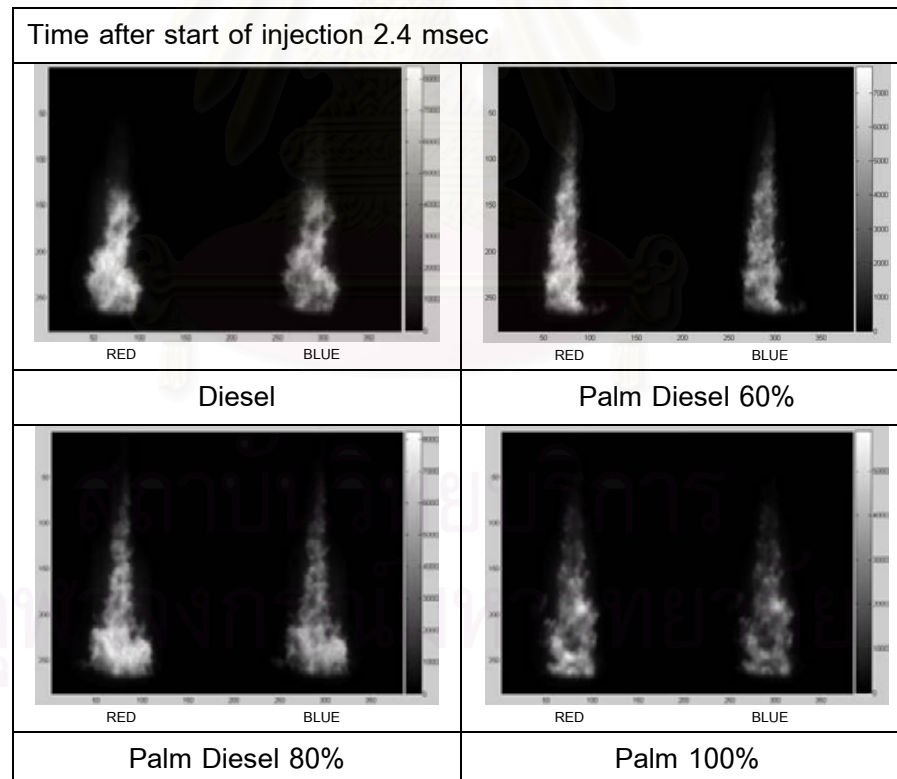
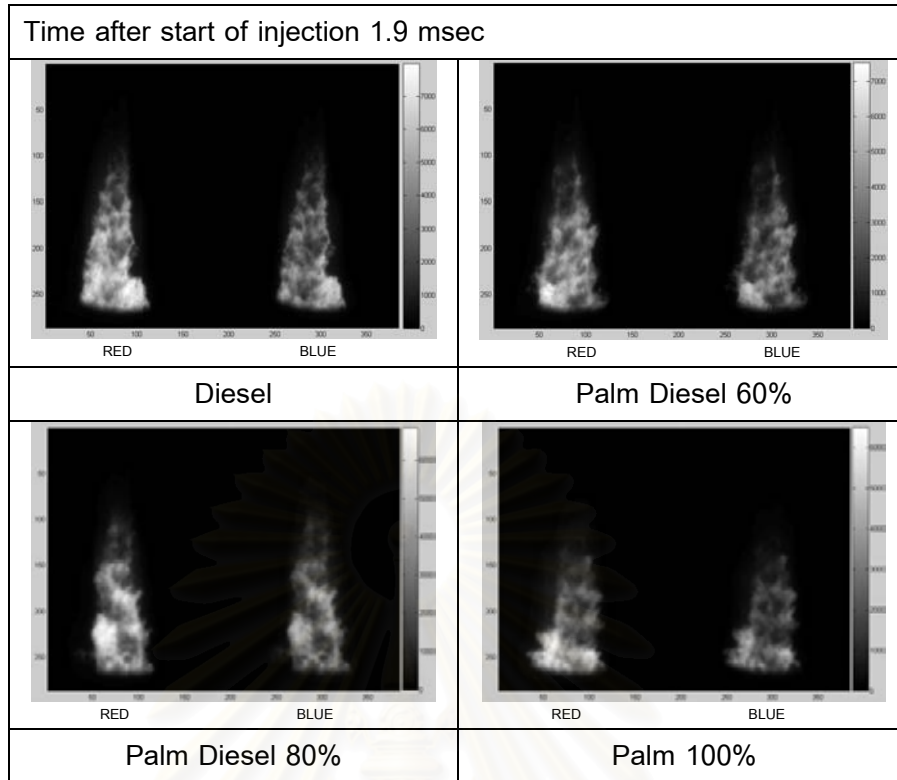


Fig. 5-46 (continue) Combustion light intensity of diesel, palm diesel 60%, 80% and palm 100%

5.1.3.2.2. Combustion flame temperature and KL factor distribution

Some of calculated results of true temperature and KL factor of diesel, palm diesel 60%, 80% and palm 100% are shown in figure 5-47 to 5-50.

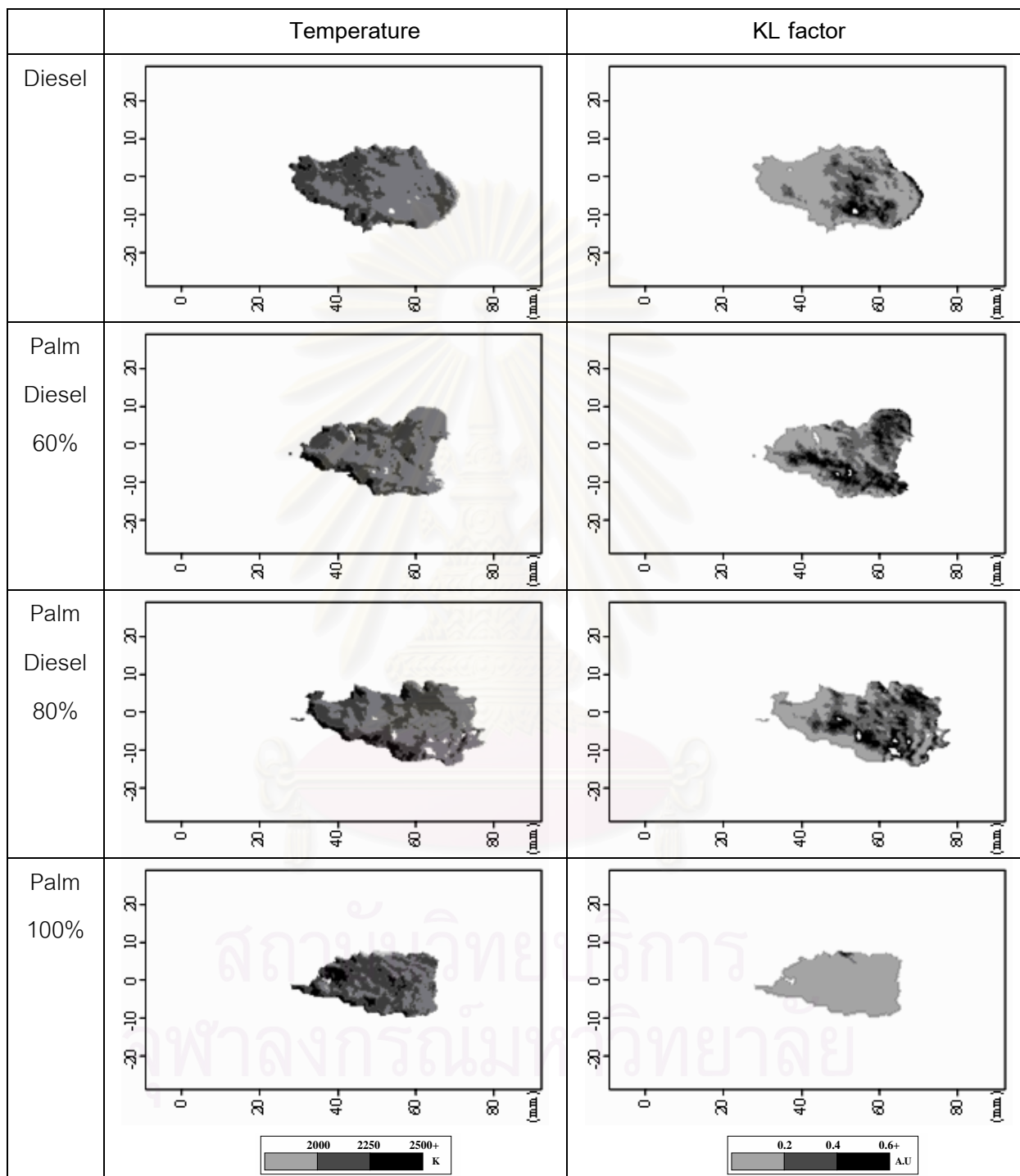


Fig.5-47 Combustion flame temperature and KL factor distribution of Diesel fuel , Palm diesel 60 %,80 % and Palm 100 % , Injection pressure 100MPa, Combustion at 3.0 MPa, 0.9 msec after start of injection, ICCD camera Gain 5.5 width 10 μ sec

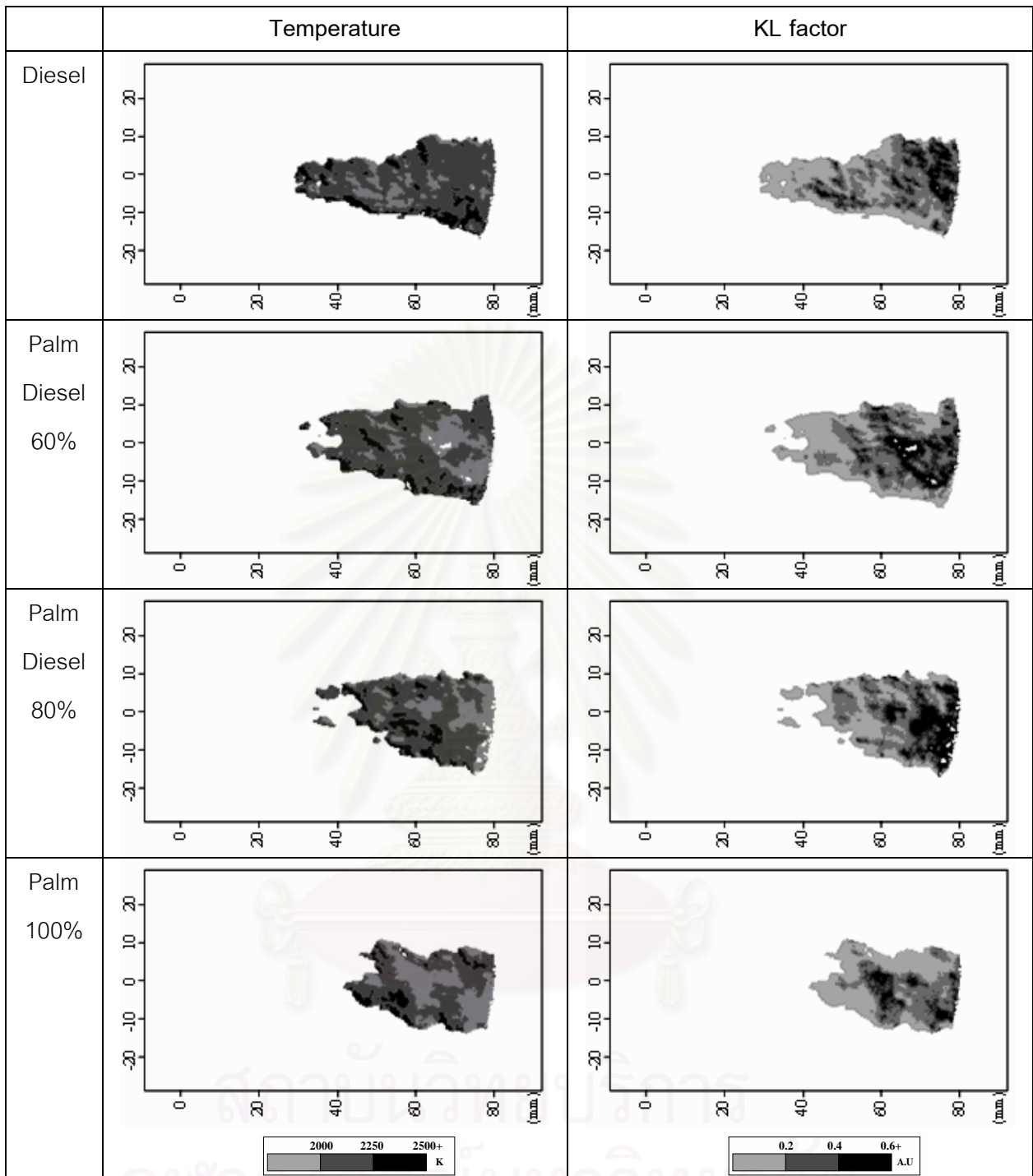


Fig.5-48 Combustion flame temperature and KL factor distribution of Diesel fuel ,Palm diesel 60 %,80 % and Palm 100 % Injection pressure 100MPa, Combustion at 3.0 MPa 1.4 msec after start of injection ICCD camera Gain 5.5 width 10 μ sec

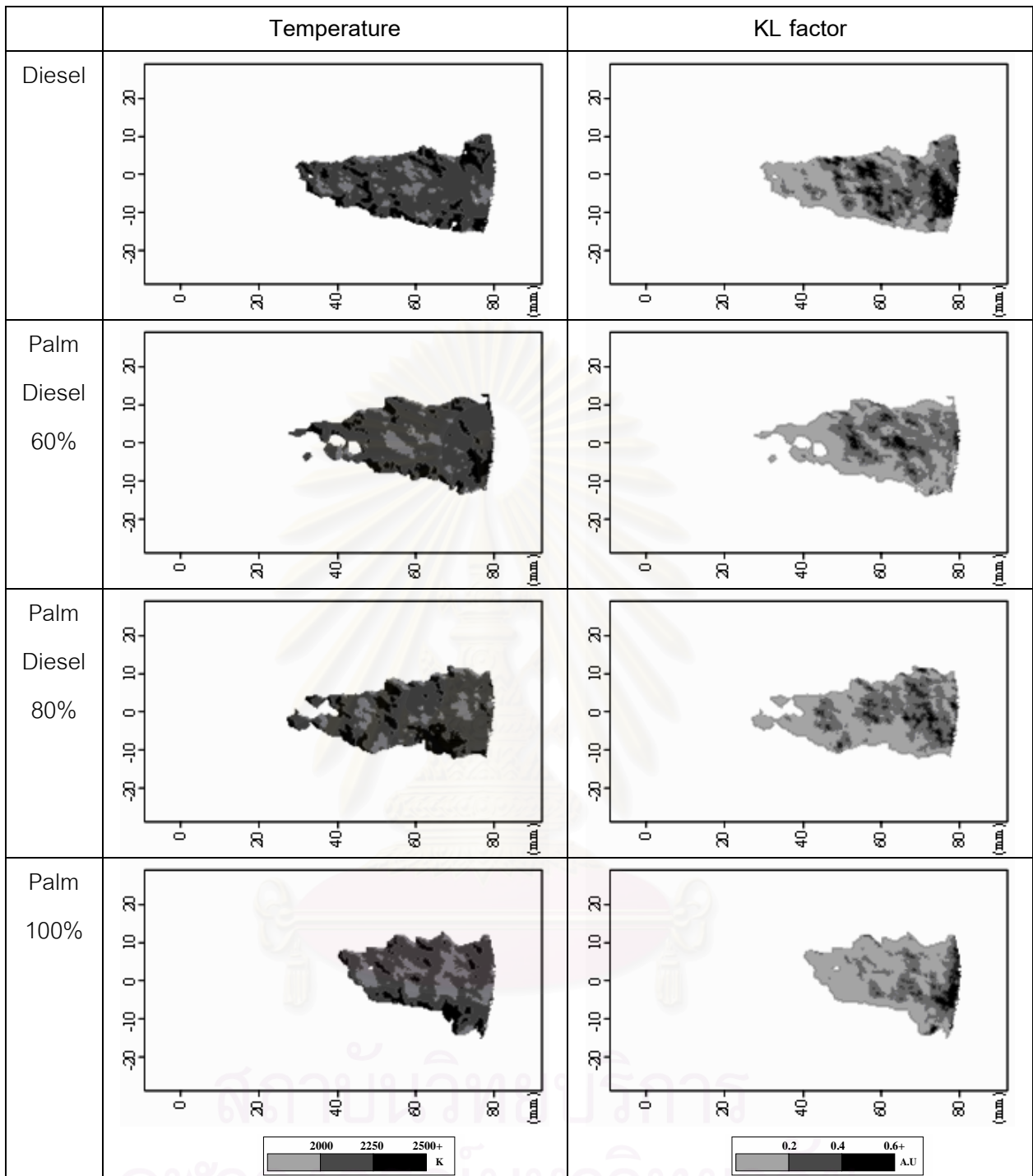


Fig.5-49 Combustion flame temperature and KL factor distribution

of Diesel fuel ,Palm diesel 60 %,80 % and Palm 100 %

Injection pressure 100MPa, Combustion at 3.0 MPa

1.9 msec after start of injection

ICCD camera Gain 5.5 width 10 μ sec

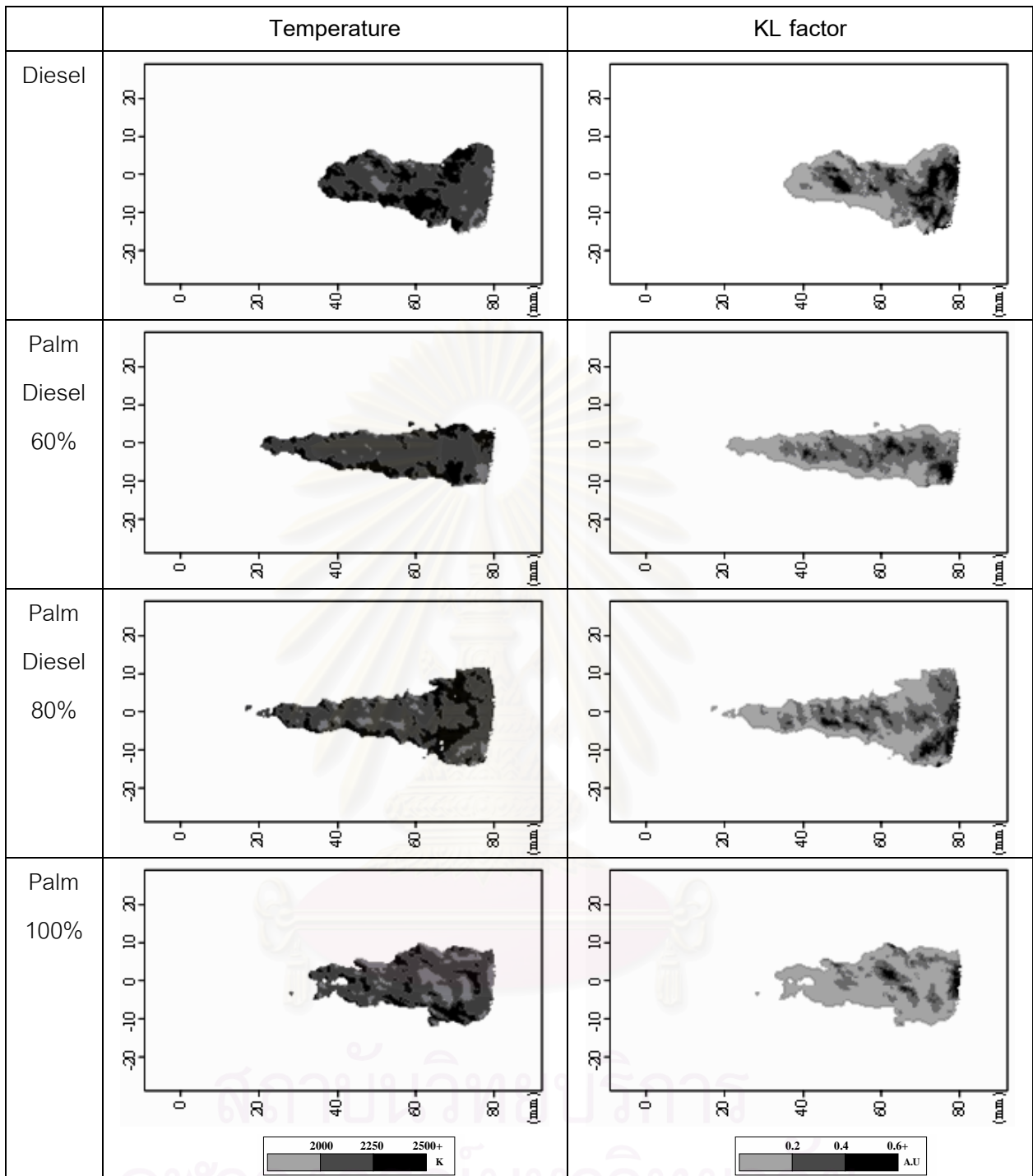


Fig.5-50 Combustion flame temperature and KL factor distribution

of Diesel fuel ,Palm diesel 60 %,80 % and Palm 100 %

Injection pressure 100MPa, Combustion at 3.0 MPa

2.4 msec after start of injection

ICCD camera Gain 5.5 width 10 μ sec

5.1.3.2.3. Combustion flame temperature histogram

The temperature histogram was calculated by counting the number of combustion flame pixel and converted them to flame area (mm^2). The temperature interval of 50K was selected and the data is shown from figure 5-51 to 5-54, taking images from instant of time 0.9, 1.4, 1.9 and 2.4 msec after start of combustion.

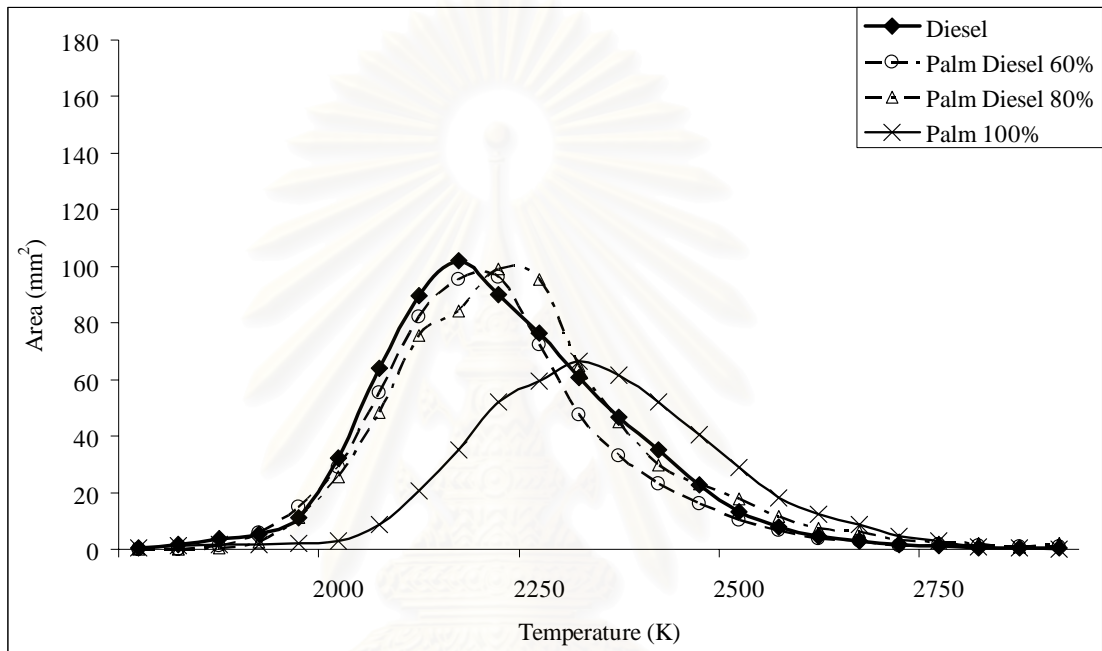


Fig. 5-51 Flame temperature histogram of Diesel, 60%,80% Palm Diesel and palm 100% at injection pressure 100 MPa Combustion at 3.0 MPa 930K 0.9 msec after start of injection

At the start of the combustion, Palm 100% combustion temperature was the highest but the flame area was smallest compared with all other fuels.

Combustion area and combustion temperature of diesel, palm 60% and palm 80% were closely same at this combustion timing.

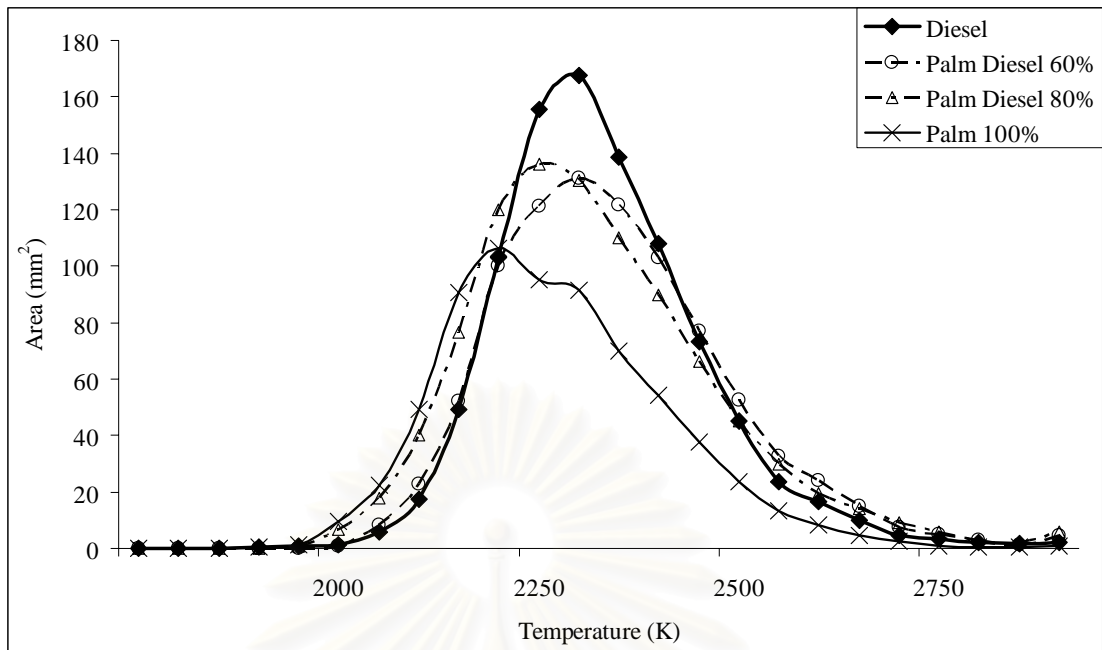


Fig. 5-52 Flame temperature histogram of Diesel, 60%,80% Palm Diesel and palm 100% at injection pressure 100 MPa Combustion at 3.0 MPa 930K 1.4 msec after start of injection

At this combustion timing, the combustion temperature of diesel fuel became the highest compared with other fuels.

There was not much difference between palm diesel 60% and palm diesel 80%. Palm 100% produced the lowest combustion temperature and area.

สถาบันวิทยบริการ
จุฬาลงกรณ์มหาวิทยาลัย

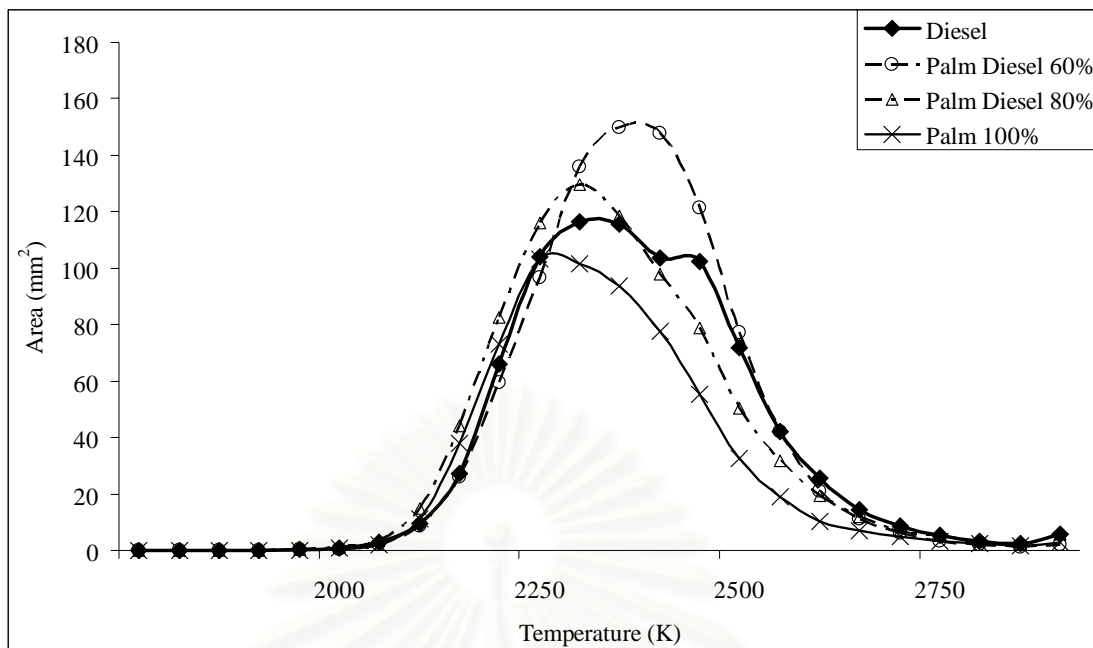


Fig. 5-53 Flame temperature histogram of Diesel, 60%,80% Palm Diesel and palm 100% at injection pressure 100 MPa Combustion at 3.0 MPa 930K 1.9 msec after start of injection

At this combustion timing, the combustion temperature of diesel fuel was still the highest. Combustion temperature and area were decreased with the higher palm blended percentage.

สถาบันวิทยบริการ
จุฬาลงกรณ์มหาวิทยาลัย

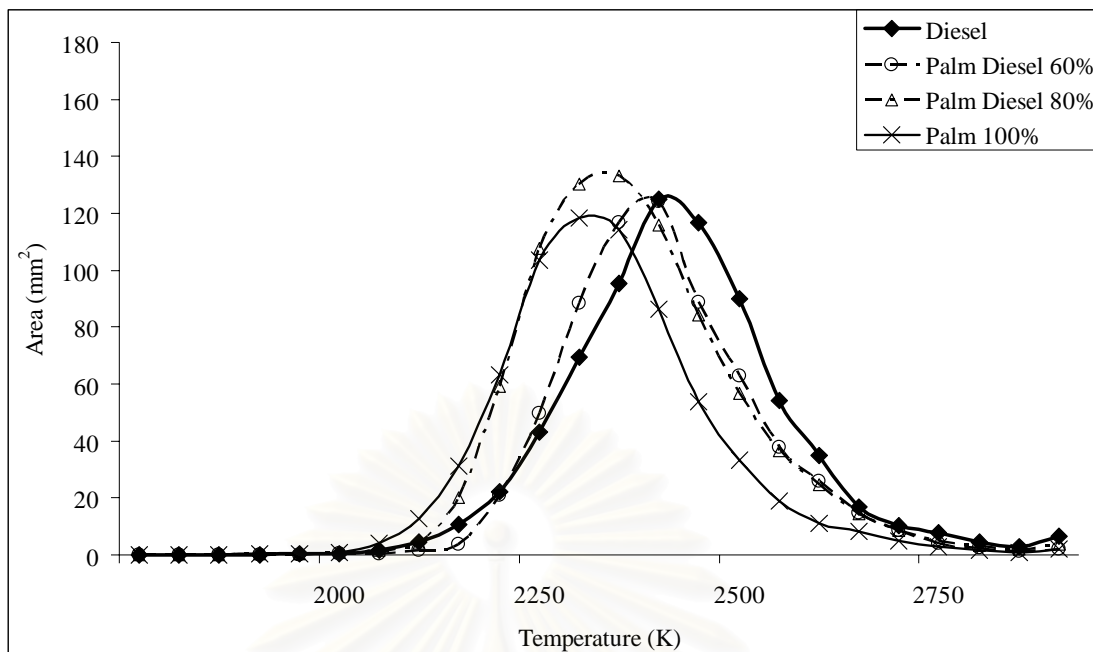


Fig. 5-54 Flame temperature histogram of Diesel, 60%,80% Palm Diesel and palm 100% at injection pressure 100 MPa Combustion at 3.0 MPa 930K 2.4 msec after start of injection

At the end of combustion, the highest to lowest combustion temperature were diesel, palm diesel 60%, palm diesel 80% and palm 100%. The combustion areas were not much difference among these fuels.

At start of combustion, flame temperature of palm 100%, palm diesel 80% and palm diesel 60% were higher than diesel. This might be caused by the short ignition delay. It was revealed that the flame temperature of palm and palm diesel were lower than diesel at the main and the end of combustion.

5.1.3.2.4. KL factor histogram

The KL factor histogram was calculated by evaluating the KL factor from the counted number of combustion flame pixel and converting them to flame area (mm^2). The KL factor interval was selected at 0.005 A.U. and the data are shown from figure 5-55 to 5-58, took the images from instant of 0.9, 1.4, 1.9 and 2.4 msec after start of combustion, respectively.

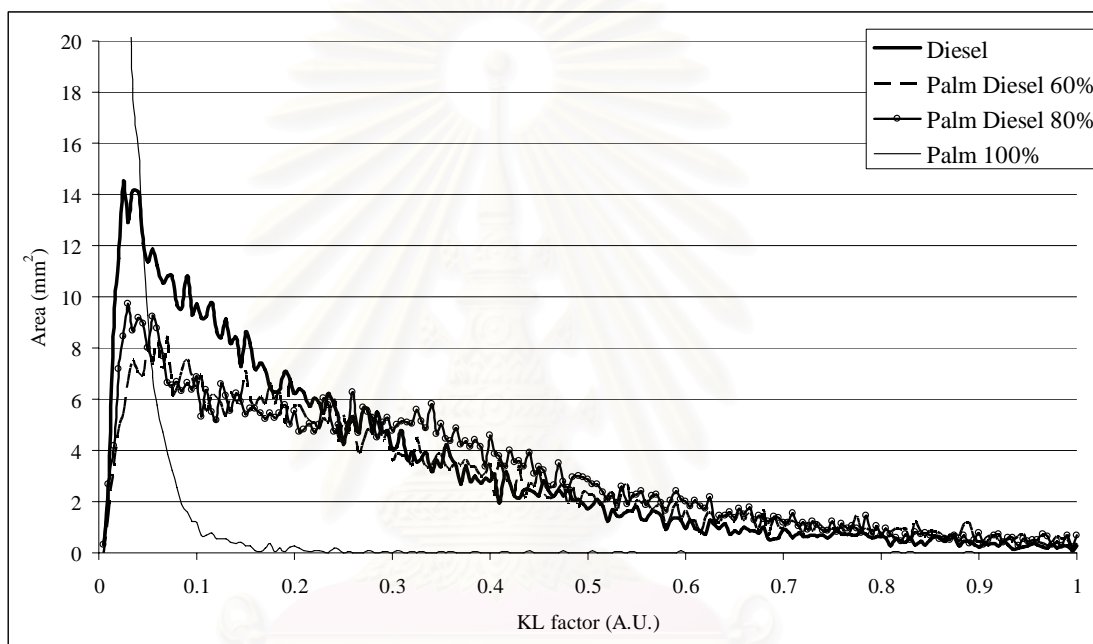


Fig. 5-55 KL factor histogram of Diesel ,60%,80% Palm Diesel and palm 100%
at injection pressure 100 MPa Combustion at 3.0 MPa 930K
0.9 msec after start of injection

At the start of combustion, KL factor of palm 100% was very low compared with other fuels. This might be caused by the highest combustion temperature of palm 100% at this time. The difference between palm diesel 60% and 80% was small.

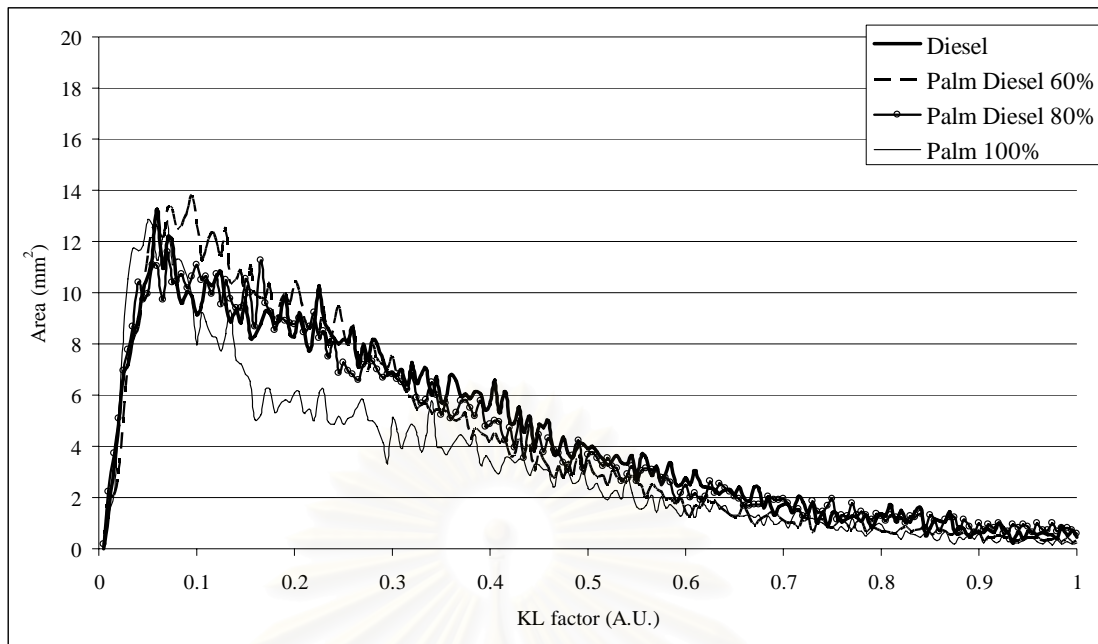


Fig. 5-56 KL factor histogram of Diesel ,60%,80% Palm Diesel and palm 100%
at injection pressure 100 MPa Combustion at 3.0 MPa 930K
1.4 msec after start of injection

At this combustion time period, KL factor of palm 100% was still smaller compared with other fuels. The difference in KL factor with palm diesel, diesel 60% and 80% was small.

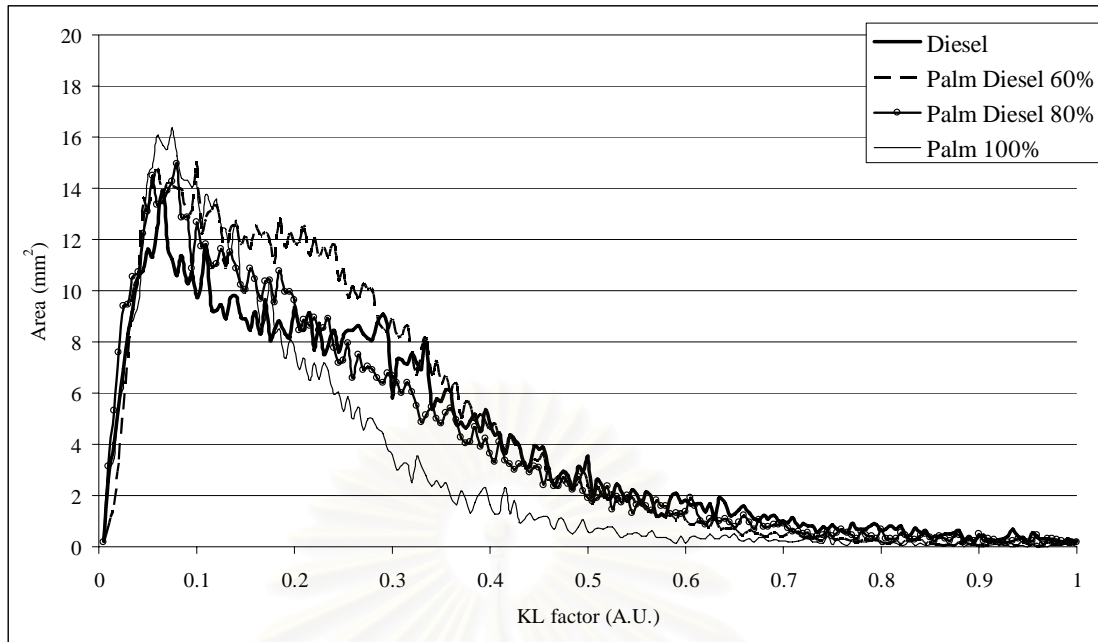


Fig. 5-57 KL factor histogram of Diesel ,60%,80% Palm Diesel and palm 100% at injection pressure 100 MPa Combustion at 3.0 MPa 930K 1.9 msec after start of injection

At this combustion time period, KL factor of palm 100% was still smaller compared with other fuels. KL factor of Palm diesel 60% seemed to be the highest but the difference of KL factor of palm diesel, diesel 60% and 80% was still small.

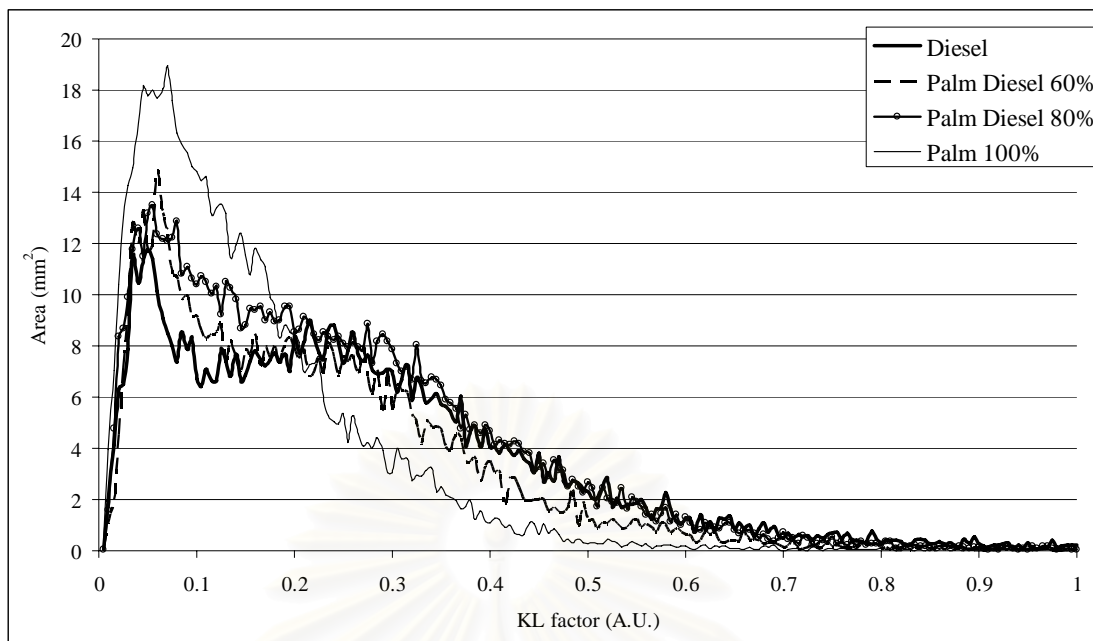


Fig. 5-58 KL factor histogram of Diesel ,60%,80% Palm Diesel and palm 100%
at injection pressure 100 MPa Combustion at 3.0 MPa 930K
2.4 msec after start of injection

At the end of the combustion, with KL factor value between 0-0.2 A.U., palm 100% was the highest but with KL factor value between 0.2-1 A.U., palm 100% was the lowest compared with other fuels.

From KL factor histogram, Palm diesel 60% seemed to produce highest KL factor and the difference with palm diesel, diesel 60% and 80% was still small. It can be seen that at the start of the combustion, KL factor of palm diesel 60% and 80% were slightly higher than diesel. Only the case of palm 100% KL factor was very low. At the main combustion, KL factor values of palm diesel 60% and 80% were higher but the difference very small.

5.1.3.2.5. The analysis of flame temperature and KL factor

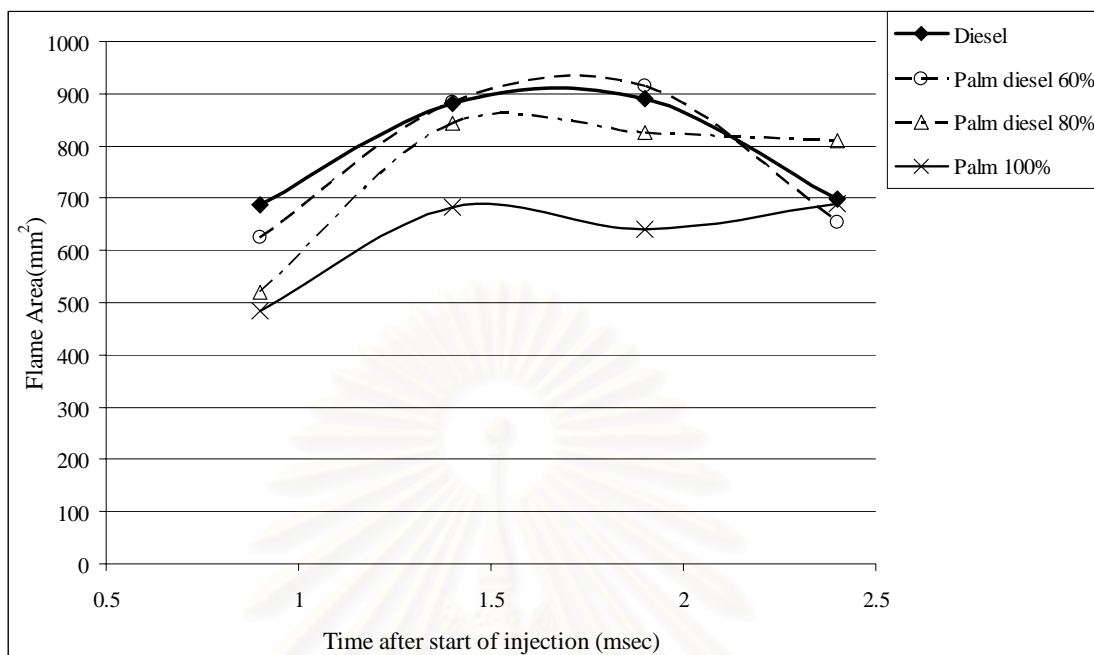


Fig. 5-59 Flame area of Diesel, 60%,80% Palm Diesel and palm 100 %
at injection pressure 100 MPa Combustion at 3.0 MPa 930K ,
0.9-2.4 msec after start of injection

The combustion flame area of fuel was decreased with the higher blending percentage of palm oil.

สถาบันวิทยบริการ
จุฬาลงกรณ์มหาวิทยาลัย

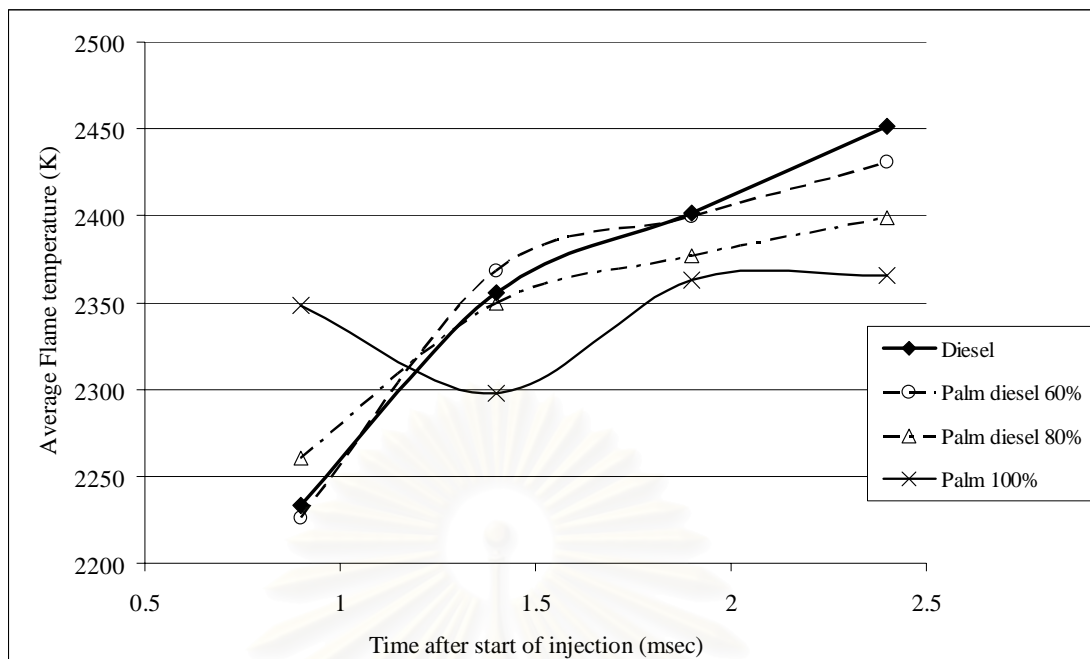


Fig. 5-60 Average temperature of Diesel 60%,80% Palm Diesel and palm 100 %
at injection pressure 100 MPa Combustion at 3.0 MPa 930K
0.9-2.4 msec after start of injection

The average combustion temperature increased with time. Increasing rate of average flame temperature of diesel was the highest compared with palm oil.

The combustion temperature of palm 100% started at the highest temperature (~2350 K) and it seemed to be constant until the end of the combustion.

สถาบันวิทยบริการ
จุฬาลงกรณ์มหาวิทยาลัย

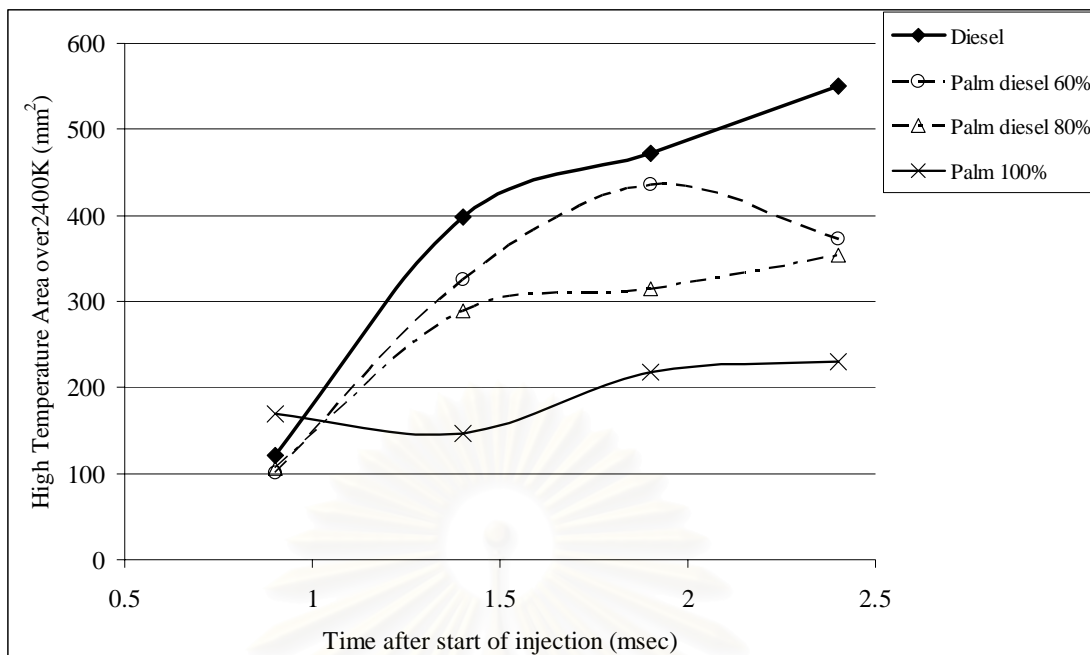


Fig. 5-61 High temperature area of Diesel 60%,80% Palm Diesel and palm 100 %
at injection pressure 100 MPa Combustion at 3.0 MPa 930K
0.9-2.4 msec after start of injection

High temperature area (>2400K) of palm diesel and palm 100% were lower than diesel. It could be concluded that the palm blended with diesel resulted in decreasing of combustion temperature.

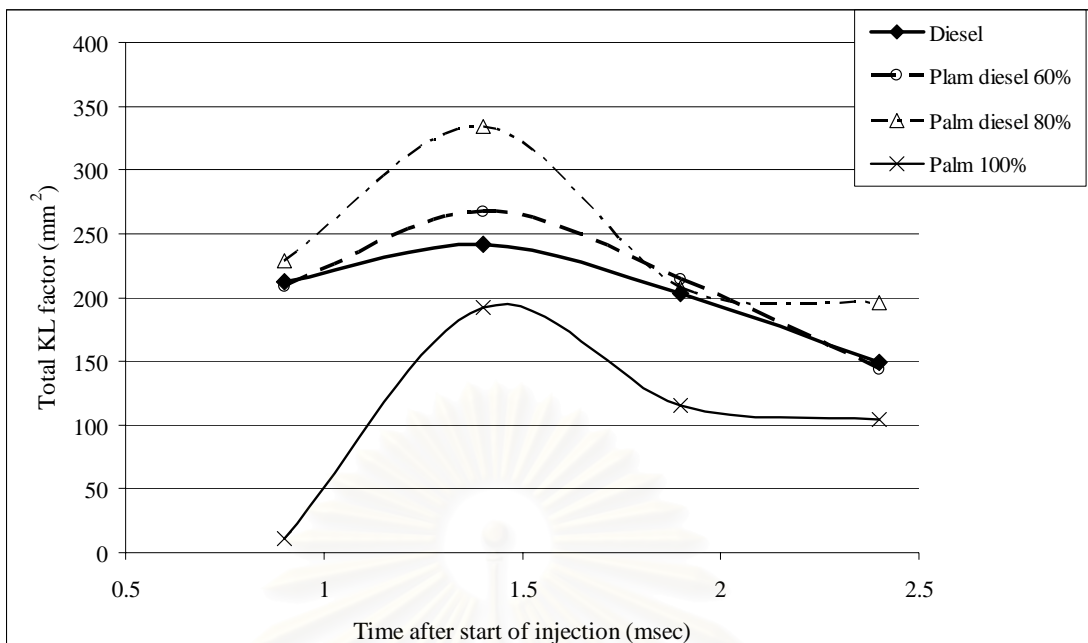


Fig. 5-62 Total KL factor of Diesel 60%,80% Palm Diesel and palm 100 %
at injection pressure 100 MPa Combustion at 3.0 MPa 930K
0.9-2.4 msec after start of injection

The total KL factor of palm diesel 60% and 80% were higher than diesel. It could be concluded that the palm blended with diesel might increase amount of soot.

In case of palm 100%, the total KL factor was very low compared with diesel.

สถาบันวิทยบริการ
จุฬาลงกรณ์มหาวิทยาลัย

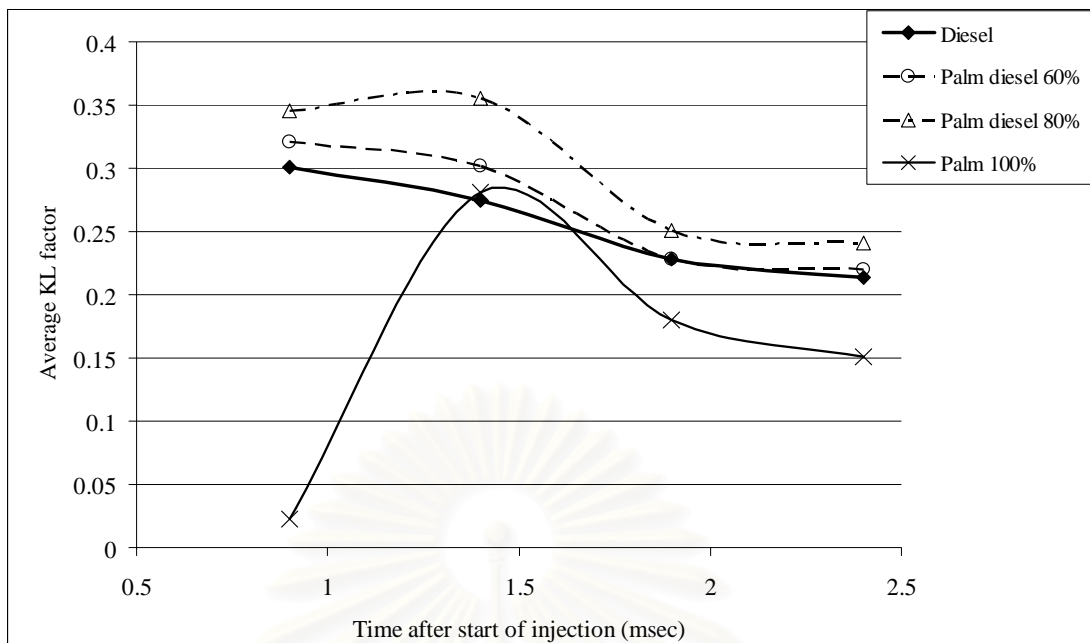


Fig. 5-63 Average KL factor of Diesel 60%,80% Palm Diesel and palm 100 % at injection pressure 100 MPa Combustion at 3.0 MPa 930K , 0.9-2.4 msec after start of injection

The average KL factor of palm diesel 60% and 80% were found higher than diesel. It could be concluded that the palm blended with diesel might increase the soot concentration of the combustion

In case of palm 100%, the average KL factor was very low compared with diesel at the start and end of combustion.

Combustion flame areas of palm diesel 60%, 80% and 100% were smaller than diesel at injection pressure of 100 MPa, as shown in figure 5-59. At the start of combustion, average flame temperature, shown in figure 5-60, of palm 100% was the highest. It might be caused by short ignition delay and fuel property. High temperature area (>2400 K) of combustion flame was calculated. It is shown in figure 5-61 that the high temperature area of palm diesel 60 %, 80% and 100% were smaller than diesel.

Average KL factor shown in figures 5-63 is the total of KL factor over the flame area, shown in figure 5-62, divided by flame area and soot concentration can be estimated. The soot concentration of palm diesel 60% and 80% were higher than diesel but in the case of palm100%, it was very low at the start of combustion.

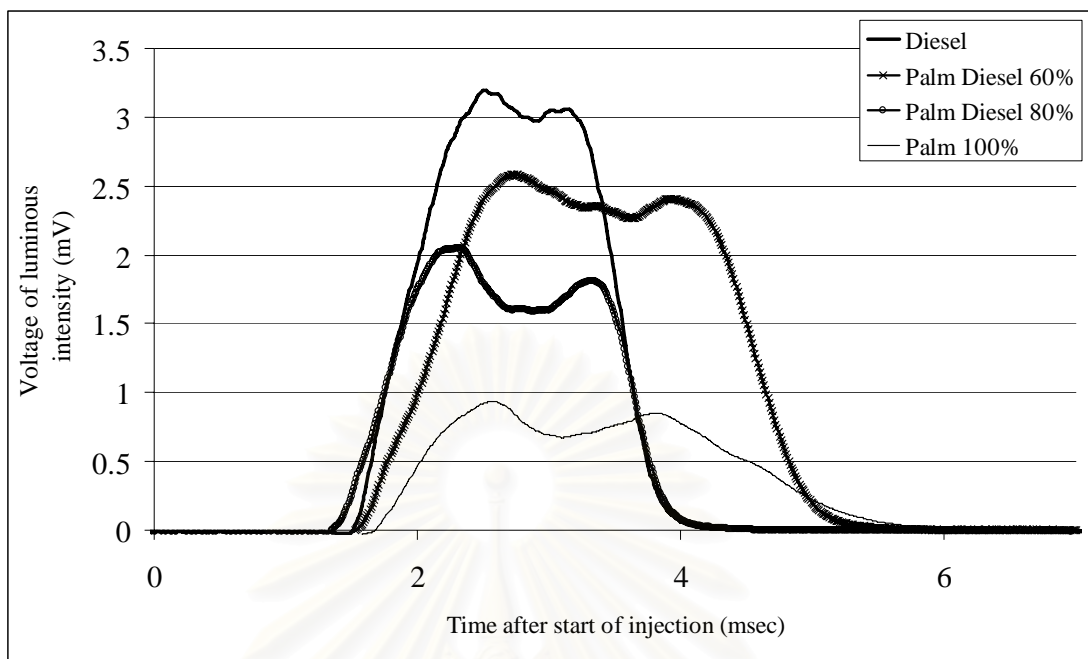


Fig. 5-64 The voltage of luminous flame intensity obtained from side photo diode

From figure 5-64, it was found that the intensity of combustion flame was decreased with the higher blending percentage and the difference between two peaks of luminous flame was extended. This might be resulted from slower burning rate of palm diesel compared to diesel.

5.2 The Study of Thai crude palm oil 10% (CPO 10%)

5.2.1 Combustion period and ignition delay

The fuel injection rate was set up as shown in figure 5-65. The injection mass was approximately 15 mg and compared with diesel fuel the injection rate was a little bit decreased.

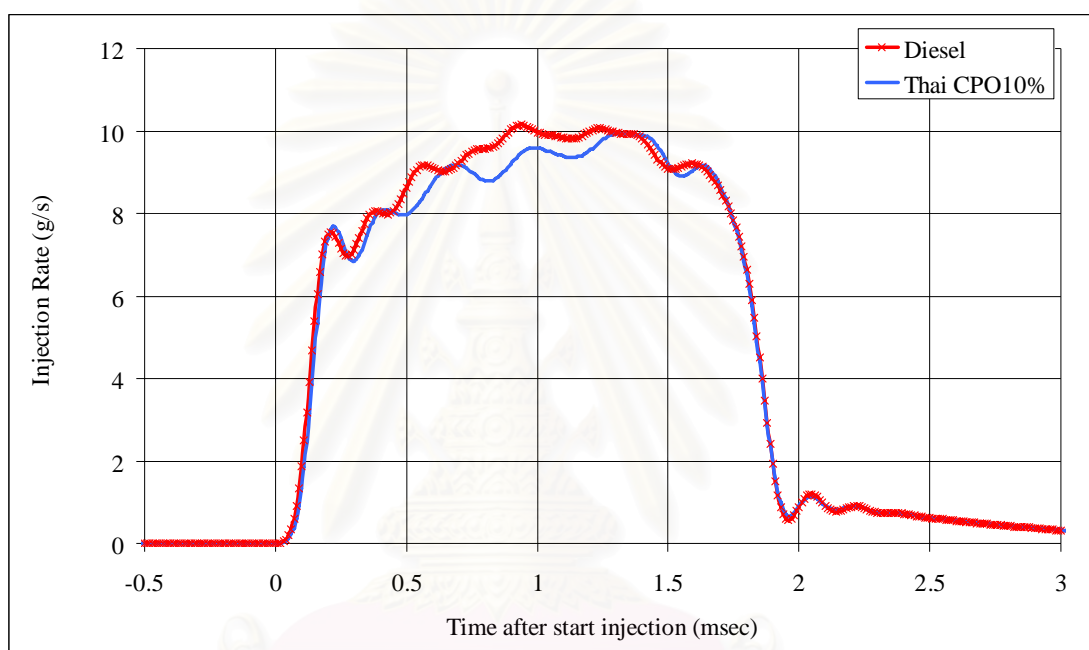


Fig. 5-65 The injection rate of Thai CPO 10% and diesel at injection pressure 100 MPa

The study on the combustion was done with heating fuel injection system up to 40°C at the combustion condition 3.0 MPa temperature around 900°C. The data obtained from photo sensor and photo diode were used to calculate ignition delay and combustion period. The result is showing in figure 5-66 and 5-67.

The amount of injection fuel became slightly smaller and the injection period became slightly shorter with CPO 10% blended, possible due to the higher viscosity of CPO fuel. The shorter combustion period of palm blended fuel might be the results of these tendencies. It was found that CPO10% had shorter ignition delay than diesel fuel around 0.1 msec.

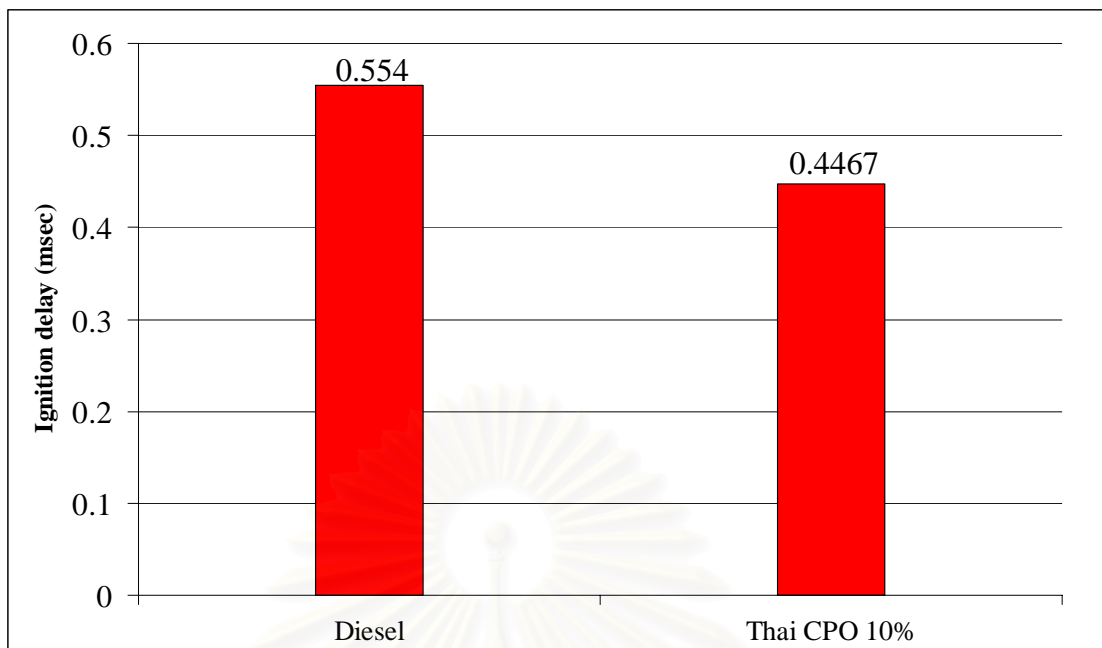


Fig. 5-66 Ignition delay of diesel and Thai CPO10%
at injection pressure 100 MPa

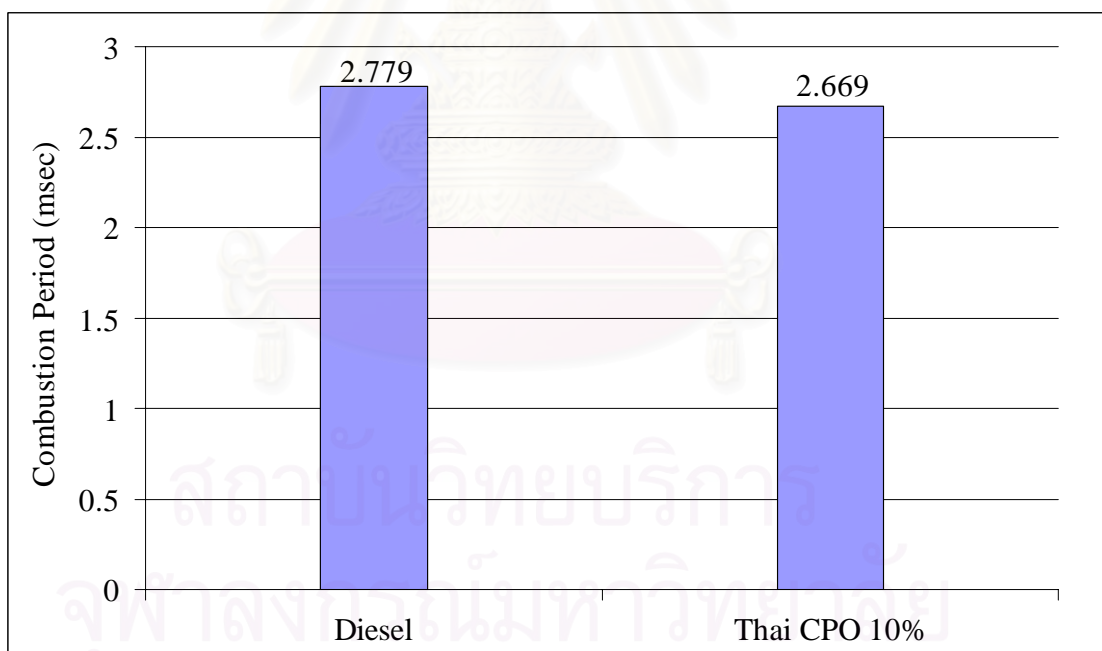


Fig. 5-67 Fuel combustion period of diesel and Thai CPO10%
at injection pressure 100 MPa

5.2.2 Combustion flame visualization

5.2.2.1. Intensity distribution of combustion flame

In each following images, the left part is corresponding with red filter and the right part is with blue filter.

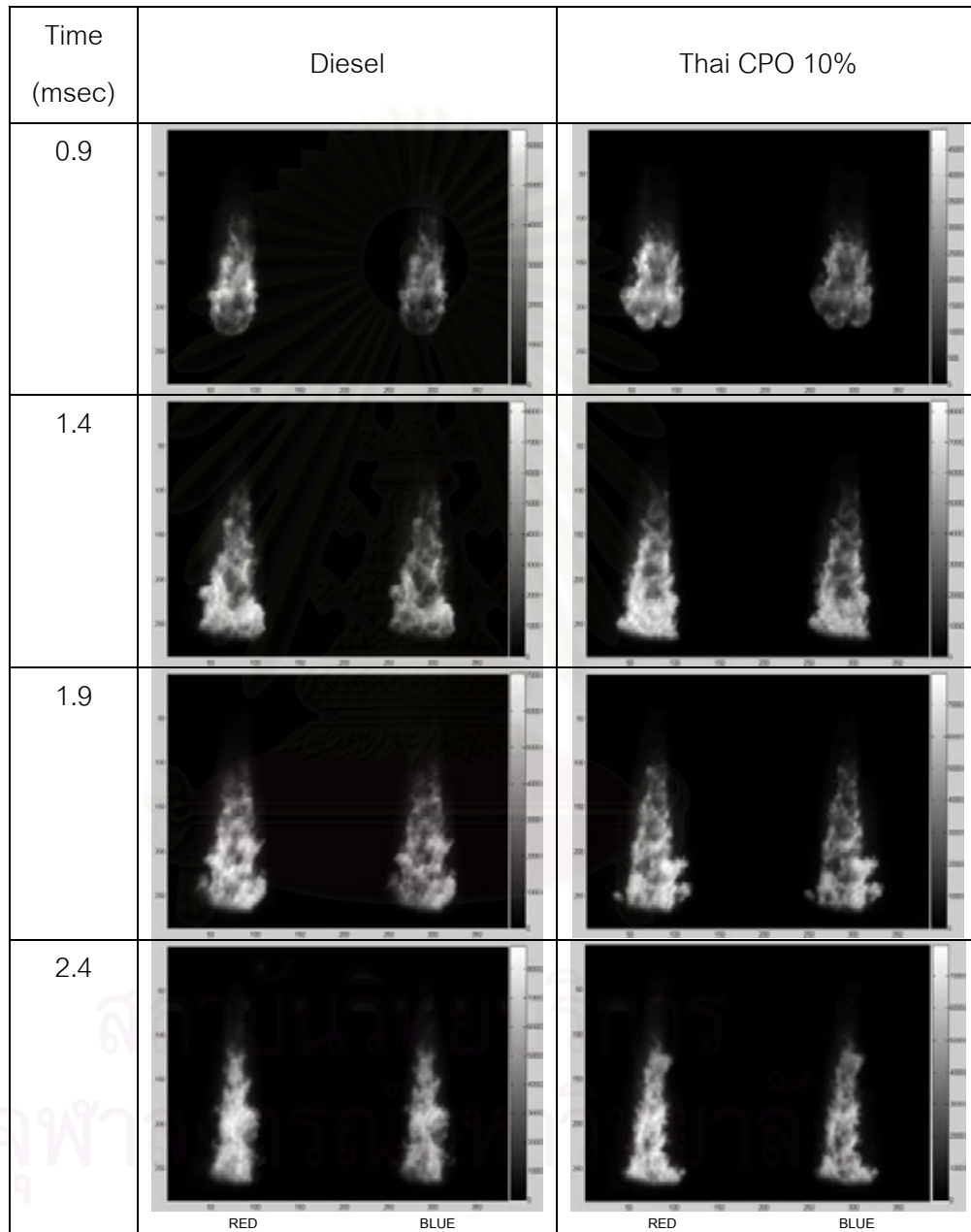


Fig. 5-68 Combustion flame intensity distribution of diesel and Thai CPO10%

5.2.2.2. Combustion flame temperature and KL factor distribution

The exposure time of ICCD camera was set 10 μ sec. The flame intensity data were compiled with two color method. The calculation results of true temperature and KL factor are shown in figures 5-69 to 72.

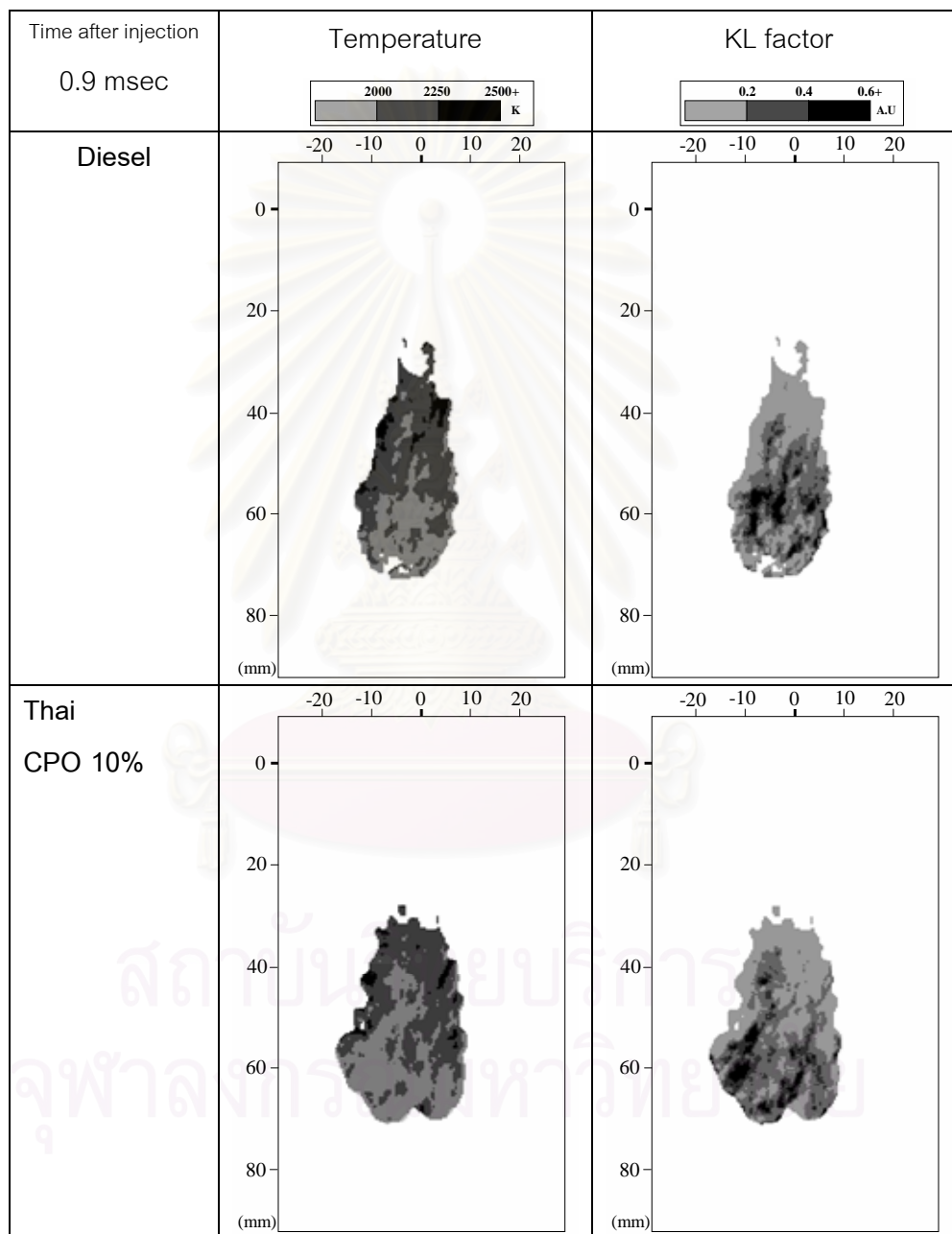


Fig.5-69 Combustion flame temperature and KL factor distribution of Diesel fuel and Thai CPO 10% Injection pressure 100MPa and 60MPa, Combustion at 3.0 MPa 0.9 msec after start of injection, ICCD camera Gain 5.5 width 10 μ sec

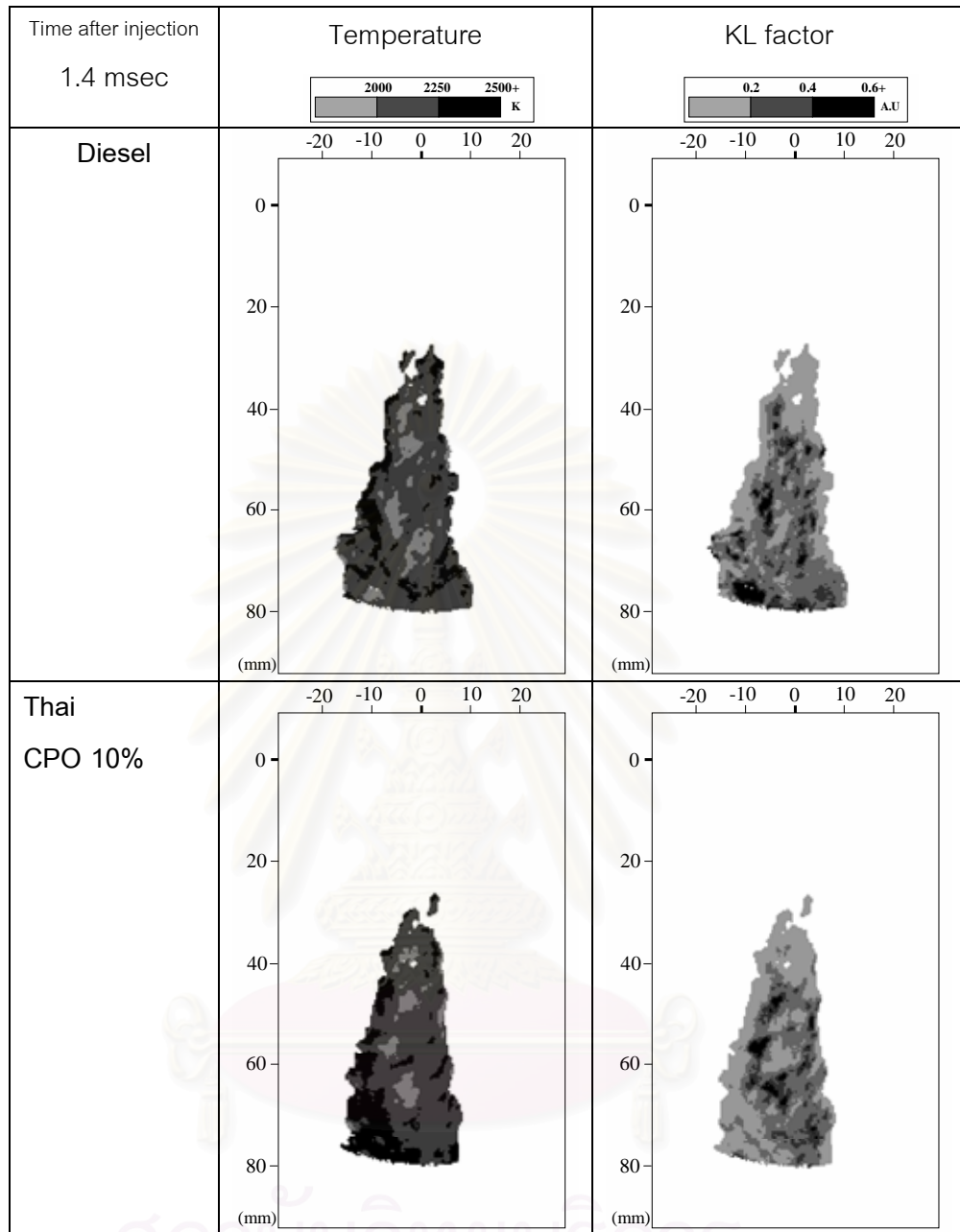


Fig.5-70 Combustion flame temperature and KL factor distribution of Diesel fuel and Thai CPO 10% Injection pressure 100MPa and 60MPa, Combustion at 3.0 MPa
1.4 msec after start of injection, ICCD camera Gain 5.5 width 10 μ sec

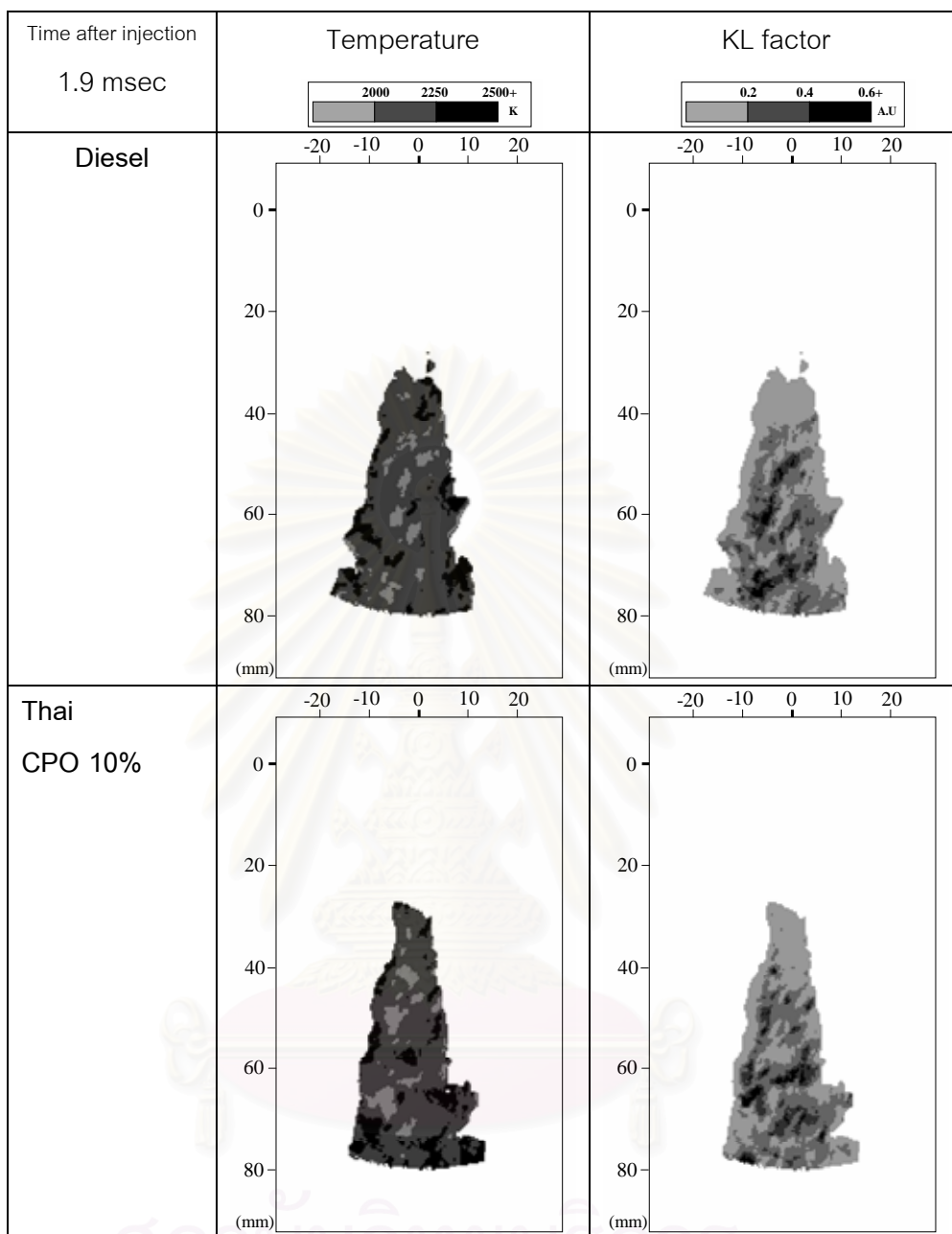


Fig.5-71 Combustion flame temperature and KL factor distribution of Diesel fuel and Thai CPO 10% Injection pressure 100MPa and 60MPa, Combustion at 3.0 MPa
1.9 msec after start of injection, ICCD camera Gain 5.5 width 10 μ sec

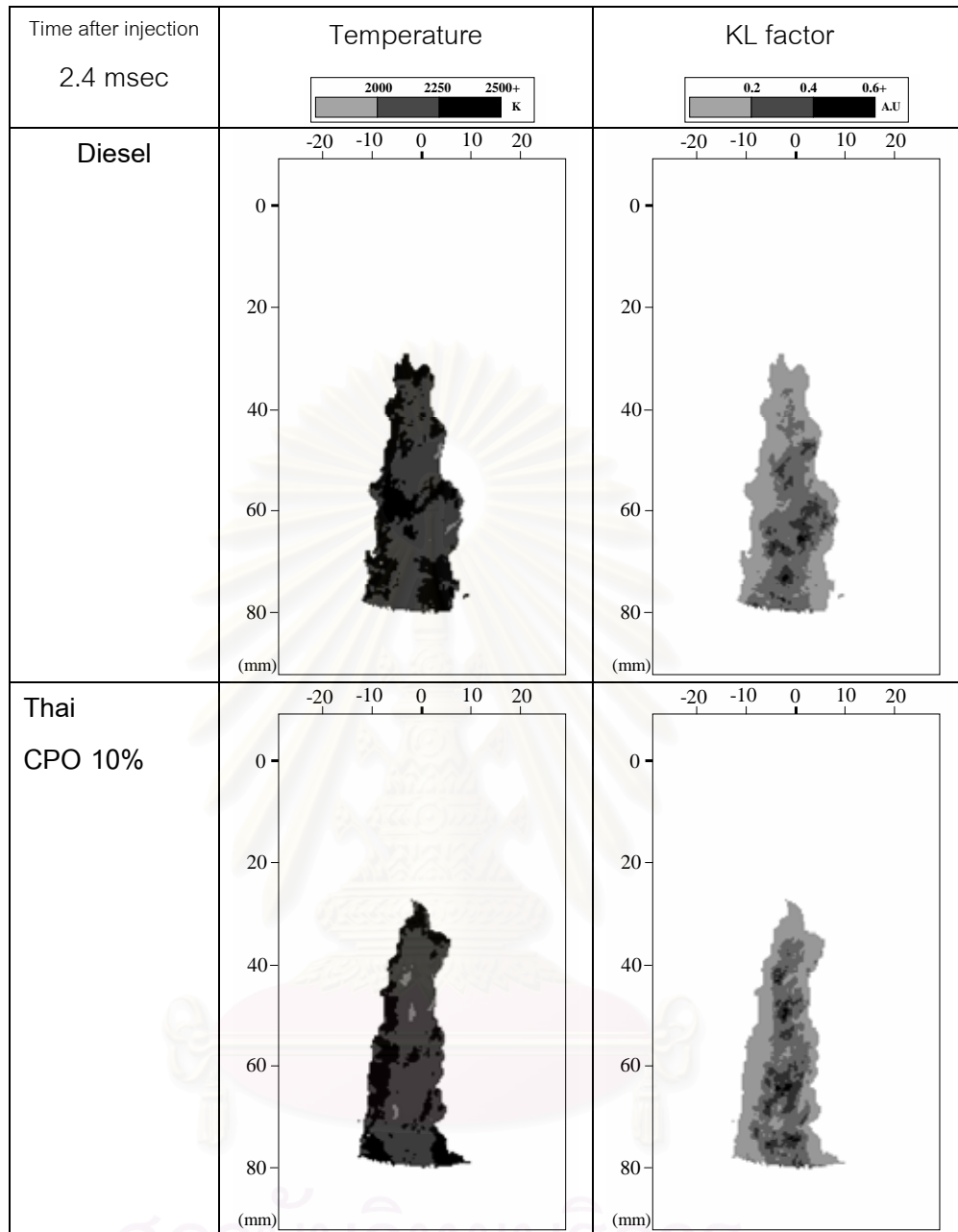


Fig.5-72 Combustion flame temperature and KL factor distribution of Diesel fuel and Thai CPO 10% Injection pressure 100MPa and 60MPa, Combustion at 3.0 MPa
2.4 msec after start of injection, ICCD camera Gain 5.5 width 10 μ sec

5.2.2.3. Combustion flame temperature histogram

The temperature histogram was calculated by counting the number of combustion flame pixel and converting them to flame area (mm^2). The temperature interval of 50 K was selected and the data is shown from figure 5-20 to 5-23; taking images from time instant of 0.9, 1.15, 1.65, 1.4, 1.65, 1.9, 2.15, 2.4 and 2.65 msec after start of combustion.

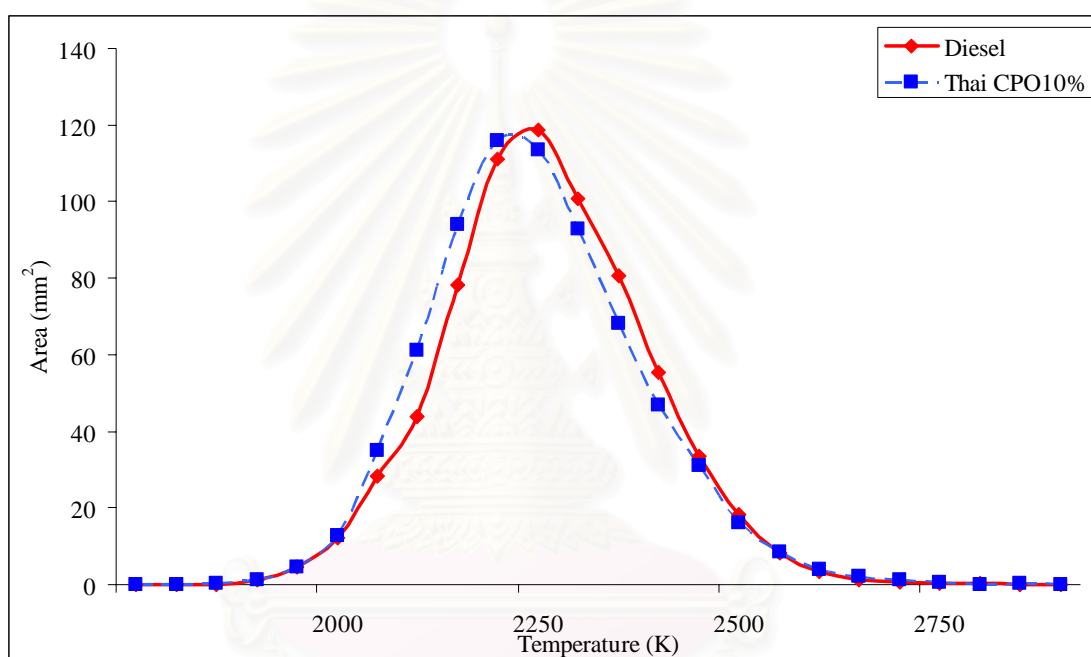


Fig. 5-73 Flame temperature histogram of Diesel and Thai CPO 10%

at injection pressure 100 MPa Combustion at 3.0 MPa 930K

0.9 msec after start of injection

สถาบันวิจัยบริการ
จุฬาลงกรณ์มหาวิทยาลัย

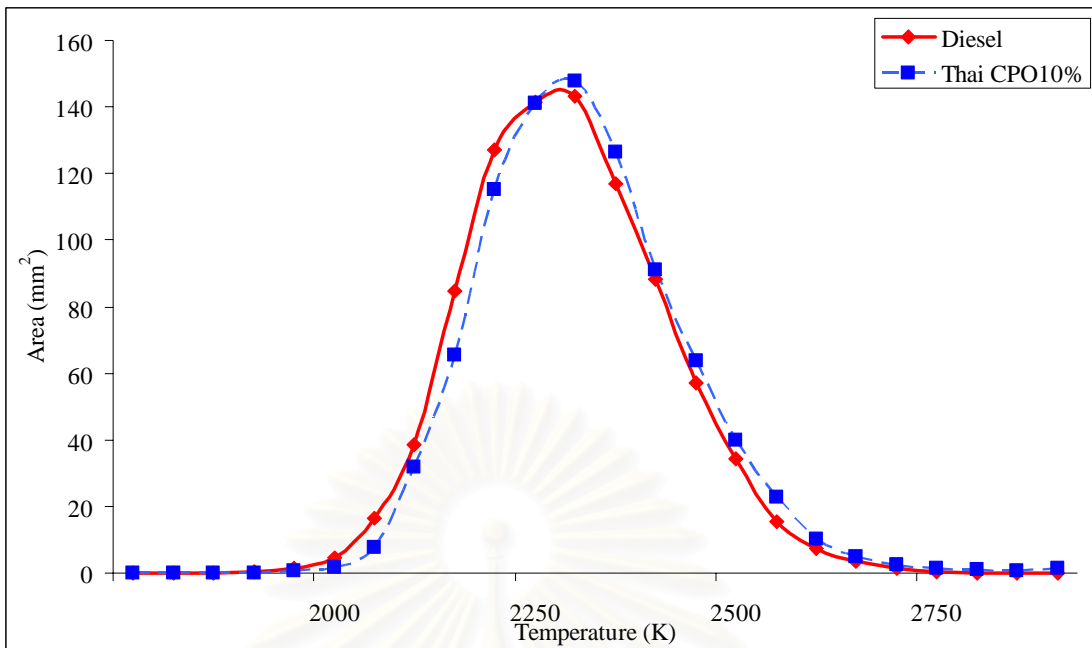


Fig. 5-74 Flame temperature histogram of Diesel and Thai CPO 10%
at injection pressure 100 MPa Combustion at 3.0 MPa 930K
1.15 msec after start of injection

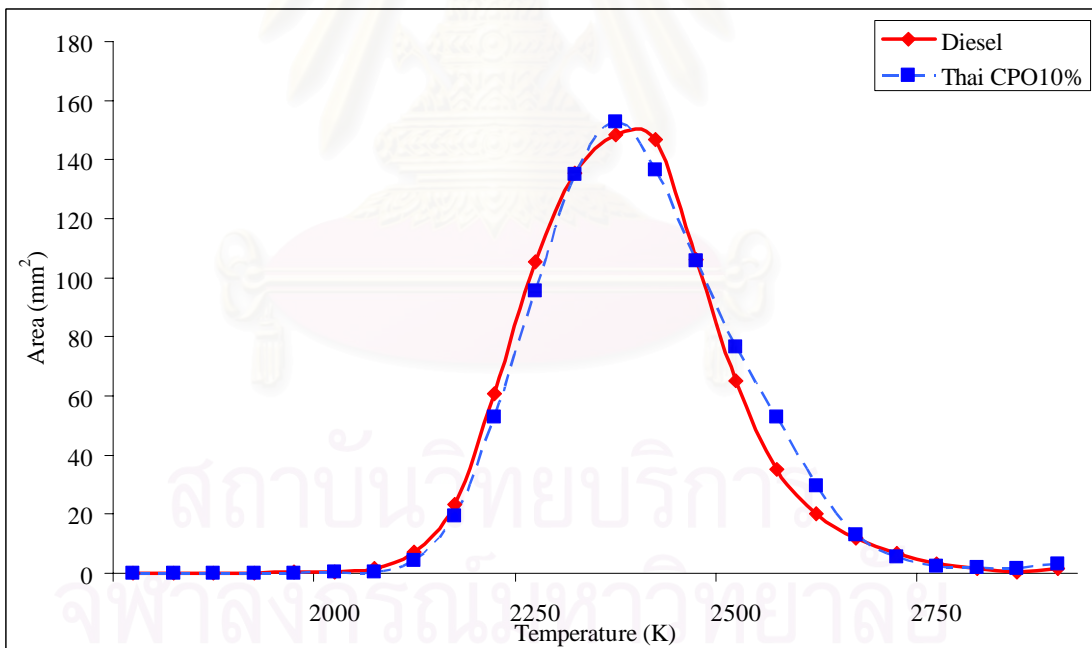


Fig. 5-75 Flame temperature histogram of Diesel and Thai CPO 10%
at injection pressure 100 MPa Combustion at 3.0 MPa 930K
1.4 msec after start of injection

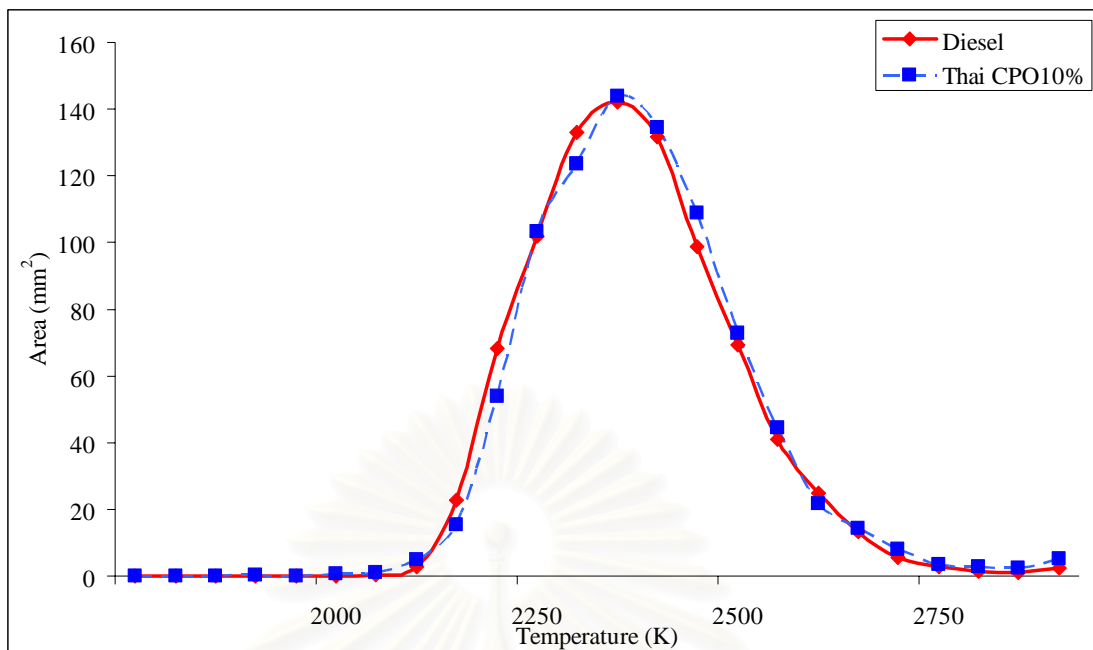


Fig. 5-76 Flame temperature histogram of Diesel and Thai CPO 10%
at injection pressure 100 MPa Combustion at 3.0 MPa 930K
1.65 msec after start of injection

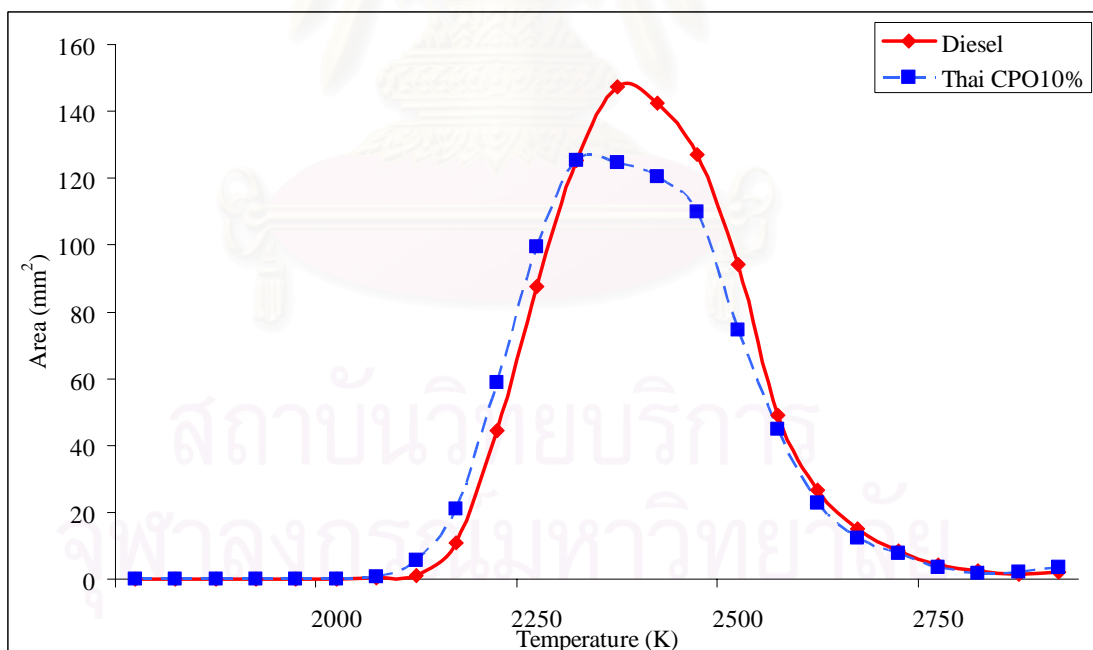


Fig. 5-77 Flame temperature histogram of Diesel and Thai CPO 10%
at injection pressure 100 MPa Combustion at 3.0 MPa 930K
1.9 msec after start of injection

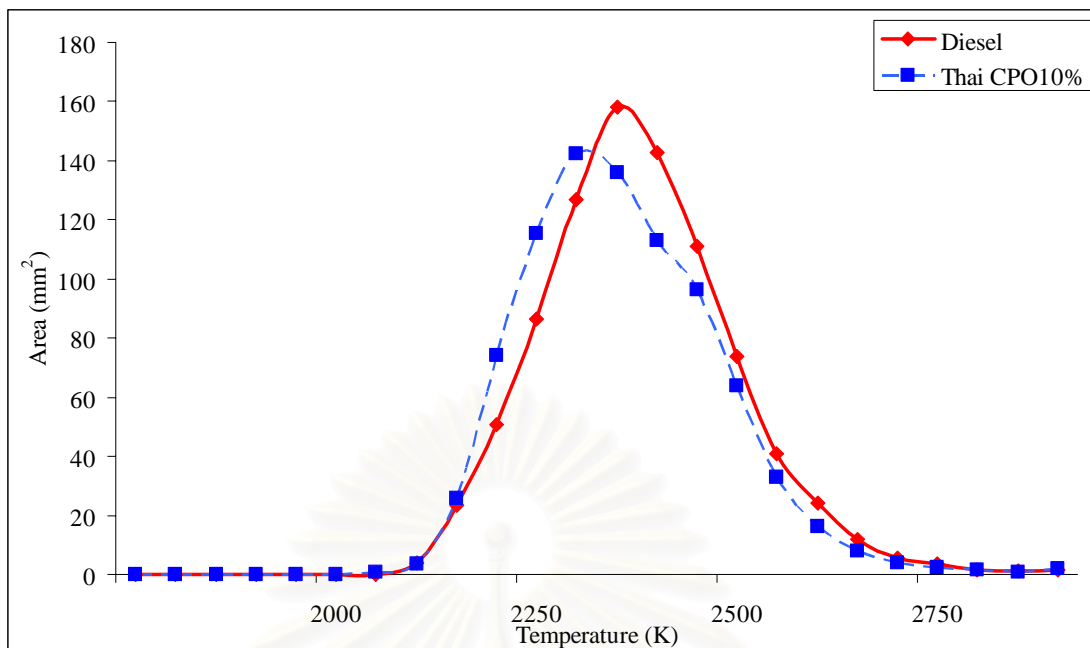


Fig. 5-78 Flame temperature histogram of Diesel and Thai CPO 10%
at injection pressure 100 MPa Combustion at 3.0 MPa 930K
2.15 msec after start of injection

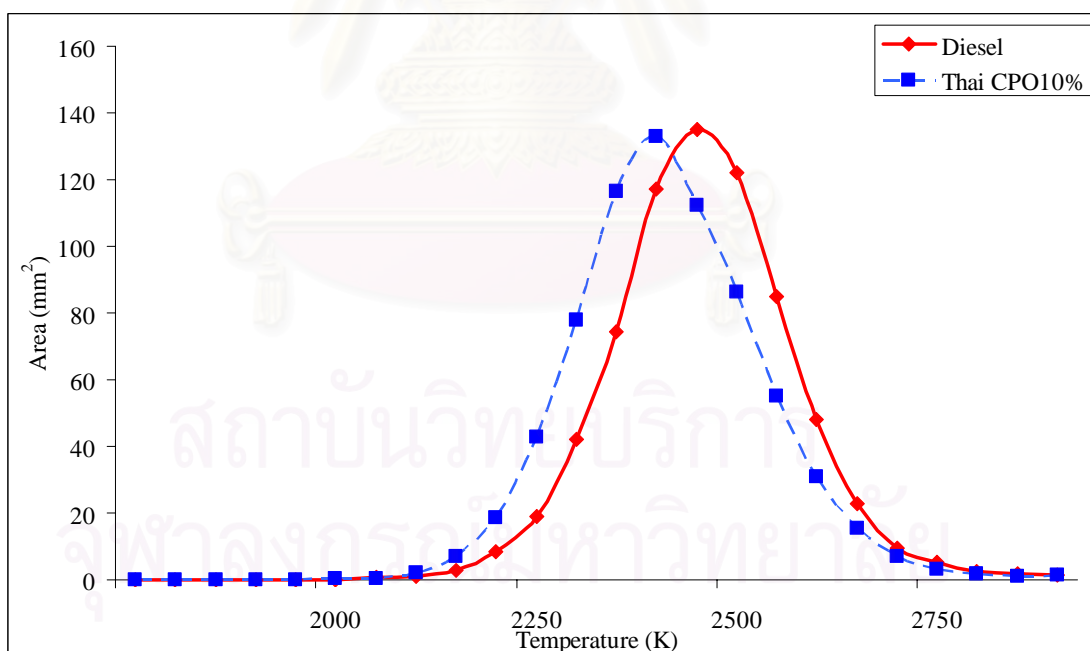


Fig. 5-79 Flame temperature histogram of Diesel and Thai CPO 10%
at injection pressure 100 MPa Combustion at 3.0 MPa 930K
2.4 msec after start of injection

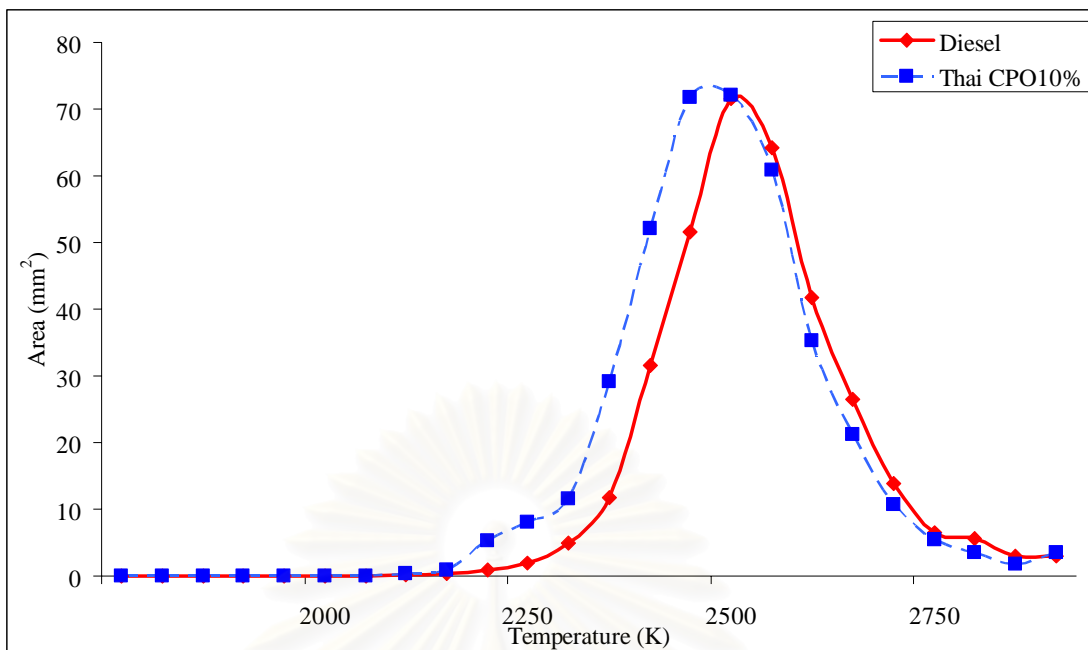


Fig. 5-80 Flame temperature histogram of Diesel and Thai CPO 10%
at injection pressure 100 MPa Combustion at 3.0 MPa 930K
2.65 msec after start of injection

The more details of combustion temperature were shown in figure 5-73 to 80. These experiments were taken with time interval of 0.25 msec, from 0.9-2.65 msec.

It was found that combustion temperature of CPO10% was lower than diesel and increased close to diesel at the main combustion period. It was became lower at the end of combustion. However, the difference was very small.

สถาบันวิทยบริการ
จุฬาลงกรณ์มหาวิทยาลัย

5.2.2.4. KL factor of Combustion flame histogram

The KL factor histogram was calculated by evaluating the KL factor from the counted number of combustion flame pixel and converting them to flame area (mm^2). The KL factor interval was selected at 0.005 A.U. and the data are shown from figure 5-81 to 5-88, took the images from instant of 0.9, 1.15, 1.4, 1.65, 1.9, 2.15, 2.4 and 2.65 msec after start of combustion, respectively.

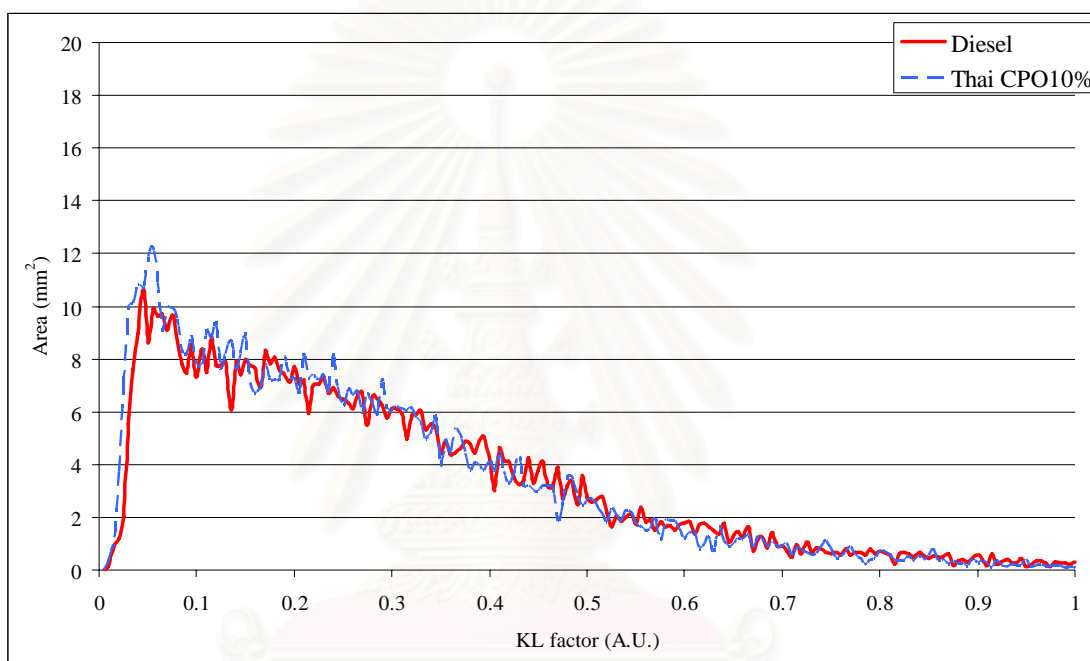


Fig. 5-81 KL factor histogram of Diesel and Thai CPO 10%
at injection pressure 100 MPa Combustion at 3.0 MPa 930K
0.9 msec after start of injection

สถาบันวิจัยประชากร
จุฬาลงกรณ์มหาวิทยาลัย

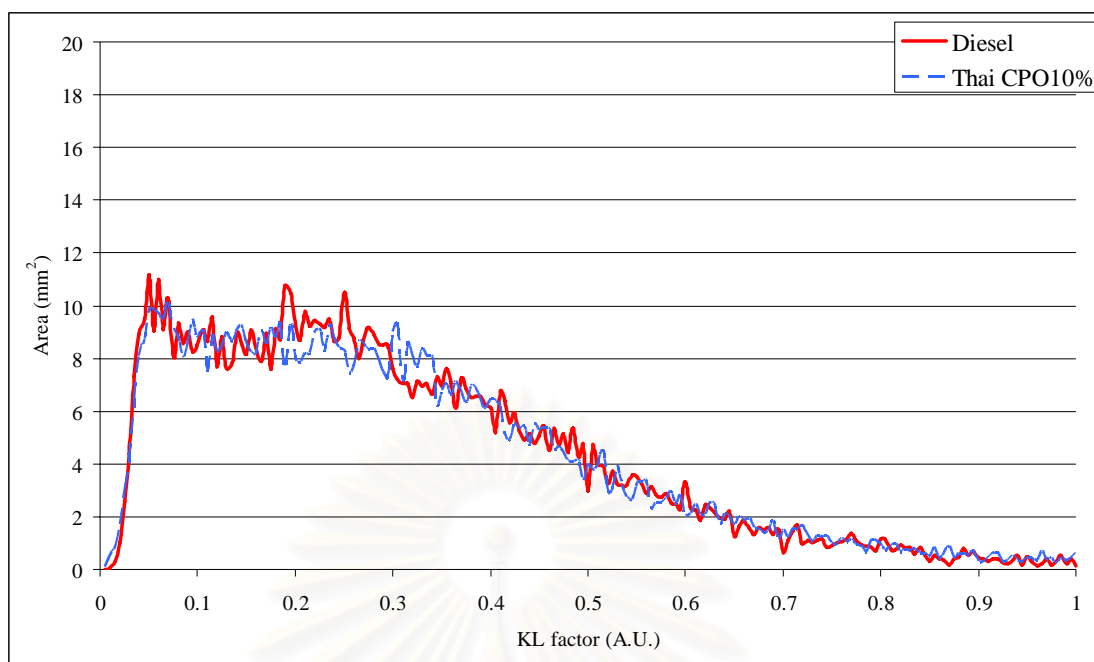


Fig. 5-82 KL factor histogram of Diesel and Thai CPO 10%
at injection pressure 100 MPa Combustion at 3.0 MPa 930K
1.15 msec after start of injection

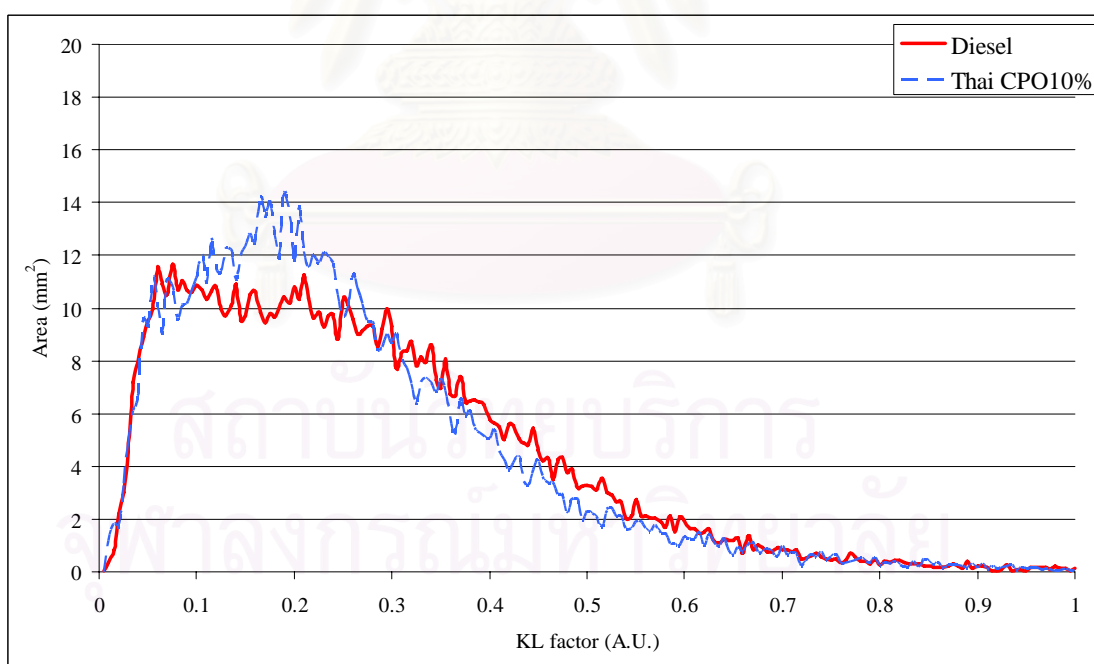


Fig. 5-83 KL factor histogram of Diesel and Thai CPO 10%
at injection pressure 100 MPa Combustion at 3.0 MPa 930K
1.4 msec after start of injection

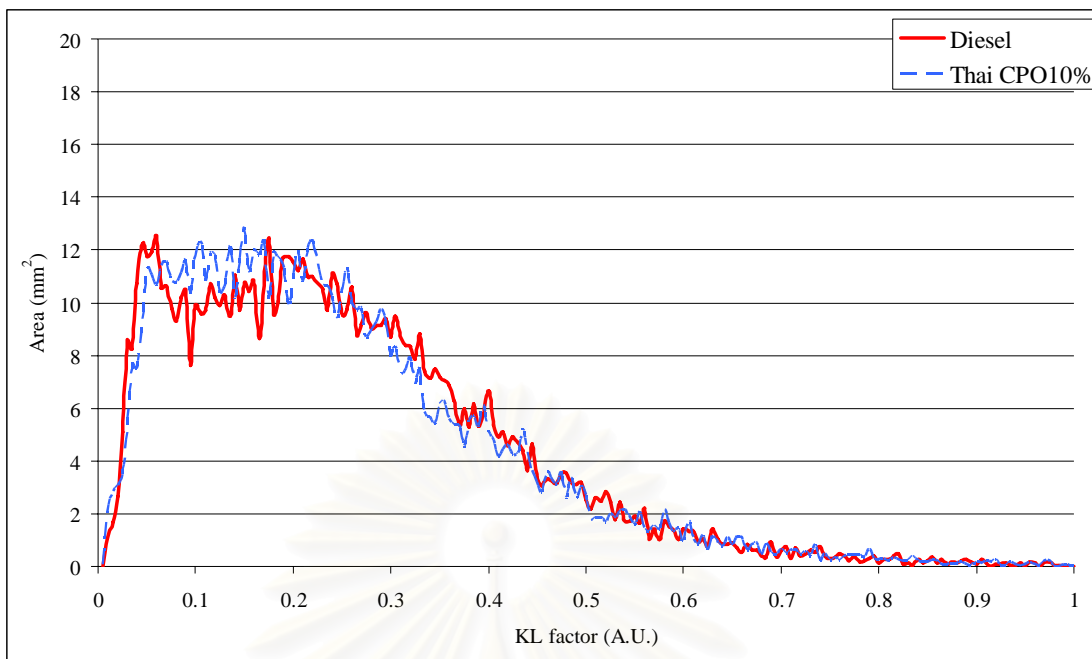


Fig. 5-84 KL factor histogram of Diesel and Thai CPO 10%
at injection pressure 100 MPa Combustion at 3.0 MPa 930K
1.65 msec after start of injection

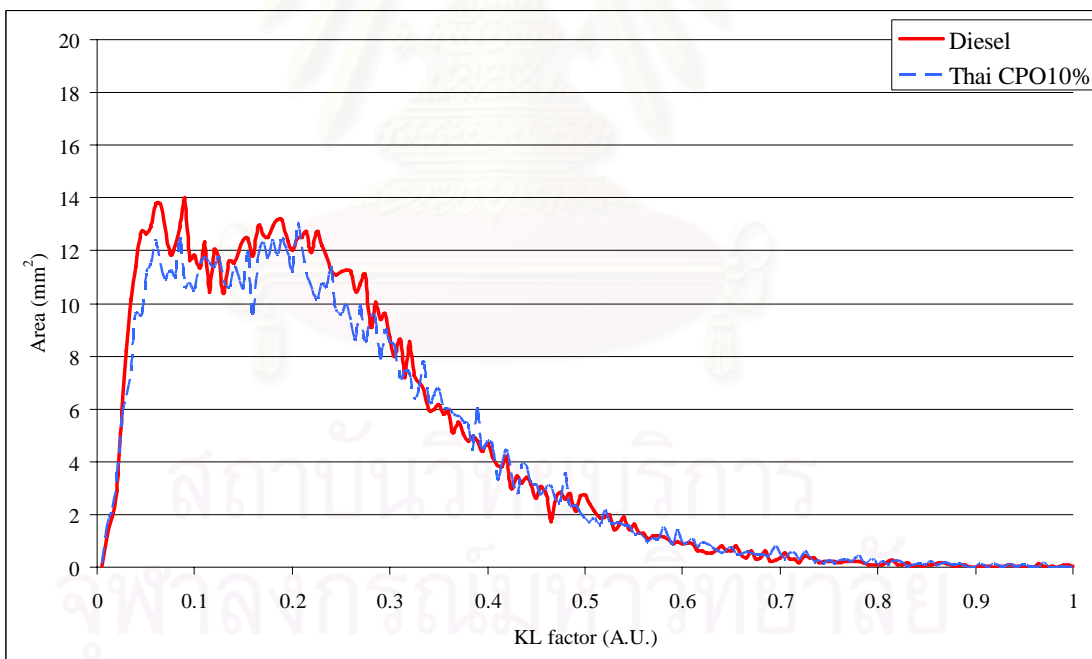


Fig. 5-85 KL factor histogram of Diesel and Thai CPO 10%
at injection pressure 100 MPa Combustion at 3.0 MPa 930K
1.9 msec after start of injection

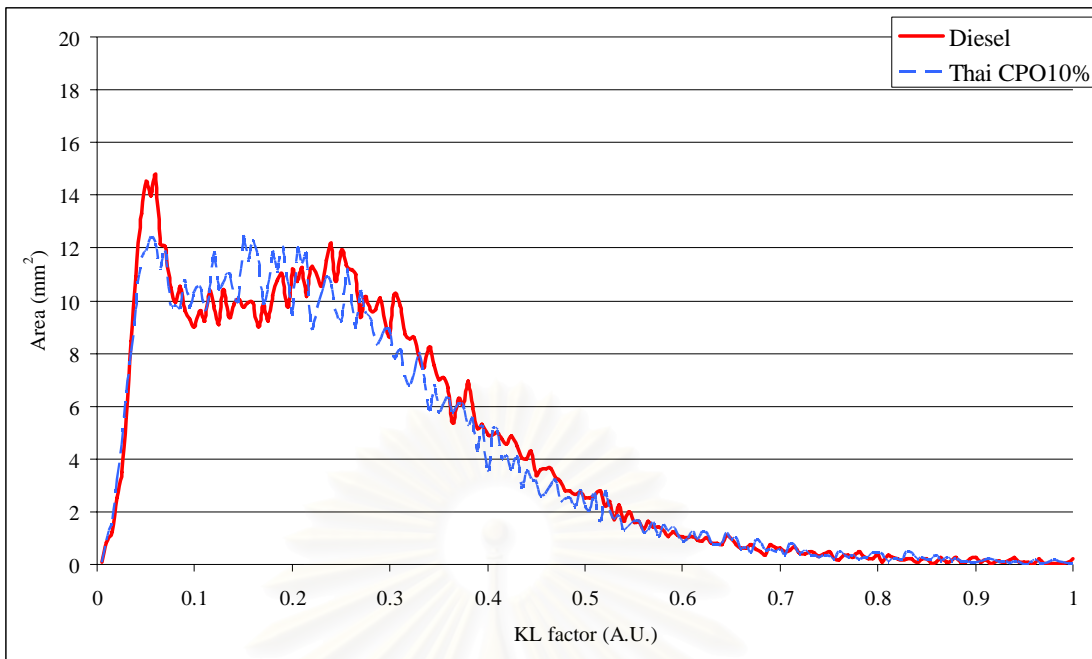


Fig. 5-86 KL factor histogram of Diesel and Thai CPO 10%
 at injection pressure 100 MPa Combustion at 3.0 MPa 930K
 2.15 msec after start of injection

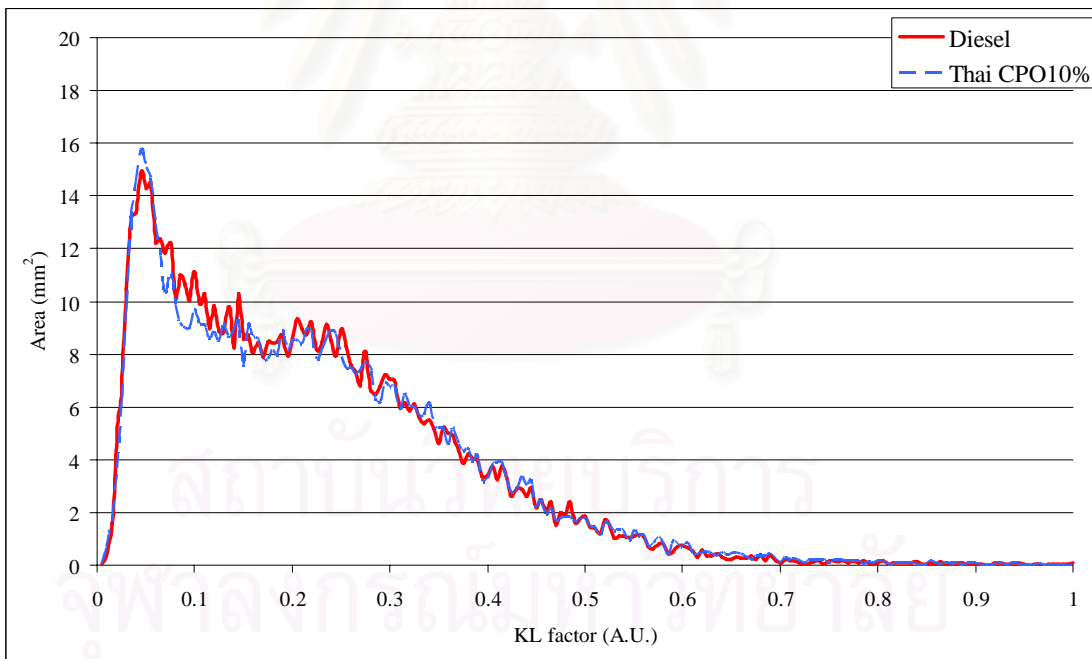


Fig. 5-87 KL factor histogram of Diesel and Thai CPO 10%
 at injection pressure 100 MPa Combustion at 3.0 MPa 930K
 2.4 msec after start of injection

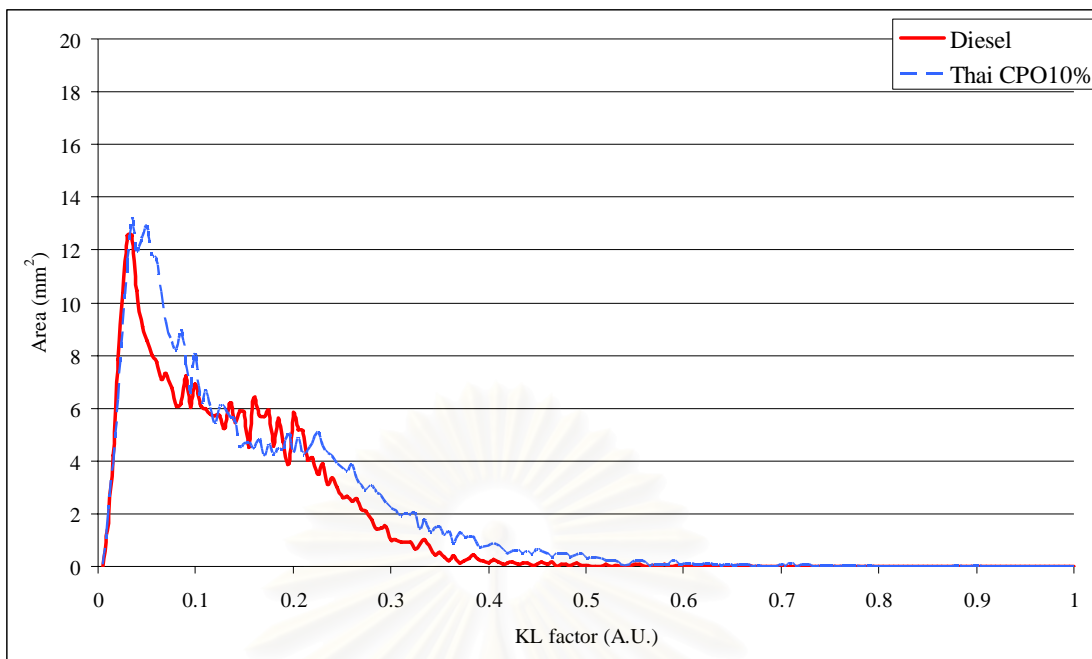


Fig. 5-88 KL factor histogram of Diesel and Thai CPO 10%
at injection pressure 100 MPa Combustion at 3.0 MPa 930K
2.65 msec after start of injection

Revealed in the KL factor histogram, KL factor of Thai palm CPO 10% was not much different compared to diesel. Hence, it could be concluded that the difference in soot emission was very small.

สถาบันวิทยบริการ
จุฬาลงกรณ์มหาวิทยาลัย

5.2.2.5. The analytical of combustion flame images

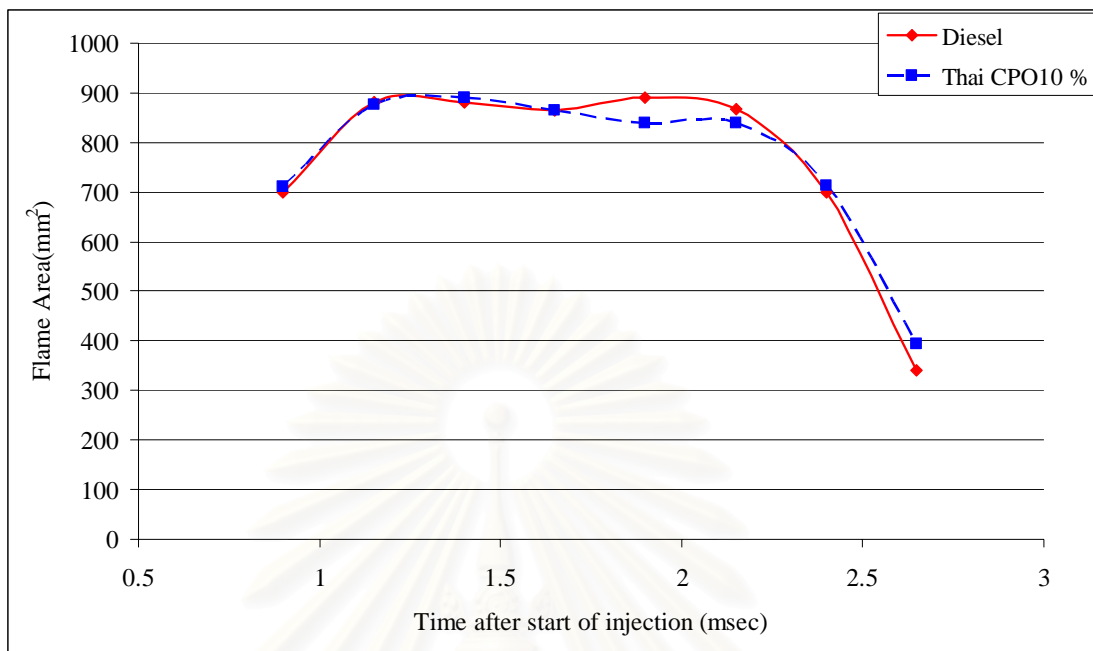


Fig. 5-89 Flame area of Diesel and Thai CPO10 % at injection pressure 100 MPa
Combustion at 3.0 MPa 930K, 0.9-2.65 msec after start of injection

Flame area of diesel and Thai CPO 10% was the same at the start to main combustion. However, there was a little bit decrease in flame area of Thai CPO 10% at the end of the combustion.

สถาบันวิทยบริการ
จุฬาลงกรณ์มหาวิทยาลัย

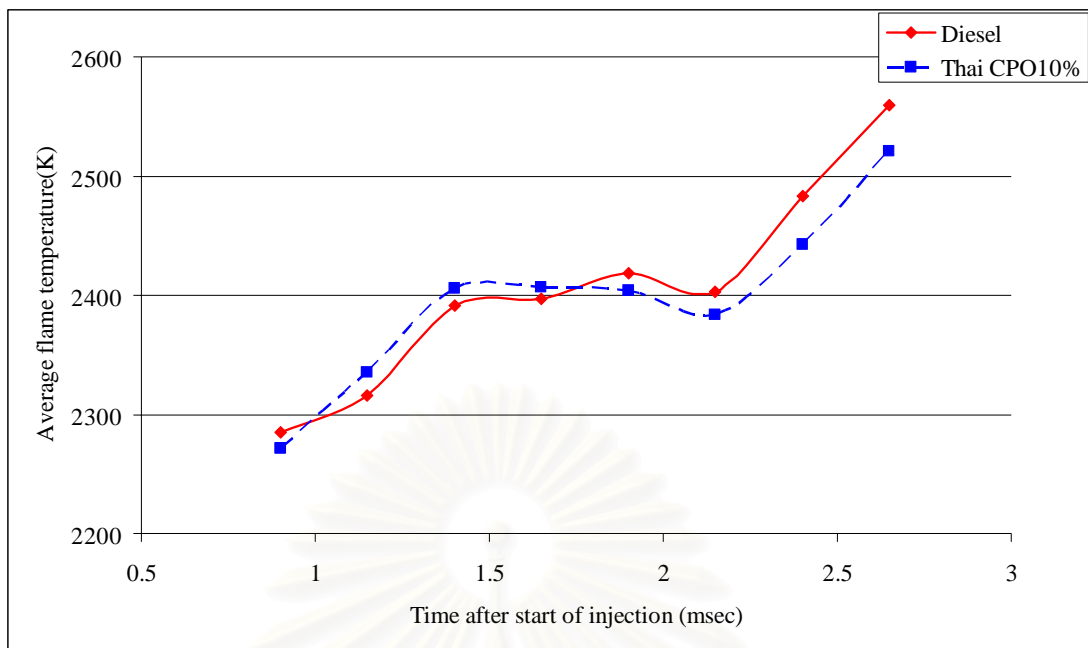


Fig. 5-90 Average flame temperature of Diesel and Thai CPO10 %
at injection pressure 100 MPa Combustion at 3.0 MPa 930K
0.9-2.65 msec after start of injection

Average combustion temperature of Thai CPO 10% was a little bit higher at the start of combustion but lower at the end combustion compared to diesel. However, the difference between both fuels was very small.

สถาบันวิทยบริการ
จุฬาลงกรณ์มหาวิทยาลัย

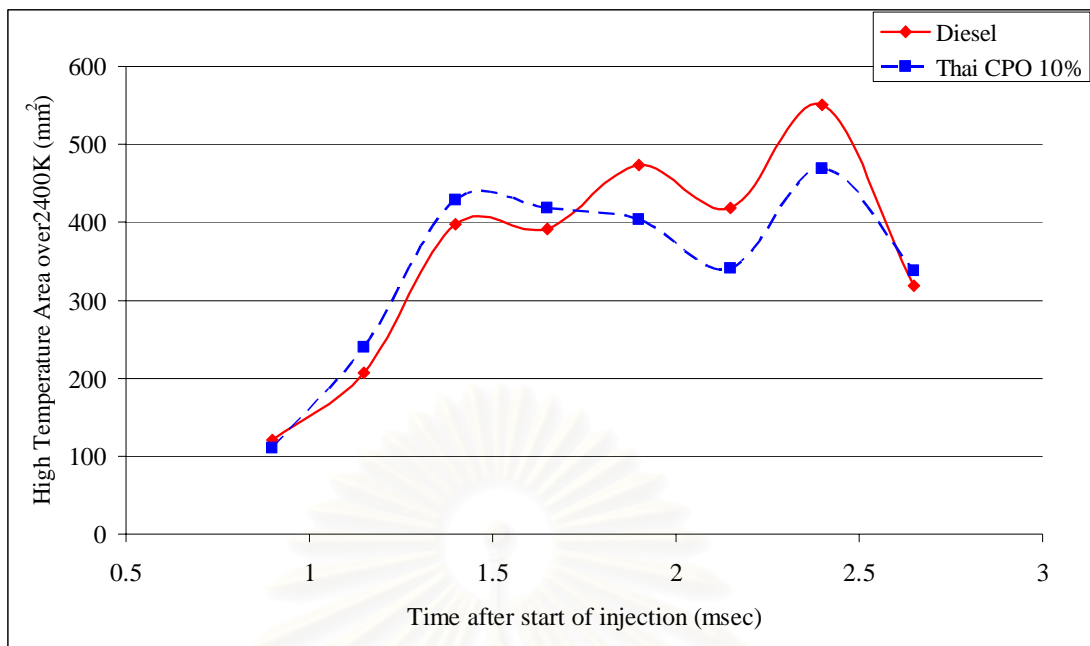


Fig. 5-91 High temperature Area of Diesel and Thai CPO10 %
at injection pressure 100 MPa Combustion at 3.0 MPa 930K
0.9-2.65 msec after start of injection

High temperature combustion area of Thai CPO 10% was a little bit higher at the start of combustion but lower at the end combustion. The difference between both fuels was very small.

สถาบันวิทยบริการ
จุฬาลงกรณ์มหาวิทยาลัย

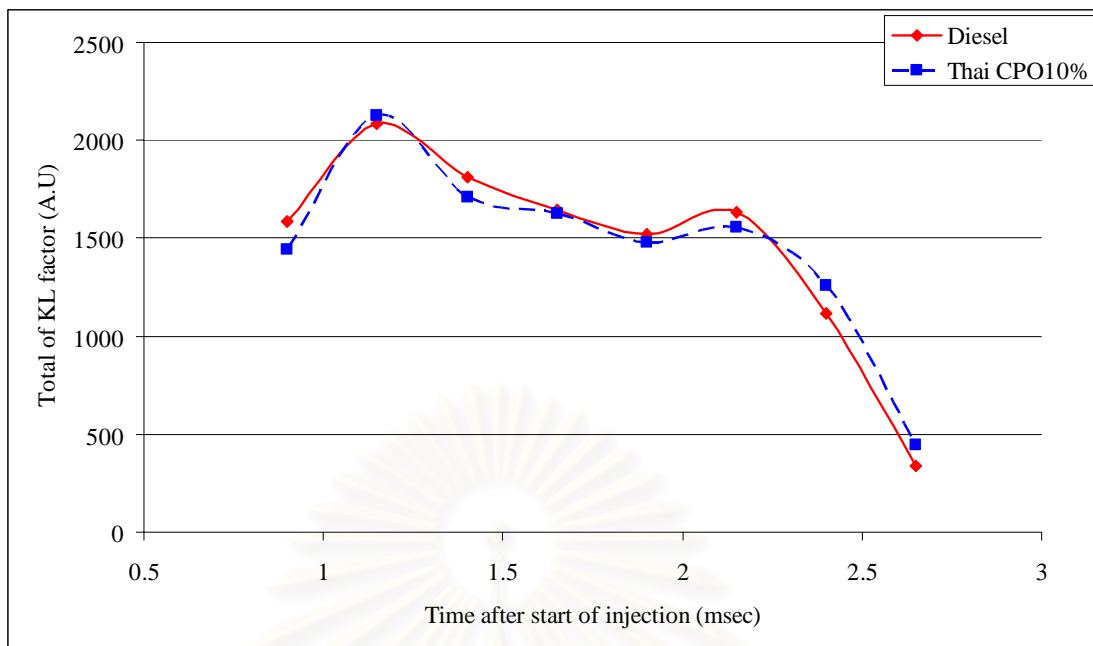


Fig. 5-92 Total KL factor of Diesel and Thai CPO10 %
at injection pressure 100 MPa, Combustion at 3.0 MPa 930K
0.9-2.65 msec after start of injection

It was found that there was very small difference in total KL factor of diesel and CPO 10%.

สถาบันวิทยบริการ
จุฬาลงกรณ์มหาวิทยาลัย

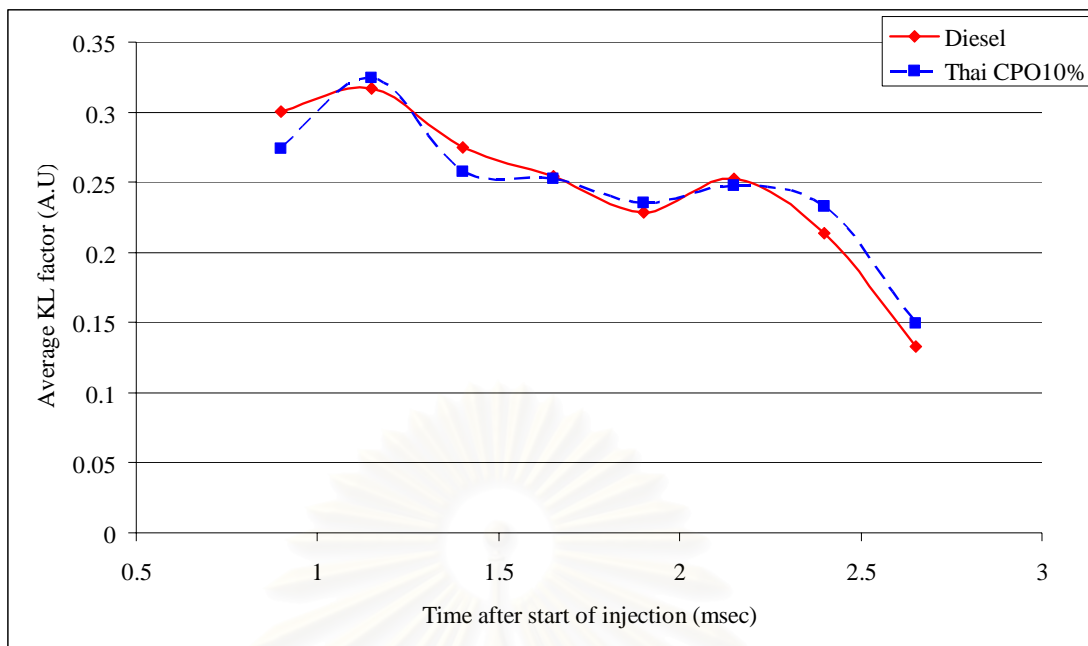


Fig. 5-93 Average KL factor of Diesel and Thai CPO10 %
at injection pressure 100 MPa Combustion at 3.0 MPa 930K ,
0.9-2.65 msec after start of injection

In the case of average KL factor, the difference between diesel and CPO10% was also very small.

The average flame temperature and high temperature area of CPO10% were slightly lower at the end of combustion, shown in figure 5-90 and 5-91. Flame area shown in figure 5-89 revealed that the flame area of CPO 10% was closely the same as diesel fuel. Also total KL factor and average KL factor were closely same as diesel, shown in figure 5-92 and 5-93.

5.3 Effect on fuel spray characteristics of high percentage palm diesel blended

5.3.1 The images of diesel and palm diesel 80% injection

The images of spray, shown in figure 5-94 and 5-95, were plotted from the raw data of the experiment of diesel fuel and palm diesel 80%, at injection pressure 100 MPa and 60 MPa.

Injection pressure 100 MPa

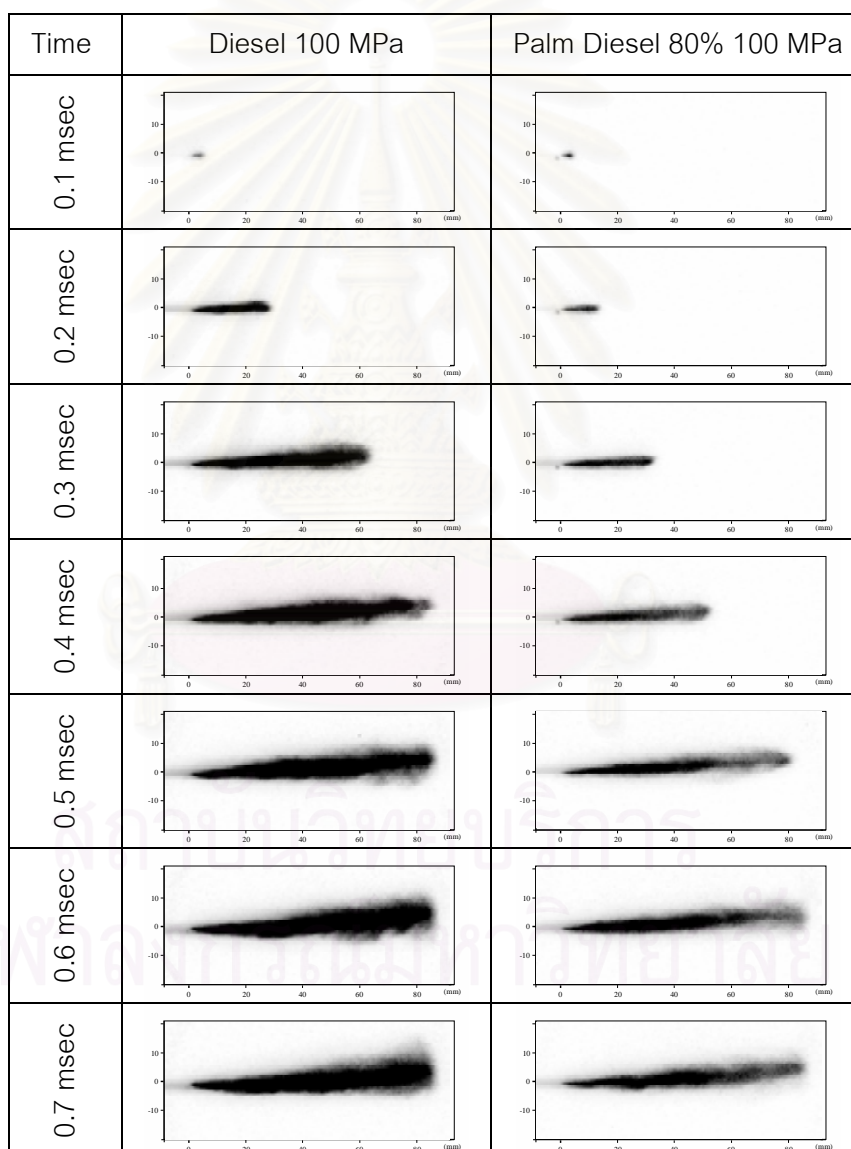


Fig. 5-94 Spray image of Diesel and Palm diesel 80%
at injection pressure 100 MPa

Injection pressure 60 MPa

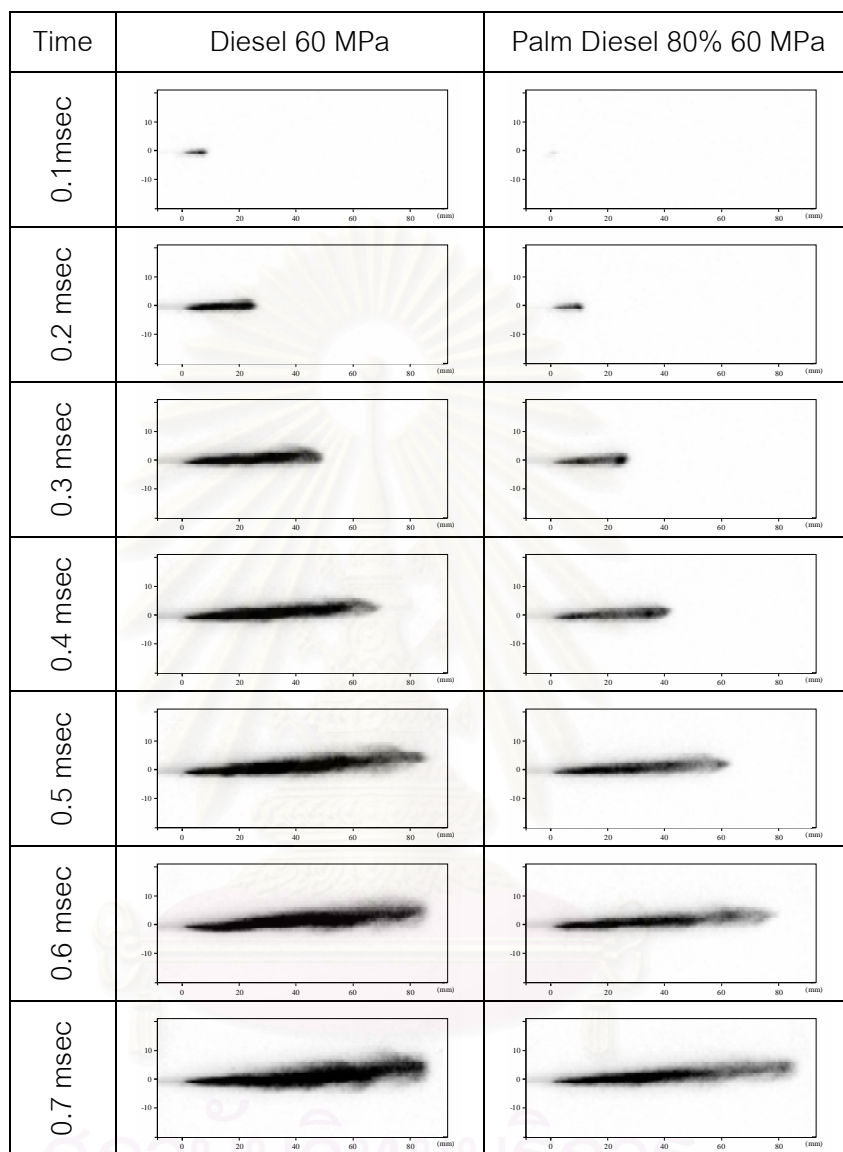


Fig. 5-95 Spray image of Diesel and Palm diesel 80%
at injection pressure 60 MPa

5.3.2 Reflected light source intensity and spray characteristics

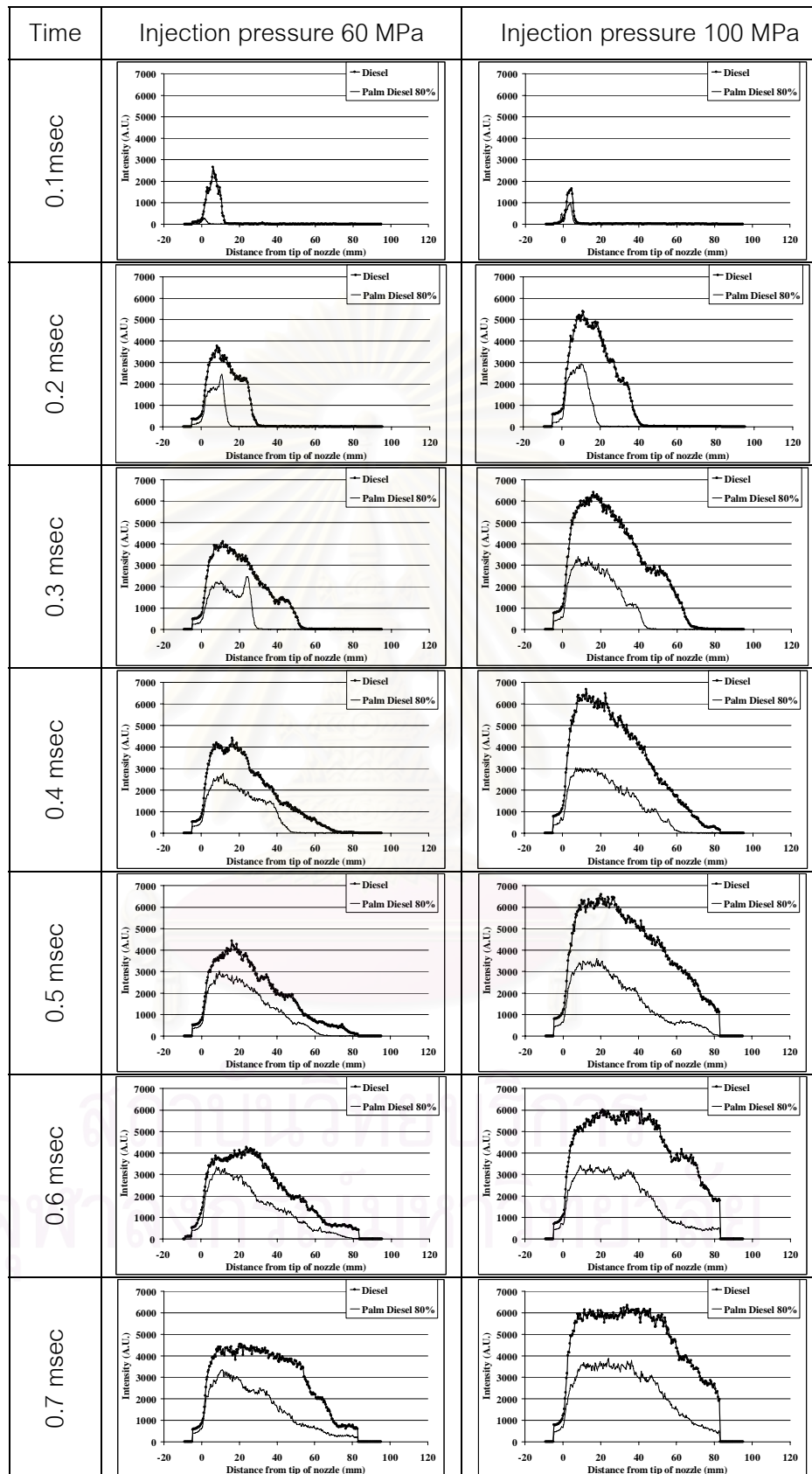


Fig. 5-96 Intensity of fuel spray at the center plane of the nozzle

Figure 5-96 is showing the section data obtained from nozzle tips plane. It is revealed that the light intensity of palm diesel 80% spray were lower than diesel at both injection pressure 100MPa and 80MPa.

5.3.3 Effect on spray characteristics

From the image data, fuel spray parameters, spray angle, spray volume and spray penetration were calculated.

5.3.3.1. Spray angle

Fuel spray angle was calculated from data at close to the peak injection rate, 1.0 msec after injection for 100MPa injection pressure and 1.2 msec after injection for 60 MPa.

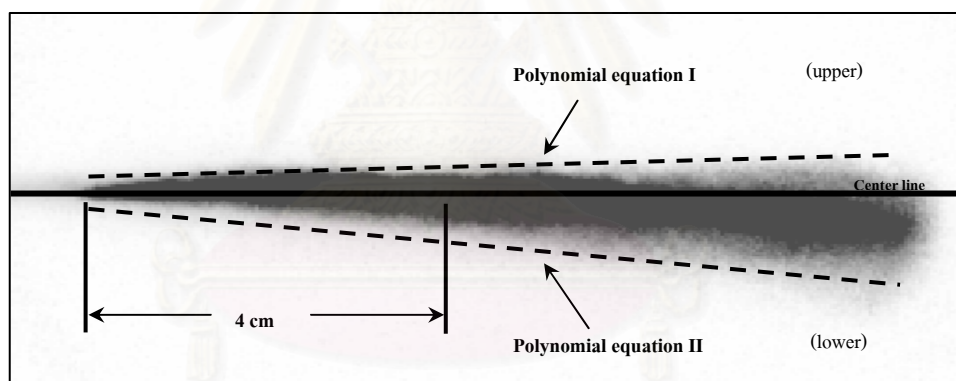


Fig. 5-97 The calculation of spray angle

By computational programming, fuel spray angle was determined from angle between upper and lower edge lines of spray, using polynomial equation I (upper) and polynomial equation II (lower) with respect to the center line. These equations were used to calculate the spray angle at 4 cm from nozzle tip, as shown in figure 5-97.

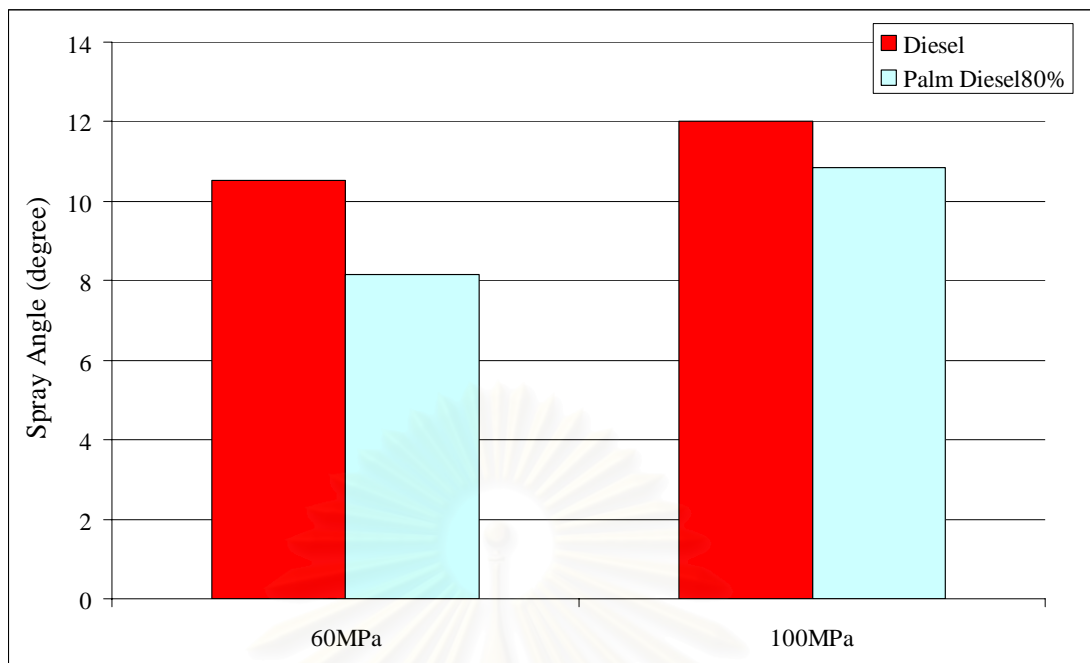


Fig. 5-98 Spray angle of Diesel and Palm diesel 80%

1.0 msec after start of injection for injection pressure 100 MPa

1.2 msec after start of injection for injection pressure 60 MPa

ICCD camera gain 9.0 width 10 μ sec

From figure 5-98, the spray angle of palm diesel 80% were smaller than diesel at injection pressure 100MPa around 1 degree and at 60MPa around 2 degree.

5.3.3.2. Spray Volume

From data obtained at 0.1-0.7 msec after start of injection, spray volume was calculated by summation of spray cross area with an assumption that the cross section shapes were circle, as shown in figure 5-99 and equation 5-1.

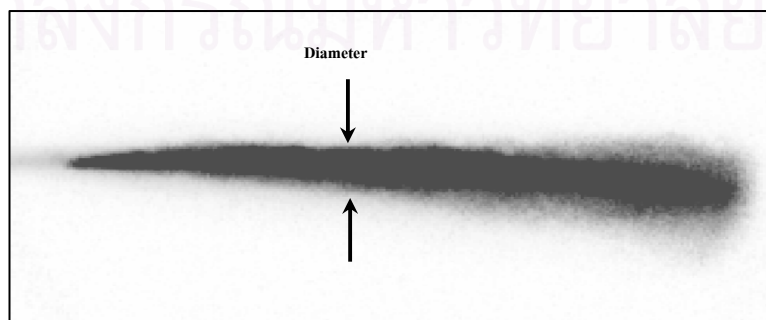


Fig. 5-99 The calculation of spray volume

$$\text{Spray volume} = \sum \left(\frac{\pi D^2}{4} \right) \quad (5-1)$$

D is spray diameter (mm)

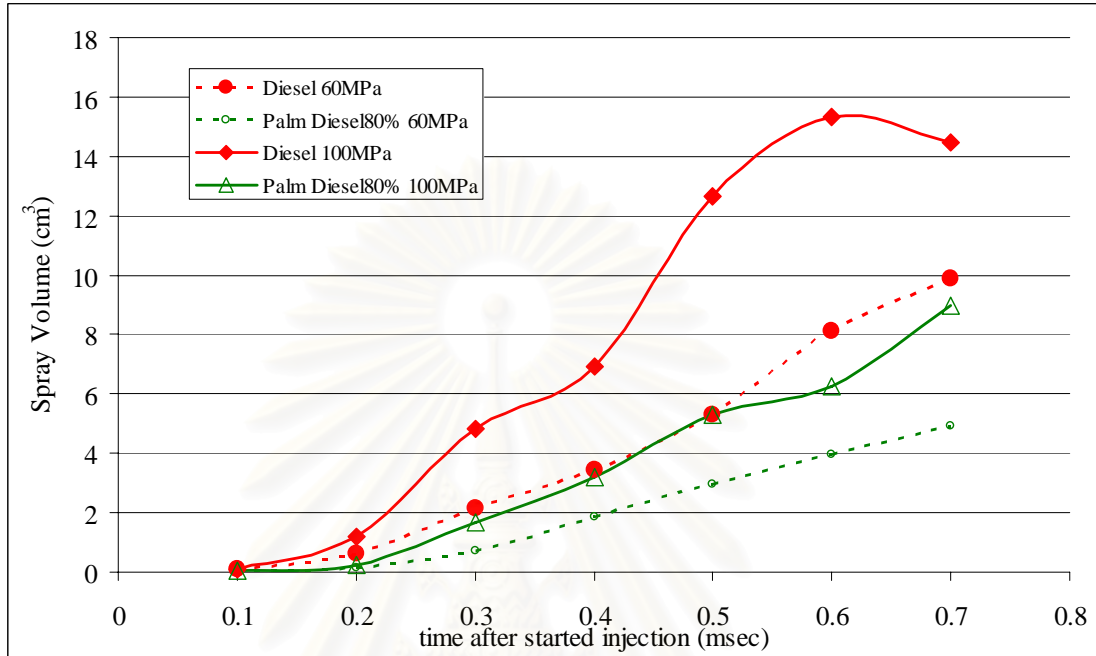


Fig. 5-100 Spray Volume of Diesel and Palm diesel 80%

It was found that spray volume was increased, with time. The increase of injection pressure could increase the spray volume.

The spray volume of palm diesel 80% was smaller than diesel at injection pressure 100MPa and 60MPa.

สถาบันวิทยบริการ
จุฬาลงกรณ์มหาวิทยาลัย

5.3.3.3. Spray penetration

The spray penetration was calculated from spray image data from the start until the limit of the observation window (0.1-0.7 msec after injection).

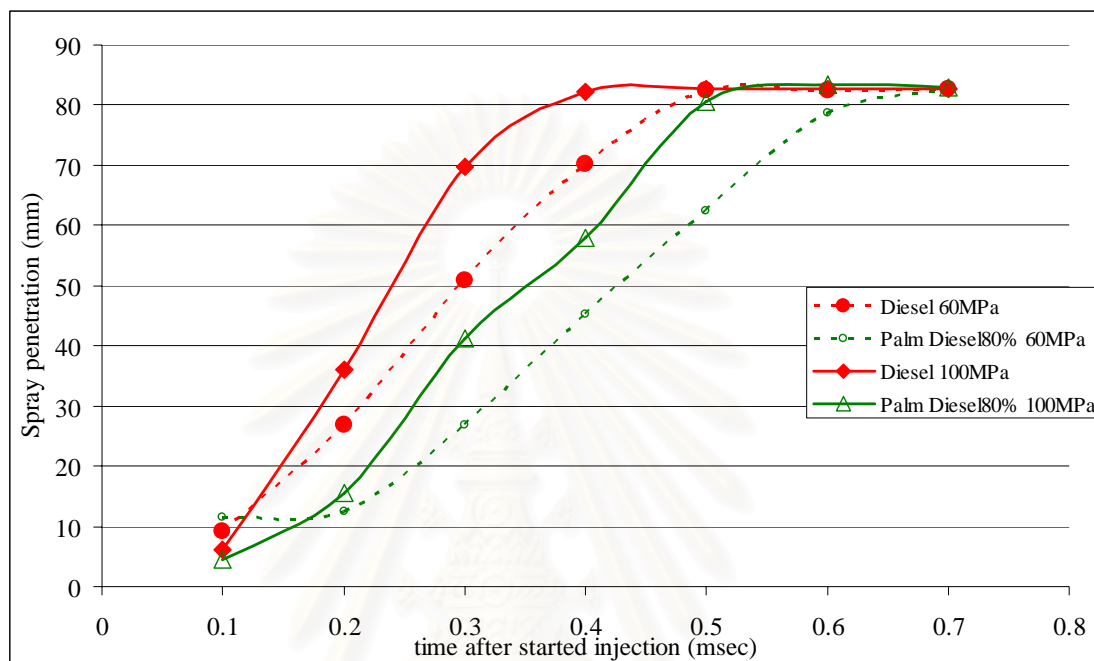


Fig. 5-101 Spray penetration of Diesel and Palm diesel 80%

It was found that the spray penetration of palm diesel 80 % was slower than diesel, around 1-1.5 msec at injection pressure 100 MPa and 60 MPa. The increase of injection pressure from 60 MPa to 100 MPa could speed up the spray penetration around 0.05 msec.

The spray angle, spray volume and spray penetration of palm diesel 80 %, shown in figures 5-97, 5-98 and 5-99 were lower than diesel. These may be due to the bad atomization of palm diesel 80%. However, the difference will be smaller if injection pressure is increased.

Figure 5-96 shows the intensity of the spray images obtained at the center plane of the nozzle with 2 injection pressure (60 and 100 MPa). The results show that the intensity of higher injection pressure was higher. In addition, the intensity of palm diesel 80% was lower than diesel fuel.

The observed trends in higher light intensity might be resulted from the 2 fuel atomization characteristics; the better atomization of fuel the higher light intensity. As the Sauter mean diameter (SMD) decreases (better atomization), the number of fuel droplet increases. This enhances the light reflection.



สถาบันวิทยบริการ
จุฬาลงกรณ์มหาวิทยาลัย

CHAPTER VI

CONCLUSION AND SUGGESTION

6.1 The study on combustion of refined palm oil

6.1.1 Ignition delay of the combustion

a) The ignition delay of palm diesel 20% were shorter than diesel at all injection pressure, though the combustion ambient were increase from 2.0 to 3.0 MPa, the ignition delay were still shorter.

b) Ignition delay was decreased with high percentage refined palm oil blended at both injection pressure 60 MPa and 100 MPa.

c) The ignition delays of palm diesel 80% and palm 100% at injection pressure 100 MPa were shorter than diesel fuel.

6.1.2 Fuel combustion period

a) Combustion period was decreased with the higher injection pressure. This might be the results of 1) short injection period and 2) better atomization as injection pressure increased.

b) The study on effect of palm blended percentage 20%, 40%, 60% revealed that at the injection pressure 60 MPa, the combustion period was rarely changed. However, in the case of injection pressure 100 MPa, the combustion period was seemed shorter.

c) Observed combustion period of palm blended at injection pressure of 100 MPa were shorter than diesel. The amount of injection fuel became slightly smaller and the injection period became slightly shorter with the increase of palm blended percentage. This may due to the higher viscosity of palm blended fuel. The shorter combustion period of palm blended fuel might be the results of these tendencies.

6.1.3 Combustion flame visualization

6.1.3.1. The study on combustion visualization of palm diesel 60% at injection pressure 60 MPa and 100MPa

a) Combustion flame areas of palm diesel 60% were smaller than that of diesel at injection pressure of 60 MPa but after increasing the injection pressure up to 100 MPa, the area size was closer to the diesel.

b) The high temperature area (over 2400K) of palm diesel 60 % was smaller than diesel. The higher the injection pressure caused the larger the high temperature area.

c) The soot concentration which estimated by average KL factor resulted that palm diesel 60% seemed to be higher than diesel at the injection pressure of 100 MPa and 60 MPa.

6.1.3.2. The Study on combustion visualization of palm diesel 60%, 80% and palm 100% at injection pressure 100 MPa

a) Combustion flame areas of palm diesel 60%, 80% and 100% were smaller than diesel at injection pressure of 100 MPa,

b) At the start of combustion, average flame temperature of palm 100% was the highest. It might be caused by short ignition delay and fuel properties.

c) High temperature area (>2400 K) of palm diesel 60 %, 80% and 100% were smaller than diesel.

d) The soot concentration (estimated by average KL factor) of palm diesel 60% and 80% were higher than diesel but in the case of palm100%, it was very low at the start of combustion.

e) The intensity of combustion flame was lower with the higher blending percentage and the difference between two peaks of luminous flame was extended. This might be due to the result from slower burning rate of palm diesel compared to diesel.

6.2 The study of Thai COP 10% blend

6.2.1 Combustion period and ignition delay

The amount of injection fuel became slightly smaller and the injection period became slightly shorter with CPO 10% blended. This is possibly due to the higher viscosity of CPO fuel. The shorter combustion period of palm blended fuel might be the results of these tendencies. It was found that CPO10% had shorter ignition delay than diesel fuel around 0.1 msec.

6.2.2 Combustion flame visualization

The average flames temperature were slightly lower and high temperature area of CPO10% were slightly smaller at the end of combustion. The flame area of CPO 10% was closer the size of diesel fuel. Also total KL factor and average KL factor were similar to the value of diesel.

6.3 The effect on spray characteristics of high percentage palm diesel blended

a) Spray angle was decreased with the high percentage palm diesel, however the difference became smaller at higher injection pressure.

b) At the same injection pressure, palm diesel 80% produced shorter the spray tip penetration and smaller spray volume compared to diesel.

c) The intensity of the spray images obtained at the center plane of the nozzle with injection pressure 100 MPa was higher than that at 60 MPa. In addition, the intensity of palm diesel 80% was lower than diesel fuel.

6.4 Suggestions

6.4.1 The experimental apparatuses

6.4.1.1 Injection systems

a) The leak of the injection system was effected the controlling at the high pressure.

b) The control of the start of experiment, line pressure and injection mass were difficult. It needs to practice.

6.4.1.2 Optical sensors

a) The position of optical sensors should rearrange to measure the luminous intensity and images at the same time.

b) The optical sensor's base should be separated from the injection system in order to eliminate the vibration of hydraulic pump when it is operated.

6.4.2 Camera calibration for two color method

6.4.2.1 Calibration for two color method

The calibration set up should be conducted with difference length set up, camera exposure time and compared with the previous data.

6.4.2.2 Calibration back ground image

From back ground image, the overlap of images was effected to the back ground. In this experiment, the back ground image was simulated from a low intensity. To obtain more clear image and data, the calibration back ground should be done in the longer exposure time as close to 10 μ sec (same as in the combustion experiment).

6.4.3 Constant for limited wave-length range ($\alpha = 1.38$)

Actually, the constant for limited wave length range (α) is not constant. To eliminate this effect, the multiple color method should be applied (more than 2 colors) to calculate this constant of each pixel intensity data.

6.4.4 Experiments

6.4.4.1 Combustion experiments

- a) More experiment should be conducted at injection pressure 60 MPa of palm diesel 80% and palm 100%
- b) The experiment at higher injection pressure and ambient pressure should be considered.

6.4.4.2 Spray experiments

- a) More experiments should be conducted with palm 100% and palm diesel 60% at injection pressure 100 MPa and 60 MPa.
- b) The relations between spray light intensity, droplet diameter, atomization and injection pressure of palm oil should be studied.
- c) The experiment should be taken care with the start of the injection, which relate to the setting up of injection system for each injection pressure and palm percentage blended.

6.4.5 Palm diesel

- a) The properties of the refine palm should be studied more, especially the density of refine palm at the experimental conditions.
- b) The blending method of palm diesel should be taken care, to make sure that the blending method and corrected percentage are obtained.

References

1. Azetsu, A.; Sato, Y.; and Wakisaka, Y. Effects of Aromatic Components in fuel on Flame Temperature and Soot Formation in Intermittent Spray Combustion. Journal of Fuels and Lubricants, SAE Transactions, 2003
2. Gary L.Borman and Kenneth W.Ragland. Combustion Engineering. Singapore: McGraw-Hill, 1998.
3. Charles Fayette Taylor. The internal combustion engine in theory and practice. 2 nd edition. United state of America, 1996.
4. Hiro Hiroyasu and Masataka Arai. Structures of Fuel Spray in Diesel Engines. SAE 900475. Society of Automotive Engineers, Warrendale, Pa., 1990.
5. Pich Prinyachan. Effects of using palm oil blending in diesel fuel for a small agricultural CI engine. Master's Thesis. Mechanical Engineering, Engineering, Chulalongkorn University., 2003.
6. Heywood, J.B. Internal combustion engine fundamentals. Singapore: McGraw-Hill, 1988.
7. Ciccarelli, G., Phil Oliver, and Steve Reynolds. Combustion theory section 5 [Online]. 2005. Available from:
<http://me.queensu.ca/courses/MECH435/5.%20Combustion%20Theory.ppt#265.11,Slide 11>
8. LaVision. 2002. Flame star II camera hand book.
9. Sato, Y. Effects of Aromatic Components in fuel on Flame Temperature and Soot Formation in Intermittent Spray Combustion. Master's Thesis. Mechanical Engineering, Engineering, University of Tokyo., 2001.
10. De Vos, J.C. A new determination of the emissivity of tungsten ribbon. Physica XX, pp. 690-714, Arnhem, Nederland., 1954.
11. Kamimoto, T. The theory of two color pyrometry. Tokai University, Japan, 2004.
(Mimeographed)
12. Autar Kaw, et al. Bisection method [Online]. 2006. Available from:
http://numericalmethods.eng.usf.edu/mws/gen/03nle/mws_gen_nle_ppt_bisection.ppt

13. Therdsak Chaisuriyaphun. Using plam oil blending in diesel fuel for indirect injection CI engine for light-duty pick-up truck application. Master's Thesis. Mechanical Engineering, Engineering, Chulalongkorn University., 2004.



สถาบันวิทยบริการ
จุฬาลงกรณ์มหาวิทยาลัย

Bibliography

1. Uyehara, O.A. et al. Flame temperature measurements in Internal combustion Engines. Transaction of the A.S.M.E, pp.17-30, 1946.
2. Owen, K., and Trevor Coley. Automotive Fuels Reference Book. 2 nd edition. United states of America: Society of Automotive Engineers, 1995.
3. Gupta, S., Poola R. and Sekar R. Effect of injection Parameters on diesel spray characteristics. SAE 2000-01-1600. Society of Automotive Engineers, Warrendale, Pa., 2000.
4. Young-Ho Won, et al. 2-D Soot Visualization in unsteady spray flame by means laser sheet scattering technique. SAE 910223. Society of Automotive Engineers, Warrendale, Pa., 1991.
5. Yamada, J., and Tanaka, Y. Manufacturing process of bio-diesel fuel. Engine technology., 2003.
6. Shao, J.,; Yan, Y.,; and Smith, S. Quantitative characterization of diesel spray using digital imaging techniques. Measurement science and technology. Institute of physics publishing, UK, 2003.
7. Blaich, B. Diesel Fuel Injection. 1 st edition. Germany: Robert Bosch GmbH, 1994.
8. Ramadhas, A.S.,; Jayaraj, S.,; and Muraleedharan, C. Use of vegetable oil as I.C. engine fuel-A review [Online]. Available from: www.Sciencedirect.com [2003,September 9]
9. Sher, E. Handbook of air pollution from internal combustion engines – Pollutant formation and control. United States of America: Academic Press, 1998.
10. Yusuf Ali, and M.A. Hanna. Alternative diesel fuels from vegetable oils. Bioresource Technology 50 (21 July 1994): 153-163.
11. Pryor, R.W., M.A. Hanna, J.L. Schinstock, and L.L. Bashford. Soybean oil fuel in a small diesel engine. Transaction of the ASAE 26: 333-337.
12. Yu C.W., Bari S, and Ameen A. A comparison of combustion characteristics of waste cooking oils as fuel in a D.I. Diesel Engine. Proc. I. MECH. E. part D journal of automobile engineering vol.216 No.3: 237-243.

13. Ziejewski, M.,and Hans J. Goettler. EMA Durability tests on high oleic sunflower and safflower oils in diesel engines. SAE paper No.961846 (26-28 August 1996).
14. Bari, C. W. Yu,and T. H. Lim. Performance deterioration and durability issues while running a diesel engine with crude palm oil. Proc. I. MECH. E. part D journal of automobile engineering vol.216 (2002): 785-792.

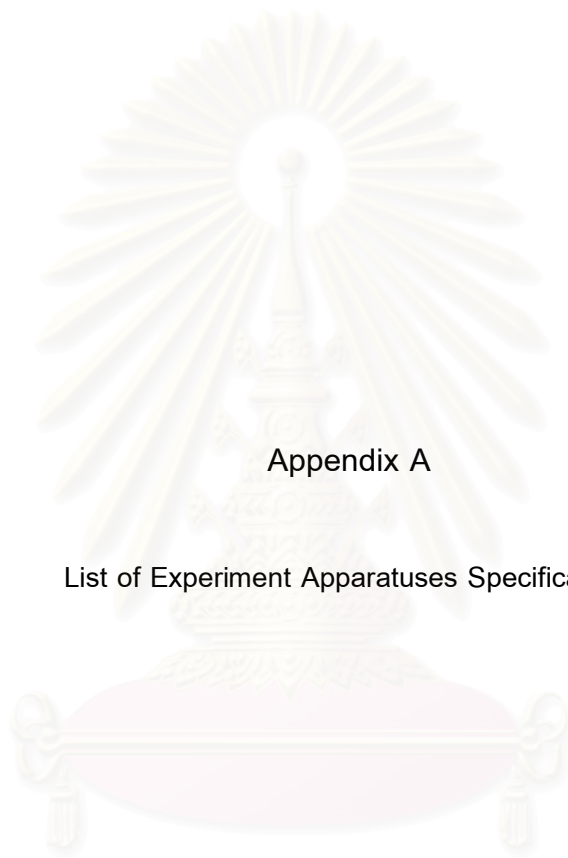


สถาบันวิทยบริการ
จุฬาลงกรณ์มหาวิทยาลัย



Appendices

สถาบันวิทยบริการ
จุฬาลงกรณ์มหาวิทยาลัย



Appendix A

List of Experiment Apparatuses Specification

สถาบันวิทยบริการ
จุฬาลงกรณ์มหาวิทยาลัย

ICCD Camera:	LA vision Flame star	
Camera sensitivity (max)	60	counts / photo electron
Reference Pos	6.3	scales setting
	(Corresponds 1 to count / phot el.)	
Min. gate	5	nsec
Dark image intensity (top)	200	counts Temp 25 °C
Read out frequency	1.8	MHz
Read out time / Frame	75	msec
RMS (single image)	2.0	counts Temp 10 °C

Computer System

Processor	P3 500 MHz	
HD	10	GB
RAM	128	MB

Lens: Nikon 105 mm , Diameter 52 mm, F1.8

Vari lens: Kenko Vari Mirage 52

Filter: 1. Center wave length	488	nm
Transmittance	46	%
Full width at half max (FWHM)	11.3	nm
2. Center wave length	634	nm
Transmittance	40	%

Full width at half max (FWHM) 8.5 nm

Tungsten lamp: TOSHIBA 5 Volt, 20 A

Regulated DC Power Supply: PAN 16-16 A KIKUSUI

Pieza Acuator Denso stacks type

Size 118.5 ± 1.6 mm, $\phi 31.2 \pm 0.2$ mm

Wight 570 g

Capacity 5.4 μ F

Maximum moving length 600 V, 105 ± 16 μ m

Power 6900 N

DC Power Supply matsusada precision

Output Voltage 0 – 650 V

Output Ampere 0 – 0.1 A

Output ripple 10 m Vrms

DA Board Micro science MDA – 2898 BPC 12 bit 2 channel

4KB(2048 data) FIFO memory

Analog (DA) input ± 5 , ± 10 , 0~+10 V

DA data out put port I/O, DMA

Clock frequency 1 MHz

AD Board Micro science ADM – 4898BPC-4-16 KW

12 bit 4 channel FIFO memory

input $\pm 10, \pm 5, \pm 2.5, \pm 2$ V

AD data out put port I/O, DMA

Clock frequency 8 MHz

Injection Pressure Sensor Kyowadengyo

Max pressure 1000 kgf / cm²Capacity 2010 ($\times 10^{-6}$) μ Strain

Clock Frequency 3 kHz

Injection rate Sensor Kyowadengyo

Max pressure 2 kgf / cm²Capacity 1850 ($\times 10^{-6}$) μ Strain

Clock Frequency 3 kHz

Mixing motor oriental motor

Frequency 50 / 60 Hz

Torque 3000 / 2600 gcm

Speed 1300 / 1550 rpm

Inside Combustion chamber pressure sensor Kyowadengyo

Max pressure 50 kgf / cm²Capacity 1527 ($\times 10^{-6}$) μ Strain

AD board Interface AZI-3141

12 bit 4 channel

FIFO memory : 4k word/ch

Input

 ± 5 , ± 10 , 0~+10 V

Conversion time

10 μ s**Radical Measurement Metal Interference**

nihonsinkukugaku MIF-W

Center Wave Length

310.3 nm

Transmittance

18.3 %

Half Band Width

16.6 nm

Photo Multiplier hamamatsa photonics silicon photo diode S1226-44BK

Wave Length

320 ~ 1000 nm

Sensitivity

0.35 A/W

Effective Size

13 mm²**Photo Multiplier hamamatsa photonics silicon photo diode S1227-1010BR**

Wave Length

320 ~ 1000 nm

Sensitivity

0.42 A/W

Effective Size

100 mm²**Photo Diode hamamatsa photonics silicon photo diode S1226-44BK**

Wave Length

320 ~ 1000 nm

Sensitivity

0.35 A/W

Effective Size

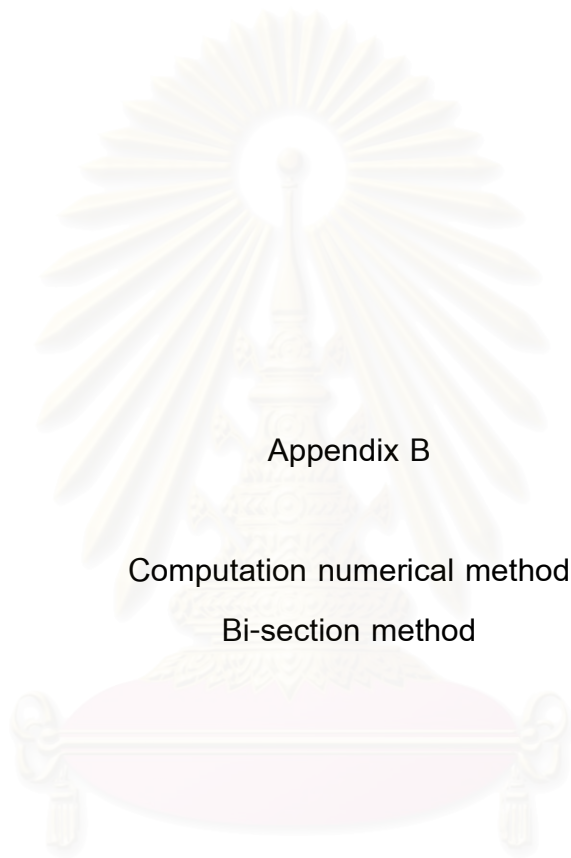
13 mm²

Photo Diode hamamatsa photonics silicon photo diode S1227-1010BR

Wave Length	320 ~ 1000	nm
Sensitivity	0.42	A / W
Effective Size	100	mm ²



สถาบันวิทยบริการ
จุฬาลงกรณ์มหาวิทยาลัย



Appendix B

Computation numerical method

Bi-section method

สถาบันวิทยบริการ
จุฬาลงกรณ์มหาวิทยาลัย

Theory of Bi-section method [12]

An equation $f(x)=0$, where $f(x)$ is a real continuous function, has at least one root between x_l and x_u if $f(x_l) f(x_u) < 0$.

$$x_m = \frac{x_l + x_u}{2} \quad (B-1)$$

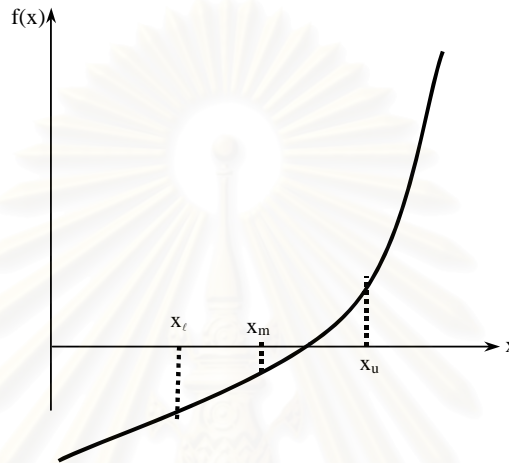


Fig. B-1 Non linear graph equation

Algorithm for Bi-section Method

Step 1:

Choose x_l and x_u as two guesses for the root such that $f(x_l) f(x_u) < 0$, or in other words, $f(x)$ changes sign between x_l and x_u .

Step 2:

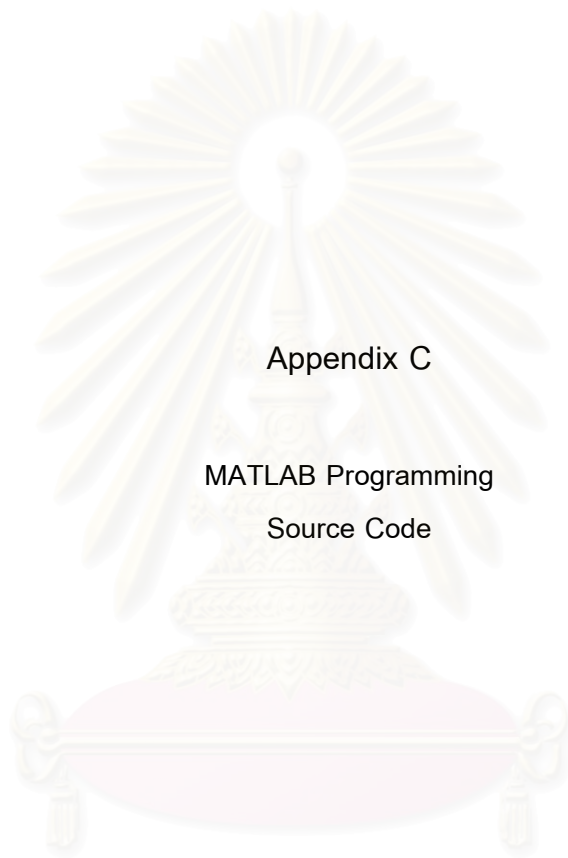
Estimate the root, x_m of the equation $f(x) = 0$ as the mid-point between x_l and x_u .

Step 3:

If $f(x_l) f(x_m) < 0$, then the root lies between x_l and x_m ; then $x_l = x_l$; $x_u = x_m$.

If $f(x_l) f(x_m) > 0$, then the root lies between x_m and x_u ; then $x_l = x_m$; $x_u = x_u$.

If $f(x_l) f(x_m) = 0$; then the root is x_m . Stop the algorithm if this is true.



Appendix C

MATLAB Programming
Source Code

สถาบันวิทยบริการ
จุฬาลงกรณ์มหาวิทยาลัย

Two Color Method
Flame temperature and KL factor

```

%Program two color 2005 by Karn Romphol ^_~(2005/9/7) gain 5.5 width 10 microsec
function T=Tm(Tr,Tb)
Xd=input('Please insert multi-INPUT file directory & name :','s');
disp('Please wait....! 2 min per file')
multiF=[Xd];
fid = fopen(multiF, 'rt');
if (fid == -1)
    error('read_file: cannot open file for reading');
end
done_yet = 0;
while (done_yet == 0)
DATA = fgetl(fid)
    if (DATA == -1);
        done_yet = 1;
    else
ZTa=[DATA,'.txt'];
W=load(ZTa);
Cali=load('D:\karn\BDFdata\20051006CariPic\calibrationpicMO5.txt');
W1=zeros(286,384);
for p=1:286;
    for u=1:384;
        if Cali(p,u) >0.25 & W(p,u) >0;
            W1(p,u)= W(p,u)./Cali(p,u);
        end
        if Cali(p,u)<=0.25;
            W1(p,u)=0;
        end
    end
end
W1;
CutPic=load('D:\karn\BDFdata\20051004cutOffPic\CutOffPic1.txt');
W2=zeros(286,384);
for g=1:286;

```

```

for e=1:384;
    if Cali(g,e)==0;,
        W2(g,e)=0;
    else
        W2(g,e)= W1(g,e).*CutPic(g,e);
    end
end
end
end
W2;
F=max(max(W))*20/100;
R=W2(1:286,2:162); %check position 82,298
B=W2(1:286,216:376);%for Data 2005/11/30 (B60%)
T=zeros(286,160);
for i=1:286
    for j=1:160
        if R(i,j)< F,
            Tm(i,j)=0;
        else
            Tr(i,j)=-22718./(log(R(i,j))-(19.246));
            Tb(i,j)=-29685./(log(B(i,j))-(22.045));
            TH(i,j)=max(Tr(i,j),Tb(i,j))+1000;
            TL(i,j)=max(Tr(i,j),Tb(i,j))+0.1;
            BklH(i,j)=0.488^1.38*log(1-exp((14388/0.488)*(1./TH(i,j)-1./Tb(i,j)))); %Max
            RklH(i,j)=0.634^1.38*log(1-exp((14388/0.634)*(1./TH(i,j)-1./Tr(i,j))));
            dklH(i,j)=-BklH(i,j)+RklH(i,j);
            BklL(i,j)=0.488^1.38*log(1-exp((14388/0.488)*(1./TL(i,j)-1./Tb(i,j)))); %Min
            RklL(i,j)=0.634^1.38*log(1-exp((14388/0.634)*(1./TL(i,j)-1./Tr(i,j))));
            dklL(i,j)=-BklL(i,j)+RklL(i,j);

            dtm(i,j)=TH(i,j)-TL(i,j);
            while dtm(i,j) > 0.1
                Tm(i,j)=(TH(i,j)+TL(i,j))/2;
                Bkl(i,j)=0.488^1.38*log(1-exp((14388/0.488)*(1./Tm(i,j)-1./Tb(i,j)))); %Mid
                Rkl(i,j)=0.634^1.38*log(1-exp((14388/0.634)*(1./Tm(i,j)-1./Tr(i,j))));
                dklm(i,j)=-Bkl(i,j)+Rkl(i,j);
            end
        end
    end
end

```



```

    if dklH(i,j).*dklL(i,j)>0,
        Tm(i,j)=0;
        Bkl(i,j)=0;
        Rkl(i,j)=0;
        dtm(i,j)=0.01;
    end

    if dklm(i,j).*dklH(i,j) > 0,
        TH(i,j)=Tm(i,j);
        dklH(i,j)=dklm(i,j);
        dtm(i,j)=TH(i,j)-TL(i,j);
    end

    if dklm(i,j).*dklL(i,j) > 0,
        TL(i,j)=Tm(i,j);
        dklL(i,j)=dklm(i,j);
        dtm(i,j)=TH(i,j)-TL(i,j);
    end

end %while
end %if

T=Tm;
end %j
end %i

ZT=[DATA,'T.txt'];
save(ZT,'T','-ASCII')

%KLfactor
WTa=load(ZTa);
WT=load(ZT);
Cali=load('D:\karn\BDFdata\20051006CariPic\calibrationpicMO5.txt');
WTa2=WTa./Cali;
R=W2(1:286,2:162);
T=WT(:,:);
K=zeros(286,160);

```


Average Temperature High, Temperature Area, Combustion Flame Area

```

X=input('Please insert multi-INPUT file directory & name :','s');
multiF=[X];
fid = fopen(multiF, 'rt');
if (fid == -1)
    error('read_file: cannot open file for reading');
end
done_yet = 0;
while (done_yet == 0)

DATA = fgetl(fid)
if (DATA == -1);
    done_yet = 1;
else

ZD=[DATA, '.txt'];
Z=[ZD];
P=load(Z);
%%%%%%%%%%%%%%%%%%%%%%%%%%%%%%%%%%%%%%%%%%%%%%%%%%%%%%%%%%%%%%%%%%%%%%%%
B=sum(sum(P(:,>2400)));
B2=B.*(30/82)^2;
C=sum(sum(P(:,>1)));
C2=C.*(30/82)^2;
D=sum(sum(P(:,>0)));
E=sum(sum(P(:,>)));
AVGTemp=E./D;

fprintf('Average of Temperature : %.3f \n', AVGTemp);
fprintf('High Temperature area(mm2): %.3f \n', B2);
fprintf('Flame area(mm2) : %.3f \n', C2);
A=input('Continue?','s');
end %if
end %while
fclose(fid);

```

Temperature Histogram

```

X=input('Please insert multi-INPUT file directory & name :','s');
multiF=[X];
fid = fopen(multiF, 'rt');
    if (fid == -1)
        error('read_file: cannot open file for reading');
    end
done_yet = 0;
while (done_yet == 0)

DATA = fgetl(fid)
    if (DATA == -1);
        done_yet = 1;
    else

ZD=[DATA, '.txt'];
Z=[ZD];
P=load(Z);

%%%%%%%%%%%%%%%%%%%%%%%%%%%%%%%%%%%%%%%%%%%%%%%%%%%%%%%%%%%%%%%%%%%%%%%%

A1=sum(sum(P(:,>2900)));
B1=A1.*(30/82)^2;

A2=sum(sum(P(:,>2850))-A1);
B2=A2.*(30/82)^2;

A3=sum(sum(P(:,>2800))-A1-A2);
B3=A3.*(30/82)^2;

A4=sum(sum(P(:,>2750))-A1-A2-A3);
B4=A4.*(30/82)^2;

A5=sum(sum(P(:,>2700))-A1-A2-A3-A4);

```

$$B5=A5.*(30/82)^2;$$

$$A6=\text{sum}(\text{sum}(P(:,>2650)))-A1-A2-A3-A4-A5;$$

$$B6=A6.*(30/82)^2;$$

$$A7=\text{sum}(\text{sum}(P(:,>2600)))-A1-A2-A3-A4-A5-A6;$$

$$B7=A7.*(30/82)^2;$$

$$A8=\text{sum}(\text{sum}(P(:,>2550)))-A1-A2-A3-A4-A5-A6-A7;$$

$$B8=A8.*(30/82)^2;$$

$$A9=\text{sum}(\text{sum}(P(:,>2500)))-A1-A2-A3-A4-A5-A6-A7-A8;$$

$$B9=A9.*(30/82)^2;$$

$$A10=\text{sum}(\text{sum}(P(:,>2450)))-A1-A2-A3-A4-A5-A6-A7-A8-A9;$$

$$B10=A10.*(30/82)^2;$$

$$A11=\text{sum}(\text{sum}(P(:,>2400)))-A1-A2-A3-A4-A5-A6-A7-A8-A9-A10;$$

$$B11=A11.*(30/82)^2;$$

$$A12=\text{sum}(\text{sum}(P(:,>2350)))-A1-A2-A3-A4-A5-A6-A7-A8-A9-A10-A11;$$

$$B12=A12.*(30/82)^2;$$

$$A13=\text{sum}(\text{sum}(P(:,>2300)))-A1-A2-A3-A4-A5-A6-A7-A8-A9-A10-A11-A12;$$

$$B13=A13.*(30/82)^2;$$

$$A14=\text{sum}(\text{sum}(P(:,>2250)))-A1-A2-A3-A4-A5-A6-A7-A8-A9-A10-A11-A12-A13;$$

$$B14=A14.*(30/82)^2;$$

$$A15=\text{sum}(\text{sum}(P(:,>2200)))-A1-A2-A3-A4-A5-A6-A7-A8-A9-A10-A11-A12-A13-A14;$$

$$B15=A15.*(30/82)^2;$$

$$A16=\text{sum}(\text{sum}(P(:,>2150)))-A1-A2-A3-A4-A5-A6-A7-A8-A9-A10-A11-A12-A13-A14-A15;$$

$$B16=A16.*(30/82)^2;$$

```

A17=sum(sum(P(:,>2100))-A1-A2-A3-A4-A5-A6-A7-A8-A9-A10-A11-A12-A13-A14-A15-
A16;
B17=A17.*(30/82)^2;

A18=sum(sum(P(:,>2050))-A1-A2-A3-A4-A5-A6-A7-A8-A9-A10-A11-A12-A13-A14-A15-
A16-A17;
B18=A18.*(30/82)^2;

A19=sum(sum(P(:,>2000))-A1-A2-A3-A4-A5-A6-A7-A8-A9-A10-A11-A12-A13-A14-A15-
A16-A17-A18;
B19=A19.*(30/82)^2;

A20=sum(sum(P(:,>1950))-A1-A2-A3-A4-A5-A6-A7-A8-A9-A10-A11-A12-A13-A14-A15-
A16-A17-A18-A19;
B20=A20.*(30/82)^2;

A21=sum(sum(P(:,>1900))-A1-A2-A3-A4-A5-A6-A7-A8-A9-A10-A11-A12-A13-A14-A15-
A16-A17-A18-A19-A20;
B21=A21.*(30/82)^2;

A22=sum(sum(P(:,>1850))-A1-A2-A3-A4-A5-A6-A7-A8-A9-A10-A11-A12-A13-A14-A15-
A16-A17-A18-A19-A20-A21;
B22=A22.*(30/82)^2;

A23=sum(sum(P(:,>1800))-A1-A2-A3-A4-A5-A6-A7-A8-A9-A10-A11-A12-A13-A14-A15-
A16-A17-A18-A19-A20-A21-A22;
B23=A23.*(30/82)^2;

A24=sum(sum(P(:,>1))-A1-A2-A3-A4-A5-A6-A7-A8-A9-A10-A11-A12-A13-A14-A15-A16-
A17-A18-A19-A20-A21-A22-A23;
B24=A24.*(30/82)^2;

Y=zeros(1,24);
Y(1,1)=B24;
Y(1,2)=B23;

```

```

Y(1,3)=B22;
Y(1,4)=B21;
Y(1,5)=B20;
Y(1,6)=B19;
Y(1,7)=B18;
Y(1,8)=B17;
Y(1,9)=B16;
Y(1,10)=B15;
Y(1,11)=B14;
Y(1,12)=B13;
Y(1,13)=B12;
Y(1,14)=B11;
Y(1,15)=B10;
Y(1,16)=B9;
Y(1,17)=B8;
Y(1,18)=B7;
Y(1,19)=B6;
Y(1,20)=B5;
Y(1,21)=B4;
Y(1,22)=B3;
Y(1,23)=B2;
Y(1,24)=B1;

disp('Temperature Area=')
Y'

%plot(Y')
%%%%%%%%%%%%%%%%%%%%%%%%%%%%%%%%%%%%%%%%%%%%%%%%%%%%%%%%%%%%%%%%%%%%%%%%%%
A=input('Continue?','s');
end %if
end %while

fclose(fid);

```

Average KL factor Total KL factor

```

X=input('Please insert multi-INPUT file directory & name :','s');

multiF=[X];

fid = fopen(multiF, 'rt');
if (fid == -1)
    error('read_file: cannot open file for reading');
end
done_yet = 0;
while (done_yet == 0)

DATA = fgetl(fid)
if (DATA == -1);
    done_yet = 1;
else

ZD=[DATA, '.txt'];
Z=[ZD];
P=load(Z);

B=sum(sum(P(:,>0)));
C=sum(sum(P(:,>)));
AVGKL=C./B;

fprintf('Integration of KLfactor: %.3f \n', C );
fprintf('Average of KLfactor : %.3f \n', AVGKL );

A=input('Continue?','s');
end %if
end %while

fclose(fid);

```


KL factor Histogram

```

X=input('Please insert multi-INPUT file directory & name :','s');
multiF=[X];
fid = fopen(multiF, 'rt');
if (fid == -1)
    error('read_file: cannot open file for reading');
end
done_yet = 0;
while (done_yet == 0)

DATA = fgetl(fid)
if (DATA == -1);
    done_yet = 1;
else

ZD=[DATA, '.txt'];
Z=[ZD];
P=load(Z);

%%%%%%%%%%%%%%%%%%%%%%%%%%%%%%%%%%%%%%%%%%%%%%%%%%%%%%%%%%%%%%%%%%%%%%%%

P1=P(:,:);
C1=zeros(286,160);
B1=zeros(1,200);

for k=1:5:1000;
    for i=1:286;
        for j=1:160;

            if P1(i,j)<(k.*0.001)+0.005 & P1(i,j)>=(k.*0.001);
                C1(i,j)=1;
            else
                C1(i,j)=0;
            end%if
        end %j
    end %i
end %k

```

```

end %i
B1(1,k)=sum(sum(C1));
end %for k
a=1:5:1000;
D=B1(1,a);
D1=D';%transpose matrix
ZT=[DATA,'his.txt'];
save(ZT,'D1','-ASCII')
%%%%%%%%%%
end %if
end %while
fclose(fid);

```

Spray Angle

```

function SAngle(SA)
X=input('Please insert multi-INPUT file directory & name :','s');
multiF=[X];
fid = fopen(multiF, 'rt');
if (fid == -1)
    error('read_file: cannot open file for reading');
end
done_yet = 0;
while (done_yet == 0)

    DATA = fgetl(fid)
    if (DATA == -1);
        done_yet = 1;
    else

        ZD=[DATA, '.txt'];
        Z=[ZD];

        S1=load(Z);
        S=S1';
    end
end

```

```

spY=81; %nozzle tip position Y
spX=28; %nozzle tip position X

spt=spY-50;
spe=spY+50;

X40=168+spX; % 1 pixel =0.02381 cm at 4 cm

spa=S(spt:spe,:);

lmax=max(max(spa));

Ysec=S(spY,:); %section at Y
%%%%%%%%%%%%%%%%%%%%%%%%%%%%%%%%%%%%%%%%%%%%%%%%%%%%%%%%%%%%%%%%%%%%%%%%
spa=S(spt:spe,:);

X40s=spa(:,X40); %section at X=4 cm
X40max=max(X40s);
%%%%%%%%%%%%%%%%%%%%%%%%%%%%%%%%%%%%%%%%%%%%%%%%%%%%%%%%%%%%%%%%%%%%%%%%

subplot(4,1,1)
imagesc(S);
grid

subplot(4,1,3)
plot(Ysec)
grid
%%%%%%%%%%%%%%%%%%%%%%%%%%%%%%%%%%%%%%%%%%%%%%%%%%%%%%%%%%%%%%%%%%%%%%%%
SH=lmax.*20/100 ; %filter at 10% from max intensity
%%%%%%%%%%%%%%%%%%%%%%%%%%%%%%%%%%%%%%%%%%%%%%%%%%%%%%%%%%%%%%%%%%%%%%%%
% set 0-1 data
Yspa=zeros(101,286);
for i=1:101;
    for j=1:286;

```

```

    if spa(i,j)< SH;
        Yspa(i,j)=0;
    else
        Yspa(i,j)=1;
    end%if
end%for
end%for
subplot(4,1,2)
imagesc(Yspa)
grid

%%%%%%%%%%%%%%%%%%%%%%%%%%%%%%%%%%%%%%%%%%%%%%%%%%%%%%%%%%%%%%%%%%%%%%%%
%Y++
YP=Yspa(1:51,:);
t1=linspace(0,0,X40);

for x1=1:X40;
    t1(x1)=sum(YP(:,x1));
end
t11=t1(spX:X40)';

%Y--
YM=Yspa(51:101,:);
t2=linspace(0,0,X40);

for x2=1:X40;
    t2(x2)=-sum(YM(:,x2));
end
t22=t2(spX:X40)';

V=1:1:X40;
subplot(4,1,4)
plot(V,t1,V,t2)
grid

```

```

%%%%%%%%%%%%%%%%%%%%%%%%%%%%%%%%%%%%%%%%%%%%%%%%%%%%%%%%%%%%%%%%%%%%%%%%
Xx=(1:1:169);
t111=t11';
up=polyfit(Xx,t111,1);

t222=t22';
um=polyfit(Xx,t222,1);

Ap=up(1);
Bp=up(2);
Am=um(1);
Bm=um(2);

YPd=(Ap.*168)+Bp;
YMd=-(Am.*168)-Bm;
%%%%%%%%%%%%%%%%%%%%%%%%%%%%%%%%%%%%%%%%%%%%%%%%%%%%%%%%%%%%%%%%%%%%%%%%
%Spray angle
SA1=atan(YPd./168);
SA2=atan(YMd./168);
SA=SA1+SA2;
SAngle=SA.*180/pi;

fprintf('Spary Angle: %.5f degree \n', SAngle );
%%%%%%%%%%%%%%%%%%%%%%%%%%%%%%%%%%%%%%%%%%%%%%%%%%%%%%%%%%%%%%%%%%%%%%%%
A=input('Continue?','s');
end %if
end %while
fclose(fid);

```

Spray Volume

```

X=input('Please insert multi-INPUT file directory & name :','s');
multiF=[X];
fid = fopen(multiF, 'rt');
if (fid == -1)
    error('read_file: cannot open file for reading');
end
done_yet = 0;
while (done_yet == 0)

DATA = fgetl(fid)
if (DATA == -1);
    done_yet = 1;
else

ZD=[DATA, '.txt'];
Z=[ZD];
P=load(Z);

%%%%%%%%%%%%%%%%%%%%%%%%%%%%%%%%%%%%%%%%%%%%%%%%%%%%%%%%%%%%%%%%%%%%%%%%

B=P(:,20:120);

B2=zeros(286,101);
Max=max(max(B));
for i=1:286
    for j=1:101
        if B(i,j)>Max*20/100,;
            B2(i,j)=1;
        else
            B2(i,j)=0;
        end
    end%j
end%i

```

```

T=linspace(0,0,286);
AT=linspace(0,0,286);
for n=1:286
    T(n)=sum(B2(n,:))*30/82; %mm
    AT(n)=pi.*(T(n)/2)^2; %mmxmm
end
SV=sum(AT)/1000;
fprintf('Spray Volume (cm3): %.3f \n', SV);
imagesc(B2)
%%%%%%%%%%%%%%%%%%%%%%%%%%%%%%%%%%%%%%%%%%%%%%%%%%%%%%%%%%%%%%%%%%%%%%%%
A=input('Continue?','s');
end %if
end %while

fclose(fid);

```

Spray Penetration

```

X=input('Please insert multi-INPUT file directory & name :','s');
multiF=[X];
fid = fopen(multiF, 'rt');
if (fid == -1)
    error('read_file: cannot open file for reading');
end
done_yet = 0;
while (done_yet == 0)
    DATA = fgetl(fid)
    if (DATA == -1);
        done_yet = 1;
    else
        ZD=[DATA, '.txt'];
        Z=[ZD];
        P=load(Z);
    end
end

```

```

%%%%%%%%%%
CutPic=load('D:\karn\BDFdata\20051004cutOffPic\CutOffPic1.txt');
P1=P.*CutPic;
B=P1(:,20:120);
B2=zeros(286,101);
Max=max(max(B));
for i=1:286
    for j=1:101
        if B(i,j)>Max*20/100;,
            B2(i,j)=B(i,j);
        else
            B2(i,j)=0;
        end
    end%j
end%i
T=linspace(0,0,256);
for m=1:286;

    if sum(B2(m,:))<10;,
        T(m)=0;
    else
        T(m)=1;
    end
end%m

B3=B2';
%subplot(2,1,1)
imagesc(B3)
grid
SP=sum(T)*30/82;

fprintf('Spray penetration (mm): %.1f \n', SP);
%%%%%%%%%%
A=input('Continue?','s');
end %if

```



```
end %while
```

```
fclose(fid);
```

Injection Rate and Injection rate shaping

```
Peak injection data
```

```
Wp=0.1611;%peak injection weight
```

```
lp=load('C:\MATLAB6p1\work\X13');
```

```
lrp=lp(:,4);
```

```
%plot(lr)
```

```
%1 set Zero Data
```

```
lsp=lrp(1:100);
```

```
Msp=sum(lsp)/100;
```

```
lr2p=lrp-Msp;
```

```
%2 cut of (-) data
```

```
lr3p=zeros(2000,1);
```

```
for b=1:2000;
```

```
    if lr2p(b) >=0;
```

```
        lr3p(b) = lr2p(b);
```

```
    else
```

```
        lr3p(b) = 0;
```

```
    end
```

```
end
```

```
%plot(lr3)
```

```
lr3p;
```

```
%2.2 convert to KPa
```

```
lr4p=lr3p;
```

```
%3 square root data
```

```
lr5p=lr4p.^(1/2);
```

```
%Area
```

```
Arp=zeros(2000,1);
```

```
for p=2:2000;
```

```

Arp(1)=0;
Arp(p)=1/2*(Ir5p(p-1)+Ir5p(p))*0.00001;
end
Arsp=sum(Arp);
% C constant data 0.017 g
C3=Wp./Arsp;
% real injection rate
Ir6p=Ir5p.*C3;
%%%%%%%%%%%%%%%%%%%%%%%%%%%%%%%%%%%%%%%%%%%%%%%%%%%%%%%%%%%%%%%%%%%%%%%%
Xrf=input('Please insert reference Injection file directory & name :','s');
W=input('Please insert calibration weight(g) :');
X1rf=[Xrf];
Irf=load(X1rf);
Irrf=Irf(:,4);
%1 set Zero Data
Isrf=Irrf(1:100);
Msrf=sum(Isrf)/100;
Ir2rf=Irrf-Msrf;

%2 cut of (-) data
Ir3rf=zeros(2000,1);
%plot(Ir3)
for b=1:2000;
    if Ir2rf(b) >=0;
        Ir3rf(b) = Ir2rf(b);
    else
        Ir3rf(b) = 0;
    end
end
%plot(Ir3)
Ir3rf;
%2.2 convert to KPa
Ir4rf=Ir3rf;
%Ir4=Ir3*(10/4090*1850/5*200/1850);
%plot(Ir4)

```

```

%3 square root data
lr5rf=lr4rf.^(1/2);

%Area
Arrf=zeros(2000,1);

for h=2:2000;
    Arrf(1)=0;
    Arrf(h)=1/2*(lr5rf(h-1)+lr5rf(h))*0.00001;

end

Arsrf=sum(Arrf);
Err=W./(C3*Arsrf);

% real injection rate
lr6rf=lr5rf.*C3;

%%%%%%%%%%%%%%%%%%%%%%%%%%%%%%%%%%%%%%%%%%%%%%%%%%%%%%%%%%%%%%%%%%%%%%%%

%Estimate spary mass from reference data
ReP=1;
while ReP==1;

X=input('Please insert Injection file directory & name :','s');
X1=[X];
l=load(X1);
lr=l(:,4);
%plot(lr)

%1 set Zero Data
ls=lr(1:100);
Ms=sum(ls)/100;
lr2=lr-Ms;

%2 cut of (-) data
lr3=zeros(2000,1);
%plot(lr3)

for j=1:2000;
    if lr2(j) >=0;
        lr3(j) = lr2(j);
    else
        lr3(j) = 0;
    end
end

```

```

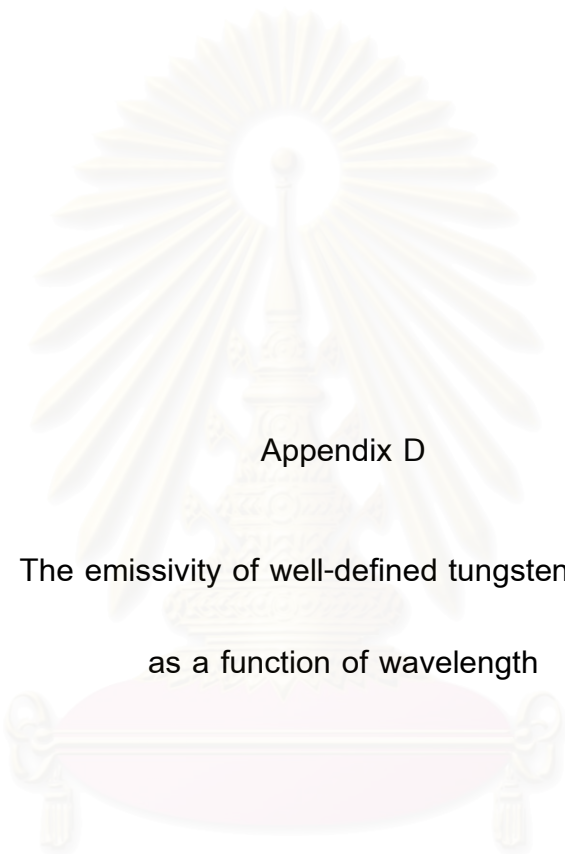
end
%plot(lr3)
lr3;
%2.2 convert to KPa
lr4=lr3;
%3 square root data
lr5=lr4.^(1/2);
%Area
Ar=zeros(2000,1);
for u=2:2000;
    Ar(1)=0;
    Ar(u)=1/2*(lr5(u-1)+lr5(u))*0.00001;
end
Ars=sum(Ar);
mass100=C3.*Ars.*Err;
ERms=(mass100-0.015)./0.015*100;
% real injection rate
lr6=lr5.*C3;
%%%%%%%%%%%%%%%%%%%%%%%%%%%%%%%%%%%%%%%%%%%%%%%%%%%%%%%%%%%%%%%%%%%%%%%%
a=1:1:2000;
a2=a/100;
plot(a2,lr6,a2,lr6rf,'r')
Mlr=max(lr6);
Mlrf=max(lr6rf);
ERlr100=(Mlr-Mlrf)./Mlr*100; %100MPa
Grid
%%%%%%%%%%%%%%%%%%%%%%%%%%%%%%%%%%%%%%%%%%%%%%%%%%%%%%%%%%%%%%%%%%%%%%%%
%Difference
fprintf('Peak injection rate of referance data:      %.5f g/s \n', Mlrf );
fprintf('Peak injection rate of  data:                %.5f g/s \n', Mlr );
fprintf('Mass of data (calculation)(100Mpa):           %.5f g \n', mass100);
fprintf('Error Mass from 0.015 g :                      %.5f Percent \n', ERms);
fprintf('Error Injection rate from referance data(100MPa) : %.5f Percent \n', ERlr100);
title(' Injection rate shaping');
xlabel('Time (msec)');

```

```
ylabel('Injection rate (g/s)');  
%%%%%%%%%%%%%%%%%%%%%%%%%%%%%%%%%%%%%%%%  
ReP=input('Continue? Yes(1) No(0) :');  
disp('*****');  
end%while
```



สถาบันวิทยบริการ
จุฬาลงกรณ์มหาวิทยาลัย



Appendix D

The emissivity of well-defined tungsten ribbon
as a function of wavelength

สถาบันวิทยบริการ
จุฬาลงกรณ์มหาวิทยาลัย

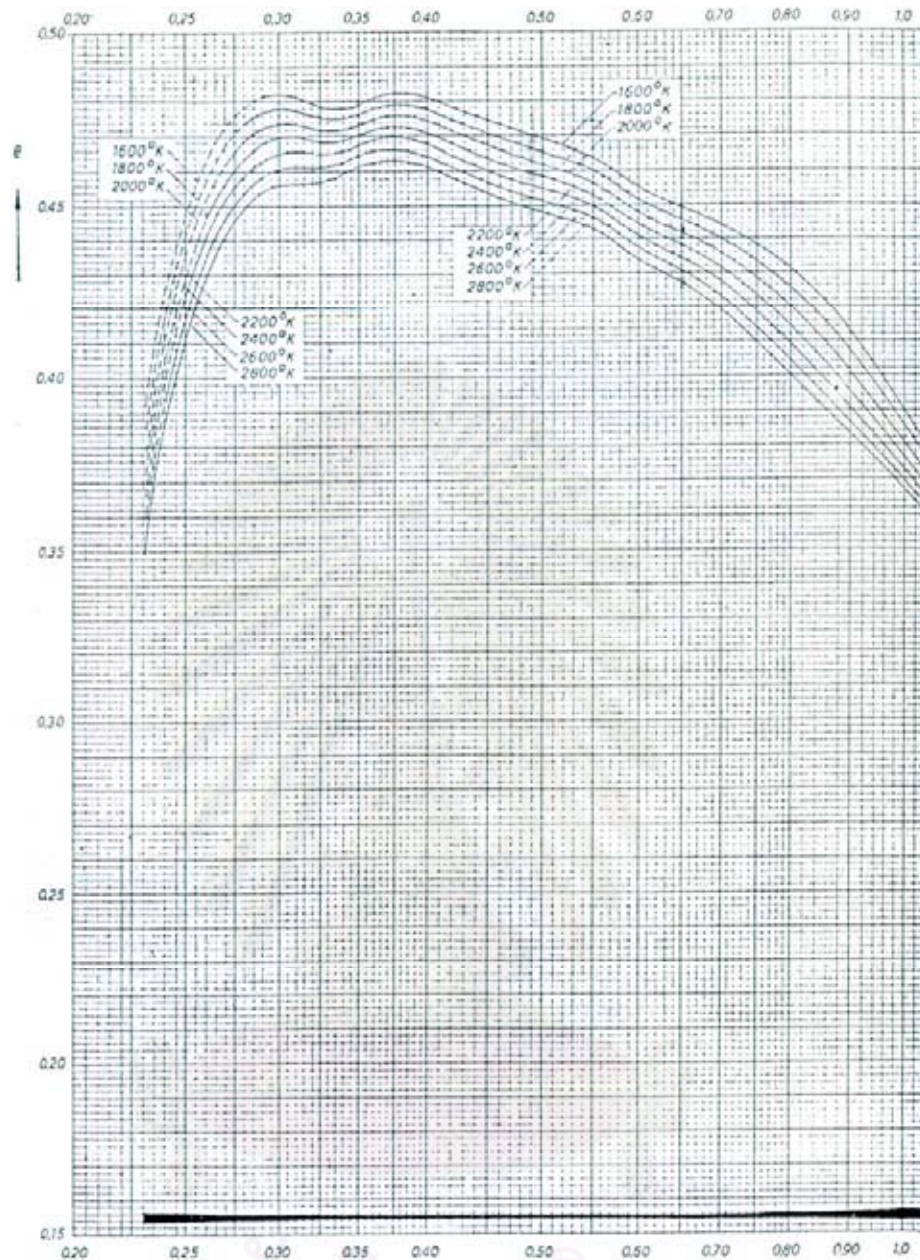
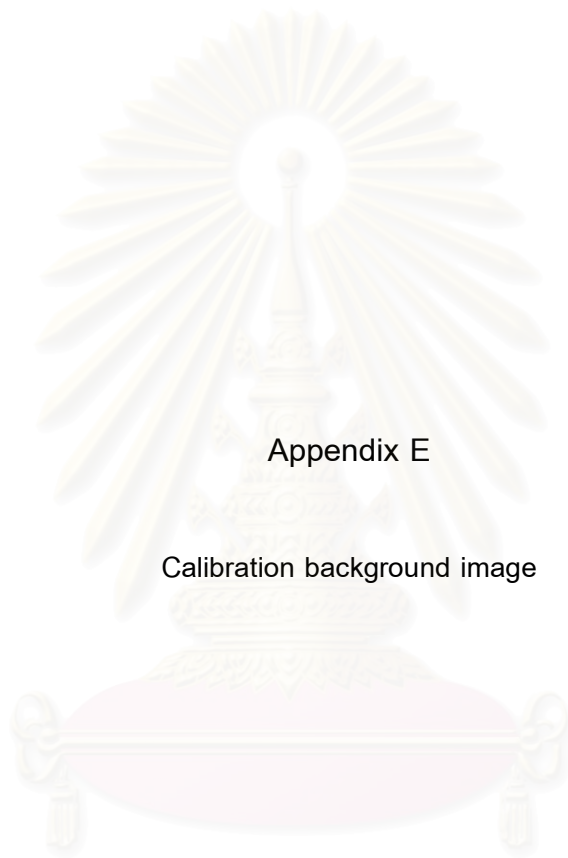


Fig. D-1 The emissivity of well-defined tungsten ribbon as a function of wave length
 at dotted parts of the curves are obtained by extrapolation.

Reference:

J.C DEVOS, Research Department of the N.V. KEMA, Arnhem, Nederland.
 Physica XX 690-714. p.713, 1954.



Appendix E

Calibration background image

สถาบันวิทยบริการ
จุฬาลงกรณ์มหาวิทยาลัย

The back ground of raw data was obtained by applied the straight light to “Frost glass”. ICCD camera was set at gain 5.5 and width 10 μsec . The image result was shown in figure E-1.

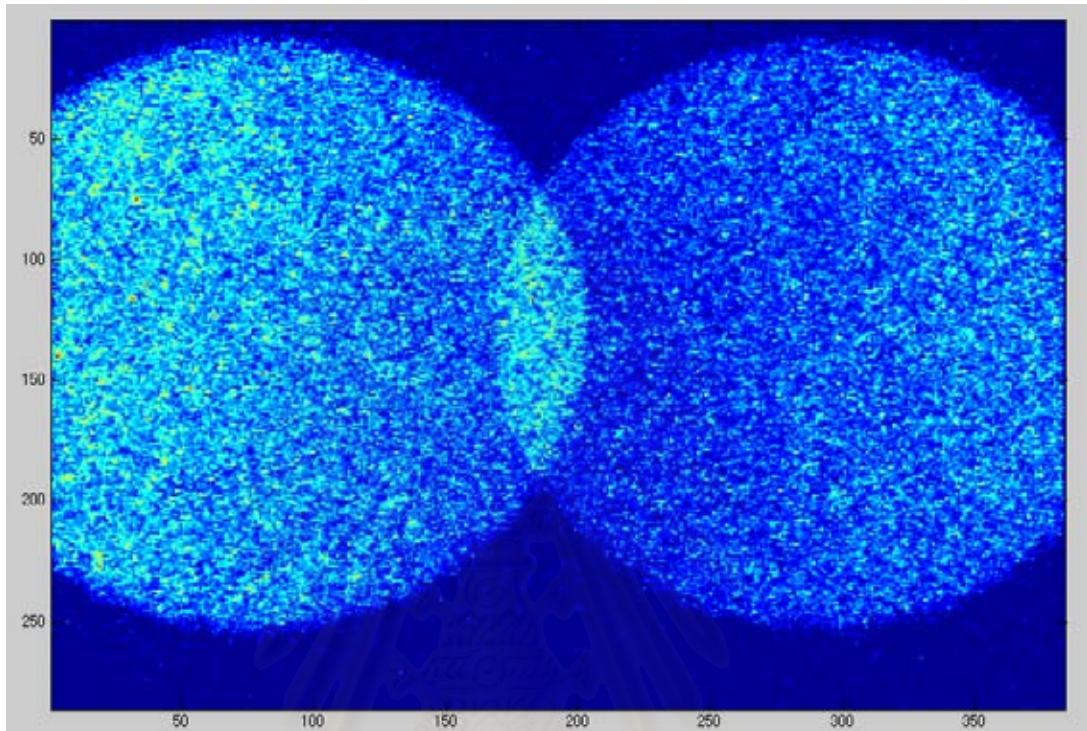


Fig.E-1 Background raw data

The image data obtain from figure E-1 was analyzed by sectioned data along X-axis and Y-axis. Both data were shown that the back ground of images was not smooth. It was caused from the over lap of 2 images and the curve of lens, shown in figure E-2 and E-3.

สถาบันวิทยบริการ
จุฬาลงกรณ์มหาวิทยาลัย

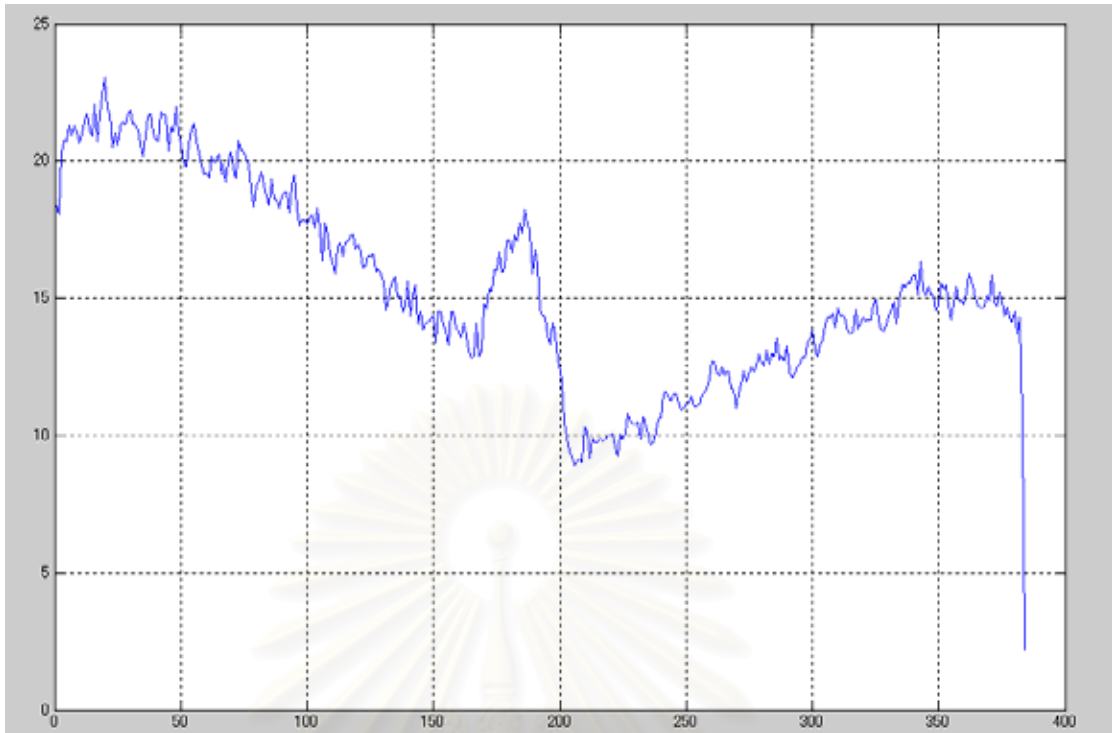


Fig.E-2 Sectional along Y-axis

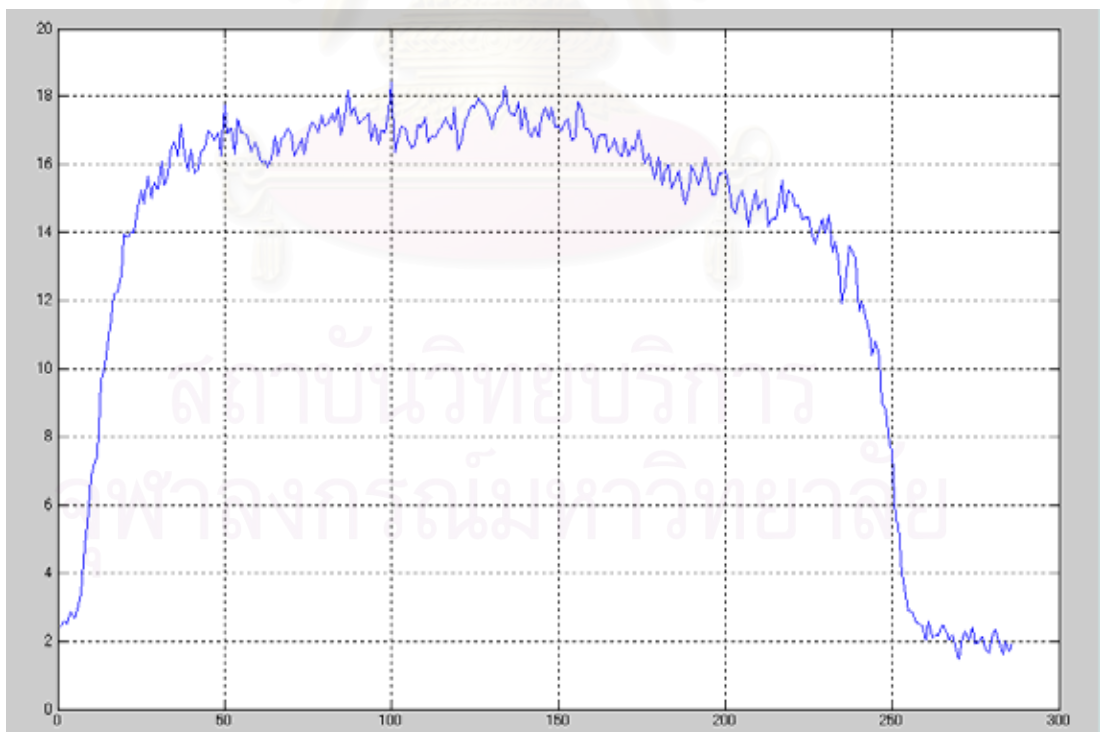


Fig.E-3 Sectional along X-axis

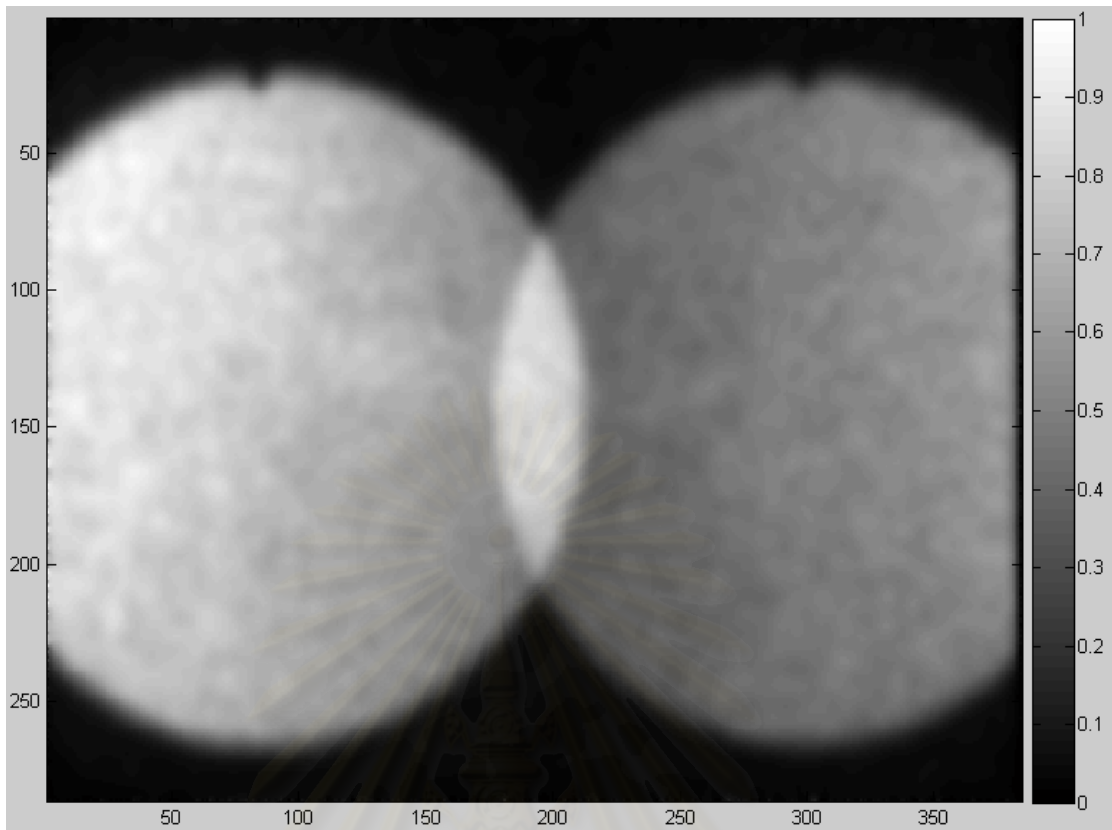


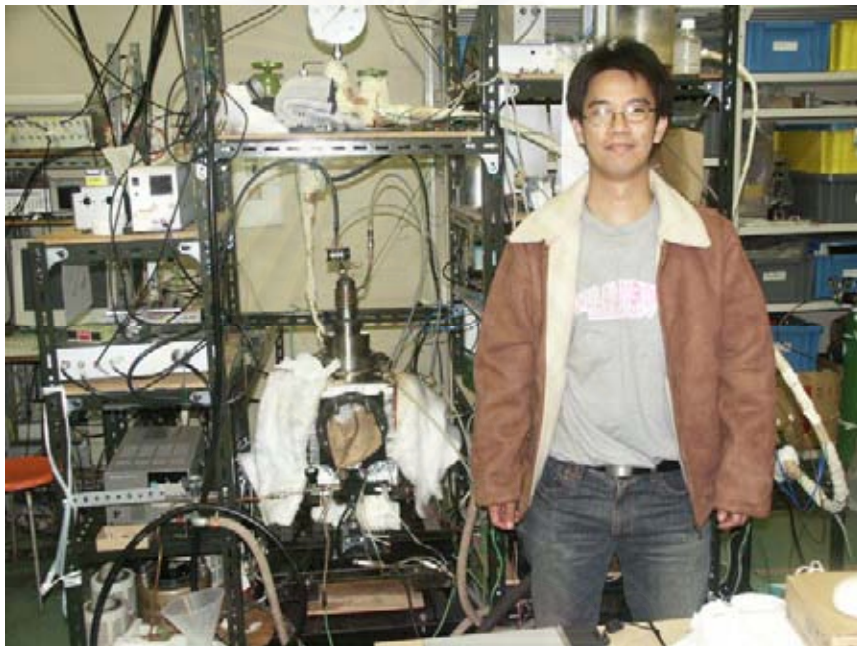
Fig.E-4 Calibration background image (by simulation)

According to raw back ground data had high image noise (low light intensity). This back ground image was simulated with an assumption that the back ground surface was smooth. By computation programming, the data were calculated by averaging them pixel by pixel and obtained the images as shown in figure E-4.

สถาบันวิทยบริการ
จุฬาลงกรณ์มหาวิทยาลัย

Author's Biography

Mr Karn RomPhol was born in 11 December 1977.in Bangkok. Graduated from department of mechanical faculty of engineering Chiang Mai university in 2000. He joined master's degree program Chulalongkorn university in 2001. In 2002, he was selected to be exchange student at Saitama University Japan. During the year 2003, he did spray combustion experiment at Tokai University, Japan.



สถาบันวิทยบริการ
จุฬาลงกรณ์มหาวิทยาลัย